Strategies for Modulating the Diverse Activities of Heat Shock Protein 70

by

Victoria A. Assimon

A dissertation submitted in partial fulfillment
of the requirements for the degree of
Doctor of Philosophy
(Chemical Biology)
in the University of Michigan
2015

Doctoral Committee:

Associate Professor Jason E. Gestwicki, Co-Chair
Professor Anna K. Mapp, Co-Chair
Professor Andrew P. Liebermann
Professor David H. Sherman
Professor Ronald W. Woodard

2015

Dedication

To my grandparents, Peter G. Assimon and Magdalini Morena.

Acknowledgements

First and foremost, I would like to thank my advisor, Professor Jason E. Gestwicki, for his patience, optimism, support, and for providing a unique interdisciplinary research environment. He has taught me a great deal about science, leadership, and collaboration. Jason has supported my intellectual curiosities, while always providing critical evaluation and direction. I feel privileged to have had the opportunity to learn from him and to have been a part of his laboratory. I would also like to thank all the members of the Gestwicki laboratory, both past and present. The work described in this thesis would not have been possible without their insights and contributions. The direct contributions of individuals have been noted in each chapter. Notable among these are Zapporah Young, Isabelle Taylor, and Xiaokai Li. Many others have continually inspired me with their passion for science, exceptional work ethic, and vibrant personalities: Tomoko Komiyama, Andrea Thompson, Matthew Smith, Leah Makley, Anne Gillies, Jennifer Rauch, Sharan Srinivasan, Bryan Dunyak, Laura Cesa, Sue-Ann Mok, Hao Shao, Jennifer Abrams, Rebecca Freilich, Kwadwo Opoku-Nsiah, and Matthew Ravalin. Additionally, I am indebted to my thesis committee, Professors Anna Mapp, Andrew Liebermann, David Sherman, and Ronald Woodard, for their insightful comments and encouragement. They have been generous with their time and have helped me to develop as a scientist. Finally, I would like to recognize Alex Martinko and my family for their constant love and support.

Table of Contents

List of Figures

List of Tables

List of Abbreviations

15-DSG	15-deoxyspergualin
5-Fam	5-Carboxyfluorescein
AdaSGC	AdamantylSGC
AR	Androgen receptor
BHI	Brain heart infusion
CFU	Colony forming units
CHIP	Carboxyl terminus of Hsc70 interacting protein
CTD	C-terminal domain
ER	Endoplasmic reticulum
ERAD	ER-associated degradation
FCPIA	Flow cytometry protein interaction assay
FP	Fluorescence polarization
FRET	Förster resonance energy transfer
G/F	Glycine-phenylalanine
Hop	Hsp70/Hsp90 organizing protein
Hsp60	Heat shock protein 60
Hsp70	Heat shock protein 70
Hsp90	Heat shock protein 90

Hsp105	Heat shock protein 105
Hsp110	Heat shock protein 110
HTS	High-throughput screening
IPTG	Isopropyl β-D-1-thiogalactopyranoside
LB	Luria–Bertani
LTP	Long-term potentiation
NBD	Nucleotide binding domain
MAPT	Microtubule-binding protein tau
MB	Methylene blue
MIC	Minimum inhibitory concentration
MoA	Mechanism of action
mP	millipolarization
MRSA	Methicillin-resistant *Staphylococcus aureus*
NEF	Nucleotide exchange factor
NMR	Nuclear magnetic resonance
NR peptide	NRLLLTG peptide
PolyQ-AR	Polyglutamine-expanded androgen receptor
PPI	Protein-protein interaction
PTM	Post-translational modification
SAR	Structure activity relationships
SEM	Standard error of the mean
SBD	Substrate binding domain

SBMA	Spinal-Bulbar Muscular Atrophy
SGC	Sulfogalactosyl ceramide
TAg	T Antigen
TPR	Tetratricopeptide repeat
VRE	Vancomycin-resistant enteroccoci
Wt	Wild-type
ZFLR	Zinc finger-like region

Abstract

Heat shock protein 70 (Hsp70) is an essential regulator of protein homeostasis. Dysfunction of protein homeostasis is directly linked to many diseases, including cancer and neurodegeneration. Thus, an understanding of Hsp70's roles in this process is expected to provide insights into the mechanisms of disease and, potentially, provide new opportunities for therapies. However, Hsp70 is also involved in essential cellular functions, so it is not clear how to safely target it. In this thesis, I first review how Hsp70 cooperates with co-chaperones to enable its many activities. Hsp70 binds to distinct co-chaperones to form complexes that have individual functions in protein folding, degradation and trafficking, suggesting that inhibition of the protein-protein interactions (PPIs) between Hsp70 and its co-chaperones might be one promising way to safely modulate this system. In Chapter 2, I performed a comprehensive, comparative study on how five TPR domain-containing co-chaperones bind to Hsp70 *in vitro*. These experiments highlighted the opportunities and challenges of targeting this PPI. In Chapter 3, I demonstrate how allosteric networks in Hsp70 can be manipulated, using both chemical and genetic approaches, in order to regulate binding to co-chaperones and tune chaperone activity in unexpected ways. Taking all this information together, I show in Chapter 4 that allosteric inhibitors of Hsp70 have surprisingly potent antibiotic activity in drug-resistant bacteria, which seem to rely on robust protein homeostasis. By better

understanding allostery and PPIs in the Hsp70 network, I made new insights into Hsp70 biology and also discovered new lead compounds for therapeutic development.

Chapter 1

Heat shock protein 70 complexes as drug targets

1.1 Abstract

Heat shock protein 70 (Hsp70) plays critical roles in proteostasis and is an emerging target for multiple diseases. However, competitive inhibition of the enzymatic activity of Hsp70 has proven challenging and, in some cases, may not be the most productive way to redirect Hsp70 function. Another approach is to inhibit Hsp70's interactions with important co-chaperones, such as J proteins, nucleotide exchange factors (NEFs) and tetratricopeptide repeat (TPR) domain-containing proteins. These co-chaperones normally bind Hsp70 and guide its many diverse cellular activities. Complexes between Hsp70 and co-chaperones have been shown to have specific functions, such as pro-folding, pro-degradation, and pro-trafficking. Thus, a promising strategy may be to block protein-protein interactions (PPIs) between Hsp70 and its co-chaperones or to target allosteric sites that disrupt or alter these contacts. Such an approach might shift the balance of Hsp70 complexes and reshape the proteome and it has the potential to restore healthy proteostasis. In this chapter, I discuss specific challenges and opportunities related to those goals.

1.2 Diversity of Hsp70 functions

Hsp70 is a molecular chaperone that plays a central role in protein quality control [1, 2]. Hsp70 binds to protein substrates to assist with their folding [3, 4], degradation [5-7], transport [8], regulation [9, 10], and aggregation prevention [11]. The capacity of Hsp70 to carry out these widely divergent functions arises, in part, from three features. First, evolution has given rise to multiple homologous Hsp70 genes [12, 13]. The resulting Hsp70 proteins populate the major subcellular compartments. For example, the cytosol of human cells has two major Hsp70 paralogs, a stress-inducible form (Hsp72/HSPA1A/B) and a constitutive form (Hsc70/HSPA8). Additionally, BiP (HSPA5) is the Hsp70 paralog in the endoplasmic reticulum (ER), while mortalin (HSPA9) is found in the mitochondria. For the purposes of this chapter, "Hsp70" will often be used to broadly refer to these chaperones because they are thought to, in many cases, have similar biochemical properties. Another source of functional diversity is Hsp70's cooperation with other chaperones, such as the heat shock proteins Hsp90 and Hsp60 [4]. Cooperation between Hsp70 and Hsp90, for example, is critical to the function of nuclear hormone receptors [8]. Finally, the full diversity of Hsp70's activities is achieved by collaborating with a large network of co-chaperones [1, 14], including J proteins, NEFs, and TPR domain-containing proteins [15]. These factors bind to Hsp70 and guide its many chaperone activities. These co-chaperones provide further diversification because each category (*e.g.* J proteins, NEFs, TPR proteins) is composed of multiple members, as discussed in more detail in subsequent sections (Figure 1.1).

1.3 Hsp70 as a therapeutic target

Hsp70 has been implicated in multiple diseases, such as neurodegenerative disorders [16], cancer [17], and infectious disease [18] and the evidence linking Hsp70 to disease has been recently reviewed [19-21]. Despite this strong connection, relatively little progress has

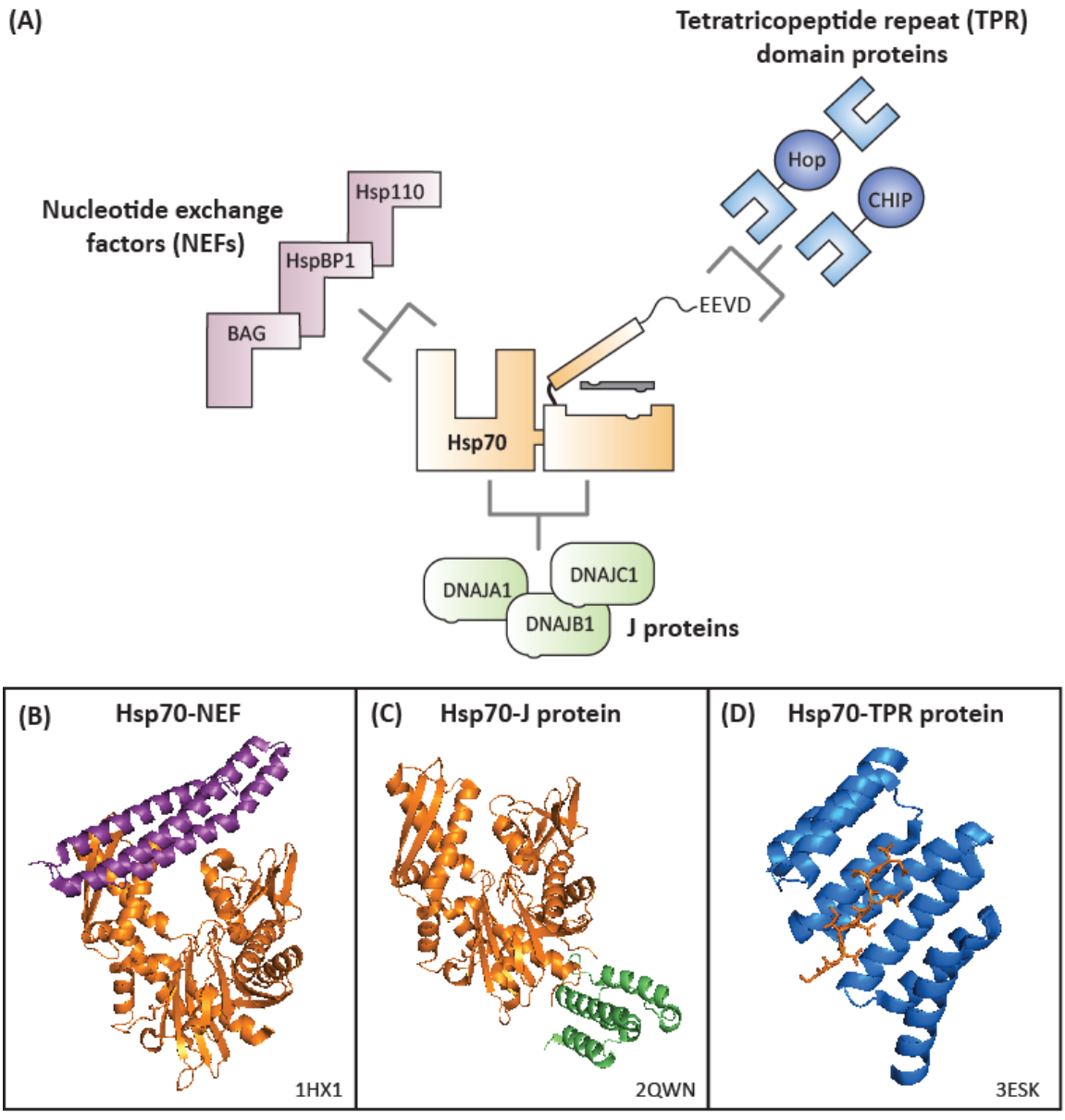

Figure 1.1 Hsp70 forms the core of a multi-protein complex and associates with numerous co-chaperones. (A) Three distinct classes of co-chaperones, NEFs (purple), J proteins (green), and TPR domain-containing proteins (blue), interact with Hsp70 (orange) and regulate its activies. The J proteins and NEFs interact with the nucleotide binding domain (NBD), while the TPR proteins bind the C-terminal region of the lid. Example structures from each class and the corresponding PDB codes are shown. All images were prepared in PyMol. (B) The BAG domain of BAG1 in complex with the NBD of Hsc70. (C) The J domain of auxilin fused to the NBD of Hsc70. (D) The TPR1A domain of Hop in complex with the substrate binding domain of Hsc70.

been made in bringing Hsp70 inhibitors to the clinic. One of the contributing factors to this lack of translational progress is that Hsp70's functional promiscuity makes it difficult to predict potential off-target effects. As discussed above, Hsp70 is involved in many key processes in the cell; thus, it is not clear how therapeutics could be used to rebalance some pathological Hsp70 functions without impacting global proteostasis. One attractive possibility may be to target the interactions between Hsp70 and its co-chaperones because these factors are thought to diversify Hsp70's functions.

A major focus of this chapter is to review the structure and function of Hsp70 multi-protein complexes and evaluate recent progress in identifying compounds that selectively target the assembly/disassembly of these complexes. The underlying model is that each complex composed of an Hsp70 (*e.g.* Hsc70, Bip, *etc.*) bound to a specific set of co-chaperones (*e.g.* J protein, NEF, or TPR domain-containing protein) might be involved in a discrete aspect of chaperone biology (*e.g.* clathrin uncoating, protein folding, degradation, *etc.*). Thus, if small molecules selectively disrupted an interaction between Hsp70 and a specific co-chaperone, then only a subset of Hsp70 biology might be impacted. In other words, the complexity of this chaperone network provides a unique opportunity to influence specific subsets of protein quality control while leaving the rest unperturbed. The challenge of this strategy is that it has been notoriously difficult to target PPIs [22-24], such as those between Hsp70 and its co-chaperones. However, new advances in high-throughput screening (HTS) methodology are rapidly changing the landscape of discovery in this area.

In fact, Hsp70 might be a particularly attractive target for deploying these methods, owing to its high number of protein-protein contacts that are important in guiding Hsp70 biology.

1.4 Structure and function of Hsp70 and its complexes

1.4.1 The domain architecture and substrate binding activity of Hsp70

Hsp70 consists of two domains, a 45 kDa N-terminal nucleotide binding domain (NBD) and a 25 kDa C-terminal substrate binding domain (SBD), which are connected by a short flexible linker [25-27]. The NBD of Hsp70 is further divided into two subdomains, lobes I and II, which are each divided into an "A" and "B" region (Figure 1.2). These lobes form a cleft that binds ATP with a nucleotide binding cassette that is related to hexokinase and actin [28]. Hsp70's SBD is composed of a 15 kDa β-sandwich subdomain with a hydrophobic

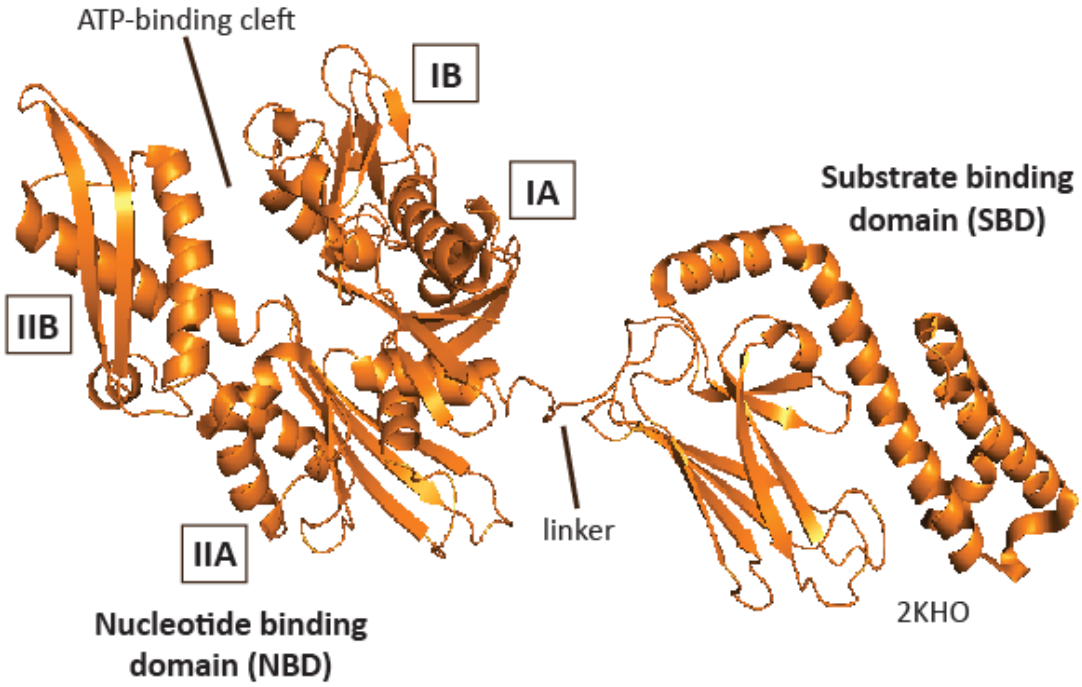

Figure 1.2 The stucture of Hsp70. Hsp70 is composed of a 45 kDa N-terminal nucleotide binding domain (NBD) connected to a 25 kDa substrate binding domain (SBD) by a short hydrophobic linker. The SBD is composed of a β-sandwich and an α-helical "lid" domain. The prokaryotic Hsp70, DnaK, is shown (PDB code 2HKO), but the general architecture appears to be conserved amongst prokaryotic and eukaryotic family members.

groove for polypeptide binding and a 10 kDa α-helical region which forms a "lid" over the polypeptide binding site [29]. Hsp70 preferentially binds hydrophobic regions of proteins and can therefore bind newly synthesized linear peptides or exposed regions on partially unfolded proteins [3, 30]. Additionally, a lack of strong sequence specificity allows Hsp70 to bind a variety of client proteins including signal transduction proteins, clathrin, nuclear hormone receptors, and cytoskeletal proteins [31, 32].

1.4.2 The ATPase cycle of Hsp70

The ATPase cycle of Hsp70 has been largely studied for the prokaryotic DnaK ortholog. In this chaperone, ATP hydrolysis involves critical allostery between the NBD and SBD. In the ATP-bound state, Hsp70 has a low affinity for substrate and retains an "open" substrate-binding cleft, but conversion to the ADP-bound state causes the α-helical lid region to "close" (Figure 1.3) [33]. In DnaK, this crosstalk between the NBD and SBD appears to be

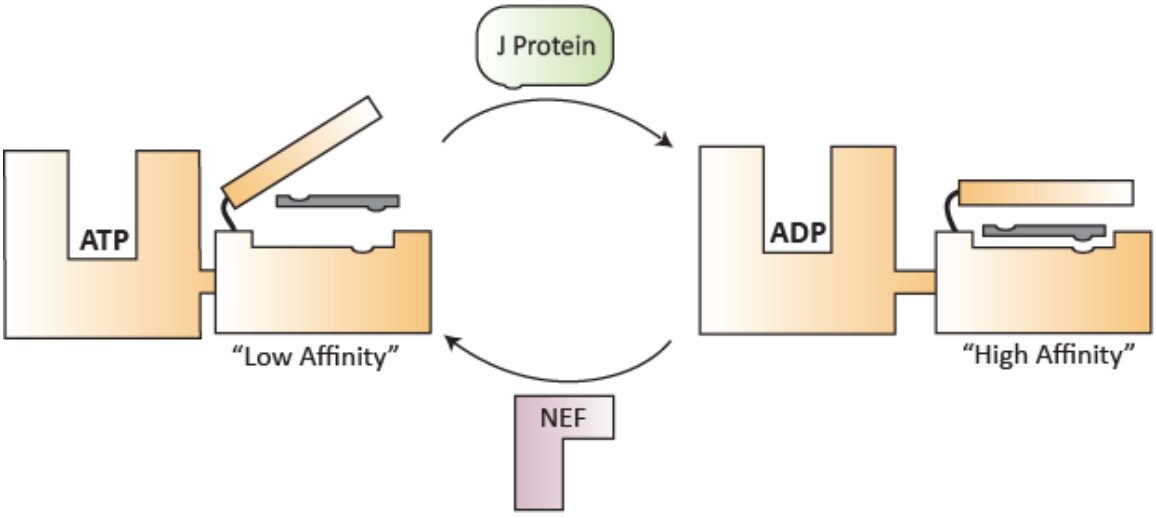

Figure 1.3 The ATPase cycle of Hsp70. Schematic of ATP hydrolysis and the role of co-chaperones. Substrate binding in the SBD coupled with J-domain co-chaperone interactions in the NBD, promote ATP hydrolysis. Conformational changes associated with ATP conversion close the "lid" and enhance affinity for the substrate. The cycle is completed when a nucleotide exchange factor interacts with the NBD and assists with ADP release.

bidirectional, because substrate binding also promotes nucleotide hydrolysis [33, 34]. Thus, ATP hydrolysis in Hsp70 is thought to be a major determinant of chaperone function. For example, mutations in the ATP binding cassette have dramatic effects on chaperone function *in vitro* and *in vivo* [35]. However, recent mutagenesis studies have further shown that the relationship between ATP hydrolysis and chaperone function is indirect [35]. For example, some mutations in DnaK that dramatically reduce ATP turnover have only modest effects on luciferase refolding. In the context of this review, these observations suggest that inhibiting the ATPase activity of Hsp70 might not always directly lead to proportional changes in functional outcomes, such as reduced client stability. Rather, modifying the interactions with co-chaperones might have a more predictable effect on chaperone functions [35].

1.4.3 Co-chaperones regulate Hsp70 structure and activity

The major families of co-chaperones bind to distinct interaction surfaces on Hsp70 (**Figure 1.1**). The J protein co-chaperones bind protein substrates and interact with Hsp70 at lobes IA and IIA of the NBD. This interaction results in an accelerated rate of ATP hydrolysis [36]. The NEF co-chaperones bind lobes IB and IIB of Hsp70's NBD and facilitate the release of ADP, which has also been shown to accelerate Hsp70's ATPase rate [37]. TPR domain-containing co-chaperones bind Hsp70's C-terminus and have been shown to modulate the fates of Hsp70 substrates [38]. Thus, these major families of co-chaperones bind Hsp70 to regulate its enzymatic activity, its choice of substrates and its triage decisions. These systems will be discussed in more detail below.

1.5 Approaches to targeting Hsp70

1.5.1 Competitive nucleotide analogs

What is the best way to chemically target Hsp70? One possible approach is to inhibit ATPase activity with competitive nucleotide analogs [20], as has been done with Hsp90 inhibitors [39]. The nucleotide binding cleft of Hsp70 is well defined and relatively deep, suggesting that it might be suitable for development of inhibitors. However, Hsp70 has a relatively tight affinity (mid-nanomolar) for nucleotide, 300-fold better than Hsp90 [40-43]. Because the cellular concentration of ATP is typically 1-5 mM, protein targets with a high affinity for ADP and ATP are much more difficult to inhibit than those with a lower affinity. Further, the ATP binding cassette in Hsp70 is highly homologous in actin and other abundant proteins. Thus, selectivity for the chaperone might be challenging. Despite these challenges, innovative work performed by Vernalis has produced competitive, orthosteric inhibitors of Hsp70, using structure-based design [44]. Consistent with their design, these compounds inhibit cancer cell viability [44] and this group has even been successful at selectively targeting BiP [45]. Additionally, a cell-based screen of molecules that trigger apoptosis resulted in the discovery of the compound Apoptozole. This molecule has been shown to bind to the NBD of Hsp70. Computational studies suggest that Apoptozole might directly compete with nucleotide for binding to Hsp70 [46, 47]. However, confirmation of this binding site by mutagenesis, competition, and/or structural studies has yet to be reported. However, Massey has reported that the path towards competitive inhibitors of Hsp70 is quantitatively more challenging than the parallel path to other related targets,

such as Hsp90 [43]. Given these hurdles, it seems prudent to pursue additional routes to the design and discovery of potent and selective small molecule modulators targeting Hsp70.

1.5.2 Inhibitors of substrate binding

Targeting the substrate binding cleft of Hsp70 is the next logical avenue, given the depth of the site and its known affinity for relatively low molecular mass peptides. This approach has been taken by Chaperone Technologies in their development of antibiotics. For example, a series of 18-20 amino acid peptides, including drosocin, pyrrhocoricin, and apidaecin, are known to interact with DnaK [18]. Of these peptides, pyrrhocoricin exhibited broad-spectrum antibacterial activity. Competition experiments indicated that this peptide has two binding sites on DnaK, one of which is thought to be adjacent to the substrate binding pocket. Interestingly, pyrrhocoricin has activity against bacteria but not mammalian cells [48], suggesting that the SBD could be leveraged to gain selectivity between different homologs of Hsp70. While this work highlights the usefulness of SBD-targeted compounds as antibiotics, it is unclear whether this strategy could be implemented in the development of therapeutics for different Hsp70 related diseases. Of particular interest is whether enough selectivity could be generated in the peptide binding groove to avoid widespread disruption of the proteome.

1.5.3 Peptide aptamers as chemical modulators of Hsp70

One promising, unbiased approach has been recently reported by Garrido and colleagues, in which they used a yeast-two hybrid experiment to identify peptide aptamers that bind either the NBD or SBD of Hsp70. These aptamers sensitize cancer cells to anti-cancer drugs *in vivo* [49, 50], strongly suggesting the potential of this approach. Thus far, it isn't clear whether these aptamers compete with nucleotide or peptide substrates or whether they have another mechanism of action. Given that these molecules were identified in a cell-based screen, it seems likely that they do not directly compete with the abundant nucleotide or substrates.

1.5.4 Targeting co-chaperones and their interactions with Hsp70

Given the significant challenges associated with the targeting of either the nucleotide or substrate binding regions of Hsp70, additional strategies are worth pursuing. A number of additional Hsp70 inhibitors have been identified, but their effects on co-chaperone interactions are not known yet [51-59]. To supplement this collection of compounds, targeting the PPIs between Hsp70 and its many co-chaperones may be an effective approach. In the following sections, I discuss each co-chaperone class in more detail and outline some of the successes and challenges associated with targeting these PPIs.

1.6 Opportunities for drugging J proteins and their interactions with Hsp70

1.6.1 Structure and function of J proteins

J proteins are a class of Hsp70 co-chaperones whose diversity in structure and function are crucial to the flexibility of the Hsp70 machinery. Evolution has dramatically expanded the

cellular repertoire of J proteins relative to Hsp70s, such that humans have over 40 J protein encoding genes, but only 13 Hsp70 genes [60, 61]. Moreover, the co-existence of many J proteins within the cytosol and nucleus suggests that they have evolved for distinct functions [62, 63]. All J proteins share a conserved J domain but they diverge in other regions, perhaps providing the functional diversity needed to recruit Hsp70 into many different cellular activities. Accordingly, various J proteins have been linked extensively with a wide array of pathological conditions including cancer, neurodegeneration, muscular dystrophy, and viral infection [64-68]. Thus, J proteins may be interesting pharmacological targets because they have the potential to impact a subset of Hsp70-dependent functions.

1.6.2 The interaction of J proteins with Hsp70

The J domain is a highly conserved structure that consists of four α-helices. The J domain interacts directly with the NBD of Hsp70 to stimulate ATP hydrolysis and allosteric conversion into a high affinity substrate binding conformation (**Figure 1.3**) [69-71]. For the bacterial DnaJ-DnaK interaction, the interface consists of the positively charged helix II of the J domain interacting electrostatically with the negatively charged NBD in lobes IA and IIA [36, 72-74]. Additionally, J domains include an invariant His-Pro-Asp (HPD) motif in the loop between helices II and III that is required for function. Though the overall four-helix architecture of the J domain is largely conserved among J proteins, subtle structural differences suggest that some functional diversity may arise from J domain interactions with Hsp70 [75]. For example, mutants in the NBD of the yeast BiP disrupt interactions with

only a subset of available J proteins [76, 77]. Although speculative, these findings suggest that it might be possible to independently target specific J domains at the contact surface with Hsp70.

1.6.3 Classification of J proteins

J proteins have been traditionally grouped into three classes based on structural homology to the *Escherichia coli* DnaJ (Figure 1.4). Class A consists of an N-terminal J domain, a glycine-phenylalanine (G/F) rich region, a zinc finger-like region (ZFLR), a barrel topology C-terminal domain (CTD) and a dimerization domain [78, 79]. Class B has the N-terminal J domain and G/F region, but lacks a ZFLR. Additionally, this class is more structurally variable at the C-terminus, but often contains two CTDs (CTDI and CTDII) [61]. Class C, the largest class, consists of proteins containing a J domain and no other structural homology to DnaJ. More recently, Kampinga and Craig have provided a revised classification system based more closely on function [79]. This classification represents an important new paradigm in thinking about J proteins and it highlights the roles of J proteins in directing the activity of Hsp70.

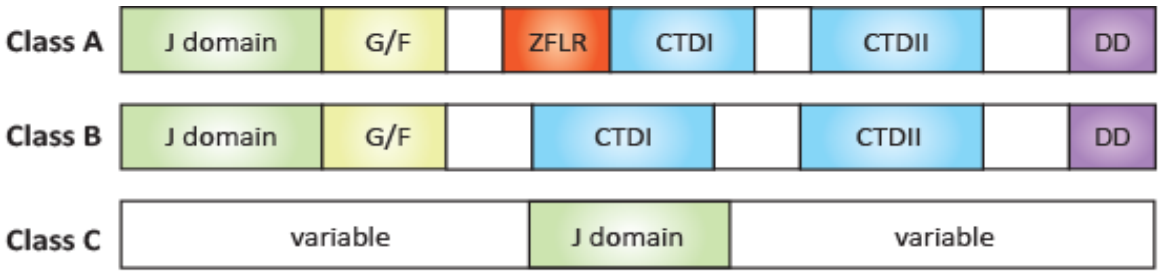

Figure 1.4 J proteins fall into three structural classes. (A) The domain architecture is depicted as a schematic beginning with the N-terminus to the left. The domain types are the J domain, G/F (glycine-phenylalanine rich region), ZFLR (zinc finger-like region), CTDI and II (C-terminal domain), and DD (dimerization domain). Class A is the most related to *E. coli* DnaJ. Class B lacks the ZFLR ,but all members have the G/F and most have one or two CTDs. Class C has no common features except the J domain, which can be located anywhere within the sequence.

1.6.4 J proteins with known specialized functions

Specific functions have been described for only some J proteins. More work is needed to clarify this area. However, some convincing and illustrative examples include auxilin (DNAJC6), which has a C-terminal J domain and a clathrin-binding domain. This J protein is exclusively involved in the Hsp70-dependent uncoating of clathrin-coated vesicles [80-82], an activity not readily redundant with other J proteins. Similarly, DNAJC7 interacts with both Hsp70 and Hsp90 and seems to play a "recycling" role in the chaperoning of specific substrates, such as the progesterone receptor [83]. In the ER, ERdj3 (DNAJB11) works with BiP to assist with ER-associated degradation (ERAD) [84, 85]. These and other examples [86] lead to a speculative model in which individual J proteins might be responsible for each of Hsp70's specific functions. In support of this idea, a systematic study of human J proteins found that a subset are able to refold luciferase, while others inhibit aggregation of heat-denatured luciferase [63], further suggesting that these co-chaperones may be specialized.

1.6.5 The interaction of J proteins with substrate

One prevailing model is that J proteins may bind to substrates and present them to Hsp70. While this concept is likely oversimplified when applied to the large family of J proteins, the interaction of these co-chaperones with substrates seems to play a crucial role in some cases. For example, Lu and coworkers deleted the J domain of Ydj1 (yeast DNAJA1) and found that the remaining portion suppresses rhodanese aggregation on its own [87]. Later work identified a shallow hydrophobic depression on the CTDI of Sis1 (yeast DNAJB1). Four

point mutants in this domain inhibited luciferase binding and refolding [88]. These studies suggest that J proteins can bind directly to substrates. Further insight into how J proteins bind to their substrates has largely been gained from peptide microarray experiments. These studies have revealed that the prokaryotic DnaJ binds ~8mer peptides enriched in hydrophobic residues [89]. Interestingly, DnaJ does not discriminate between L-peptides and D-peptides, indicating that peptide binding involves side chain interactions [89, 90]. However, a crystal structure of the Ydj1 C-terminus bound to the peptide GWLYEIS suggests that the peptide forms a β-strand alongside a β-sheet in CTDI and several contacts are made with the peptide backbone [91]. This discrepancy may be due to species differences and the fact that the general rules for J protein-substrate interactions are not yet clear. However, it is reasonable to hypothesize that formation of Hsp70-J protein-substrate complexes may be important in directing Hsp70 to "choose" specific substrates.

1.6.6 J proteins interact with disease-relevant substrates

The interaction between J proteins and substrates appears to be important for several disease-relevant proteins [92]. For example, DNAJB1 and DNAJB6 inhibit the aggregation and toxicity of mHtt, which is involved in Huntington's disease [93-95]. However, another J protein, DNAJA1, co-localizes with mHtt aggregates [96] and its over-expression increases mHtt aggregation [97]. These observations suggest that individual J proteins, such as DNAJB1 and DNAJA1, might have unique roles in protein quality control. This concept is further illustrated by studies on the Hsp70 substrate, tau [98], in which DNAJB1 inhibits aggregation of tau *in vitro* [99], while DNAJA1 over-expression causes the proteasomal

degradation of tau [100]. Together, these observations suggest that the interactions between J proteins and their substrates might be interesting drug targets, but that more information is needed about how this network is assembled.

1.6.7 The J protein and Hsp70 interaction can be chemically modulated

While the interactions between J proteins and their substrates have not been pharmacologically targeted, several compounds impact the ability of J proteins to act on Hsp70s. This PPI is an attractive drug target because of the importance of J proteins regulating Hsp70's ATP turnover. The first of the compounds to interfere with this PPI was 15-deoxyspergualin (15-DSG), a modified natural product that stimulates cytosolic Hsp70 ATP hydrolysis [101-103]. Chemical screens for structurally similar molecules identified R/1, a compound that specifically inhibits the J protein-stimulated ATPase activity of the yeast cytosolic Hsp70, Ssa1 [104] (Figure 1.5). These findings suggested that drug-like molecules could be identified that alter interactions between J proteins and Hsp70s. In further support of this idea, an unrelated class of molecules, the sulfogalactosyl ceramide (SGC) mimics, were developed. SGC is a cell surface receptor that binds the NBD of multiple members of the Hsp70 family [105, 106]. Park and coworkers developed a soluble mimic of SGC called adamantylSGC (AdaSGC). AdaSGC inhibits the J protein-stimulated ATPase activity of Hsp70, but not its intrinsic (*i.e*. unstimulated) activity, suggesting that it may directly inhibit the J domain-Hsp70 interaction [107].

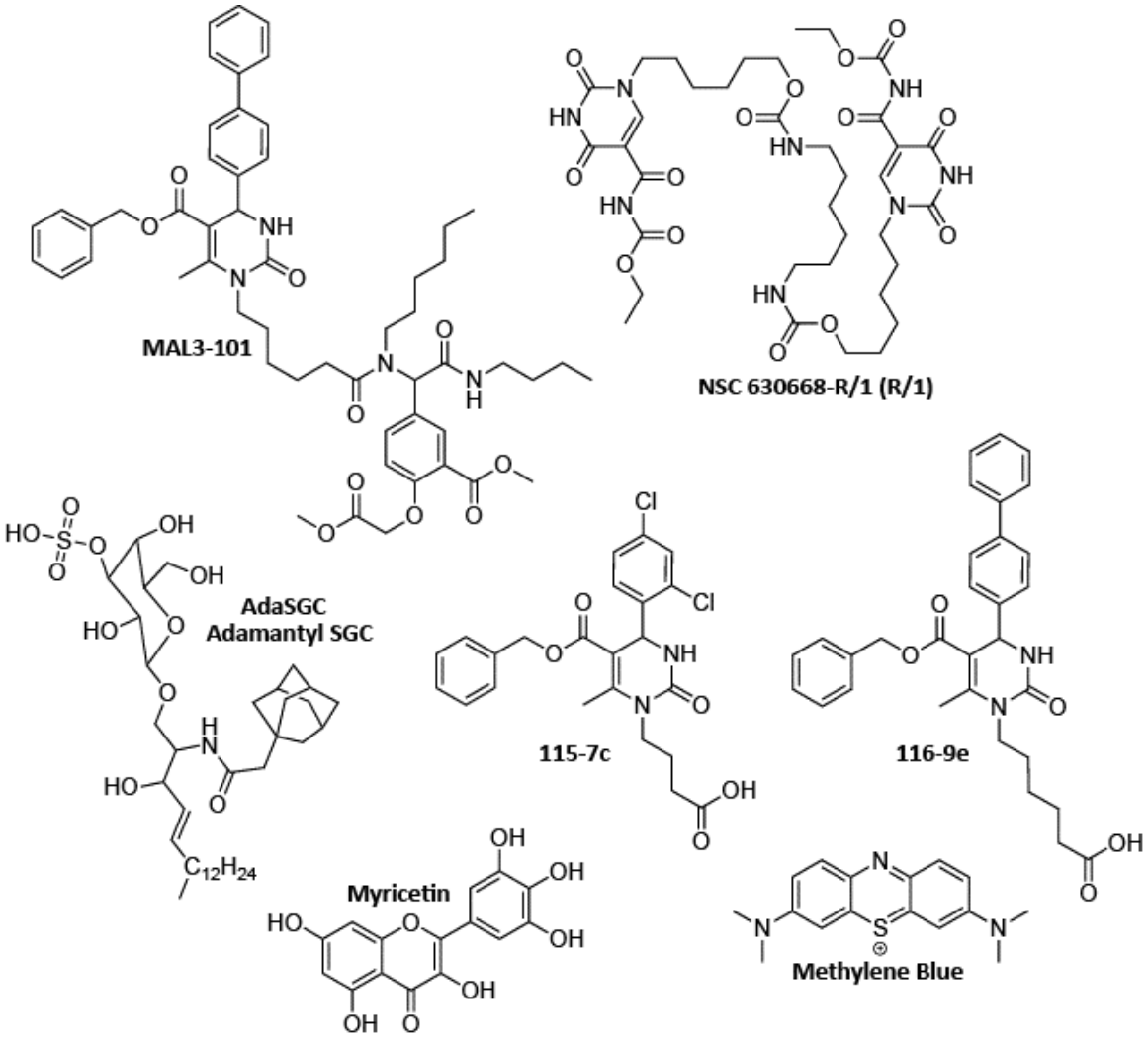

Figure 1.5 Structures of chemical modulators of the Hsp70-J protein interaction.

1.6.8 Dihydropyrimidines as chemical modulators of the J protein-Hsp70 complex

More recent HTS efforts have identified a broader range of compounds that specifically influence J protein-stimulated Hsp70 ATPase activity. For example, screening of a collection of dihydropyrimidines identified MAL3-101, which had no effect on intrinsic Hsp70 ATP turnover, but inhibited J protein-stimulated turnover [108]. Subsequent screening and structural studies confirmed this outcome and showed that the dihydropyrimidines bind to a region at the J protein-Hsp70 interface [109-111]. Moreover,

these studies also found that some dihydropyrimidines promote J protein activity, while others are inhibitory. For example, 115-7c is able to stimulate the ATPase activity of Hsp70 synergistically with DnaJ [109]. 115-7c binds better to the DnaJ-DnaK complex than DnaK alone. Additionally, nuclear magnetic resonance (NMR) studies found that 115-7c binds adjacent to the J domain binding site on DnaK. However, the related compound 116-9e, which (similar to MAL3-101) has a diphenyl substitution on the dihydropyrimidine ring (Figure 1.5), inhibits DnaJ stimulation of ATPase activity, without impacting NEF function [109]. Interestingly, MAL3-101 seems to discriminate between J proteins because it inhibits Ssa1 stimulation by SV40 large T Antigen (TAg), a viral J protein, but had less potent activity against the combination of Ssa1 and Ydj1. This finding suggests that it may be possible to achieve J protein specific inhibition even by targeting the J protein-Hsp70 interface. MAL3-101 was subsequently found to have potent anti-cancer effects in a multiple myeloma cell line and mouse model [112], while other dihydropyrimidines have been found to control the stability of other Hsp70 substrates, including tau, polyglutamine proteins, and Akt [52, 83, 113, 114]. This growing body of work suggests that targeting the Hsp70-J protein interface may be a productive approach for guiding Hsp70 functions. Importantly, these compounds are not generally cytotoxic and they do not activate a stress response [52, 113, 114], consistent with the idea that disrupting PPIs in the Hsp70 complex may be relatively well tolerated.

1.6.9 Allosteric inhibitors of the J protein-Hsp70 complex

Other chemical series also appear to have activity against the Hsp70-J protein interaction. Interestingly, some of these compounds have mechanisms different than the dihydropyrimidines. For example, a HTS effort against the DnaK-DnaJ pair identified the flavinoid myricetin (Figure 1.5), which inhibits DnaJ-stimulated ATPase and substrate binding activities, without affecting intrinsic or NEF stimulated activity [52, 115]. NMR revealed that myricetin binds the NBD in a region between the IB and IA subdomains, which is more than 20 Å away from the J domain binding site [115]. However, myricetin blocks binding of DnaJ to DnaK, suggesting that it acts across a long distance allosteric pathway. Additional HTS efforts have shown that methylene blue (MB) blocks J stimulation of ATP turnover *in vitro* (Figure 1.5). However, like myricetin, MB's effects in cells and animals are complex and it is likely to have targets other than Hsp70s [52, 83, 116]. Despite this complexity, MB and myricetin have clearly shown Hsp70-dependent effects on pathological substrates in cellular and animal models [52, 83, 117] and they reduce Akt levels in cancer cells [114]. Interestingly, these effects are blocked by co-administration of 115-7c, the dihydropyrimidine activator of J protein function [52], further suggesting that the Hsp70-J protein contact is critical. Finally, a larger HTS effort using more than 55,000 compounds identified zafirlukast as an inhibitor of the DnaK-DnaJ combination [118] and a screen of more than 300,000 compounds identified an inhibitor of TAg [119]. These efforts further illustrate that a screening strategy employing reconstituted chaperone complexes can be used to identify specific inhibitors of a PPI in the Hsp70 system.

The effects of small molecules on disease-relevant Hsp70 substrates are an initial indication that this is a promising avenue of investigation. However, J protein biology is complex and more work is needed to rationally refine these studies to focus on specific J protein-Hsp70 pairs. More specifically, if a discrete Hsp70-J protein pair can be clearly attributed to a distinct pathobiology, then HTS approaches might be employed to selectively disrupt (or even promote) the key PPIs.

1.7 Opportunities for drugging NEFs and their interactions with Hsp70

1.7.1 Human NEFs are unique in structure and function

NEFs provide another potential "handle" for targeting the Hsp70 chaperone complex. NEFs bind Hsp70 and help to facilitate the exchange of ADP for ATP. The biochemistry of the NEF family of co-chaperones has classically been investigated using the prokaryotic NEF, GrpE, as a model [120]. However, the eukaryotic cytosol does not contain a GrpE homolog. Rather, there are three main subclasses of human NEFs: Hsp110, HspBP1, and the BAG proteins, all of which are structurally distinct with little to no sequence homology. Consistent with their diverse structures, they also differ in their mode of binding to Hsp70s and their roles in guiding Hsp70 biology (Figure 1.6). For example, BAG2 is associated with proteasomal degradation of the Hsp70 substrate, tau, while BAG1-Hsp70 is linked to increased tau stability [121, 122]. These observations suggest that the formation of specific NEF-Hsp70 complexes may help decide the fate of Hsp70-bound substrates. Additionally, these findings illustrate that differential disruption of specific Hsp70-NEF contacts might be beneficial in disease. For example, members of the NEF family are differentially

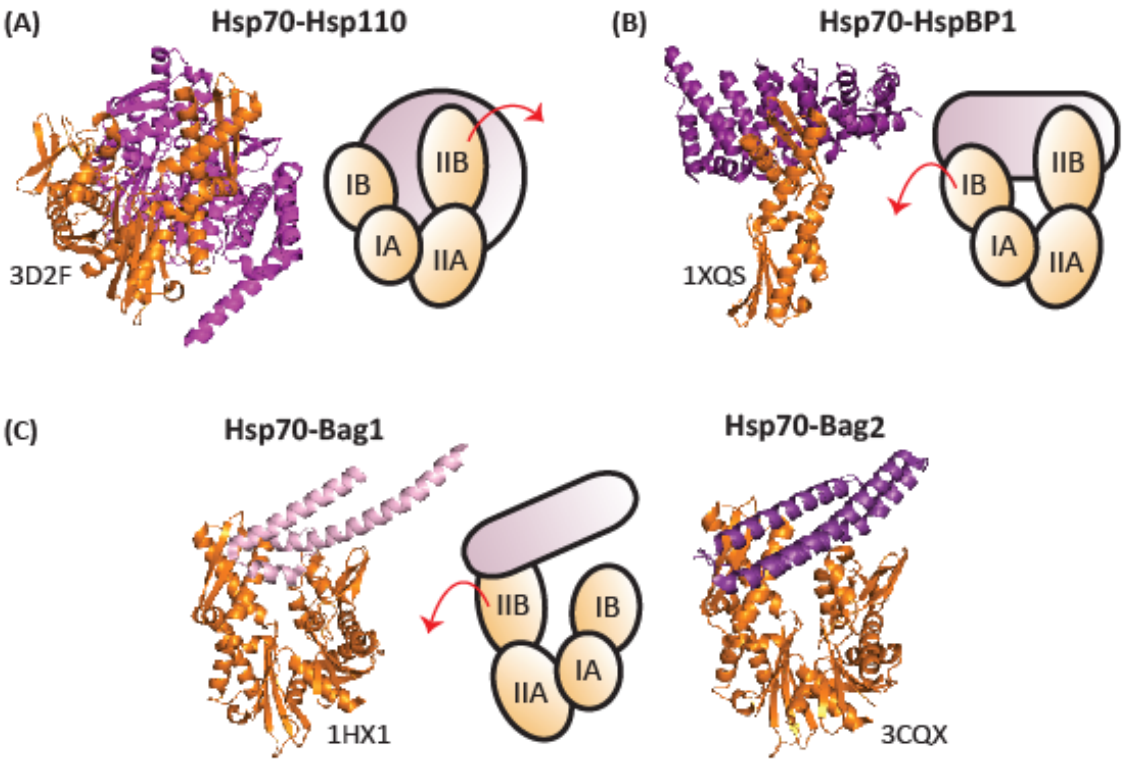

Figure 1.6 Structures of Hsp70-NEF complexes. (A) Crystal structure of yeast Hsp110, Sse1, and human Hsp70 NBD. Complex formation between Hsp70 and Hsp110 leads to a rotation in lobe IIB allowing nucleotide release. (B) Crystal structure of HspBP1 and lobe II of Hsp70's NBD. HspBP1 wraps around lobe IIB displacing lobe I and opening the nucleotide cleft. (C) Crystal structures of Hsp70 NBD in complex with the BAG domain of BAG1 and BAG2. Association between Hsp70 and the BAG proteins cause an outward rotation of lobe II, promoting nucleotide exchange. In all figures Hsp70 is colored in light orange and NEFs are colored in purple with PDB codes indicated. Images were prepared in PyMol.

expressed in multiple diseases, including cancer, Alzheimer's, cardiomyopathies, and ischemia [123-126], highlighting the rationale for developing chemical modulators of NEF-Hsp70.

1.7.2 Human Hsp110 has multiple isoforms

Hsp110 was originally observed and classified as a heat shock protein based on the appearance of a 110 kDa band in the lysates of Chinese Hamster Ovary cells upon heat shock [127]. In humans the major cytosolic Hsp110 protein is called Hsp105 (HSPH1).

Hsp105 has two major isoforms α and β [128]. Hsp105β results from alternative splicing at exon 12 and lacks 43 amino acids from its C-terminus. Recently, a mutant of Hsp110 that skips exon 9 and results in a truncated form of Hsp110, Hsp110ΔE9, has also been described [129]. This truncated Hsp110ΔE9 is able to act as a dominant negative mutant, abrogating Hsp110 chaperone activity and sensitizing cancer cells to chemotherapy treatments [129]. Since Hsp110 has been shown to protect cancer cells against apoptotic death [130], strategies to block its function or its interactions with Hsp70 could be promising cancer therapies.

1.7.3 Domain architecture and chaperone function of Hsp110

Hsp110 is a relative of the Hsp70 family of chaperones. Therefore, it has very similar domain architecture, with the main differences including a longer acidic loop region between the β-sandwich and α-helical lid of the SBD and a larger unstructured C-terminal extension [131, 132]. Despite the structural similarity, Hsp110 only functions as a holdase and has no ability to refold substrates without the help of the Hsp70 machinery [132-136]. Furthermore, while Hsp110 homologs bind nucleotide, this function seems to be dispensable for their NEF activity [137]. The crystal structure of the complex between Hsp70 and yeast Hsp110, Sse1, shows that the interaction covers a large surface area involving their respective NBDs [138, 139]. This interaction between Hsp70 and Hsp110 causes several rotations in Hsp70's NBD, especially in lobe IIB [140], allowing ADP release (Figure 1.6).

1.7.4 Strategies for targeting the Hsp110-Hsp70 interaction

The large buried surface area between Hsp70 and Hsp110 may make targeting this interaction difficult. The problem in PPI systems like this is that binding energy is often distributed across a large and complex topology, precluding easy inhibition by small (<500 Da) molecules. However, inhibiting PPIs with large surface areas is not unprecedented and compounds with potency values in the low nM range have been reported [141]. A common feature of previous successful strategies is that the small molecules tend to target so-called "hotspots" of the PPI, meaning the inhibitor binds in a region on one partner containing a small number of residues that are responsible for the majority of the binding strength [142, 143]. Thus, it will be important to identify residues that are critical to the Hsp70-NEF interaction. Another common feature of successful PPI inhibitors is that they bind in allosteric sites to impact the topology of protein-protein contact surfaces from a distance [143]. This approach lets the small molecule bind in a relatively concise pocket and impact larger surfaces to block PPIs. It seems likely that similar mechanisms will need to be employed to target the Hsp110-Hsp70 interaction.

1.7.5 The structure of HspBP1 and its interactions with Hsp70

Similar issues should be considered when designing inhibitors for the other major classes of NEFs. For example, HspBP1 is a 40 kDa protein that is composed of two structural domains, a largely unstructured N-terminal domain and a C-terminal domain that is mostly α-helical and is responsible for HspBP1 binding to Hsp70 [144]. This C-terminal region has been shown to be sufficient for eliciting Hsp70 nucleotide release [144, 145] and co-crystal

structures suggest that HspBP1's C-terminal domain interacts with lobe II of Hsp70's NBD (Figure 1.6) [145]. Importantly, this interaction is not the same as the PPI between Hsp70 and Hsp110, suggesting that this contact might be selectively inhibited. This goal might be attractive because of HspBP1's links to cancer and chemotherapy resistance [146].

1.7.6 The BAG family of NEFs and their interactions with Hsp70

Additional lessons about how to potentially target the Hsp70-NEF interaction are illustrated by the BAG family of co-chaperones, which includes BAG1-6. BAG proteins are defined by a characteristic C-terminal BAG domain that binds lobe IB and IIB of Hsp70's NBD and facilitates nucleotide release [147, 148]. This BAG domain typically consists of 110 to 124 amino acids and forms a three-helix bundle with the second and third helices providing the binding interface for Hsp70 [37, 149]. The association between the BAG domain and Hsp70 causes a 14° rotation in lobe II, which results in an opening of the nucleotide binding cleft and promotes ADP release (Figure 1.6) [37]. Interestingly, while all BAG proteins interact with Hsp70 through their conserved BAG domains, their N-terminal region is highly variable (Figure 1.7). This diversity is likely to be key for pathway specificity. BAG proteins may use these domains to determine the timing and location of nucleotide-dependent delivery of Hsp70-bound cargo.

One of the major questions in this field is whether the structural differences between the major NEF classes can be exploited to produce selective inhibitors of the various families. Similarly, can different members of the BAG family be individually targeted? Further, it is

not yet clear how many NEF functions are dependent on Hsp70 and how many are independent.

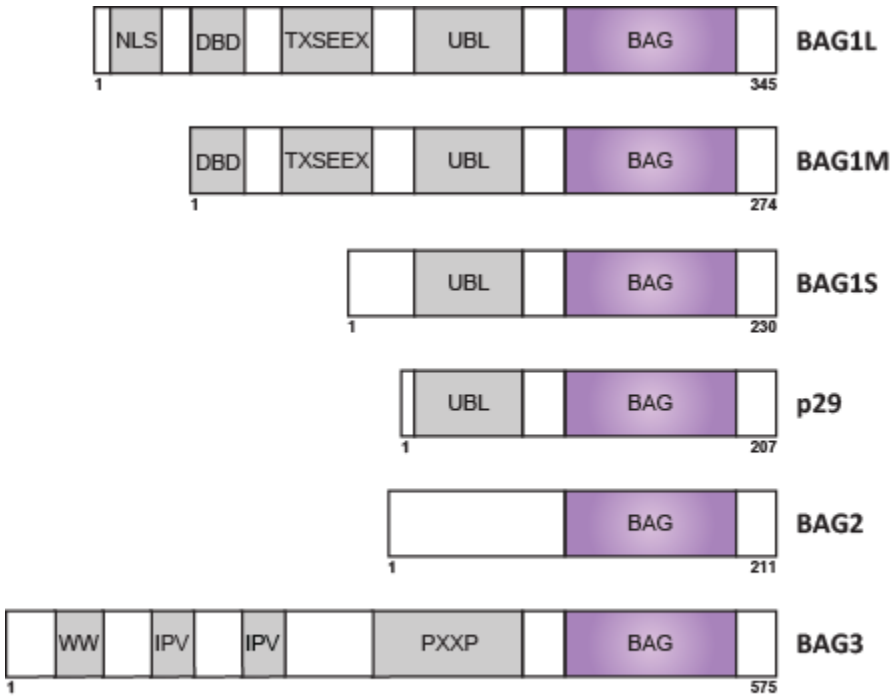

Figure 1.7 Domain architecture of BAG proteins. While all proteins share a C-terminal BAG domain, their N-termini are highly variable in composition and structure.

1.8 Opportunities for drugging TPR proteins and their interactions with Hsp70

1.8.1 The structure of TPR domains

Hsp70 also cooperates with a number of TPR domain-containing proteins. The TPR motif is defined by a degenerate 34 amino acid sequence that forms an amphipathic antiparallel α-helix [40, 150-153] and a TPR domain is typically assembled from 3 to 16 tandem TPR motifs. Although first identified in subunits of the anaphase promoting complex [154, 155], the TPR domain has since been found to be a common feature of PPs, including those between Hsp70 and its co-chaperones.

1.8.2 TPR co-chaperones have diverse cellular functions

Members of the family of TPR co-chaperones, as a whole, share little homology outside their TPR domains and they typically have regions involved in functions unrelated to Hsp70/Hsp90 binding [40, 150-153]. For example, the TPR co-chaperone CHIP (carboxyl terminus of Hsc70 interacting protein) is an ubiquitin E3 ligase with an effector Ubox domain [156]. This co-chaperone directs ubiquitination of Hsp70-bound substrates, marking them for proteasome-mediated degradation [157, 158]. In contrast, the TPR co-chaperone Hop (Hsp70/Hsp90 organizing protein) has three TPR domains: TPR1, TPR2A, and TPR2B. Of these domains, TPR1 and TPR2A mediate the association with Hsp70 and Hsp90, respectively [159, 160]. Thus, Hop facilitates the coordination of Hsp70 and Hsp90, ultimately allowing for the transfer of substrate between these two chaperone systems [161, 162]. This coordination allows Hop to play a central role in the folding of proteins, such as nuclear hormone receptors [163, 164]. Thus, when Hop and CHIP compete for binding to Hsp70 through their TPR domains, they establish a choice between two opposing fates: folding *vs.* degradation. These findings highlight the field's current model for combinatorial assembly of Hsp70 complexes, in which mutually exclusive binding of Hsp70 to specific co-chaperones dictates the fate of substrates [165-167]. Taken together, these features suggest that chaperone complexes may have the potential to be chemically modulated in order to "tune" the proteome.

1.8.3 TPR co-chaperones bind to the C-terminal EEVD of Hsp70/90

TPR co-chaperones interact with the disordered C-terminus of Hsp70. Mutagenesis studies [160, 168, 169] and co-crystal structures of the TPR domains of Hop and CHIP with Hsp70 C-terminal peptides [159, 170] illustrate the importance of the C-terminal EEVD amino acids in mediating these PPIs [168, 171]. Based on these findings, the EEVD motif of Hsp70 has been generalized as the minimal binding site for TPR co-chaperones. This motif is also present in the extreme C-terminus of the evolutionarily unrelated molecular chaperone Hsp90, but not in the prokaryotic DnaK, mitochondrial or ER-resident Hsp70 homologs. These observations highlight the role of the EEVD motif as a recruitment element that anchors TPR co-chaperones to the cytoplasmic Hsp70 and Hsp90 chaperone systems. However, there is not much known about how TPR co-chaperones "compete" for binding to Hsp70. Thus, compounds that block the EEVD-TPR interaction might be exciting probes for understanding chaperone biology and these compounds may serve as leads for drug discovery. This possibility will be the subject of my thesis work in chapter 2.

The importance of EEVD-TPR domain contacts in facilitating PPIs between Hsp70/90 and TPR co-chaperones is well appreciated within the chaperone field. However, much less attention has been paid to interaction surfaces outside this canonical binding site. Immunoprecipitation experiments as well as *in vitro* binding studies performed on the Hsp70-Hop complex, demonstrate that binding involves secondary contacts outside the EEVD motif [160, 172]. Recent structural work illustrates that the TPR domain of CHIP engages with both the lid of Hsp70's SBD and the EEVD motif. NMR binding studies indicate that these secondary lid contacts are very weak (K_D >100 uM) [173]. Additionally,

sequences outside of the TPR domain of Hop, CHIP, and other TPR co-chaperones cause differential binding to Hsp90 mutants [174, 175]. Together, these findings suggest that interactions between TPR proteins and Hsp70 are more complex than the minimal TPR-EEVD interactions. Thus, many key fundamental questions remain unanswered: What are the molecular interactions between Hsp70 and TPR co-chaperones? Do these interactions differ among TPR co-chaperones? What molecular events influence the choice to bind one TPR protein over another? Because TPR co-chaperone structures are divergent in nature, additional contacts outside the EEVD-TPR binding site may provide an avenue for the development of chemical probes that can modulate specific TPR-chaperone interactions. Such compounds would be useful in further dissecting the complex mechanisms of Hsp70 and individual TPR co-chaperones in protein quality control.

1.8.4 Small molecule inhibitors of Hsp70/90-TPR co-chaperone complexes

The development of small molecule modulators of Hsp70-TPR complexes is still in its infancy. However, in the Hsp90 system, Yi and co-workers have targeted the TPR domain of Hop and identified pyrimidotriazinediones as inhibitors of that PPI [176]. Additionally, derivatives of the natural product sansalvamide A have been shown to modulate Hsp90 interactions with TPR co-chaperones [177, 178]. Taken together, this work suggests that the Hsp70-TPR interactions may also be amenable to inhibition. However, further studies are still needed because the binding sites and mechanisms of these molecules are not yet clear. Compared to the other PPIs (*e.g*. J proteins and NEFs), the interactions between TPR domains and Hsp70s are relatively more concise, which might accelerate discovery in that

area. The challenges will be in understanding how to engender selectivity and guide the "choice" of TPR partner.

There are compelling reasons to target the PPIs between Hsp70 and its co-chaperones. These contacts help shape Hsp70 activities and, as such, they might be targeted to redirect the protein quality control system. Molecules that disrupt the assembly and disassembly of the Hsp70 complex might supplement other types of Hsp70 inhibitors, such as competitive inhibitors of ATP and substrate binding, providing a more complete suite of chemical probes and potential therapeutics. However, the number of PPIs in the Hsp70 complex means that there are a large number of contacts yet to be explored.

1.9 Analysis and prospectus

1.9.1 Assays are needed for characterizing chemical modulators of Hsp70 complexes

PPIs are notoriously difficult to inhibit and the specific interactions involved in binding to Hsp70 are particularly challenging, given their large buried surface areas. What strategies might be used to disrupt these contacts? Based on growing evidence from other PPI inhibitor discovery programs [22-24], it seems likely that compounds that are able to bind to allosteric sites might be in the best position to target the types of PPIs in the Hsp70 system. Another key tool will likely be the development of HTS platforms that are specifically suited to finding inhibitors of PPIs. Recent developments in this area include AlphaLISA, flow cytometry protein interaction assay (FCPIA), and gray box screening [115, 118]. These assay platforms might lower the barrier to uncovering suitable compounds.

Also, the creation of chemical libraries enriched for more complex small molecules (natural product-like) may further accelerate discovery in this area [179]. A clever combination of these methods might overcome the challenges associated with targeting the Hsp70 complex.

1.9.2 Targeting Hsp70 multi-protein complexes could have global effects on the proteome

One major question that looms large over this field is how the global proteome will respond to inhibitors of Hsp70 (both orthostatic and allosteric). This concept has not been rigorously tested and it remains uncertain how cells will respond to different types of Hsp70 inhibitors. What will happen to protein stability and turnover when Hsp70 function is blocked or even "tuned"? The answers to this question may depend on how the molecule works (*e.g.* competitive inhibitor of ATP binding, allosteric inhibitor of J proteins, *etc.*) and whether it is selective for specific Hsp70 paralogs. It seems likely that the only way to address these significant concerns is to develop potent inhibitors and then use them to develop empirical models.

1.9.3 Thesis outline

In this thesis, I first characterize Hsp70-TPR domain-containing co-chaperone interactions with the goal of understanding whether these PPIs might serve as good drug targets (chapter 2). Then, I study how allostery within the Hsp70 system translates to effects on co-chaperone binding, revealing an interesting control network in the NBD (chapter 3). Finally, I apply that knowledge of Hsp70 co-chaperone dynamics to a translational

objective, identifying potent new antibiotics that target the bacterial DnaK system (chapter 4). The impact of these new findings and their implications for future work are discussed in chapter 5.

Notes

Portions of this chapter were published as “Hsp70 Protein complexes as drug targets” 2013 *Current Pharmaceutical Design*, 19(3), 404-17. Victoria A. Assimon, Anne T. Gillies, Jennifer N. Rauch, and Jason E. Gestwicki contributed to this review.

1.10 References

1. Mayer, M.P. and B. Bukau, *Hsp70 chaperones: cellular functions and molecular mechanism.* Cell Mol Life Sci, 2005. **62**(6): p. 670-84.
2. Bukau, B., J. Weissman, and A. Horwich, *Molecular chaperones and protein quality control.* Cell, 2006. **125**(3): p. 443-51.
3. Frydman, J., *Folding of newly translated proteins in vivo: the role of molecular chaperones.* Annu Rev Biochem, 2001. **70**: p. 603-47.
4. Hartl, F.U., A. Bracher, and M. Hayer-Hartl, *Molecular chaperones in protein folding and proteostasis.* Nature, 2011. **475**(7356): p. 324-32.
5. Bercovich, B., et al., *Ubiquitin-dependent degradation of certain protein substrates in vitro requires the molecular chaperone Hsc70.* J Biol Chem, 1997. **272**(14): p. 9002-10.
6. Arndt, V., C. Rogon, and J. Hohfeld, *To be, or not to be--molecular chaperones in protein degradation.* Cell Mol Life Sci, 2007. **64**(19-20): p. 2525-41.
7. Kettern, N., et al., *Chaperone-assisted degradation: multiple paths to destruction.* Biol Chem, 2010. **391**(5): p. 481-9.
8. Pratt, W.B. and D.O. Toft, *Regulation of signaling protein function and trafficking by the hsp90/hsp70-based chaperone machinery.* Exp Biol Med (Maywood), 2003. **228**(2): p. 111-33.
9. Gamer, J., H. Bujard, and B. Bukau, *Physical interaction between heat shock proteins DnaK, DnaJ, and GrpE and the bacterial heat shock transcription factor sigma 32.* Cell, 1992. **69**(5): p. 833-42.
10. Rodriguez, F., et al., *Molecular basis for regulation of the heat shock transcription factor sigma32 by the DnaK and DnaJ chaperones.* Mol Cell, 2008. **32**(3): p. 347-58.
11. Tyedmers, J., A. Mogk, and B. Bukau, *Cellular strategies for controlling protein aggregation.* Nat Rev Mol Cell Biol, 2010. **11**(11): p. 777-88.
12. Daugaard, M., M. Rohde, and M. Jaattela, *The heat shock protein 70 family: Highly homologous proteins with overlapping and distinct functions.* FEBS Lett, 2007. **581**(19): p. 3702-10.
13. Brocchieri, L., E. Conway de Macario, and A.J. Macario, *hsp70 genes in the human genome: Conservation and differentiation patterns predict a wide array of overlapping and specialized functions.* BMC Evol Biol, 2008. **8**: p. 19.
14. Hohfeld, J., D.M. Cyr, and C. Patterson, *From the cradle to the grave: molecular chaperones that may choose between folding and degradation.* EMBO Rep, 2001. **2**(10): p. 885-90.
15. Meimaridou, E., S.B. Gooljar, and J.P. Chapple, *From hatching to dispatching: the multiple cellular roles of the Hsp70 molecular chaperone machinery.* J Mol Endocrinol, 2009. **42**(1): p. 1-9.
16. Broadley, S.A. and F.U. Hartl, *The role of molecular chaperones in human misfolding diseases.* FEBS Lett, 2009. **583**(16): p. 2647-53.
17. Mosser, D.D. and R.I. Morimoto, *Molecular chaperones and the stress of oncogenesis.* Oncogene, 2004. **23**(16): p. 2907-18.

18. Otvos, L., et al., *Interaction between heat shock proteins and antimicrobial peptides.* Biochemistry, 2000. **39**(46): p. 14150-14159.
19. Evans, C.G., L. Chang, and J.E. Gestwicki, *Heat shock protein 70 (hsp70) as an emerging drug target.* J Med Chem, 2010. **53**(12): p. 4585-602.
20. Brodsky, J.L. and G. Chiosis, *Hsp70 molecular chaperones: emerging roles in human disease and identification of small molecule modulators.* Curr Top Med Chem, 2006. **6**(11): p. 1215-25.
21. Patury, S., Y. Miyata, and J.E. Gestwicki, *Pharmacological targeting of the Hsp70 chaperone.* Curr Top Med Chem, 2009. **9**(15): p. 1337-51.
22. Gestwicki, J.E. and P.S. Marinec, *Chemical control over protein-protein interactions: beyond inhibitors.* Comb Chem High Throughput Screen, 2007. **10**(8): p. 667-75.
23. Berg, T., *Modulation of protein-protein interactions with small organic molecules.* Angew Chem Int Ed Engl, 2003. **42**(22): p. 2462-81.
24. Arkin, M.R. and J.A. Wells, *Small-molecule inhibitors of protein-protein interactions: progressing towards the dream.* Nat Rev Drug Discov, 2004. **3**(4): p. 301-17.
25. Bertelsen, E.B., et al., *Solution conformation of wild-type E. coli Hsp70 (DnaK) chaperone complexed with ADP and substrate.* Proc Natl Acad Sci U S A, 2009. **106**(21): p. 8471-6.
26. Zhuravleva, A. and L.M. Gierasch, *Allosteric signal transmission in the nucleotide-binding domain of 70-kDa heat shock protein (Hsp70) molecular chaperones.* Proceedings of the National Academy of Sciences of the United States of America, 2011. **108**(17): p. 6987-6992.
27. Kityk, R., et al., *Structure and Dynamics of the ATP-Bound Open Conformation of Hsp70 Chaperones.* Molecular Cell, 2012. **48**(6): p. 863-874.
28. Bork, P., C. Sander, and A. Valencia, *An ATPase domain common to prokaryotic cell cycle proteins, sugar kinases, actin, and hsp70 heat shock proteins.* Proc Natl Acad Sci U S A, 1992. **89**(16): p. 7290-4.
29. Wang, H., et al., *NMR solution structure of the 21 kDa chaperone protein DnaK substrate binding domain: a preview of chaperone-protein interaction.* Biochemistry, 1998. **37**(22): p. 7929-40.
30. Zhu, X., et al., *Structural analysis of substrate binding by the molecular chaperone DnaK.* Science, 1996. **272**(5268): p. 1606-14.
31. Young, J.C., J.M. Barral, and F. Ulrich Hartl, *More than folding: localized functions of cytosolic chaperones.* Trends Biochem Sci, 2003. **28**(10): p. 541-7.
32. Gaestel, M., *Molecular chaperones in signal transduction.* Handb Exp Pharmacol, 2006(172): p. 93-109.
33. Mayer, M.P., et al., *Multistep mechanism of substrate binding determines chaperone activity of Hsp70.* Nat Struct Biol, 2000. **7**(7): p. 586-93.
34. Vogel, M., M.P. Mayer, and B. Bukau, *Allosteric regulation of Hsp70 chaperones involves a conserved interdomain linker.* J Biol Chem, 2006. **281**(50): p. 38705-11.
35. Chang, L., et al., *Mutagenesis reveals the complex relationships between ATPase rate and the chaperone activities of Escherichia coli heat shock protein 70 (Hsp70/DnaK).* J Biol Chem, 2010. **285**(28): p. 21282-91.

36. Ahmad, A., et al., *Heat shock protein 70 kDa chaperone/DnaJ cochaperone complex employs an unusual dynamic interface.* Proc Natl Acad Sci U S A, 2011. **108**(47): p. 18966-71.
37. Sondermann, H., et al., *Structure of a Bag/Hsc70 complex: convergent functional evolution of Hsp70 nucleotide exchange factors.* Science, 2001. **291**(5508): p. 1553-7.
38. Liu, F.H., et al., *Specific interaction of the 70-kDa heat shock cognate protein with the tetratricopeptide repeats.* J Biol Chem, 1999. **274**(48): p. 34425-32.
39. Whitesell, L. and S.L. Lindquist, *HSP90 and the chaperoning of cancer.* Nature Reviews Cancer, 2005. **5**(10): p. 761-772.
40. Allan, R.K. and T. Ratajczak, *Versatile TPR domains accommodate different modes of target protein recognition and function.* Cell Stress & Chaperones, 2011. **16**(4): p. 353-367.
41. Borges, J.C. and C.H.I. Ramos, *Spectroscopic and thermodynamic measurements of nucleotide-induced changes in the human 70-kDa heat shock cognate protein.* Archives of Biochemistry and Biophysics, 2006. **452**(1): p. 46-54.
42. Williamson, D.S., et al., *Novel Adenosine-Derived Inhibitors of 70 kDa Heat Shock Protein, Discovered Through Structure-Based Design.* Journal of Medicinal Chemistry, 2009. **52**(6): p. 1510-1513.
43. Massey, A.J., *ATPases as drug targets: insights from heat shock proteins 70 and 90.* J Med Chem, 2010. **53**(20): p. 7280-6.
44. Massey, A.J., et al., *A novel, small molecule inhibitor of Hsc70/Hsp70 potentiates Hsp90 inhibitor induced apoptosis in HCT116 colon carcinoma cells.* Cancer Chemother Pharmacol, 2011. **66**(3): p. 535-45.
45. Macias, A.T., et al., *Adenosine-derived inhibitors of 78 kDa glucose regulated protein (Grp78) ATPase: insights into isoform selectivity.* J Med Chem, 2010. **54**(12): p. 4034-41.
46. Williams, D.R., et al., *An apoptosis-inducing small molecule that binds to heat shock protein 70.* Angewandte Chemie-International Edition, 2008. **47**(39): p. 7466-7469.
47. Cho, H.J., et al., *A Small Molecule That Binds to an ATPase Domain of Hsc70 Promotes Membrane Trafficking of Mutant Cystic Fibrosis Transmembrane Conductance Regulator.* Journal of the American Chemical Society, 2011. **133**(50): p. 20267-20276.
48. Kragol, G., et al., *The antibacterial peptide pyrrhocoricin inhibits the ATPase actions of DnaK and prevents chaperone-assisted protein folding.* Biochemistry, 2001. **40**(10): p. 3016-3026.
49. Rerole, A.L., et al., *Peptides and aptamers targeting HSP70: a novel approach for anticancer chemotherapy.* Cancer Res, 2011. **71**(2): p. 484-95.
50. Rerole, A.L., G. Jego, and C. Garrido, *Hsp70: anti-apoptotic and tumorigenic protein.* Methods Mol Biol, 2011. **787**: p. 205-30.
51. Williams, D.R., et al., *An apoptosis-inducing small molecule that binds to heat shock protein 70.* Angew Chem Int Ed Engl, 2008. **47**(39): p. 7466-9.
52. Jinwal, U.K., et al., *Chemical manipulation of hsp70 ATPase activity regulates tau stability.* J Neurosci, 2009. **29**(39): p. 12079-88.

53. Cellitti, J., et al., *Small molecule DnaK modulators targeting the beta-domain.* Chem Biol Drug Des, 2009. **74**(4): p. 349-57.
54. Hassan, A.Q., et al., *The Novolactone Natural Product Disrupts the Allosteric Regulation of Hsp70.* Chemistry & Biology, 2015. **22**(1): p. 87-97.
55. Rodina, A., et al., *Identification of an Allosteric Pocket on Human Hsp70 Reveals a Mode of Inhibition of This Therapeutically Important Protein.* Chemistry & Biology, 2013. **20**(12): p. 1469-1480.
56. Taldone, T., et al., *Heat Shock Protein 70 Inhibitors. 2. 2,5 '-Thiodipyrimidines, 5-(Phenylthio)pyrimidines, 2-(Pyridin-3-ylthio)pyrimidines, and 3-(Phenylthio)pyridines as Reversible Binders to an Allosteric Site on Heat Shock Protein 70.* Journal of Medicinal Chemistry, 2014. **57**(4): p. 1208-1224.
57. Rodina, A., et al., *Affinity Purification Probes of Potential Use To Investigate the Endogenous Hsp70 Interactome in Cancer.* Acs Chemical Biology, 2014. **9**(8): p. 1698-1705.
58. Howe, M.K., et al., *Identification of an Allosteric Small-Molecule Inhibitor Selective for the Inducible Form of Heat Shock Protein 70.* Chemistry & Biology, 2014. **21**(12): p. 1648-1659.
59. Daguer, J.P., et al., *DNA display of fragment pairs as a tool for the discovery of novel biologically active small molecules.* Chemical Science, 2015. **6**(1): p. 739-744.
60. Qiu, X.B., et al., *The diversity of the DnaJ/Hsp40 family, the crucial partners for Hsp70 chaperones.* Cell Mol Life Sci, 2006. **63**(22): p. 2560-70.
61. Kampinga, H.H., et al., *Guidelines for the nomenclature of the human heat shock proteins.* Cell Stress Chaperones, 2009. **14**(1): p. 105-11.
62. Caplan, A.J., D.M. Cyr, and M.G. Douglas, *YDJ1p facilitates polypeptide translocation across different intracellular membranes by a conserved mechanism.* Cell, 1992. **71**(7): p. 1143-55.
63. Hageman, J., et al., *The diverse members of the mammalian HSP70 machine show distinct chaperone-like activities.* Biochem J, 2011. **435**(1): p. 127-42.
64. Sterrenberg, J.N., G.L. Blatch, and A.L. Edkins, *Human DNAJ in cancer and stem cells.* Cancer Lett, 2011. **312**(2): p. 129-42.
65. Kalia, S.K., L.V. Kalia, and P.J. McLean, *Molecular chaperones as rational drug targets for Parkinson's disease therapeutics.* CNS Neurol Disord Drug Targets, 2010. **9**(6): p. 741-53.
66. Mitra, A., L.A. Shevde, and R.S. Samant, *Multi-faceted role of HSP40 in cancer.* Clin Exp Metastasis, 2009. **26**(6): p. 559-67.
67. Harms, M.B., et al., *Exome sequencing reveals DNAJB6 mutations in dominantly-inherited myopathy.* Ann Neurol, 2012. **71**(3): p. 407-16.
68. Knox, C., et al., *Heat shock protein 40 (Hsp40) plays a key role in the virus life cycle.* Virus Res, 2011. **160**(1-2): p. 15-24.
69. Langer, T., et al., *Successive action of DnaK, DnaJ and GroEL along the pathway of chaperone-mediated protein folding.* Nature, 1992. **356**(6371): p. 683-9.
70. Wall, D., M. Zylicz, and C. Georgopoulos, *The conserved G/F motif of the DnaJ chaperone is necessary for the activation of the substrate binding properties of the DnaK chaperone.* J Biol Chem, 1995. **270**(5): p. 2139-44.

71. Szabo, A., et al., *The ATP hydrolysis-dependent reaction cycle of the Escherichia coli Hsp70 system DnaK, DnaJ, and GrpE.* Proc Natl Acad Sci U S A, 1994. **91**(22): p. 10345-9.
72. Greene, M.K., K. Maskos, and S.J. Landry, *Role of the J-domain in the cooperation of Hsp40 with Hsp70.* Proc Natl Acad Sci U S A, 1998. **95**(11): p. 6108-13.
73. Gassler, C.S., et al., *Mutations in the DnaK chaperone affecting interaction with the DnaJ cochaperone.* Proc Natl Acad Sci U S A, 1998. **95**(26): p. 15229-34.
74. Suh, W.C., et al., *Interaction of the Hsp70 molecular chaperone, DnaK, with its cochaperone DnaJ.* Proc Natl Acad Sci U S A, 1998. **95**(26): p. 15223-8.
75. Hennessy, F., et al., *Not all J domains are created equal: implications for the specificity of Hsp40-Hsp70 interactions.* Protein Sci, 2005. **14**(7): p. 1697-709.
76. Awad, W., et al., *BiP mutants that are unable to interact with endoplasmic reticulum DnaJ proteins provide insights into interdomain interactions in BiP.* Proc Natl Acad Sci U S A, 2008. **105**(4): p. 1164-9.
77. Vembar, S.S., et al., *J domain co-chaperone specificity defines the role of BiP during protein translocation.* J Biol Chem, 2010. **285**(29): p. 22484-94.
78. Cheetham, M.E. and A.J. Caplan, *Structure, function and evolution of DnaJ: conservation and adaptation of chaperone function.* Cell Stress Chaperones, 1998. **3**(1): p. 28-36.
79. Kampinga, H.H. and E.A. Craig, *The HSP70 chaperone machinery: J proteins as drivers of functional specificity.* Nat Rev Mol Cell Biol, 2010. **11**(8): p. 579-92.
80. Holstein, S.E., H. Ungewickell, and E. Ungewickell, *Mechanism of clathrin basket dissociation: separate functions of protein domains of the DnaJ homologue auxilin.* J Cell Biol, 1996. **135**(4): p. 925-37.
81. Xing, Y., et al., *Structure of clathrin coat with bound Hsc70 and auxilin: mechanism of Hsc70-facilitated disassembly.* EMBO J, 2010. **29**(3): p. 655-65.
82. Bocking, T., et al., *Single-molecule analysis of a molecular disassemblase reveals the mechanism of Hsc70-driven clathrin uncoating.* Nat Struct Mol Biol, 2011. **18**(3): p. 295-301.
83. Wang, A.M., et al., *Inhibition of hsp70 by methylene blue affects signaling protein function and ubiquitination and modulates polyglutamine protein degradation.* J Biol Chem, 2010. **285**(21): p. 15714-23.
84. Nakanishi, K., et al., *Localization and function in endoplasmic reticulum stress tolerance of ERdj3, a new member of Hsp40 family protein.* Cell Stress Chaperones, 2004. **9**(3): p. 253-64.
85. Shen, Y. and L.M. Hendershot, *ERdj3, a stress-inducible endoplasmic reticulum DnaJ homologue, serves as a cofactor for BiP's interactions with unfolded substrates.* Mol Biol Cell, 2005. **16**(1): p. 40-50.
86. Fan, C.Y., et al., *Exchangeable chaperone modules contribute to specification of type I and type II Hsp40 cellular function.* Mol Biol Cell, 2004. **15**(2): p. 761-73.
87. Lu, Z. and D.M. Cyr, *The conserved carboxyl terminus and zinc finger-like domain of the co-chaperone Ydj1 assist Hsp70 in protein folding.* J Biol Chem, 1998. **273**(10): p. 5970-8.

88. Lee, S., et al., *Identification of essential residues in the type II Hsp40 Sis1 that function in polypeptide binding.* J Biol Chem, 2002. **277**(24): p. 21675-82.
89. Rudiger, S., J. Schneider-Mergener, and B. Bukau, *Its substrate specificity characterizes the DnaJ co-chaperone as a scanning factor for the DnaK chaperone.* EMBO J, 2001. **20**(5): p. 1042-50.
90. Feifel, B., H.J. Schonfeld, and P. Christen, *D-peptide ligands for the co-chaperone DnaJ.* J Biol Chem, 1998. **273**(20): p. 11999-2002.
91. Li, J., X. Qian, and B. Sha, *The crystal structure of the yeast Hsp40 Ydj1 complexed with its peptide substrate.* Structure, 2003. **11**(12): p. 1475-83.
92. Arawaka, S., Y. Machiya, and T. Kato, *Heat shock proteins as suppressors of accumulation of toxic prefibrillar intermediates and misfolded proteins in neurodegenerative diseases.* Curr Pharm Biotechnol, 2010. **11**(2): p. 158-66.
93. Jana, N.R., et al., *Polyglutamine length-dependent interaction of Hsp40 and Hsp70 family chaperones with truncated N-terminal huntingtin: their role in suppression of aggregation and cellular toxicity.* Hum Mol Genet, 2000. **9**(13): p. 2009-18.
94. Zhou, H., S.H. Li, and X.J. Li, *Chaperone suppression of cellular toxicity of huntingtin is independent of polyglutamine aggregation.* J Biol Chem, 2001. **276**(51): p. 48417-24.
95. Chuang, J.Z., et al., *Characterization of a brain-enriched chaperone, MRJ, that inhibits Huntingtin aggregation and toxicity independently.* J Biol Chem, 2002. **277**(22): p. 19831-8.
96. Hay, D.G., et al., *Progressive decrease in chaperone protein levels in a mouse model of Huntington's disease and induction of stress proteins as a therapeutic approach.* Hum Mol Genet, 2004. **13**(13): p. 1389-405.
97. Wyttenbach, A., et al., *Effects of heat shock, heat shock protein 40 (HDJ-2), and proteasome inhibition on protein aggregation in cellular models of Huntington's disease.* Proc Natl Acad Sci U S A, 2000. **97**(6): p. 2898-903.
98. Miyata, Y., et al., *Molecular chaperones and regulation of tau quality control: strategies for drug discovery in tauopathies.* Future Med Chem, 2011. **3**(12): p. 1523-37.
99. Sahara, N., et al., *Molecular chaperone-mediated tau protein metabolism counteracts the formation of granular tau oligomers in human brain.* J Neurosci Res, 2007. **85**(14): p. 3098-108.
100. Abisambra, J.F., et al., *DnaJA1 Antagonizes Constitutive Hsp70-Mediated Stabilization of Tau.* J Mol Biol, 2012.
101. Nadler, S.G., et al., *Interaction of the immunosuppressant deoxyspergualin with a member of the Hsp70 family of heat shock proteins.* Science, 1992. **258**(5081): p. 484-6.
102. Brodsky, J.L., *Selectivity of the molecular chaperone-specific immunosuppressive agent 15-deoxyspergualin: modulation of Hsc70 ATPase activity without compromising DnaJ chaperone interactions.* Biochem Pharmacol, 1999. **57**(8): p. 877-80.

103. Nadeau, K., et al., *Quantitation of the interaction of the immunosuppressant deoxyspergualin and analogs with Hsc70 and Hsp90.* Biochemistry, 1994. **33**(9): p. 2561-7.
104. Fewell, S.W., B.W. Day, and J.L. Brodsky, *Identification of an inhibitor of hsc70-mediated protein translocation and ATP hydrolysis.* J Biol Chem, 2001. **276**(2): p. 910-4.
105. Mamelak, D., et al., *Hsp70s contain a specific sulfogalactolipid binding site. Differential aglycone influence on sulfogalactosyl ceramide binding by recombinant prokaryotic and eukaryotic hsp70 family members.* Biochemistry, 2001. **40**(12): p. 3572-82.
106. Mamelak, D. and C. Lingwood, *The ATPase domain of hsp70 possesses a unique binding specificity for 3'-sulfogalactolipids.* J Biol Chem, 2001. **276**(1): p. 449-56.
107. Park, H.J., et al., *A soluble sulfogalactosyl ceramide mimic promotes Delta F508 CFTR escape from endoplasmic reticulum associated degradation.* Chem Biol, 2009. **16**(4): p. 461-70.
108. Fewell, S.W., et al., *Small molecule modulators of endogenous and co-chaperone-stimulated Hsp70 ATPase activity.* J Biol Chem, 2004. **279**(49): p. 51131-40.
109. Wisen, S., et al., *Binding of a small molecule at a protein-protein interface regulates the chaperone activity of hsp70-hsp40.* ACS Chem Biol, 2010. **5**(6): p. 611-22.
110. Chang, L., et al., *High-throughput screen for small molecules that modulate the ATPase activity of the molecular chaperone DnaK.* Anal Biochem, 2008. **372**(2): p. 167-76.
111. Wisen, S., et al., *Chemical modulators of heat shock protein 70 (Hsp70) by sequential, microwave-accelerated reactions on solid phase.* Bioorg Med Chem Lett, 2008. **18**(1): p. 60-5.
112. Braunstein, M.J., et al., *Antimyeloma Effects of the Heat Shock Protein 70 Molecular Chaperone Inhibitor MAL3-101.* J Oncol, 2011. **2011**: p. 232037.
113. Walter, G.M., et al., *Ordered assembly of heat shock proteins, Hsp26, Hsp70, Hsp90, and Hsp104, on expanded polyglutamine fragments revealed by chemical probes.* J Biol Chem, 2011. **286**(47): p. 40486-93.
114. Koren, J., 3rd, et al., *Facilitating Akt clearance via manipulation of Hsp70 activity and levels.* J Biol Chem, 2010. **285**(4): p. 2498-505.
115. Chang, L., et al., *Chemical screens against a reconstituted multiprotein complex: myricetin blocks DnaJ regulation of DnaK through an allosteric mechanism.* Chem Biol, 2011. **18**(2): p. 210-21.
116. Congdon, E.E., et al., *Methylthioninium chloride (methylene blue) induces autophagy and attenuates tauopathy in vitro and in vivo.* Autophagy, 2012. **8**(4).
117. O'Leary, J.C., 3rd, et al., *Phenothiazine-mediated rescue of cognition in tau transgenic mice requires neuroprotection and reduced soluble tau burden.* Mol Neurodegener, 2010. **5**: p. 45.
118. Miyata, Y., et al., *High-throughput screen for Escherichia coli heat shock protein 70 (Hsp70/DnaK): ATPase assay in low volume by exploiting energy transfer.* J Biomol Screen, 2010. **15**(10): p. 1211-9.

119. Seguin, S.P., et al., *High-throughput screening identifies a bisphenol inhibitor of SV40 large T antigen ATPase activity.* J Biomol Screen, 2012. **17**(2): p. 194-203.
120. Harrison, C., *GrpE, a nucleotide exchange factor for DnaK.* Cell Stress Chaperones, 2003. **8**(3): p. 218-24.
121. Carrettiero, D.C., et al., *The cochaperone BAG2 sweeps paired helical filament-insoluble tau from the microtubule.* J Neurosci, 2009. **29**(7): p. 2151-61.
122. Elliott, E., P. Tsvetkov, and I. Ginzburg, *BAG-1 associates with Hsc70.Tau complex and regulates the proteasomal degradation of Tau protein.* J Biol Chem, 2007. **282**(51): p. 37276-84.
123. Souza, A.P., et al., *HspBP1 levels are elevated in breast tumor tissue and inversely related to tumor aggressiveness.* Cell Stress Chaperones, 2009. **14**(3): p. 301-10.
124. Elliott, E., O. Laufer, and I. Ginzburg, *BAG-1M is up-regulated in hippocampus of Alzheimer's disease patients and associates with tau and APP proteins.* J Neurochem, 2009. **109**(4): p. 1168-78.
125. Knoll, R., et al., *The cardiac mechanical stretch sensor machinery involves a Z disc complex that is defective in a subset of human dilated cardiomyopathy.* Cell, 2002. **111**(7): p. 943-55.
126. Nakamura, J., et al., *Targeted disruption of Hsp110/105 gene protects against ischemic stress.* Stroke, 2008. **39**(10): p. 2853-9.
127. Subjeck, J.R., et al., *Heat shock proteins and biological response to hyperthermia.* Br J Cancer Suppl, 1982. **5**: p. 127-31.
128. Ishihara, K., K. Yasuda, and T. Hatayama, *Molecular cloning, expression and localization of human 105 kDa heat shock protein, hsp105.* Biochim Biophys Acta, 1999. **1444**(1): p. 138-42.
129. Dorard, C., et al., *Expression of a mutant HSP110 sensitizes colorectal cancer cells to chemotherapy and improves disease prognosis.* Nat Med, 2011. **17**(10): p. 1283-9.
130. Hosaka, S., et al., *Synthetic small interfering RNA targeting heat shock protein 105 induces apoptosis of various cancer cells both in vitro and in vivo.* Cancer Sci, 2006. **97**(7): p. 623-32.
131. Liu, Q. and W.A. Hendrickson, *Insights into Hsp70 chaperone activity from a crystal structure of the yeast Hsp110 Sse1.* Cell, 2007. **131**(1): p. 106-20.
132. Oh, H.J., et al., *The chaperoning activity of hsp110. Identification of functional domains by use of targeted deletions.* J Biol Chem, 1999. **274**(22): p. 15712-8.
133. Dragovic, Z., et al., *Molecular chaperones of the Hsp110 family act as nucleotide exchange factors of Hsp70s.* EMBO J, 2006. **25**(11): p. 2519-28.
134. Goeckeler, J.L., et al., *Overexpression of yeast Hsp110 homolog Sse1p suppresses ydj1-151 thermosensitivity and restores Hsp90-dependent activity.* Mol Biol Cell, 2002. **13**(8): p. 2760-70.
135. Oh, H.J., X. Chen, and J.R. Subjeck, *Hsp110 protects heat-denatured proteins and confers cellular thermoresistance.* J Biol Chem, 1997. **272**(50): p. 31636-40.
136. Yamagishi, N., et al., *Characterization of stress sensitivity and chaperone activity of Hsp105 in mammalian cells.* Biochem Biophys Res Commun, 2011. **409**(1): p. 90-5.

137. Shaner, L., et al., *The function of the yeast molecular chaperone Sse1 is mechanistically distinct from the closely related hsp70 family.* J Biol Chem, 2004. **279**(21): p. 21992-2001.
138. Schuermann, J.P., et al., *Structure of the Hsp110:Hsc70 nucleotide exchange machine.* Mol Cell, 2008. **31**(2): p. 232-43.
139. Polier, S., et al., *Structural basis for the cooperation of Hsp70 and Hsp110 chaperones in protein folding.* Cell, 2008. **133**(6): p. 1068-79.
140. Hendrickson, W.A. and Q. Liu, *Exchange we can believe in.* Structure, 2008. **16**(8): p. 1153-5.
141. Wilson, C.G. and M.R. Arkin, *Small-molecule inhibitors of IL-2/IL-2R: lessons learned and applied.* Curr Top Microbiol Immunol, 2011. **348**: p. 25-59.
142. DeLano, W.L., et al., *Convergent solutions to binding at a protein-protein interface.* Science, 2000. **287**(5456): p. 1279-83.
143. Wells, J.A. and C.L. McClendon, *Reaching for high-hanging fruit in drug discovery at protein-protein interfaces.* Nature, 2007. **450**(7172): p. 1001-9.
144. McLellan, C.A., D.A. Raynes, and V. Guerriero, *HspBP1, an Hsp70 cochaperone, has two structural domains and is capable of altering the conformation of the Hsp70 ATPase domain.* J Biol Chem, 2003. **278**(21): p. 19017-22.
145. Shomura, Y., et al., *Regulation of Hsp70 function by HspBP1: structural analysis reveals an alternate mechanism for Hsp70 nucleotide exchange.* Mol Cell, 2005. **17**(3): p. 367-79.
146. Tanimura, S., et al., *Anticancer drugs up-regulate HspBP1 and thereby antagonize the prosurvival function of Hsp70 in tumor cells.* J Biol Chem, 2007. **282**(49): p. 35430-9.
147. Takayama, S., Z. Xie, and J.C. Reed, *An evolutionarily conserved family of Hsp70/Hsc70 molecular chaperone regulators.* J Biol Chem, 1999. **274**(2): p. 781-6.
148. Takayama, S., et al., *BAG-1 modulates the chaperone activity of Hsp70/Hsc70.* EMBO J, 1997. **16**(16): p. 4887-96.
149. Briknarova, K., et al., *Structural analysis of BAG1 cochaperone and its interactions with Hsc70 heat shock protein.* Nat Struct Biol, 2001. **8**(4): p. 349-52.
150. Goebl, M. and M. Yanagida, *THE TPR SNAP HELIX - A NOVEL PROTEIN REPEAT MOTIF FROM MITOSIS TO TRANSCRIPTION.* Trends in Biochemical Sciences, 1991. **16**(5): p. 173-177.
151. Lamb, J.R., S. Tugendreich, and P. Hieter, *Tetratrico peptide repeat interactions: to TPR or not to TPR?* Trends in Biochemical Sciences, 1995. **20**(7): p. 257-259.
152. Blatch, G.L., et al., *Isolation of a mouse cDNA encoding mSTI1, a stress-inducible protein containing the TPR motif.* Gene, 1997. **194**(2): p. 277-282.
153. D'Andrea, L.D. and L. Regan, *TPR proteins: the versatile helix.* Trends in Biochemical Sciences, 2003. **28**(12): p. 655-662.
154. Sikorski, R.S., et al., *A repeating amino acid motif in CDC23 defines a family of proteins and a new relationship among genes required for mitosis and RNA synthesis.* Cell, 1990. **60**(2): p. 307-317.
155. Hirano, T., et al., *Snap helix with knob and hole: Essential repeats in S. pombe nuclear protein nuc2 +.* Cell, 1990. **60**(2): p. 319-328.

156. Zhang, M., et al., *Chaperoned ubiquitylation--crystal structures of the CHIP U box E3 ubiquitin ligase and a CHIP-Ubc13-Uev1a complex.* Mol Cell, 2005. **20**(4): p. 525-38.
157. Connell, P., et al., *The co-chaperone CHIP regulates protein triage decisions mediated by heat-shock proteins.* Nat Cell Biol, 2001. **3**(1): p. 93-6.
158. Qian, S.B., et al., *CHIP-mediated stress recovery by sequential ubiquitination of substrates and Hsp70.* Nature, 2006. **440**(7083): p. 551-5.
159. Scheufler, C., et al., *Structure of TPR domain-peptide complexes: Critical elements in the assembly of the Hsp70-Hsp90 multichaperone machine.* Cell, 2000. **101**(2): p. 199-210.
160. Brinker, A., et al., *Ligand discrimination by TPR domains - Relevance and selectivity of EEVD-recognition in Hsp70 center dot Hop center dot Hsp90 complexes.* Journal of Biological Chemistry, 2002. **277**(22): p. 19265-19275.
161. Chen, S. and D.F. Smith, *Hop as an adaptor in the heat shock protein 70 (Hsp70) and hsp90 chaperone machinery.* J Biol Chem, 1998. **273**(52): p. 35194-200.
162. Morishima, Y., et al., *Stepwise assembly of a glucocorticoid receptor.hsp90 heterocomplex resolves two sequential ATP-dependent events involving first hsp70 and then hsp90 in opening of the steroid binding pocket.* J Biol Chem, 2000. **275**(24): p. 18054-60.
163. Hutchison, K.A., et al., *Proof that hsp70 is required for assembly of the glucocorticoid receptor into a heterocomplex with hsp90.* J Biol Chem, 1994. **269**(7): p. 5043-9.
164. Smith, D.F., *Dynamics of heat shock protein 90-progesterone receptor binding and the disactivation loop model for steroid receptor complexes.* Mol Endocrinol, 1993. **7**(11): p. 1418-29.
165. Young, J.C., J.M. Barral, and F.U. Hartl, *More than folding: localized functions of cytosolic chaperones.* Trends in Biochemical Sciences, 2003. **28**(10): p. 541-547.
166. Meimaridou, E., S.B. Gooljar, and J.P. Chapple, *From hatching to dispatching: the multiple cellular roles of the Hsp70 molecular chaperone machinery.* Journal of Molecular Endocrinology, 2009. **42**(1-2): p. 1-9.
167. Hohfeld, J., D.M. Cyr, and C. Patterson, *From the cradle to the grave: molecular chaperones that may choose between folding and degradation.* Embo Reports, 2001. **2**(10): p. 885-890.
168. Wu, S.J., et al., *Different combinations of the heat-shock cognate protein 70 (hsc70) C-terminal functional groups are utilized to interact with distinct tetratricopeptide repeat-containing proteins.* Biochemical Journal, 2001. **359**: p. 419-426.
169. Ballinger, C.A., et al., *Identification of CHIP, a novel tetratricopeptide repeat-containing protein that interacts with heat shock proteins and negatively regulates chaperone functions.* Molecular and Cellular Biology, 1999. **19**(6): p. 4535-4545.
170. Wang, L., et al., *Molecular Mechanism of the Negative Regulation of Smad1/5 Protein by Carboxyl Terminus of Hsc70-interacting Protein (CHIP).* Journal of Biological Chemistry, 2011. **286**(18).
171. Liu, F.H., et al., *Specific interaction of the 70-kDa heat shock cognate protein with the tetratricopeptide repeats.* Journal of Biological Chemistry, 1999. **274**(48): p. 34425-34432.

172. Carrigan, P.E., et al., *Multiple domains of the co-chaperone Hop are important for Hsp70 binding.* Journal of Biological Chemistry, 2004. **279**(16): p. 16185-16193.
173. Zhang, H.Q., et al., *A Bipartite Interaction between Hsp70 and CHIP Regulates Ubiquitination of Chaperoned Client Proteins.* Structure, 2015. **23**(3): p. 472-482.
174. Cheung-Flynn, J., et al., *C-terminal sequences outside the tetratricopeptide repeat domain of FKBP51 and FKBP52 cause differential binding to hsp90.* Journal of Biological Chemistry, 2003. **278**(19): p. 17388-17394.
175. Chen, S.Y., et al., *Differential interactions of p23 and the TPR-containing proteins Hop, Cyp40, FKBP52 and FKBP51 with Hsp90 mutants.* Cell Stress & Chaperones, 1998. **3**(2): p. 118-129.
176. Yi, F., et al., *An AlphaScreen (TM)-Based High-Throughput Screen to Identify Inhibitors of Hsp90-Cochaperone Interaction.* Journal of Biomolecular Screening, 2009. **14**(3): p. 273-281.
177. Vasko, R.C., et al., *Mechanistic Studies of Sansalvamide A-Amide: An Allosteric Modulator of Hsp90.* Acs Medicinal Chemistry Letters, 2010. **1**(1): p. 4-8.
178. Ardi, V.C., et al., *Macrocycles That Inhibit the Binding between Heat Shock Protein 90 and TPR-Containing Proteins.* Acs Chemical Biology, 2011. **6**(12): p. 1357-1366.
179. Schreiber, S.L., *Target-oriented and diversity-oriented organic synthesis in drug discovery.* Science, 2000. **287**(5460): p. 1964-9.

Chapter 2

Specific binding of tetratricopeptide repeat (TPR) proteins to Hsp70 and Hsp90 is regulated by affinity and phosphorylation

2.1 Abstract

The heat shock proteins Hsp70 and Hsp90 require the help of tetratricopeptide repeat (TPR) domain-containing co-chaperones for many of their functions. Each monomer of Hsp70 or Hsp90 can only interact with a single TPR co-chaperone at a time and each member of the TPR co-chaperone family brings distinct functions into the complex. Thus, competition for TPR binding sites on Hsp70 and Hsp90 appears to shape chaperone activity. Recent structural and biophysical efforts have improved our understanding of chaperone-TPR contacts, focusing on the C-terminal EEVD motif that is present in both chaperones. To better understand these important protein-protein interactions (PPIs) on a wider scale, I measured the affinity of five TPR co-chaperones, CHIP, Hop, DNAJC7, FKBP51, and FKBP52, for the C-termini of four members of the chaperone family, Hsc70, Hsp72, Hsp90α, and Hsp90β, *in vitro*. These studies identified some surprising selectivity amongst the chaperone-TPR pairs, including the selective binding of FKBP51/52 to Hsp90α/β. These results also revealed that other TPR co-chaperones are only able to weakly discriminate between the chaperones or between their paralogs. I also explored whether mimicking phosphorylation of serine and threonine residues near the EEVD motif

might impact TPR co-chaperone affinity. The results suggested that phosphorylation selectively shapes TPR interactions, with dramatic effects on CHIP, but not other co-chaperones. Together, these findings suggest that both intrinsic affinity and post-translational modifications tune the interactions between Hsp70/90 and the TPR co-chaperones.

2.2 Introduction

2.2.1 Hsp70 and Hsp90 require the help of TPR co-chaperones for many of their functions

The molecular chaperones Hsp70 and Hsp90 are essential regulators of cellular protein quality control, where they use ATP turnover to play broad roles in protein folding, trafficking, and degradation [1-6]. In part, Hsp70 and Hsp90 are able to engage in so many different pathways because they collaborate with co-chaperones [7]. Co-chaperones, including the tetratricopeptide repeat (TPR) domain-containing proteins, bind to chaperones and help determine whether "clients" will be folded, degraded, or sent to other fates. Thus, active chaperone complexes are often considered to include both the core chaperone (*e.g.* Hsp70 or Hsp90) and its associated co-chaperones. Because of this, there is great interest in studying the protein-protein interactions (PPIs) between chaperones and co-chaperones in order to better understand how these complexes form, how they are regulated, and how "decisions" are made. This knowledge is important because imbalances in protein quality control have been linked to a range of diseases, including cancer and neurodegeneration [8-13].

2.2.2 Structure and diverse functions of TPR domain-containing co-chaperones

TPR domains are comprised of tandem 34 amino acid motifs, which form amphipathic antiparallel α-helix hairpins that stack on one another [14]. Two of the most well studied TPR domain-containing proteins are Hop (Hsp70/Hsp90 organizing protein) and CHIP (carboxyl terminus of Hsc70 interacting protein) [15-18]. Like all co-chaperones of this class, Hop and CHIP have no homology outside of the TPR domain. It is this diversity that allows the TPR co-chaperones to bring unique capabilities into chaperone complexes. For example, Hop uses multiple TPR domains to bind both Hsp70 and Hsp90 at the same time, coordinating these two chaperone systems and favoring client folding [19-24]. In contrast, CHIP is an ubiquitin E3 ligase with a TPR domain and an effector U-box domain [25]. This co-chaperone favors addition of polyubiquitin chains to Hsp70/90-bound clients, promoting their proteasomal degradation [26, 27]. Other important TPR proteins include FKBP51 and FKBP52, which work with Hsp70 and Hsp90 during the maturation and trafficking of steroid hormone receptors [28-30], and DNAJC7, which contains a J-domain [31, 32]. Together, these observations suggest that the ultimate fate of chaperone-bound clients (*e.g.* whether they are folded, degraded, trafficked, or matured) may be guided, in part, by the "choice" of which TPR co-chaperone is bound.

2.2.3 TPR domains bind to the C-termini of cytosolic Hsp70s and Hsp90s

The constitutive and heat-inducible paralogs of Hsp70 in the cytoplasm, termed Hsc70 (HSPA8) and Hsp72 (HSPA1A) respectively, contain a highly conserved EEVD motif at their respective C-termini. This four amino acid sequence binds to the concave face of the TPR

domains, as revealed by mutagenesis and structural studies [33-35]. In the bound form, key contacts are made between the chaperone's carboxy terminus and conserved cationic residues in the TPR domain. Like Hsp70s, both paralogs of Hsp90 in the cytosol (Hsp90α and Hsp90β) contain this same conserved, C-terminal EEVD motif. The striking thing about this observation is that, outside of this small motif, the two Hsp90s share no structural or sequence homology with the Hsp70s. Yet, the sequence of all four chaperones terminates with the same four amino acids, EEVD. In contrast, the other paralogs of Hsp70 and Hsp90, which are located in the endoplasmic reticulum, mitochondria and chloroplast, do not have EEVD motifs, suggesting that the TPR interactions may have evolved to specifically mediate quality control in the cytosol and nucleus.

2.2.4 An all-inclusive study of Hsp70/90-TPR protein interactions has not been preformed

More information about the PPIs between TPR co-chaperones and cytoplasmic Hsp70s/Hsp90s, might help us understand a key step in protein quality control. Indeed, pioneering studies by multiple groups have examined the structures and affinities of important TPR-EEVD interactions, including Hop-Hsp70/90 [3, 36, 37], PP5-Hsp70/90 [38, 39], CHIP-Hsp70/90 [40-43], and FKBP52-Hsp90 [44]. However, a comprehensive study of PPIs has not yet been reported. Such a side-by-side comparison is important because the competition for TPR-domain proteins in the cytosol appears to be a major determinant of quality control. In this study, I used a fluorescence polarization (FP) platform to systematically compare the affinities of five different human TPR co-chaperones (Hop, CHIP, DNAJC7, FKBP51, and FKBP52) for the C-termini of the four cytosolic Hsp70s/90s. I

found that some co-chaperones, such as FKBP51 and FKBP52, have a strong preference for Hsp90s over Hsp70s. Other chaperones, including Hop, CHIP, and DNAJC7, have a modest (~2-fold) preference for Hsp70s. Using chimeric peptides, I found that a single residue adjacent to the EEVD motif was important for some of this selectivity. Interestingly, none of the TPR co-chaperones could discriminate between the paralogs of Hsp70 or Hsp90, suggesting that they might work with both forms equally. Finally, I confirmed that mimicking phosphorylation of the C-termini of Hsp70s and Hsp90s dramatically alters their affinity for CHIP, while also finding that this is not the case for other TPR co-chaperones. Together, these studies provide a resource for understanding how interactions in this system are regulated.

2.3 Results and discussion

2.3.1 The binding of Hsp70 to TPR co-chaperones is mediated by Hsp70's EEVD motif

Previous work had suggested that the EEVD motif provides the majority of the TPR interaction affinity, with less affinity (typically <20%) coming from secondary contacts [42, 45-48]. Secondary contacts are potentially appealing because they might provide a means of selectively targeting specific Hsp70-TPR co-chaperone complexes with small molecule inhibitors. However, in the systems studied previously, the secondary affinities were relatively weak (K_D >100 μM) [42]. To ask whether this was also the case in other TPR-chaperone complexes, I generated a mutant Hsp72 construct that lacked an EEVD motif (Hsp72ΔEEVD). This mutant was normal in binding nucleotide (Appendix 2.6.1A) and a client peptide derived from the MHC class I antigen HLA-B2702 (Fam-HLA) (Appendix

2.6.1B), showing that the EEVD motif does not directly contribute to these activities. I next tested whether this otherwise functional Hsp72ΔEEVD mutant could compete with the Hsp72 tracer (Fam-GSGPTIEEVD) for binding to TPR co-chaperones (Appendix 2.6.2). I found that Hsp72ΔEEVD was unable to compete for tracer binding, even at 40 μM, whereas wild-type (wt) Hsp72 could (Appendix 2.6.2B). These results suggest that interactions outside of the canonical EEVD-TPR binding site are relatively weak, consistent with recent structural studies on Hsp70 and CHIP [42]. Based on this result, I decided to focus strictly on the C-termini of Hsp70s and Hsp90s to further understand their interactions with TPR proteins.

2.3.2 Preferences of the TPR co-chaperones for binding to Hsp70 and Hsp90

In an effort to understand what factors influence binding to the molecular chaperones, I first determined the affinity of chaperone C-termini for full-length TPR proteins using a FP assay. In these studies, I focused on some of the best-studied TPR co-chaperones: CHIP, Hop, DNAJC7, FKBP51, and FKBP52. In addition, I included HIP as a negative control because this co-chaperone binds Hsp70s in a region outside the EEVD motif [49]. For our FP experiments, I measured the ability of TPR proteins to interact with fluorescently labeled peptides corresponding to the C-termini of Hsc70 (Fam-SSGPTIEEVD), Hsp72 (Fam-GSGPTIEEVD), Hsp90α (Fam-DDTSRMEEVD), and Hsp90β (Fam-EDASRMEEVD). Using this platform, I found that CHIP, Hop, and DNAJC7 bound to both Hsp70s and Hsp90s (Figure 2.1A). Of these complexes, CHIP had the tightest affinity, binding Hsc70 with a K_D of 0.62 ± 0.06 μM and Hsp72 with a K_D of 0.51 ± 0.03 μM. I also found that CHIP, Hop, and DNAJC7

(A) Summary of binding affinities of TPR co-chaperones for Hsp70 and Hsp90 C-termini.

	K_D (μM)			
TPR Protein	SSGPTIEEVD (Hsc70)	GSGPTIEEVD (Hsp72)	DDTSRMEEVD (Hsp90α)	EDASRMEEVD (Hsp90β)
CHIP	0.62 ± 0.06	0.51 ± 0.03	1.03 ± 0.07	1.32 ± 0.11
Hop	2.70 ± 0.14	2.64 ± 0.13	5.39 ± 0.62	6.26 ± 0.87
DNAJC7	2.97 ± 0.31	2.47 ± 0.21	6.83 ± 1.63	6.19 ± 0.97
FKBP51	>100	>100	1.24 ± 0.08	2.05 ± 0.14
FKBP52	>75	>75	1.61 ± 0.36	1.02 ± 0.14
Hip	>40	>40	>40	>40

(B) DNAJC7 binds to both Hsp70s and Hsp90s. (C) FKBP52 binds specifically to Hsp90s. (D) Hip does not interact with the C-termini of Hsp70s or Hsp90s.

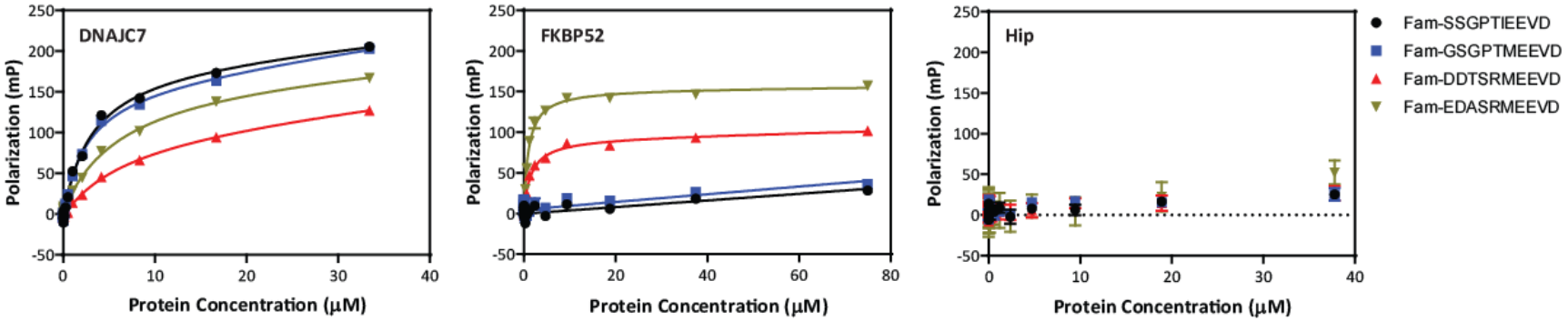

Figure 2.1 Binding of full-length TPR co-chaperones to the C-termini of cytosolic Hsp70s and Hsp90s. (A) Summary of affinity values, measured by FP. Experiments were performed at least twice in triplicate. Results are shown as the average and standard error of the mean (SEM). Representative binding curves are shown for (B) DNAJC7 (C) FKBP52, and (D) the negative control Hip.

bound Hsc70 and Hsp72 with ~2-fold tighter affinity than Hsp90α and Hsp90β (**Figure 2.1** and **Appendix 2.6.3**). Interestingly, I found that the FKBP51 and FKBP52 did not interact with appreciable affinity (K_D >75 μM) with Hsp70s. Rather, they specifically bound to Hsp90α and Hsp90β with K_D values between 1 and 2 μM (**Figure 2.1** and **Appendix 2.6.3**). Another important observation was that no specificity was observed between paralogs (*i.e.* Hsc70 versus Hsp72), suggesting that TPR co-chaperones do not discriminate between them. The negative control, Hip, did not interact with any of the C-terminal tracers, as expected. Finally, a reversed Hsp90 peptide (Fam-DVEEM) had no affinity for any of the TPR co-chaperones (**Appendix 2.6.4**), consistent with previous results [41].

2.3.3 The Met residue of the Hsp90 C-terminus (MEEVD) influences binding preferences

Some of the TPR co-chaperones appeared to bind Hsp70s slightly tighter than Hsp90s (see **Figure 2.1**). To understand the origin of this difference, I first aligned the amino acid sequences of cytosolic Hsp70s, revealing conservation of either IEEVD or VEEVD. A similar alignment of eukaryotic Hsp90 sequences showed that these proteins all terminate with MEEVD. Thus, it appeared that the identity of the residue immediately adjacent to the EEVD (Ile or Met) might account for some of the binding preferences, consistent with previous models [35]. To test this hypothesis, I first generated a chimeric mutant in which the Ile residue of an Hsp70 tracer was replaced with a Met (Fam-GSGPTMEEVD). This chimera had a weakened interaction with CHIP, Hop, and DNAJC7 (**Figure 2.2A** and **2.2C**), instead having an "Hsp90-like" affinity. This result suggested that the Met residue of Hsp90s might be important in the affinity differences between Hsp70s and Hsp90s.

However, placing the Met in the context of Hsp70 C-terminus was not able to provide binding to FKBP51 and FKBP52 (K_D > 75 μM) (Figure 2.2C and Appendix 2.6.5), so other features must be responsible for the selectivity of FKBP51/52 for Hsp90s. To further explore the role of the Ile/Met residues, I generated the corresponding mutant Hsp90α tracer in which I switched the Met residue to an Ile (Fam-DDTSRIEEVD) and tested its

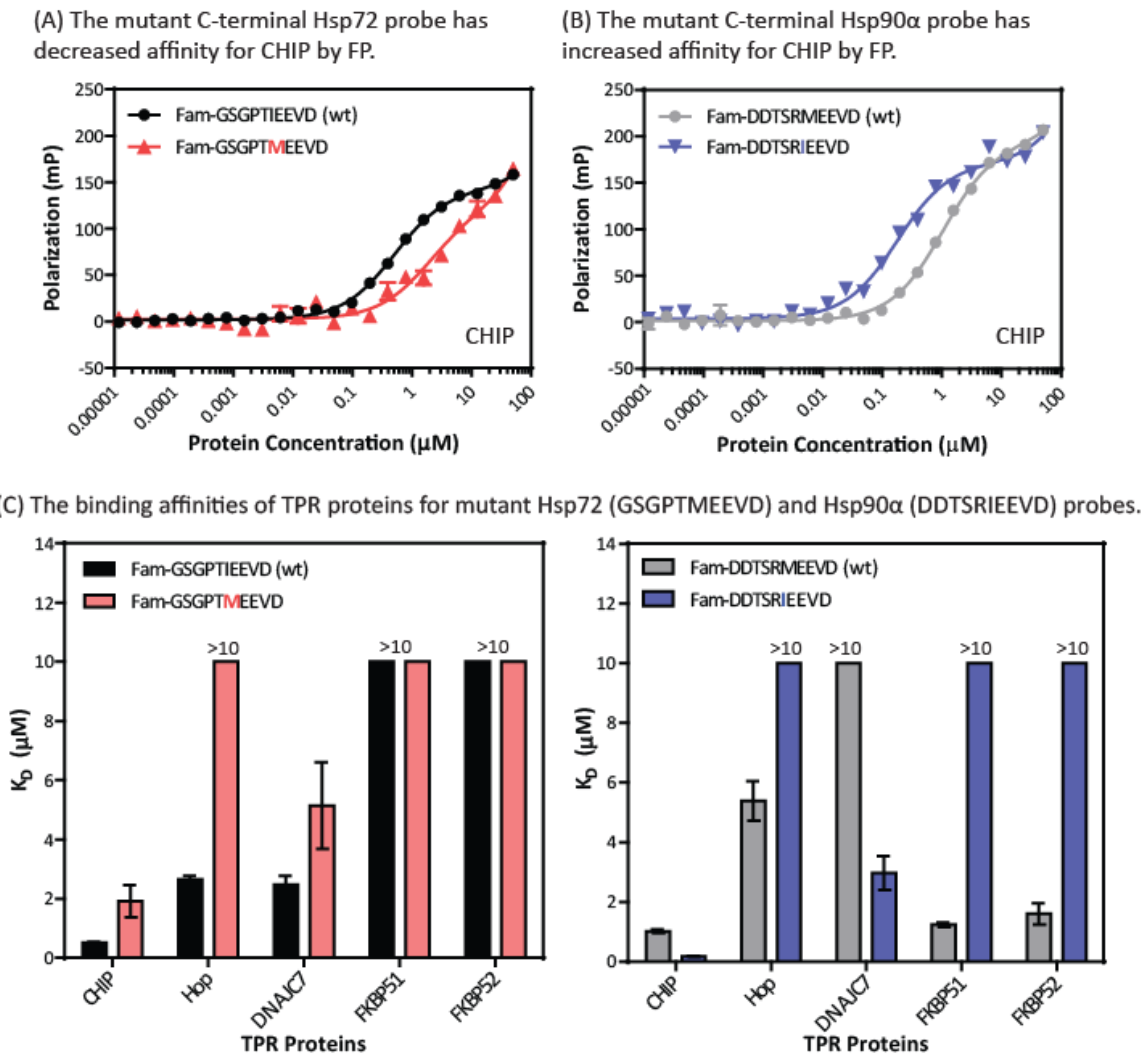

Figure 2.2 The Ile residue of Hsp72 (GSGPTIEEVD) and Met residue of Hsp90α (DDTSRMEEVD) strongly influence binding preferences. (A) CHIP preferentially binds the C-terminus of Hsp72 (GSGPTIEEVD) over the C-terminus of Hsp90α (DDTSRMEEVD). A mutant C-terminal Hsp72 probe (GSGPTMEEVD) has decreased affinity for CHIP. (B) A mutant C-terminal Hsp90α probe (DDTSRMEEVD) has increased affinity for CHIP. (C) The binding affinities of TPR proteins for mutant Hsp72 (GSGPTMEEVD) and Hsp90α (DDTSRMEEVD) C-terminal tracers. Affinities were measured by FP using full-length TPR proteins. Experiments were performed at least twice in triplicate. Results are shown as the average and the error bars represent SEM.

binding. FKBP51 and FKBP52 no longer bound the mutant Hsp90α (K_D >25 μM) (**Figure 2.2C** and **Appendix 2.6.5**), reducing the affinity by at least 12-fold compared to wt Hsp90α. Co-crystal structures of FKBP52 bound to a MEEVD peptide show the Met of MEEVD forms a critical hydrogen bond with Lys-282 of FKBP52's TPR domain, which is important in stabilizing the binding of this peptide [44]. Similarly, the mutant had other binding preferences that mirrored those of Hsp70's. For example, CHIP and DNAJC7 had increased affinity (≥2-fold) for the mutant in comparison to the wt (**Figure 2.2C** and **Appendix 2.6.5**). However, the mutant did not bind Hop (K_D >25 μM), so residues other than the Ile/Met must be critical. Taken together, these data illustrate that the Ile/Met position is a major contributor to differences between the binding affinities for Hsp70s and Hsp90s.

2.3.4 Polar contacts dominate binding of TPR co-chaperones to Hsp70/Hsp90

The EEVD motif is strongly electronegative and the corresponding surface of the TPR domain tends to be electropositive (**Figure 2.3A**) [25, 35, 50]. To explore the role of possible polar interactions in selectivity, I mutated the last Glu of the EEVD motif to either a neutral Ala (Fam-DDTSRMEAVD) or a cationic Lys (Fam-DDTSRMEKVD). Using FP, I found that all of the TPR proteins had slightly decreased affinity for the Ala mutant tracer (**Figure 2.3C**). FKBP51 was most sensitive to this change, binding the Ala mutant with a K_D of 4.63 ± 0.38 μM, a ~4-fold decrease in affinity. The mutant Lys tracer (Fam-DDTSRMEKVD) had significantly decreased affinity for all TPR proteins (≥3-fold). Again, FKBP51 and FKBP52 were most sensitive to this change (K_D > 25). Next, I performed additional FP assays in which binding of wt Hsp70 and Hsp90 C-terminal tracers to TPR co-chaperones was

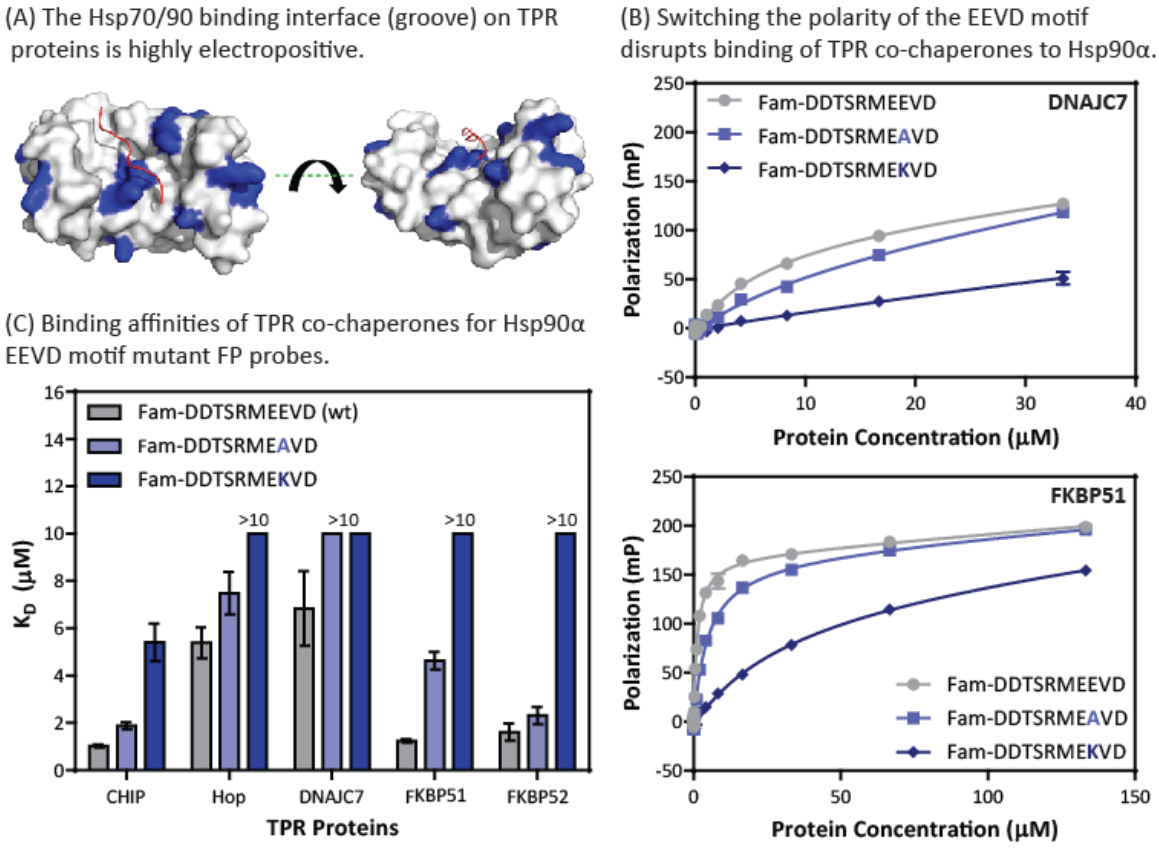

Figure 2.3 The binding of TPR co-chaperones to Hsp70/90 involves polar contacts in the EEVD motif. (A) The Hsp70/90 binding interface of TPR co-chaperones has a strong electropositive character. Surface representation of Hop's TPR1 domain (PBD code = 1ELW) is shown as an example. Cationic residues (Lys and Arg) are highlighted in blue. Images were prepared using PyMOL. (B) Switching a glutamic acid in the EEVD motif to an alanine slightly decreased the affinity of TPR co-chaperones for Hsp70/90, while replacement with a lysine greatly decreased binding. (C) Affinities of TPR co-chaperones for Hsp90α mutant tracers DDTSRMEAVD and DDTSRMEKVD. (D) Binding of TPR co-chaperones to C-termini of Hsp70s and Hsp90s is pH dependent. Representative CHIP results are shown. There was no change in the intrinsic fluorescence of the Fam fluorophore under these pH conditions (data not shown). All affinities were measured by FP using full-length TPR proteins. Experiments were performed at least twice in triplicate. Results are shown as the average and the error bars represent SEM.

measured at elevated pH. All of the TPR co-chaperones had reduced affinity at high pH (Figure 2.3D and Appendix 2.6.6), supporting the idea that polar contacts are critical for the formation of EEVD-TPR domain complexes. However, the binding preferences did not dramatically switch, so pH seems unlikely to regulate TPR preferences.

2.3.5 TPR1 and TPR2A of Hop selectively bind to the C-termini of Hsp70 and Hsp90

Hop is unique among the TPR co-chaperones studied here in that it contains three TPR domains that are termed: TPR1, TPR2A, and TPR2B (Figure 2.4A). Previous co-crystallographic and *in vitro* binding studies have shown that TPR1, when studied as an isolated protein, prefers to bind the C-terminus of Hsp70, whereas the isolated TPR2A domain binds tighter to Hsp90's C-terminus [35]. In the co-crystal structures, the N-terminal portions of the peptides seemed to dictate selectivity by occupying different hydrophobic patches within their respective TPR domains. I wanted to test whether this discrimination was preserved in full length Hop because it seemed possible that the binding properties could be significantly altered in the context of the multi-domain protein, instead of isolated domains. Accordingly, I introduced single point mutations into full-length Hop that disrupt the critical "carboxylate clamps" required for EEVD binding. Two of the point mutations (K8A and R77A) were in the TPR1 domain, while the other mutations (N223A and R305A) were in Hop's TPR2A domain (Figure 2.4A and 2.4B). Using my FP assay, I tested the ability of these mutant proteins to interact with Hsp70 and Hsp90 tracers. Hop^{K8A} and Hop^{R77A} did not interact with appreciable affinity (K_D >25 μM) to Hsp70, but had normal affinity for Hsp90s (K_D values ~ 6 to 8 μM) (Fig 2.4C and Appendix 2.6.7).

(A) The domain architecture of the TPR co-chaperone Hop.

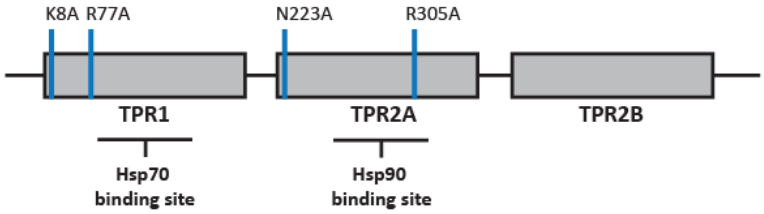

(B) Structures of Hop TPR1 and TPR2A domains bound to Hsp70/90 C-terminal ligands.

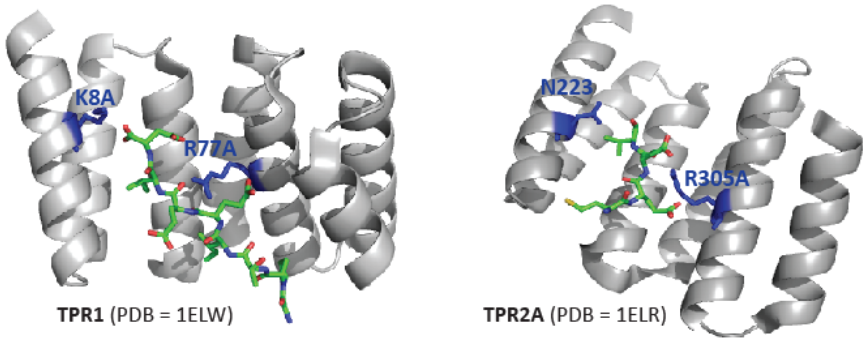

(C) Summary of binding affinities of Hop mutants for Hsp70 and Hsp90 C-termini.

	K_D (μM)			
Hop Mutant	SSGPTIEEVD (Hsc70)	GSGPTIEEVD (Hsp72)	DDTSRMEEVD (Hsp90α)	EDASRMEEVD (Hsp90β)
K8A	>25	>25	6.53 ± 0.94	8.30 ± 1.68
R77A	>25	>25	6.49 ± 0.97	9.81 ± 2.31
N223A	3.33 ± 0.20	2.94 ± 0.30	>25	>25
R305A	4.05 ± 0.32	3.82 ± 0.20	>25	>25
wt	2.70 ± 0.14	2.64 ± 0.13	5.39 ± 0.62	6.26 ± 0.87

(D) Hop R77A binds specifically to Hsp90s. (E) Hop R305A binds specifically to Hsp70s.

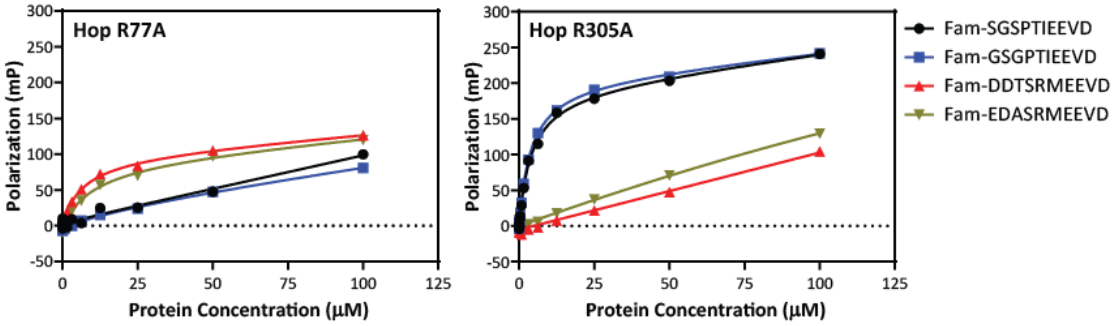

Figure 2.4 Hop's TPR1 and TPR2A domains selectively interact with the C-termini of Hsp70 and Hsp90. (A) Schematic of the domain architecture of Hop. Blue lines indicate point mutations made in Hop's TPR1 and TPR2A domains. (B) Structures of Hop's TPR1 domain (PBD = 1ELW) and TPR2A domain (PBD = 1ELR). Residues that were mutated in these domains are highlighted in blue. Hsp70/90 C-terminal peptides are shown in green. Structures were prepared using PyMOL. (C) Table summarizing binding affinities of Hop point mutants (K8A, R77A, N223A, and R305A) for chaperone tracers. Affinities were measured by FP using full-length Hop. Experiments were performed at least twice in triplicate. Results are shown as the average and error bars represent SEM. Representative binding curves are shown. (D) Hop R77A binds specifically to Hsp90s. (E) Hop R305A binds specifically to Hsp70s.

Conversely, TPR2A mutants, Hop^{N223A} and Hop^{R305A}, selectively interacted with Hsp70 (K_D of 2-4 μM) but not Hsp90s. Taken together, this work supports the conclusions made from studying individual domains of Hop.

2.3.6 Phosphorylation of Hsp70/Hsp90 C-termini dramatically affects binding to CHIP

It has recently been shown that phosphorylation of serine and threonine residues in the C-termini of Hsp70 and Hsp90 influences binding to CHIP [51]. Thus, I wondered if phosphorylation might be a general regulatory mechanism for TPR binding. To test this idea, I generated FP tracers that mimicked phosphorylation (Figure 2.5A) and measured their binding to TPR proteins. Consistent with previous data [51], the affinity of CHIP for the mutant Hsc70 Fam-SSGPTEIEEVD and Hsp90α Fam-DDTERMEEVD tracers was reduced by more than 8-fold (Figure 2.5A). Also, Hop had mildly enhanced binding (~2-fold) to pseudophosphorylated Hsp70 and Hsp90 C-termini (Figure 2.5B). Interestingly, the binding of DNAJC7, FKBP51, and FKBP52 to either chaperone was unaffected (Figure 2.5B). Thus, mimicking phosphorylation of the C-termini of Hsp70 and Hsp90 seemed to tune the affinity for select TPR co-chaperones but not others.

2.4 Conclusions

2.4.1 Specific binding of TPR co-chaperones to Hsp70 and Hsp90 is influenced by affinity and phosphorylation

The molecular chaperones Hsp70 and Hsp90 work with TPR co-chaperones to mediate protein triage and quality control. In this study, I characterized how TPR co-chaperones,

(A) CHIP has decreased affinity for pseudophosphorylated Hsp70/90 C-termini.

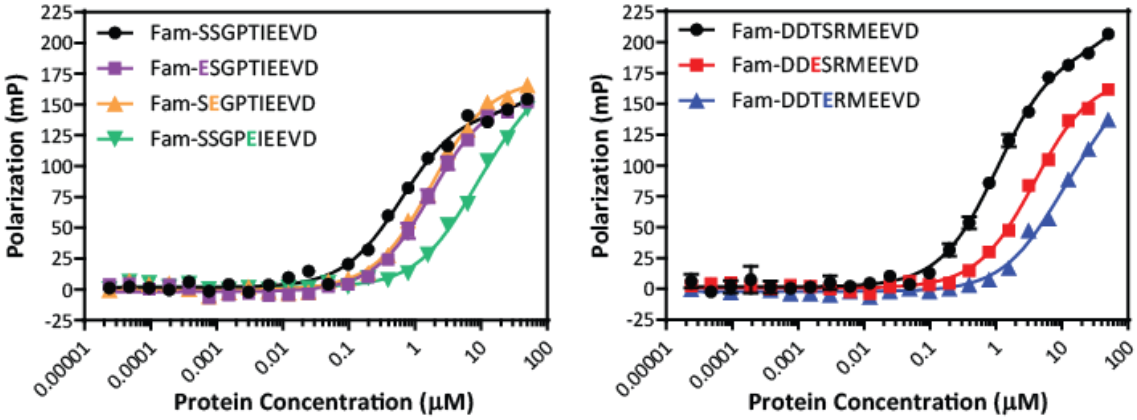

(B) Binding affinities of TPR co-chaperones for pseudophosphorylated Hsp70/90 C-termini.

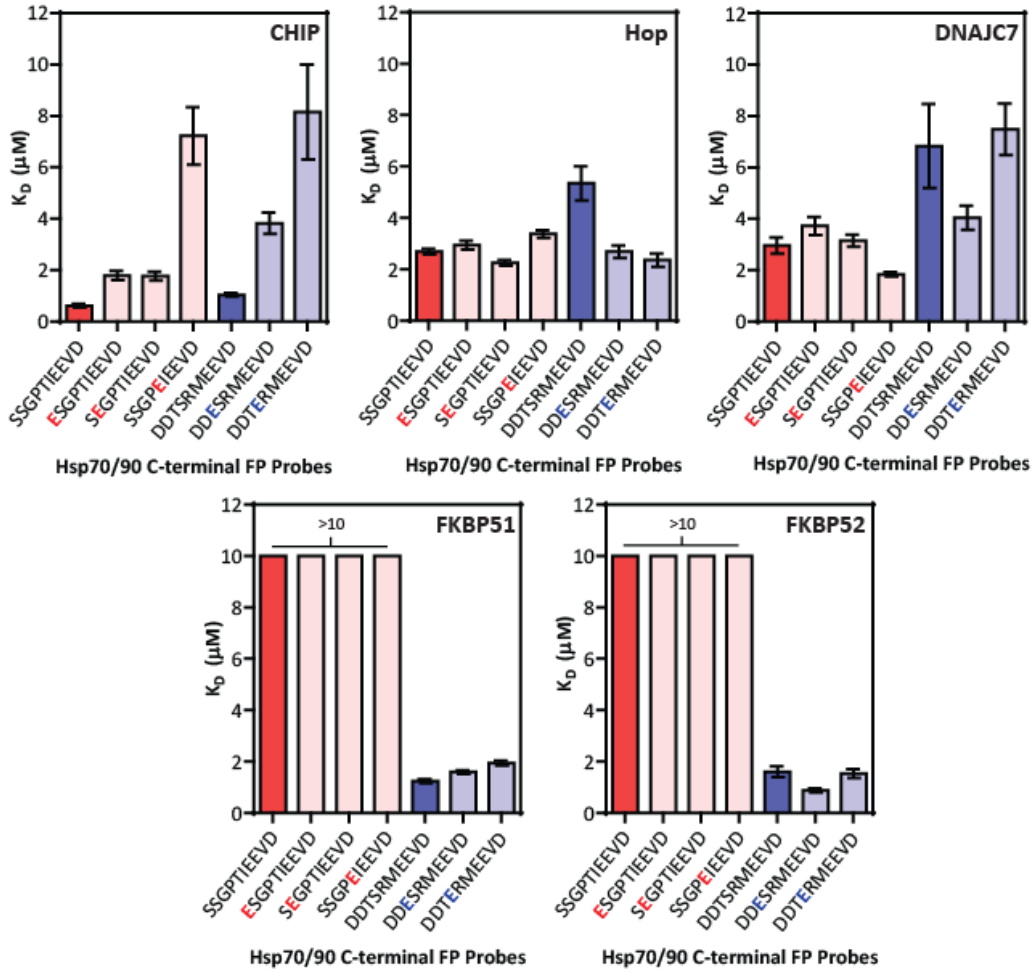

Figure 2.5 Mimicking phosphorylation of Hsp70/90 selectively weakens binding to CHIP. (A) CHIP has decreased affinity for Hsp70/90 C-termini that contain phosphomimetic residues. (B) Binding affinities of other TPR co-chaperones for mutant Hsp70/90 C-termini. All affinities measured by FP using full-length TPR proteins. Experiments were performed at least twice in triplicate. Results are shown as the average and error bars represent SEM.

including CHIP, Hop, DNAJC7, FKBP51, and FKBP52, bind the C-termini of four cytosolic human Hsp70s and Hsp90s *in vitro*. Some TPR co-chaperones showed a preference for chaperones. For example, CHIP, Hop, and DNAJC7 had a 2-fold overall preference for Hsp70s over Hsp90s. Using point mutants, I learned that the Ile/Met residue adjacent to the EEVD motif was one feature that gives rise to these differences. Moreover, I found that mimicking phosphorylation of Ser/Thr residues in the C-termini reduced affinity for CHIP and modestly enhanced affinity for Hop, but that this modification had little effect on the interactions with other TPR proteins. This result was surprising, given the dramatic increase in size and charge at these sites and their proximity to the EEVD-TPR contact. Finally, no specificity was observed when comparing chaperone paralogs (*i.e.* Hsc70 versus Hsp72) in any of these platforms. This was also surprising because the expression of the paralogs is regulated by quite different mechanisms and a few reports have started to identify pathways that rely on one and not the other [52-54]. However, from the TPR's point of view, they appear to be degenerate. Together, these studies expand our understanding of chaperone-TPR PPIs. It is important to emphasize that some of these conclusions have been suggested by previous studies (*vide infra*). The comprehensive approach taken here was designed to provide the full spectrum of interaction affinities and reveal broader patterns. Some of the surprising results from this approach include the findings that FKBP51 and FKBP52 do not bind Hsp70s and that pseudophosphorylation has no effect on binding to DNAJC7, FKBP51, and FKBP52. Thus, TPR interactions are perhaps tuned by unexpected ways.

2.4.2 Features other than affinity of the EEVD-TPR contacts could influence complex formation between TPR co-chaperones and Hsp70/90

What are the implications of these results for understanding chaperone-mediated quality control? Before this work, one formal possibility was that different TPR co-chaperones might display a clear hierarchy of affinity constants. This scenario would have suggested a model in which certain TPR co-chaperones could effectively outcompete others to drive quality control "decisions." However, with a few exceptions (*e.g.* FKBP51/52 binding exclusively to Hsp90s and selectivity within Hop TPR domains), there were not dramatic differences between the observed affinity constants (see Figure 2.1). So, what other factors might contribute to selectivity in this system? One possibility is that secondary contacts (*e.g.* those outside the EEVD motif) might help tune the interactions. However, there appears to be comparatively little energy in these interactions, so their contributions might be expected to be relatively small. Another possibility is that the expression levels of the individual TPR domain co-chaperones, rather than their intrinsic affinity values, may dominate which complexes are most likely to form. For example, Hop expression is known to be induced in response to certain stress conditions, such as infection [55], which could reshape the dynamics of which TPR interactions are favored. However, this model seems unsatisfying by itself. Rather, an addition to this model is suggested by the observations that mimicking phosphorylation dramatically weakens the affinity of the CHIP-Hsp70/Hsp90 complexes, while enhancing the corresponding Hop complexes. Specifically, it seems plausible that post-translational modifications (PTMs) might help guide which TPR co-chaperone is bound by the specific chaperone. In the case of phosphorylation, contact

with CHIP is apparently disfavored, while interactions with other TPR co-chaperones are spared or even enhanced (in the case of Hop). This mechanism is appealing because it would allow quality control "decisions" to be shaped by signaling pathways, providing a way for cells and organisms to adjust their proteomes in response to cues or changing conditions. Even this model seems rather incomplete, so I also favor the idea that other features might ultimately be found to contribute to the choice of which TPR co-chaperone is bound. These features might include the structure of the client, whether it directly interacts with co-chaperones, and the subcellular co-localization of all the components. Future work will need to explore how these factors guide the selection of TPR-chaperone pairs. These results suggest that, except for the special cases of FKBPs and individual Hop domains, features other than affinity of the EEVD-TPR contacts might play dominant roles.

2.4.3 Strategies for targeting Hsp70/90-TPR co-chaperone complexes

There has been great interest in targeting these PPIs to treat diseases [56-60]. Many of these strategies are focused on inhibiting EEVD-TPR contacts, such as that between Hop and Hsp70/90, which are important in cancer. However, our results suggest that such approaches may have unintended consequences. For example, androgen receptor (AR) is dependent on Hop-Hsp70 for its maturation [61], but it also requires CHIP-Hsp70 for its degradation [62, 63]. Thus, it is not clear what effect an EEVD-TPR inhibitor might ultimately have on levels of that client. One might conceivably achieve greater selectivity by developing inhibitors of the secondary contacts between chaperones and TPR co-chaperones, which presumably occur at sites that are less degenerate than the EEVD-TPR

contact. However, like others [42], I found that the energy contributed by secondary contacts (*e.g.* those outside the EEVD) contribute relatively little binding free energy. Thus, it may be difficult to identify compounds that compete with the PPIs by binding at these secondary contacts. Despite this challenge, some progress has been made with derivatives of the natural product sansalvamide A, which inhibit some Hsp90-TPR interactions but not others [59, 60]. Although the mechanisms are not yet clear, these molecules are thought to act at allosteric sites on Hsp90, avoiding the problem of weak affinity in the secondary contacts. It is becoming more widely appreciated that allosteric inhibitors are effective against otherwise "undruggable" PPIs [64]. Our results support the continued focus on allosteric sites, rather than TPR-EEVD inhibitors, in the pursuit of reagents for fine-tuning protein quality control.

2.5 Experimental procedures

2.5.1 Plasmids

Human CHIP, Hop, FKBP51, and FKBP52 were expressed from a pET151 vector such that they contained an N-terminal His-tag and TEV cleavage site. Site-directed mutagenesis for Hop mutants (K8A, R77A, N223A, and R305A) was performed using the Phusion Site-Directed Mutagenesis Kit protocol (New England Biolabs, Ipswich, MA). Human DNAJC7, Hsc70 (HSPA8), Hsp72 (HSPA1A), and Hsp72ΔEEVD were expressed from a pMCSG7 vector with an N-terminal His-tag and TEV cleavage site. Lastly, HIP was expressed from a pET28a vector with an N-terminal His-tag and Thrombin cleavage site.

2.5.2 Protein expression and purification

Hsc70, Hsp72, Hsp72ΔEEVD proteins were expressed in *E. coli* BL21 (DE3) cells. Liter cultures of terrific broth were grown at 37 °C until an OD_{600} of 0.6. Cultures were cooled to 25 °C and induced with isopropyl β-D-1-thiogalactopyranoside (IPTG; final concentration of 500 µM). Afterwards, cultures were grown overnight at 25 °C. For protein purification, cell pellets were re-suspended in His-binding buffer (50 mM TRIS, 10 mM Imidazole, 500 mM NaCl, pH 8) supplemented with protease inhibitors. Cells were lysed by sonication, pelleted by centrifugation, and the supernatant was applied to Ni-NTA His-Bind Resin (Novagen, Darmstadt, Germany). The resin was washed with His-binding buffer, followed by His-washing buffer (50 mM TRIS, 30 mM Imidazole, 300 mM NaCl, pH 8). The protein was then removed from the resin using His-elution buffer (50 mM TRIS, 300 mM Imidazole, 300 mM NaCl, pH 8). Before further purification by an ATP-agarose column (Sigma), $MgCl_2$ and KCl was added to the eluted sample (final concentration: $MgCl_2$ = 10 mM, KCl =10 mM). The sample was then applied to the ATP-agarose column, was first washed with buffer A (25 mM HEPES, 5 mM $MgCl_2$, 10 mM KCl, pH 7.5) and then was washed with buffer B (25 mM HEPES, 5 mM $MgCl_2$, 1M KCl, pH 7.5). The column was then washed a third time with buffer A and then eluted in buffer A containing 3 mM ATP. The pure protein was concentrated and exchanged into buffer A for storage. Note that the N-terminal His-tags were not removed.

Human CHIP, Hop, Hop mutants, FKBP51, and FKBP52 were expressed in *E. coli* BL21 (DE3) cells. Liter cultures of terrific broth were grown at 37 °C until an OD_{600} of 0.6. Cultures were

cooled to 18 °C before induction with IPTG (final concentration of 500 µM) and then grown overnight. For protein purification, cell pellets were lysed and first purified using the batch Ni-NTA His-Bind resin protocol described above. The N-terminal His-tag was then removed using TEV protease. The sample was then further purified by size exclusion chromatography using a prep grade XK 16/100 Superdex 200 column (GE Healthcare Life Sciences) in a 50 mM HEPES, 10 mM NaCl, pH 7.4 buffer. Human HIP was purified using previously described methods [65].

The human TPR protein DNAJC7 was expressed in *E. coli* BL21 (DE3) cells. Liter cultures of terrific broth were grown at 37 °C until an OD_{600} of 0.6 was reached. Cultures were then cooled to 18 °C before induction with IPTG (500 µM) and then grown overnight. Cell pellets were re-suspended in DNAJC7 His-binding buffer (50 mM TRIS, 10 mM Imidazole, 750 mM NaCl, pH 8) supplemented with protease inhibitors. Cells were lysed by sonication, subjected to centrifugation, and the supernatant was then applied to Ni-NTA His-Bind Resin (Novagen, Darmstadt, Germany). The resin was washed with the DNAJC7 His-binding buffer, followed by an extensive wash with DNAJC7 His-washing buffer 1 (50 mM TRIS, 30 mM Imidazole, 750 mM NaCl, 3% ethanol, pH 8). The resin was washed a third time with DNAJC7 His-washing buffer 2 (50 mM TRIS, 30 mM Imidazole, 100 mM NaCl, 3% ethanol, pH 8). Finally, the protein was then removed from the resin with the His-elution buffer (50 mM TRIS, 300 mM Imidazole, 300 mM NaCl, pH 8). The purified protein was concentrated and exchanged into a 50 mM TRIS, 300 mM NaCl, pH 7.4 buffer for storage. Note that the N-terminal His-tag was not removed.

2.5.3 Preparation of apo Hsp70 protein

Hsp70 protein was made apo (*e.g.* nucleotide free) using extensive dialysis in 3 mL cassettes (catalog number = 66330, Life Technologies). First, the protein was dialyzed into 25 mM HEPES, 10 mM KCl, 5 mM EDTA, pH 7.5 at 4 °C for two days. Next, it was dialyzed into 25 mM HEPES, 10 mM KCl, pH 7.5 at 4 °C for another two days and then stored at -80 °C. Fresh buffers were made daily.

2.5.4 Fluorescence polarization assays

2.5.4.1 General procedures

All Experiments were performed in 384-well, black, low volume, round-bottom plates (catalog number = 4511, Corning, NY). Polarization values in millipolarization units (mP) were measured at an excitation wavelength at 485 nm and an emission wavelength at 530 nm using a Molecular Devices Spectramax M5 plate reader (Sunnyvale, CA). For binding experiments, equilibrium-binding isotherms were constructed by plotting FP readings as a function of the protein concentration at a fixed concentration of a tracer. All experiments were performed at least twice in triplicate. Results are shown as the average and standard error of the mean (SEM). All experimental data were analyzed using GraphPad Prism 6 software.

2.5.4.2 TPR co-chaperones binding to Hsp70/90 C-terminal probes

Fluorescent C-terminal Hsp70 and Hsp90 peptides were custom ordered from GenScript (Piscataway, NJ) and designed to have an N-terminal 5-Carboxyfluorescein (5-Fam) via a 6-

carbon spacer (aminohexanoic acid). These probes were stored as 5 mM DMSO stocks at -30 °C. Before use, the tracer solutions were diluted in the assay buffer (50 mM HEPES, 10 mM NaCl, 0.01% Triton X-100, pH 7.4 or 9.4) to a working concentration of 0.1 µM. Note that 5-Fam (pK_a ~6.4) has pH-sensitive fluorescence, so no binding experiments were performed at low pH values. To each well was added 16 µL of a TPR co-chaperone (CHIP, Hop, DNAJC7, FKBP51, FKBP52, or HIP) from a 2-fold dilution series made using the assay buffer. Final concentrations of protein ranged from 0 to 125 µM. Next, 4 µL of a 0.1 µM 5-Fam-labeled C-terminal Hsp70/90 peptide was added to each well, to give a final concentration of 20 nM and a total assay volume of 20 µL. The plate was covered from light and allowed to incubate at room temperature for 30 minutes, which was determined to be at equilibrium.

2.5.4.3 FP competition experiment with C-terminal Hsp70/90 probes

I also determined the ability of full length Hsp72 or Hsp72ΔEEVD to compete with the C-terminal Hsp72 probe (5Fam-GSGPTIEEVD) for binding to a TPR protein (CHIP, Hop, or DNAJC7). First, 6 µL of a TPR co-chaperone was added to each well (final concentration: CHIP = 0.5 µM, Hop = 2.5 µM, or DnaJC7 = 2.5 µM). This amount equals the concentration of the TPR co-chaperone at which 50% of the FP probe (5Fam-GSGPTIEEVD) is bound, based on binding experiments. Next, 10 µL of Hsp72 or Hsp72ΔEEVD from a 2-fold dilution made using the assay buffer (50 mM HEPES, 10 mM NaCl, 0.01% Triton X-100, pH 7.4) was added. Final concentrations of Hsp72/Hsp72ΔEEVD ranged from 0 to 40 µM. Finally, 4 µL of a 0.1 µM 5Fam-GSGPTIEEVD was added to each well, to give a final concentration of 20

nM and a total assay volume of 20 µL. The plate was covered from light and allowed to incubate at room temperature for 30 minutes.

2.5.4.4 Binding of a fluorescent ATP analog to Hsp72/Hsp72ΔEEVD

The fluorescent ATP analog, Fam-ATP (N^6-(6-Amino)hexyl-ATP-5Fam), was purchased from Jena Bioscience (catalog number = NU-805-5FM, Jena, Germany). To a plate, was added 10 µL of a 2-fold dilution series of protein (Hsp72 or Hsp72ΔEEVD). Dilution series were made using the assay buffer (100 mM TRIS, 20 mM KCl, 6 mM $MgCl_2$, 0.001% Triton X-100, pH 7.4). Final concentrations of proteins ranged from 0 to 25 µM. Apo (nucleotide free) Hsp72/Hsp72ΔEEVD must be used in order to achieve substantial and reproducible binding to the Fam-ATP probe. Next, 6 µL of a 3.3 mM solution of ATP or ADP was added to each well, to give a final concentration 1 mM. Finally, 4 µL of a 0.1 µM Fam-ATP was added to each well, to give a final concentration of 20 nM and a total assay volume of 20 µL. The plate was allowed to incubate at room temperature covered from light for 30 minutes.

2.5.4.5 FP competition experiment with Fam-ATP

I also determined the ability of unlabeled ATP to compete with the Fam-ATP probe for binding to Hsp72/Hsp72ΔEEVD. First, apo Hsp72 or Hsp72ΔEEVD was added to each well to give a final concentration 0.5 µM. This amount equals the concentration of Hsp72/Hsp72ΔEEVD at which 50% of the FP probe (Fam-ATP) is bound based on binding experiments. Next, a 2-fold dilution of ATP made using the assay buffer (100 mM TRIS, 20 mM KCl, 6 mM $MgCl_2$, 0.001% Triton X-100, pH 7.4). Final concentrations of ATP ranged

from 0 to 300 µM. Finally, Fam-ATP was added to each well, to give a final concentration of 20 nM and a total assay volume of 20 µL. The plate was covered from light and allowed to incubate at room temperature for 30 minutes in order to reach equilibrium.

2.5.4.6 Binding of Fam-HLA substrate to Hsp72/Hsp72ΔEEVD

HLA substrate FP probe was custom ordered form the University of Michigan Proteomics & Peptide Synthesis Core. This probe was designed to have a 5-Fam N-terminal of the following sequence: RENLRIALRY. This probe the stored as 5 mM DMSO stocks at -30 °C. Before use, probes were diluted in the assay buffer (100 mM TRIS, 20 mM KCl, 6 mM $MgCl_2$, 0.001% Triton X-100, pH 7.4) to a working concentration of 0.1 µM. To a plate, was added 10 µL of a 2-fold dilution series of protein (Hsp72, Hsp72ΔEEVD, or CHIP). Dilution series were made using the assay buffer. Final concentrations of the protein ranged from 0 to 25 µM. Apo (nucleotide free) Hsp72/Hsp72ΔEEVD must be used in order achieve substantial and reproducible binding to the Fam-HLA probe. Next, 6 µL of a 3.3 mM solution of ATP or ADP was added to each well, to give a final concentration 1 mM. Finally, 4 µL of a 0.1 µM Fam-HLA was added to each well, to give a final concentration of 20 nM and a total assay volume of 20 µL. The plate was allowed to incubate at room temperature covered from light for 1 hour.

Notes

This chapter has be submitted for publication as “Specific binding of tetratricopeptide repeat (TPR) proteins to heat shock protein 70 (Hsp70) and heat shock protein 90 (Hsp90)

is regulated by affinity and phosphorylation" to *Biochemistry.* Victoria A. Assimon and Jason E. Gestwicki designed the experiments. Victoria A. Assimon conducted all experiments. We thank Dr. Daniel R. Southworth (University of Michigan) for his generous gift of CHIP, Hop, FKBP51, and FKBP52 expression vectors. We would also like to thank Dr. Yoichi Osawa (University of Michigan) for his generous gift of the Hip expression vector.

2.6 Appendix

2.6.1 Hsp72ΔEEVD is able to engage with nucleotide and substrate

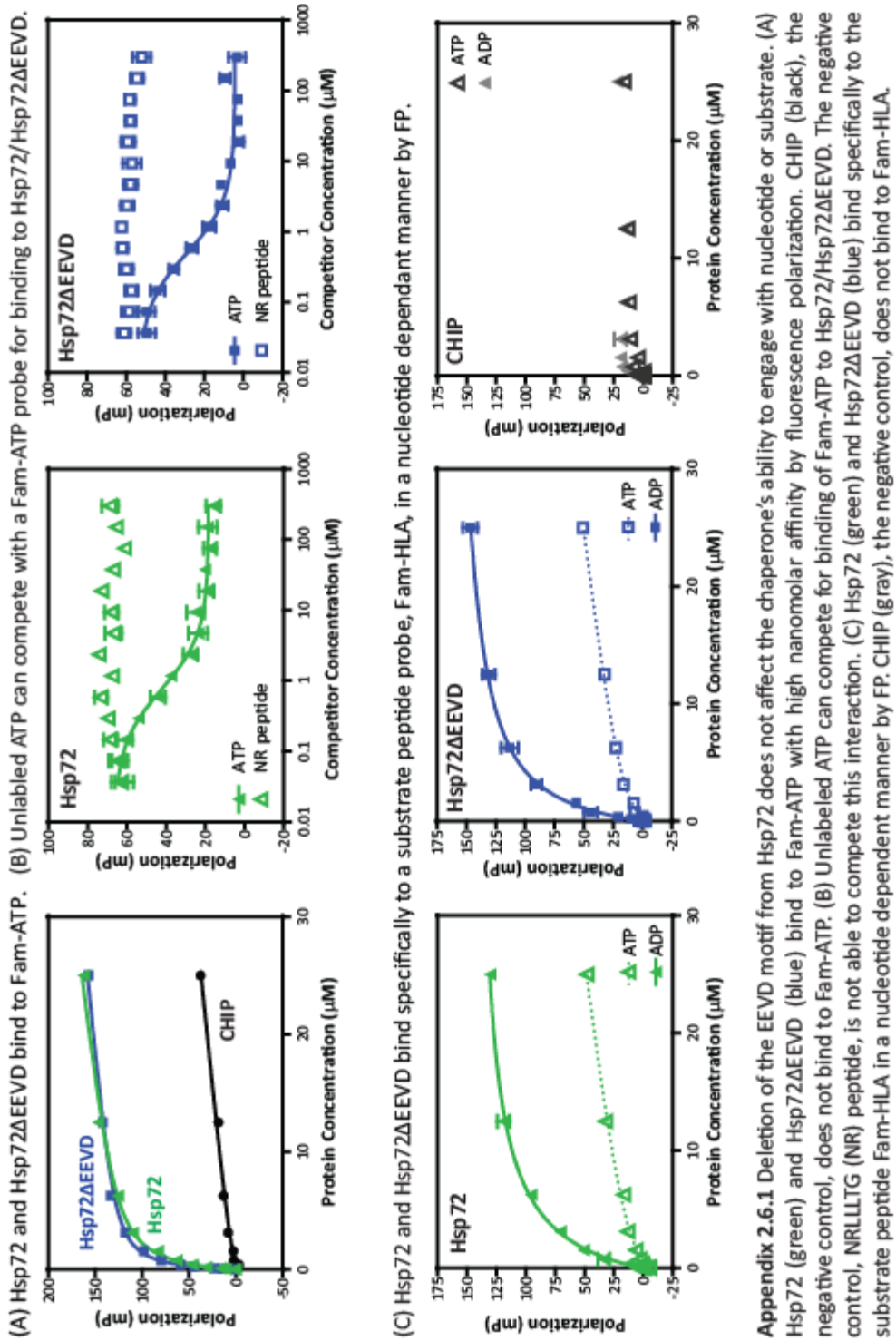

Appendix 2.6.1 Deletion of the EEVD motif from Hsp72 does not affect the chaperone's ability to engage with nucleotide or substrate. (A) Hsp72 (green) and Hsp72ΔEEVD (blue) bind to Fam-ATP with high nanomolar affinity by fluorescence polarization. CHIP (black), the negative control, does not bind to Fam-ATP. (B) Unlabeled ATP can compete for binding of Fam-ATP to Hsp72/Hsp72ΔEEVD. The negative control, NRLLLTG (NR) peptide, is not able to compete this interaction. (C) Hsp72 (green) and Hsp72ΔEEVD (blue) bind specifically to the substrate peptide Fam-HLA in a nucleotide dependent manner by FP. CHIP (gray), the negative control, does not bind to Fam-HLA.

2.6.2 The binding of Hsp70 to TPR co-chaperones is mediated by Hsp70's EEVD motif

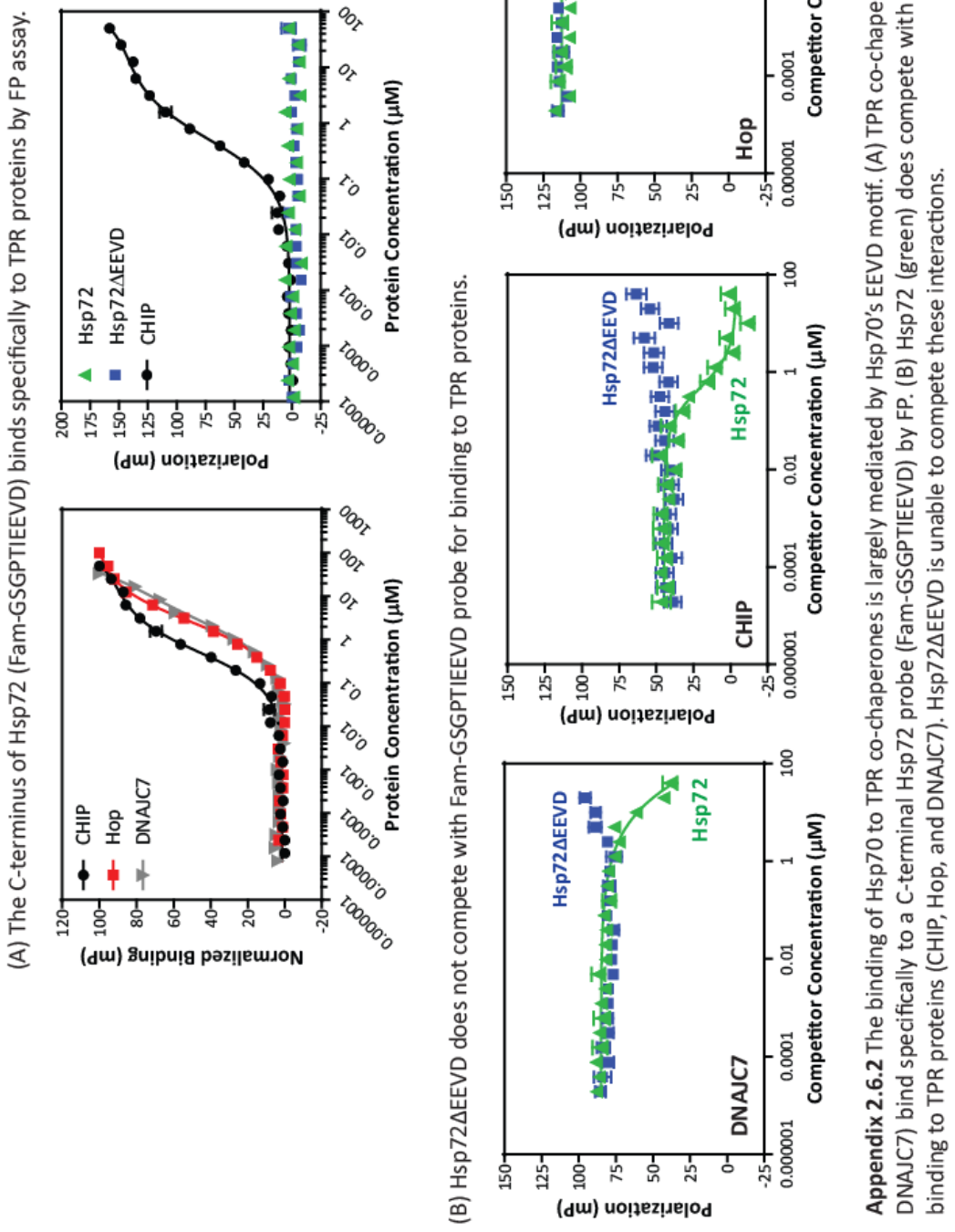

Appendix 2.6.2 The binding of Hsp70 to TPR co-chaperones is largely mediated by Hsp70's EEVD motif. (A) TPR co-chaperones (CHIP, Hop, and DNAJC7) bind specifically to a C-terminal Hsp72 probe (Fam-GSGPTIEEVD) by FP. (B) Hsp72 (green) does compete with Fam-GSGPTIEEVD for binding to TPR proteins (CHIP, Hop, and DNAJC7). Hsp72ΔEEVD is unable to compete these interactions.

2.6.3 TPR co-chaperones differentially interact with the C-termini of cytosolic Hsp70s/90s

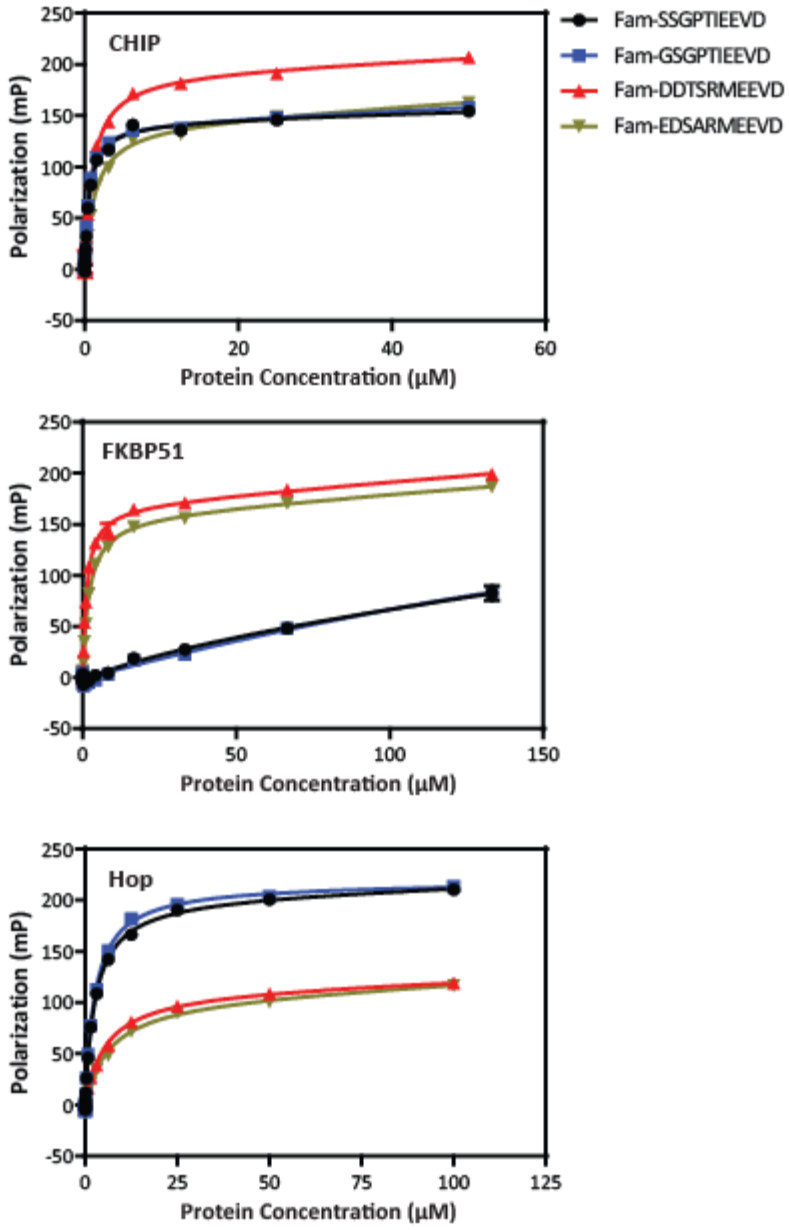

Appendix 2.6.3 TPR co-chaperones differentially interact with the C-termini of cytosolic Hsp70s and Hsp90s. Binding curves are shown for the following TPR co-chaperones: CHIP, FKBP51, and Hop. Affinities were measured by FP using C-terminal Hsp70/90 peptide probes and full length TPR proteins. These experiments were performed at least twice in triplicate. Results are shown as the average and SEM.

2.6.4 The orientation of the EEVD is important for the interaction between TPR co-chaperones and the C-termini of Hsp70/90

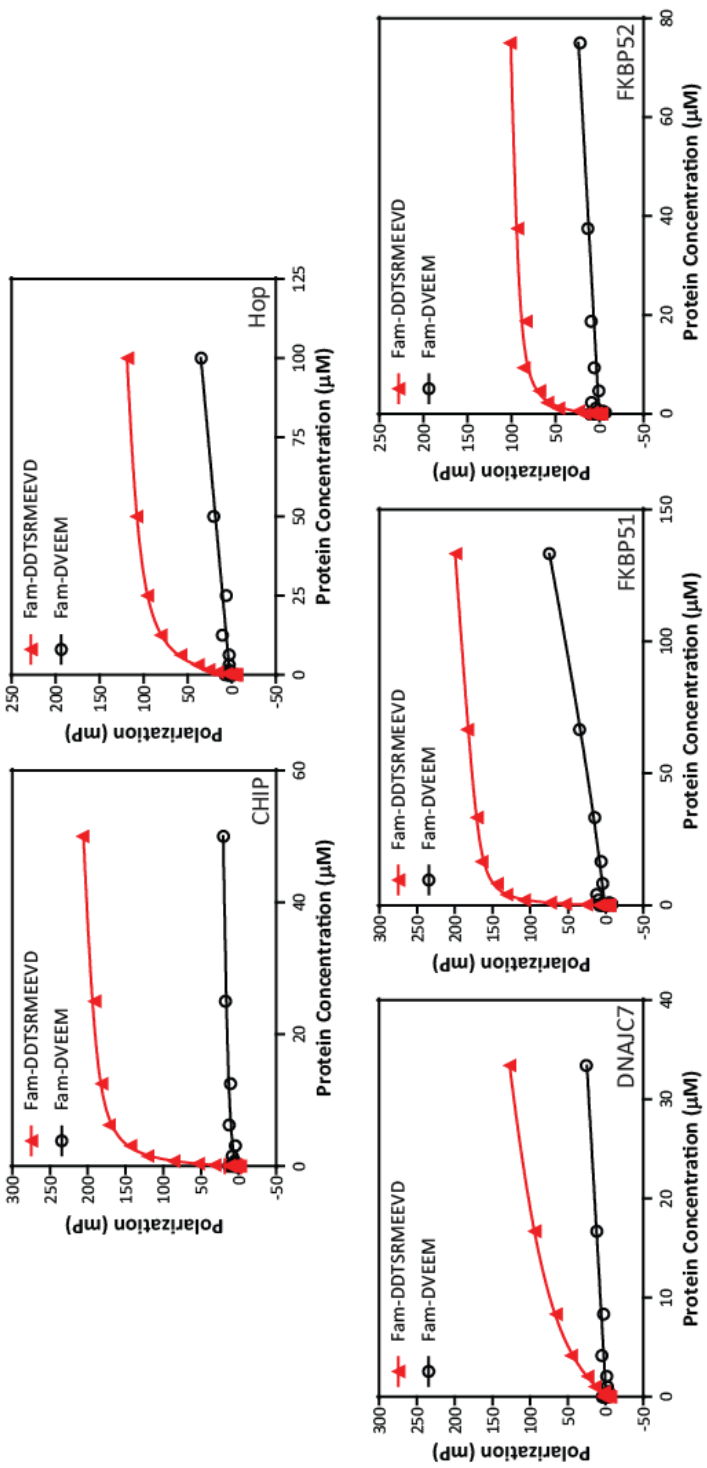

Appendix 2.6.4 The orientation of the EEVD is important for the interaction between TPR co-chaperones and the C-termini of Hsp70/90. The reverse C-terminal peptide FP probe, Fam-DVEEM, has no affinity for TPR co-chaperones. These experiments were performed at least twice in triplicate. Results are shown as the average and SEM.

2.6.5 The Ile of the C-terminus Hsp70 (GSGPTIEEVD) and the Met of the C-terminus Hsp90α (DDTSRMEEVD) strongly influence binding preferences of TPR co-chaperones

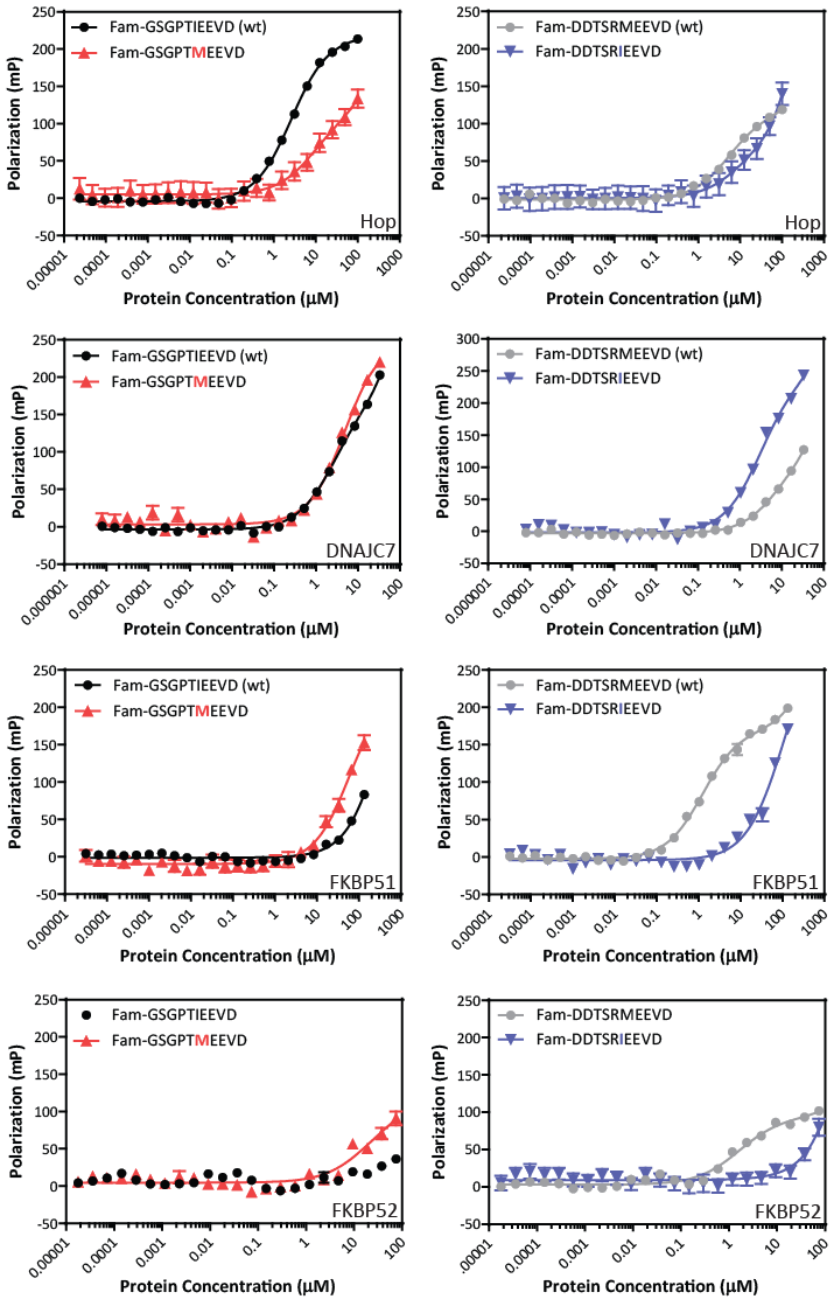

Appendix 2.6.5 The Ile residue of the C-terminus Hsp70 (GSGPTIEEVD) and the Met residue of the C-terminus Hsp90α (DDTSRMEEVD) strongly influence binding preferences of TPR co-chaperones. The binding curves of TPR co-chaperones (Hop, DNAJC7, FKBP51, and FKBP52) to C-terminal mutant Hsp70 (Fam- GSGPTMEEVD) and Hsp90 (Fam-DDTSRIEEVD) FP probes are shown. Affinities were measured by FP using full length TPR proteins. These experiments were performed at least twice in triplicate. Results are shown as the average and SEM.

2.6.6 The binding of TPR co-chaperones to Hsp70/90 involves polar contacts

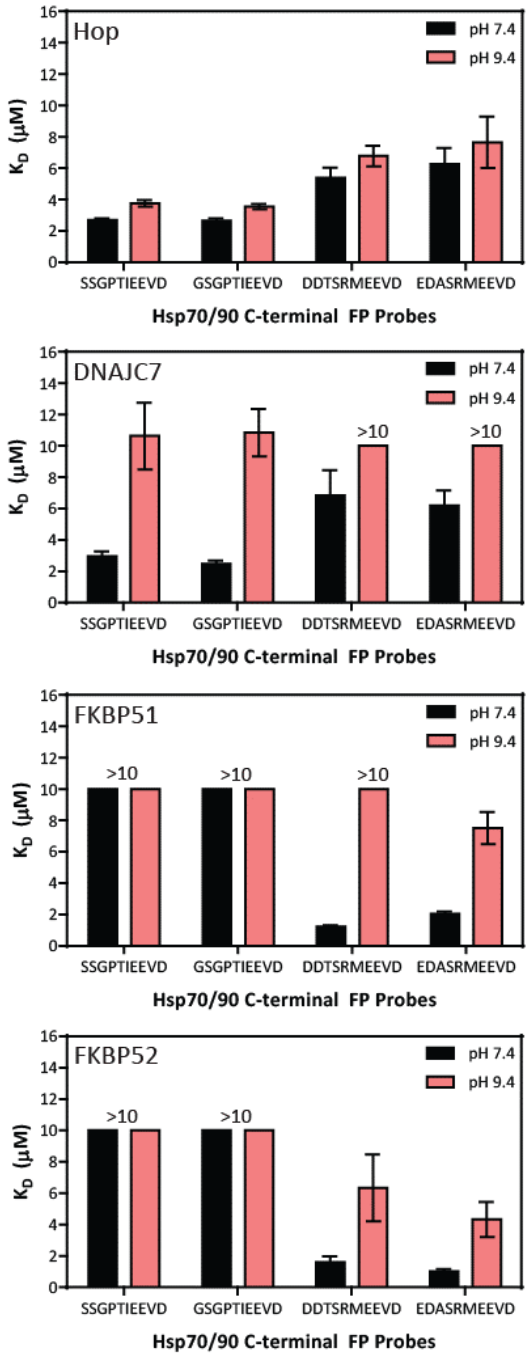

Appendix 2.6.6 The binding of TPR co-chaperones to Hsp70/90 involves polar contacts in the EEVD motif. Consistent with the role of this polar interaction, the binding of TPR co-chaperones to C-termini of Hsp70s and Hsp90s is pH dependent. The binding affinities of TPR co-chaperones (Hop, DNAJC7, FKBP51, and FKBP52) for Hsp70/90 C-terminal FP probes at pH 7.4 and 9.4 are shown. These experiments were performed at least twice in triplicate. Results are shown as the average and SEM.

2.6.7 Hop's TPR1 and TPR2A domains selectively interact with the C-termini of Hsp70 and Hsp90, respectively

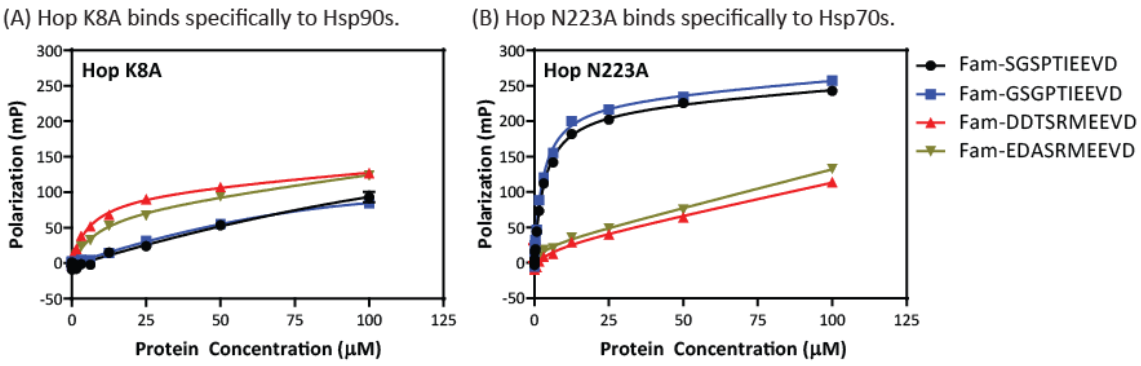

Appendix 2.6.7 Binding of Hop mutants (K8A and N223A) to Hsp70/90 C-termini by FP. All experiments were performed at least twice in triplicate. Results are shown as the average and SEM.

2.7 References

1. Kundrat, L. and L. Regan, *Balance between folding and degradation for Hsp90-dependent client proteins: a key role for CHIP.* Biochemistry, 2010. **49**(35): p. 7428-38.
2. Chiang, H.L., et al., *A Role for a 70-Kilodaton Heat-Shock Protein in Lysosomal Degradation of Intracellular Proteins.* Science, 1989. **246**(4928): p. 382-385.
3. Bercovich, B., et al., *Ubiquitin-dependent degradation of certain protein substrates in vitro requires the molecular chaperone Hsc70.* Journal of Biological Chemistry, 1997. **272**(14): p. 9002-9010.
4. Bukau, B., J. Weissman, and A. Horwich, *Molecular chaperones and protein quality control.* Cell, 2006. **125**(3): p. 443-51.
5. Hartl, F.U. and M. Hayer-Hartl, *Protein folding - Molecular chaperones in the cytosol: from nascent chain to folded protein.* Science, 2002. **295**(5561): p. 1852-1858.
6. Young, J.C., et al., *Pathways of chaperone-mediated protein folding in the cytosol.* Nature Reviews Molecular Cell Biology, 2004. **5**(10): p. 781-791.
7. Hohfeld, J., D.M. Cyr, and C. Patterson, *From the cradle to the grave: molecular chaperones that may choose between folding and degradation.* Embo Reports, 2001. **2**(10): p. 885-890.
8. Gong, M. and N. Hubner, *Molecular genetics of human hypertension.* Clinical Science, 2006. **110**(3): p. 315-326.
9. Cummings, C.J., et al., *Over-expression of inducible HSP70 chaperone suppresses neuropathology and improves motor function in SCA1 mice.* Human Molecular Genetics, 2001. **10**(14): p. 1511-1518.
10. Warrick, J.M., et al., *Suppression of polyglutamine-mediated neurodegeneration in Drosophila by the molecular chaperone HSP70.* Nature Genetics, 1999. **23**(4): p. 425-428.
11. Yaglom, J.A., V.L. Gabai, and M.Y. Sherman, *High levels of heat shock protein Hsp72 in cancer cells suppress default senescence pathways.* Cancer Research, 2007. **67**(5): p. 2373-2381.
12. Neckers, L., E. Mimnaugh, and T.W. Schulte, *Hsp90 as an anti-cancer target.* Drug Resistance Updates, 1999. **2**(3): p. 165-172.
13. Waza, M., et al., *Modulation of Hsp90 function in neurodegenerative disorders: a molecular-targeted therapy against disease-causing protein.* Journal of Molecular Medicine-Jmm, 2006. **84**(8): p. 635-646.
14. D'Andrea, L.D. and L. Regan, *TPR proteins: the versatile helix.* Trends in Biochemical Sciences, 2003. **28**(12): p. 655-662.
15. Nicolet, C.M. and E.A. Craig, *Isolation and Characterization of Sti1, a Stress-Inducible Gene from Saccharomyces-Cerevisiae.* Molecular and Cellular Biology, 1989. **9**(9): p. 3638-3646.

16. Smith, D.F., et al., *Identification of a 60-Kilodalton Stress-Related Protein, P60, Which Interacts with Hsp90 and Hsp70.* Molecular and Cellular Biology, 1993. **13**(2): p. 869-876.
17. Ballinger, C.A., et al., *Identification of CHIP, a novel tetratricopeptide repeat-containing protein that interacts with heat shock proteins and negatively regulates chaperone functions.* Molecular and Cellular Biology, 1999. **19**(6): p. 4535-4545.
18. Ballinger, C.A., et al., *Identification of CHIP, a novel striated muscle-restricted TPR-containing protein that negatively regulates chaperone functions.* Faseb Journal, 1999. **13**(4): p. A442-A442.
19. Hernandez, M.P., W.P. Sullivan, and D.O. Toft, *The assembly and intermolecular properties of the hsp70-Hop-hsp90 molecular chaperone complex.* Journal of Biological Chemistry, 2002. **277**(41): p. 38294-38304.
20. Johnson, B.D., et al., *Hop modulates hsp70/hsp90 interactions in protein folding.* Journal of Biological Chemistry, 1998. **273**(6): p. 3679-3686.
21. Chen, S.Y. and D.F. Smith, *Hop as an adaptor in the heat shock protein 70 (Hsp70) and Hsp90 chaperone machinery.* Journal of Biological Chemistry, 1998. **273**(52): p. 35194-35200.
22. Morishima, Y., et al., *Stepwise assembly of a glucocorticoid receptor center dot hsp90 heterocomplex resolves two sequential ATP-dependent events involving first hsp70 and then hsp90 in opening of the steroid binding pocket.* Journal of Biological Chemistry, 2000. **275**(24): p. 18054-18060.
23. Hutchison, K.A., et al., *Proof That Hsp70 Is Required for Assembly of the Glucocorticoid Receptor into a Heterocomplex with Hsp90.* Journal of Biological Chemistry, 1994. **269**(7): p. 5043-5049.
24. Smith, D.F., *Dynamics of Heat-Shock Protein 90-Progesterone Receptor-Binding and the Disactivation Loop Model for Steroid-Receptor Complexes.* Molecular Endocrinology, 1993. **7**(11): p. 1418-1429.
25. Zhang, M.H., et al., *Chaperoned ubiquitylation - Crystal structures of the CHIPU box E3 ubiquitin ligase and a CHIP-Ubc13-Uev1a complex.* Molecular Cell, 2005. **20**(4): p. 525-538.
26. Connell, P., et al., *The co-chaperone CHIP regulates protein triage decisions mediated by heat-shock proteins.* Nature Cell Biology, 2001. **3**(1): p. 93-96.
27. Qian, S.B., et al., *CHIP-mediated stress recovery by sequential ubiquitination of substrates and Hsp70.* Nature, 2006. **440**(7083): p. 551-555.
28. Davies, T.H., Y.M. Ning, and E.R. Sanchez, *A new first step in activation of steroid receptors - Hormone-induced switching of FKBP51 and FKBP52 immunophilins.* Journal of Biological Chemistry, 2002. **277**(7): p. 4597-4600.
29. Jaaskelainen, T., H. Makkonen, and J.J. Palvimo, *Steroid up-regulation of FKBP51 and its role in hormone signaling.* Current Opinion in Pharmacology, 2011. **11**(4): p. 326-331.
30. Riggs, D.L., et al., *Noncatalytic role of the FKBP52 peptidyl-prolyl isomerase domain in the regulation of steroid hormone signaling.* Molecular and Cellular Biology, 2007. **27**(24): p. 8658-8669.

31. Brychzy, A., et al., *Cofactor Tpr2 combines two TPR domains and a J domain to regulate the Hsp70/Hsp90 chaperone system.* Embo Journal, 2003. **22**(14): p. 3613-3623.
32. Moffatt, N.S.C., et al., *Role of the cochaperone Tpr2 in Hsp90 chaperoning.* Biochemistry, 2008. **47**(31): p. 8203-8213.
33. Russell, L.C., et al., *Identification of conserved residues required for the binding of a tetratricopeptide repeat domain to heat shock protein 90.* Journal of Biological Chemistry, 1999. **274**(29): p. 20060-20063.
34. Carrello, A., et al., *The common tetratricopeptide repeat acceptor site for steroid receptor-associated immunophilins and Hop is located in the dimerization domain of hsp90.* Journal of Biological Chemistry, 1999. **274**(5): p. 2682-2689.
35. Scheufler, C., et al., *Structure of TPR domain-peptide complexes: critical elements in the assembly of the Hsp70-Hsp90 multichaperone machine.* Cell, 2000. **101**(2): p. 199-210.
36. Southworth, D.R. and D.A. Agard, *Client-Loading Conformation of the Hsp90 Molecular Chaperone Revealed in the Cryo-EM Structure of the Human Hsp90:Hop Complex.* Molecular Cell, 2011. **42**(6): p. 771-781.
37. Kirschke, E., et al., *Glucocorticoid receptor function regulated by coordinated action of the Hsp90 and Hsp70 chaperone cycles.* Cell, 2014. **157**(7): p. 1685-97.
38. Cliff, M.J., et al., *Conformational diversity in the TPR domain-mediated interaction of protein phosphatase 5 with Hsp90.* Structure, 2006. **14**(3): p. 415-426.
39. Connarn, J.N., et al., *The Molecular Chaperone Hsp70 Activates Protein Phosphatase 5 (PP5) by Binding the Tetratricopeptide Repeat (TPR) Domain.* Journal of Biological Chemistry, 2014. **289**(5): p. 2908-2917.
40. Wang, L., et al., *Molecular Mechanism of the Negative Regulation of Smad1/5 Protein by Carboxyl Terminus of Hsc70-interacting Protein (CHIP).* Journal of Biological Chemistry, 2011. **286**(18).
41. Smith, M.C., et al., *The E3 Ubiquitin Ligase CHIP and the Molecular Chaperone Hsc70 Form a Dynamic, Tethered Complex.* Biochemistry, 2013. **52**(32): p. 5354-5364.
42. Zhang, H.Q., et al., *A Bipartite Interaction between Hsp70 and CHIP Regulates Ubiquitination of Chaperoned Client Proteins.* Structure, 2015. **23**(3): p. 472-482.
43. Kundrat, L. and L. Regan, *Identification of Residues on Hsp70 and Hsp90 Ubiquitinated by the Cochaperone CHIP.* Journal of Molecular Biology, 2010. **395**(3): p. 587-594.
44. Wu, B.L., et al., *3D structure of human FK506-binding protein 52: Implications for the assembly of the glucocorticoid receptor/Hsp90/immunophilin heterocomplex.* Proceedings of the National Academy of Sciences of the United States of America, 2004. **101**(22): p. 8348-8353.
45. Carrigan, P.E., et al., *Multiple domains of the co-chaperone Hop are important for Hsp70 binding.* Journal of Biological Chemistry, 2004. **279**(16): p. 16185-16193.
46. Brinker, A., et al., *Ligand discrimination by TPR domains - Relevance and selectivity of EEVD-recognition in Hsp70 center dot Hop center dot Hsp90 complexes.* Journal of Biological Chemistry, 2002. **277**(22): p. 19265-19275.

47. Cheung-Flynn, J., et al., *C-terminal sequences outside the tetratricopeptide repeat domain of FKBP51 and FKBP52 cause differential binding to hsp90.* Journal of Biological Chemistry, 2003. **278**(19): p. 17388-17394.
48. Chen, S.Y., et al., *Differential interactions of p23 and the TPR-containing proteins Hop, Cyp40, FKBP52 and FKBP51 with Hsp90 mutants.* Cell Stress & Chaperones, 1998. **3**(2): p. 118-129.
49. Li, Z., F.U. Hartl, and A. Bracher, *Structure and function of Hip, an attenuator of the Hsp70 chaperone cycle.* Nature Structural & Molecular Biology, 2013. **20**(8): p. 929-+.
50. Sinars, C.R., et al., *Structure of the large FK506-binding protein FKBP51, an Hsp90-binding protein and a component of steroid receptor complexes.* Proceedings of the National Academy of Sciences of the United States of America, 2003. **100**(3): p. 868-873.
51. Muller, P., et al., *C-terminal phosphorylation of Hsp70 and Hsp90 regulates alternate binding to co-chaperones CHIP and HOP to determine cellular protein folding/degradation balances.* Oncogene, 2013. **32**(25): p. 3101-3110.
52. Patel, P.D., et al., *Paralog-selective Hsp90 inhibitors define tumor-specific regulation of HER2.* Nature Chemical Biology, 2013. **9**(11): p. 677-+.
53. Fontaine, S.N., et al., *Isoform-selective Genetic Inhibition of Constitutive Cytosolic Hsp70 Activity Promotes Client Tau Degradation Using an Altered Co-chaperone Complement.* Journal of Biological Chemistry, 2015. **290**(21): p. 13115-13127.
54. Jinwal, U.K., et al., *Imbalance of Hsp70 family variants fosters tau accumulation.* Faseb Journal, 2013. **27**(4): p. 1450-1459.
55. Heine, H., et al., *Bacterial lipopolysaccharide induces expression of the stress response genes hop and H411.* J Biol Chem, 1999. **274**(30): p. 21049-55.
56. Yi, F. and L. Regan, *A Novel Class of Small Molecule Inhibitors of Hsp90.* Acs Chemical Biology, 2008. **3**(10): p. 645-654.
57. Zhang, T., et al., *A novel Hsp90 inhibitor to disrupt Hsp90/Cdc37 complex against pancreatic cancer cells.* Molecular Cancer Therapeutics, 2008. **7**(1): p. 162-170.
58. Pimienta, G., K.M. Herbert, and L. Regan, *A Compound That Inhibits the HOP-Hsp90 Complex Formation and Has Unique Killing Effects in Breast Cancer Cell Lines.* Molecular Pharmaceutics, 2011. **8**(6): p. 2252-2261.
59. Vasko, R.C., et al., *Mechanistic Studies of Sansalvamide A-Amide: An Allosteric Modulator of Hsp90.* Acs Medicinal Chemistry Letters, 2010. **1**(1): p. 4-8.
60. Ardi, V.C., et al., *Macrocycles That Inhibit the Binding between Heat Shock Protein 90 and TPR-Containing Proteins.* Acs Chemical Biology, 2011. **6**(12): p. 1357-1366.
61. Heemers, H.V. and D.J. Tindall, *Androgen receptor (AR) coregulators: A diversity of functions converging on and regulating the AR transcriptional complex.* Endocrine Reviews, 2007. **28**(7): p. 778-808.
62. Sarkar, S., et al., *Androgen receptor degradation by the E3 ligase CHIP modulates mitotic arrest in prostate cancer cells.* Oncogene, 2014. **33**(1): p. 26-33.
63. Adachi, H., et al., *CHIP overexpression reduces mutant androgen receptor protein and ameliorates phenotypes of the spinal and bulbar muscular atrophy transgenic mouse model.* Journal of Neuroscience, 2007. **27**(19): p. 5115-5126.

64. Thompson, A.D., et al., *Fine-tuning multiprotein complexes using small molecules.* ACS chemical biology, 2012. **7**(8): p. 1311-20.
65. Morishima, Y., et al., *Heme-dependent activation of neuronal nitric oxide synthase by cytosol is due to an Hsp70-dependent, thioredoxin-mediated thiol-disulfide interchange in the heme/substrate binding cleft.* Biochemistry, 2011. **50**(33): p. 7146-56.

Chapter 3

Mutagenesis of Hsp70 reveals a complex and tunable allosteric network: Connecting drug binding sites to function and protein-protein interactions

3.1 Abstract

Hsp70 plays important roles in maintaining the integrity of the proteome and thus, is an emerging target for multiple diseases. In models of neurodegeneration, such as Spinal-Bulbar Muscular Atrophy (SBMA), MKT-077 and its analogs have been shown to bind selectively to an allosteric pocket on Hsp70 and relieve disease phenotypes. However, the molecular mechanism by which these molecules modulate Hsp70's functions has not been fully elucidated. In this chapter, I performed alanine-scanning mutagenesis on MKT-077's binding pocket and studied the effects of these mutations using a host of *in vitro* chaperone assays. I found that mutations within the MKT-077 binding pocket of Hsp70 dysregulate key allosteric networks, which ultimately leads to the trapping of Hsp70 in an ADP-like conformation where it can no longer refold substrates. These findings provide new strategies for how to tune Hsp70's functions in order to treat diseases of protein misfolding.

3.2 Introduction

3.2.1 Allosteric inhibitors as an alternative approach to targeting Hsp70 complexes

As introduced in chapter 1, the molecular chaperone Hsp70 has important roles in maintaining protein homeostasis and it is associated with diseases of protein misfolding. Thus, Hsp70 is considered to be a promising new drug target. The goal of my thesis is to explore ways of safely manipulating this chaperone. Towards that goal I performed a comprehensive study of how TPR co-chaperones interact with Hsp70 (chapter 2). An important conclusion of this study was that it would be very challenging to directly interfere with TPR-Hsp70 interactions using small molecules (*e.g.* orthosteric inhibitors). However, another way to manipulate Hsp70 and its co-chaperones would be to interfere with allostery. As discussed in chapter 1, Hsp70 is a highly allosteric machine and its co-chaperone interactions are allosterically controlled. Indeed, the Gestwicki laboratory has performed multiple, unbiased chemical screens to identify inhibitors of Hsp70 complexes, leading to the identification of molecules that appear to act at allosteric sites [1-4]. Additionally, we have validated and optimized compounds, based on the rhodacyanine dye MKT-077, that are known to interact with an allosteric site on Hsp70. The goal of this chapter is to understand the mechanism of these molecules and to explore how they might tune functions of Hsp70 complexes.

3.2.2 Allosteric inhibitors of Hsp70 have promising activity in models of neurodegeneration

Work by the Gestwicki laboratory and its collaborators has suggested that MKT-077 analogs have promise for the treatment of multiple diseases. For example, in collaboration with Chad A. Dickey (University of South Florida), we demonstrated that an MKT-077 analog, YM-1, reduced the accumulation of microtubule-binding protein tau (MAPT) and

rescued long-term potentiation (LTP) deficits in hippocampal slices from a mouse model of Alzheimer's disease (rTg4510 mice) [5]. Additionally, Andrew P. Lieberman's group (University of Michigan) found that YM-1 treatment reduced the accumulation of polyglutamine-expanded androgen receptor (polyQ-AR) in cellular and *Drosophila melanogaster* models SBMA [6]. In both cases, the activity of YM-1 was dependent on Hsp70, illustrating that this chaperone is a major cellular target. Taken together, these data suggest that YM-1 and more recent analogs might serve as potential drug leads [7, 8]. The emergence of these molecules also presented a unique opportunity for my thesis work. Specifically, these molecules could provide a blueprint for how to target Hsp70 complexes. In other words, I wanted to use MKT-077 molecules to understand how allostery controls chaperone functions in the Hsp70 system.

3.2.3 ATP hydrolysis involves critical allostery between Hsp70's domains

Allosteric networks span both domains of Hsp70. As previously discussed in chapter 1, Hsp70 consists of two domains, a nucleotide binding domain (NBD) and substrate binding domain (SBD). These domains are connected by a short flexible linker [9-11]. The NBD of Hsp70 is further divided into two subdomains, lobes I and II, which are each divided into an "A" and "B" region (**Figure 1.2**). These lobes form a cleft that binds ATP with a nucleotide binding cassette [12]. Hsp70's SBD is composed of a β-sandwich subdomain with a hydrophobic groove for polypeptide binding and an α-helical region which forms a "lid" over the peptide binding site. In the ATP-bound state, Hsp70 has an "open" substrate-binding cleft and a low affinity for substrates. However, conversion to the ADP-bound state

causes the α-helical lid region to "close," increasing Hsp70's affinity for substrates (Figure 1.3) [13]. Thus, ATP hydrolysis involves critical allostery between the NBD and SBD.

3.2.4 Structural and experimental studies reveal allosteric hotspots on Hsp70

A wealth of structural and computational data has provided mechanistic clues that help to explain why transitioning through different nucleotide states affects conformational changes in Hsp70. For example, in collaboration with Heather Carlson (University of Michigan) we performed molecular dynamics simulations of the NBD in its ATP, ADP, and apo forms and found a nucleotide dependent rotation of the IIB subdomain. This movement involved "hinge" residues, such as Hsc70^{G229} (DnaK^{G228}), at the interface of the IIB and IIA subdomains (Figure 3.1) [14]. The motion of this residue, along with its nearby

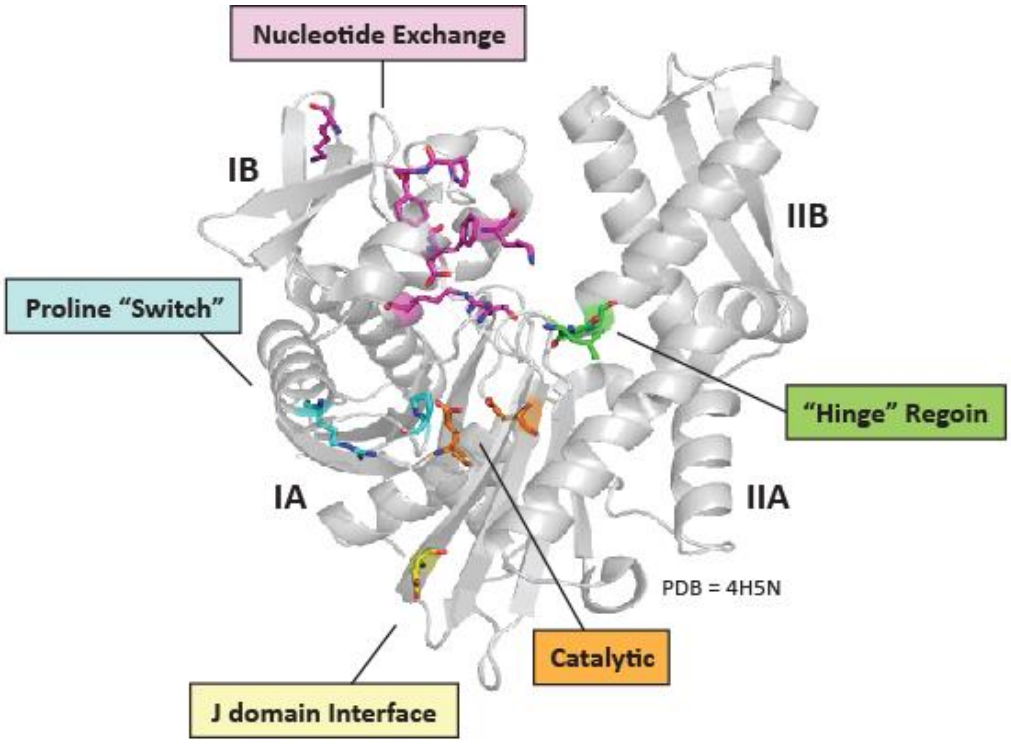

Figure 3.1 Hsp70 has multiple allosteric hotspots in its nucleotide binding domain. The location of various allosteric hotspots on the NBD of Hsp70 are shown. This image was prepared using PyMol.

neighbors, tended to move in coordination during conversion from the ATP- to the ADP(P_i)-bound state. Similarly, highly conserved proline (Hsc70^{P147}/DnaK^{P143}) and arginine (Hsc70^{R155}/DnaK^{R151}) residues are thought to adopt different conformations in response to the nucleotide state of Hsp70 and together act as a "switch" that controls the opening and closing of the SBD (**Figure 3.1**) [15]. Mutations of catalytic residues (Hsc70^{E175}/DnaK^{E171} and Hsc70^{D206}/DnaK^{D201}), located between lobes IA and IIA, have also been shown to impair nucleotide-induced changes in conformation (**Figure 3.1**) [16, 17]. Further, mutating any of these highly conserved allosteric residues disrupts chaperone function. Interestingly, all these residues are located at the interfaces of the lobes (IA, IIA, IB, and IIB) of the NBD. Thus, these studies suggest that nucleotide-dependent conformational changes are controlled by a handful of allosteric networks and that these residues are linked to reorientations of the NBD subdomains [18, 19].

Further insights into the allosteric pathways of Hsp70 come from studies aimed at understanding PPIs with co-chaperones, especially in the prokaryotic DnaK-DnaJ-GrpE system. For example, mutations in the IB subdomain, such as DnaK^{K55}, have been shown to block GrpE binding [20, 21]. Other residues in this region are also thought to be important for modulating nucleotide exchange [20-22] (**Figure 3.1**). Additionally, mutagenesis has been used to study residues on DnaK involved in DnaJ binding, such as DnaK^{E217} [23] (**Figure 3.1**). These mutations have been extensively studied and been shown to impair DnaK's ATPase activity and ability to refold model substrates [22], suggesting that the allosteric networks in Hsp70/DnaK are closely linked to PPIs with co-chaperones.

Finally, the linker region, which connects the NBD and SBD, has been shown to influence long-range allostery between Hsp70's domains. For example, the linker stimulates ATPase activity when present on a truncated NBD construct by binding to a hydrophobic cleft between subdomains IA and IIA [24]. Additionally, mutations in the linker region of DnaK impair DnaJ-stimulated ATP hydrolysis and dysregulate DnaK's ability to release substrate in response to ATP. Taken together, these studies illustrate that there are multiple allosteric hotspots, both within subdomains and between subdomains.

3.2.5 How do allosteric Hsp70 inhibitors work?

Using NMR and computational approaches, Erik R. P. Zuiderweg (University of Michigan), Saurav Misra (Case Western University), and Giorgio Colombo (ICRM, Milano Italy) have all shown that MKT-077 and its analogs interact with an allosteric site on the NBD of Hsp70. This site is located at the interface between lobes IA and IIA, adjacent to, but not overlapping with, the nucleotide pocket (**Figure 3.1**) [25]. Interestingly, MKT-077 only interacted with Hsp70's NBD in its ADP-bound form and not its apo- or ATP-bound states [25, 26]. Molecular dynamics studies suggest that the allosteric site in lobes IA/IIA is only open enough to allow compound binding in the ADP-bound state. Based on this knowledge and the promising activity of the compounds in disease models, I wanted to further probe the mechanism of action (MoA). This goal was important because optimization of the molecules would benefit from additional knowledge of the MoA. The Gestwicki laboratory has developed a battery of biochemical assays (*e.g.* ATP binding, ATP turnover, substrate

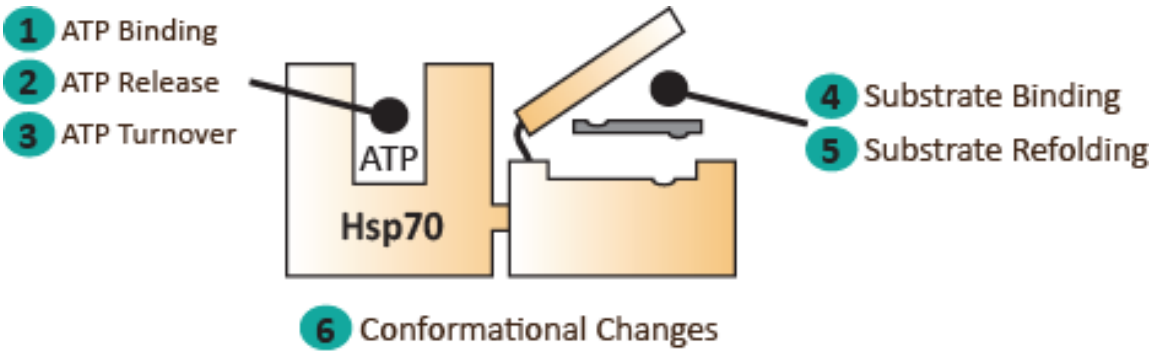

Figure 3.2 Hsp70 has many measureable *in vitro* activities.

binding, substrate refolding, *etc.*) (Figure 3.2) that seemed ideally suited for this type of inquiry. Unfortunately, the fluorescent properties of MKT-077 analogs precluded their use in most of our biochemical assays (data not shown). Thus, an alternative approach was needed to better elucidate MKT-077's MoA.

3.3 Results and discussion

3.3.1 Using mutagenesis to study the mechanism of allosteric Hsp70 inhibitors

To better understand how MKT-077 might regulate the structure and function of Hsp70 complexes, I performed alanine-scanning mutagenesis on MKT-077's binding pocket (Figure 3.3). Protein engineering, particularly alanine-scanning mutagenesis, has proven to be a powerful method for elucidating the protein function, including the discovery of allosteric networks [27]. The strategy that I took was to systematically replace each residue that the Zuiderweg group had identified in NMR titration studies with MKT-077, as discussed above (Figure 3.3). These residues were predicted to contact MKT-077 and to communicate the allosteric effects of compound. Thus, I made the following mutants in full length Hsc70: R76A, Y149A, Y149W, F150A, D206A, T222A, T222M, D225A, T2226A,

H227A, and L228A. The Y149W and T222M mutants were designed to block the binding of MKT-077 molecules to Hsp70. These mutations could be particularly useful (*i.e*. serve as dominant-negatives) in future cellular studies. Each of the mutant proteins expressed in *E. coli* and were purified using the standard wt Hsc70 procedure (Appendix 3.6.1). My strategy was to test each of the mutants in a battery of biochemical tests for chaperone functions, including ATP binding, ATP turnover, co-chaperone interactions, and client refolding (Figure 3.2). As discussed in Chapter 1, Hsp70 structure-function relationships are complex, so I will systematically describe the design and results of each assay and reserve interpretations until all of the parameters are measured. My hypothesis is that some of the residues chosen for mutation might link the MKT-077 binding site to known allosteric networks in Hsp70. Conversely, other residues might be important for binding to MKT-077, but these might not be directly involved in allosteric communication. It is important to

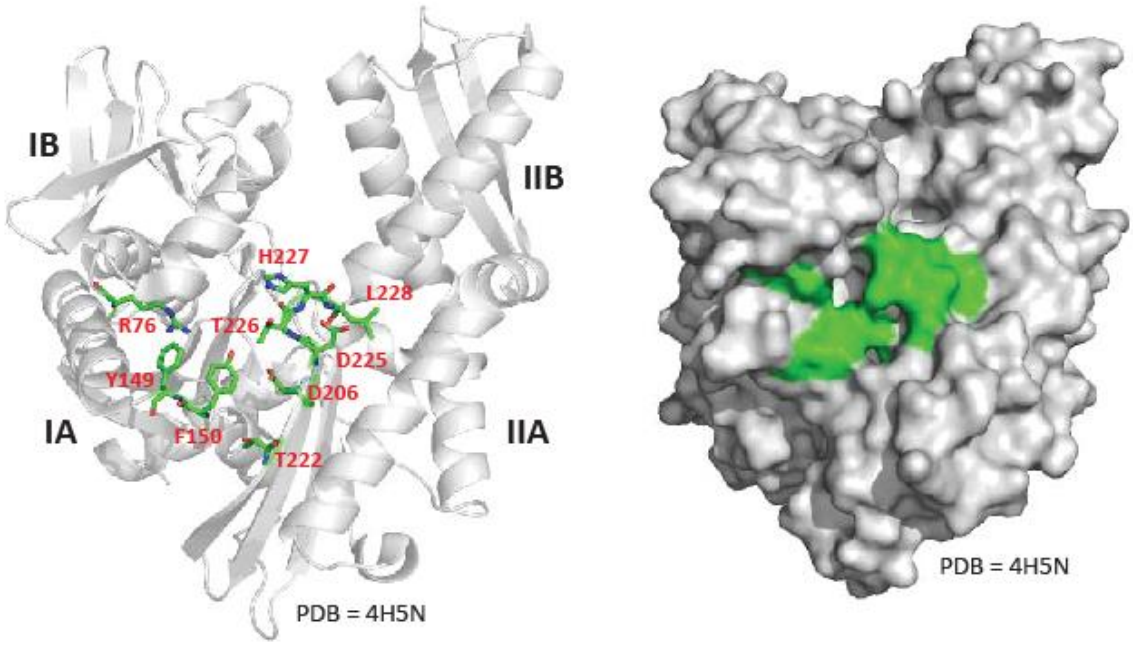

Figure 3.3 The location of Hsp70 MKT-077 binding pocket mutants. The location of mutations in Hsp70 are shown in green. Because the mutations are all present in the NBD, only this domain is shown for clarity (gray). All images were prepared in PyMol.

differentiate between these possibilities, because it could help guide the design of next-generation Hsp70 inhibitors. Further, this approach may reveal a new allosteric network in the Hsp70 system.

3.3.2 Hsc70 mutants bind nucleotide

Using these mutants, I first assessed whether they had normal affinity for nucleotide. I measured this interaction by fluorescence polarization (FP) using a fluorescently labeled ATP analog (Fam-ATP) (**Figure 3.4**). The NBD of wt Hsc70 was used as the positive control and the SBD of wt Hsc70 was used as a negative control (**Figure 3.4A**). Wt Hsc70 bound to the tracer with a K_D of 0.75 ± 0.07 μM and SBD did not bind, as expected. The majority of the Hsc70 mutants had an affinity that was similar to wt Hsc70 (high nanomolar to low micromolar) (**Figure 3.4C** and **Appendix 3.6.2**). Only H227A had a significantly reduced binding affinity (K_D >10μM). Thus, most of the mutants exhibited normal binding to nucleotide. This result is consistent with the location of the MKT-077 binding site, which is not overlapping with ATP-binding residues.

3.3.3 NEFs promote the release of nucleotide from Hsc70 mutants

As discussed is chapter 1, NEFs cause nucleotide dissociation from Hsp70. I next wanted to explore whether my mutations affected NEF activity by measuring the release of nucleotide. Towards this goal, I employed a competitive FP assay that measures release of Fam-ATP in the presence of human NEFs (*i.e.* BAG1, BAG2, or BAG3). We found that a subset of the mutants (D206A, T226A, H227A, and L228A) had a modest dynamic range

(A) The nucleotide binding domain of Hsc70 interacts specifically with Fam-ATP.

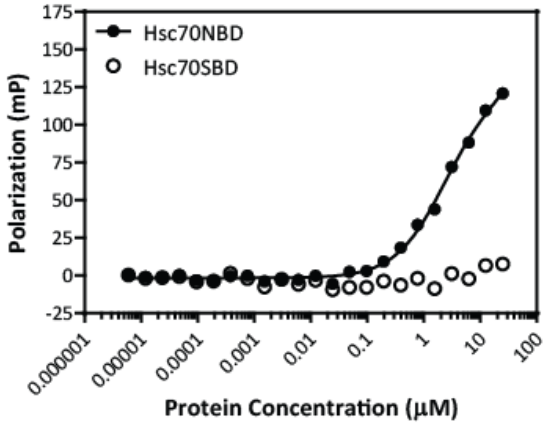

(B) Hsc70 mutants have differential affinities for Fam-ATP.

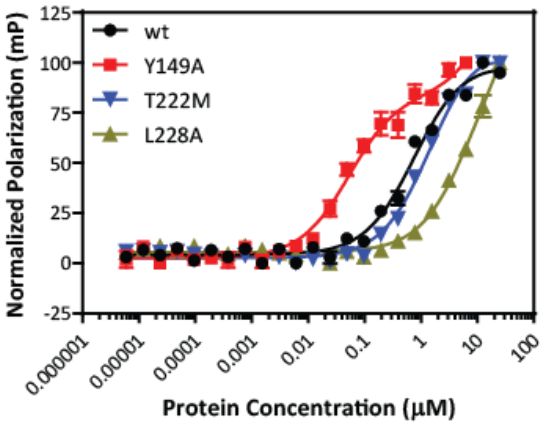

(C) Summary of binding affinities of Hsc70 mutants to Fam-ATP by fluorescence polarization.

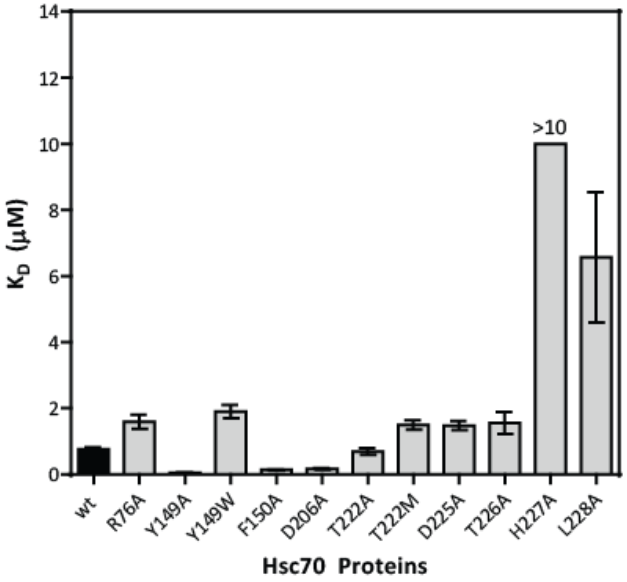

Hsc70 Proteins	K_D (µM)
wt	0.75 ± 0.07
R76A	1.59 ± 0.21
Y149A	0.05 ± 0.01
Y149W	1.90 ± 0.20
F150A	0.14 ± 0.01
D206A	0.17 ± 0.02
T222A	0.69 ± 0.10
T222M	1.50 ± 0.14
D225A	1.48 ± 0.14
T226A	1.55 ± 0.34
H227A	>10
L228A	6.57 ± 1.98

Figure 3.4 Hsc70 MKT-077 binding site mutants can engage with nucleotide. (A) The nucleotide binding domain of Hsc70 (black) binds to Fam-ATP with low micromolar affinity by FP. The substrate binding domain of Hsc70 (white), the negative control, does not bind to Fam-ATP. (B) Hsc70 mutants have differential affinities for Fam-ATP. Representative binding curves are shown for the following proteins: wt Hsc70, Y149A, T222M, and L228A. (C) Summary of binding affinities of Hsc70 mutants for Fam-ATP. All experiments were performed at least twice in triplicate. Results are shown as the average and SEM.

(<60 mP units) for binding the Fam-ATP (Appendix 3.6.2). Thus, these mutants were precluded from this study. Consistent with previous results, BAG1 (EC_{50} = 0.69 ± 0.27 µM), BAG2 (EC_{50} = 0.63 ± 0.12 µM), and BAG3 (EC_{50} = 0.37 ± 0.08 µM) all promoted the release of Fam-ATP from wt Hsc70 [28] (Figure 3.5 and Appendix 3.6.3). Similarly, all the Hsc70

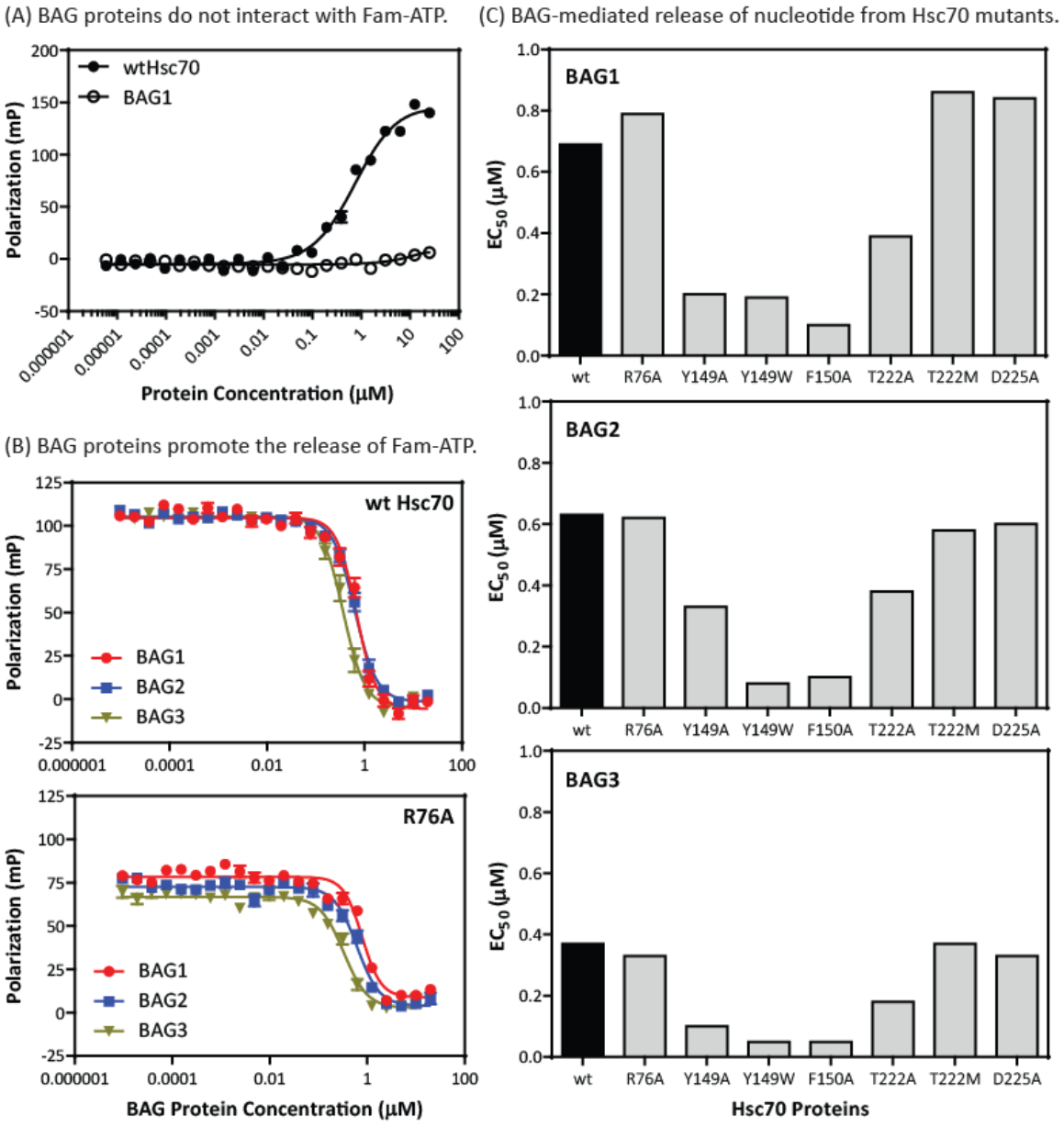

Figure 3.5 BAG proteins promote the release of nucleotide from Hsc70 mutants. (A) The nucleotide exchange factor BAG1 (white) does not interact with Fam-ATP by FP. (B) BAG proteins promote the release of Fam-ATP. Representative competition curves are shown for wt Hsc70 and R76A. (C) Bar graphs summarizing the ability of BAG 1, 2, and 3 to promote the release of nucleotide from Hsc70 mutants. All experiments were performed at least twice in triplicate. Results are shown as the average and SEM.

mutants that were tested were sensitive to the BAG proteins. The potency of the BAG proteins was nearly the same as wt for most of the Hsc70 mutants (R76A, T222A, T226A, and D225A). Interestingly, Y149W and F150A mutants were even more susceptible to

nucleotide release by BAG proteins (EC_{50} = 0.05 – 0.20 µM). Thus, with some exceptions, most of the mutants had normal responses to BAG proteins.

3.3.4 Hsc70 mutants hydrolyze ATP

As mentioned in chapter 1, the ATPase rate of Hsp70 is stimulated by J proteins. Thus, I wanted to measure the ability of a J protein (DNAJA2) to stimulate turnover of ATP for each Hsc70 mutant. Towards this goal, I calculated the K_m and V_{max} values for DNAJA2-mediated stimulation of wt Hsc70 and mutants (Table 3.1 and Appendix 3.6.4), using a standard malachite green assay. With the exception of D206A and T222M, I found that the mutants had little impact on DNAJA2-mediated ATPase activity. Using K_m as an approximation of binding to Hsc70, I found the affinities of most mutants for DNAJA2 were similar to wt Hsc70 (K_m = 34.0 ± 11.0 nM). Two mutants, D206A and T222M, were only weakly stimulated by DNAJA2, such that the curves could not be reliably fit (Table 3.1 and Appendix 3.6.4). With the exception of Y149W (V_{max} = 4.8 ± 0.5 µM) and the ATPase dead mutants (D206A and T222M), the maximum stimulation

Table 3.1 The ATPase activity of Hsc70 mutants.

Hsc70 Protein	Intrinsic ATPase Rate	DJA2 Stimulation	
	$pmolP_i/\mu M/min$	$Vmax_J$ $pmolP_i/\mu M/min$	Km_J nM
wt	**1.8 ± 0.1**	**20.3 ± 1.9**	**34.0 ± 11.0**
R76A	5.3 ± 0.3	12.4 ± 2.1	23.1 ± 14.3
Y145A	3.9 ± 0.1	25.1 ± 2.2	59.2 ± 18.4
Y145W	1.5 ± 0.1	4.8 ± 0.5	32.2 ± 11.2
F150A	2.3 ± 0.1	8.7 ± 1.8	72.6 ± 53.6
D206A	1.6 ± 0.1	NF	NF
T222A	2.1 ± 0.1	11.8 ± 0.8	37.9 ± 8.5
T222M	1.8 ± 0.1	NF	NF
D225A	1.8 ± 0.1	16.2 ± 1.5	94.4 ± 32.7
T226A	2.7 ± 0.2	13.9 ± 1.8	26.5 ± 11.9
H227A	1.5 ± 0.1	9.7 ± 2.3	167.8 ± 155.6
L228A	1.2 ± 0.1	12.6 ± 2.2	89.8 ± 58.5

Gray boxes indicate that either the ATPase rate was not stimulated, as defined by a mutant in which the SEM of the K_m or V_{max} encompassed zero, or when a non-linear fit could not be obtained. Such proteins were deemed nonfunctional (NF). The V_{max} value (calculated by the equation described in the Experimental Procedures) represents the increase in ATPase rate compared to a solvent control. All these experiments were performed at least twice in triplicate. Results are shown as the average and SEM. Raw data can be found in Appendix 3.6.4.

(V_{max}) of the mutants by DNAJA2 was within 3-fold of wt Hsc70 (V_{max} = 20.3 ± 1.9 μM) (**Table 3.1** and **Appendix 3.6.4**). Thus, with some exceptions, most of the point mutants within the MKT-077 binding site had only modest effects on ATP turnover.

3.3.5 Hsc70 mutants do not bind substrate in a nucleotide-dependent manner

The NBD and SBD of Hsp70 are normally in allosteric communication, such that ATP binding in the NBD triggers conformational changes that weaken the SBD's affinity for client peptides. Hydrolysis of nucleotide causes the lid region of the SBD to "close," which greatly increases Hsp70's affinity for clients by slowing the off-rate of these substrates (**Figure 1.3**) [13]. To explore if the mutations had any effect on this communication, I measured binding to a model client and tested whether different nucleotides could affect the apparent affinity. Specifically, I developed a FP platform in which I measured the binding of an Hsc70 protein to a fluorescently labeled client peptide derived from the MHC class I antigen HLA-B2702 (Fam-HLA). As expected, wt Hsc70 had no appreciable affinity for Fam-HLA in the presence of ATP (K_D >25 μM), but bound the tracer with low micromolar affinity in the presence of ADP (K_D = 5.51 ± 0.97 μM) (**Figure 3.6B**). Only two out of the eleven mutants, Y149A and H227A, behaved like the wild-type protein. Instead, most of them bound the Fam-HLA tracer with low micromolar affinity in the presence of either ATP or ADP. Moreover, one mutant (Y149W) bound the Fam-HLA better in the presence of ATP (**Figure 3.6C** and **Appendix 3.6.5**), which is the opposite of wild-type. This was my first indication that the MKT-077 binding site might be important for allosteric communication.

(A) The substrate binding domain of Hsc70 interacts specifically with Fam-HLA.

(B) Hsc70 binds to the substrate peptide probe, Fam-HLA, in a nucleotide dependent manner.

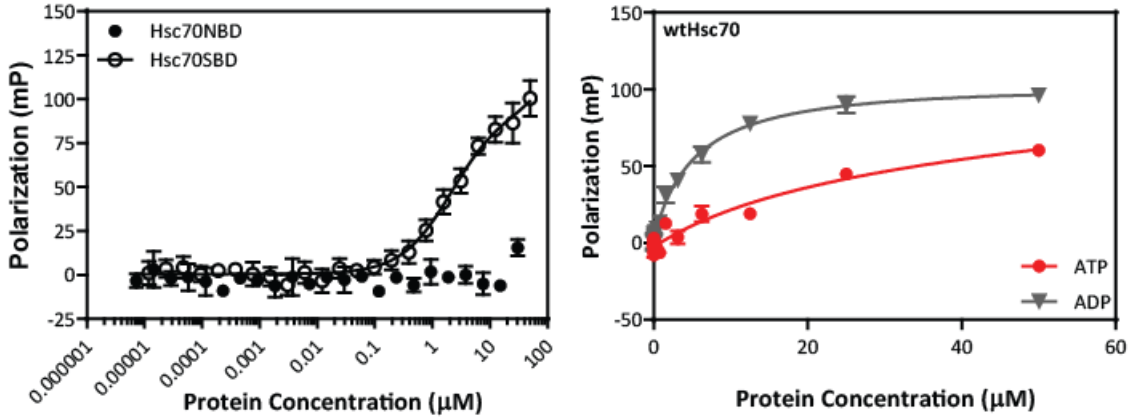

(C) Multiple Hsc70 mutants do not exhibit a nucleotide dependence when binding Fam-HLA.

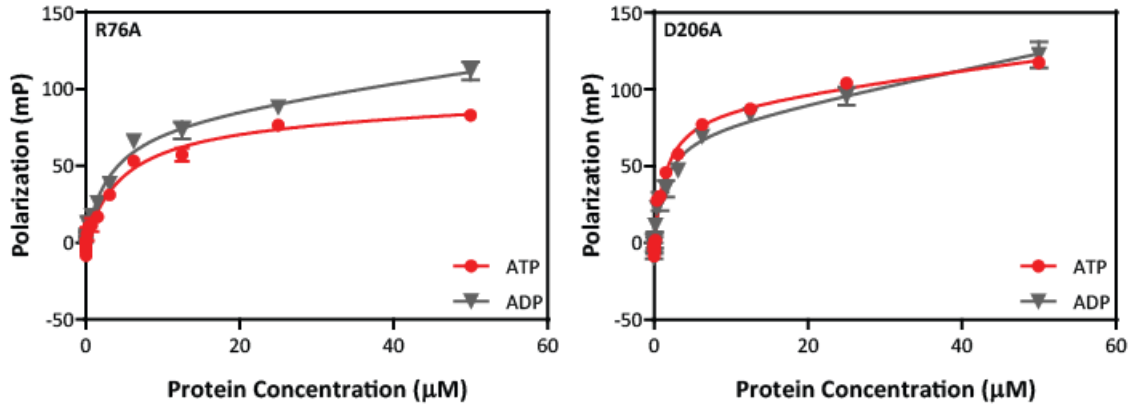

(D) Summary of Hsc70 mutants binding to Fam-HLA in the presence of ATP or ADP.

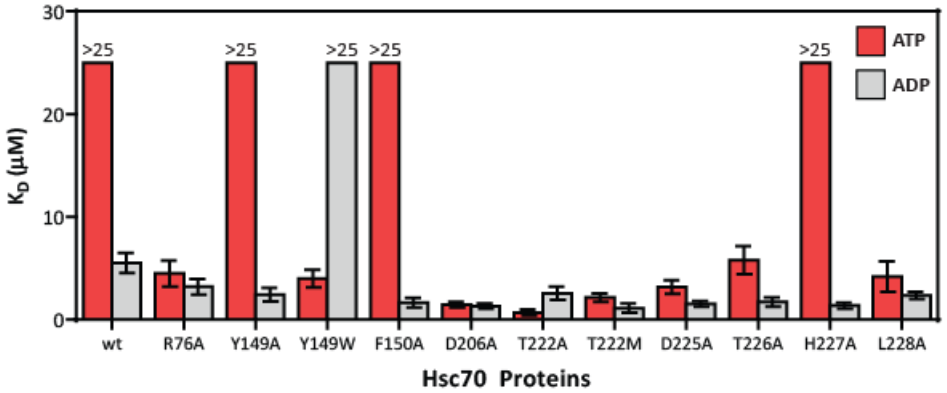

Figure 3.6 Hsc70 mutants do not bind substrate in a nucleotide dependent manner. (A) The substrate binding domain of Hsc70 (white) binds to Fam-HLA with low micromolar affinity by FP. The nucleotide binding domain of Hsc70 (black), the negative control, does not bind to Fam-HLA. (B) Wt Hsc70 has low micromolar affinity for Fam-HLA, in presence of ADP (gray). In the presence of ATP, wt Hsc70 does not have appreciable affinity for Fam-HLA. (C) Multiple Hsc70 mutants do not exhibit a nucleotide dependence when binding Fam-HLA. Representative binding curves are shown for R76A and D206A. (D) Summary of binding affinities of Hsc70 mutants to Fam-HLA in the presence of ATP (red) or ADP (gray).

3.3.6 Hsc70 mutants are deficient in their ability to refold substrates

One of the main roles of Hsc70 is to facilitate protein folding [29, 30]. This activity is often measured *in vitro* using a standard luciferase refolding assay, in which denatured firefly luciferase is restored to its active state by Hsc70 and a J protein in the presence of ATP [31]. Consistent with previous reports, low concentrations of DNAJA2 stimulated the ability of wt Hsc70 to refold luciferase in this platform. The same behavior was also observed for the F150A, T222A, D225A, and L228A mutants. Interestingly, the L228A mutation enhanced the refolding ability of the Hsc70-DNAJA2 complex. All of the other mutants where completely deficient at refolding (Figure 3.7B and Appendix 3.6.6). This result is consistent with the apparent defects in allosteric communication between the NBD and SBD, which is known to be required for proper client interactions. Next, we tested whether

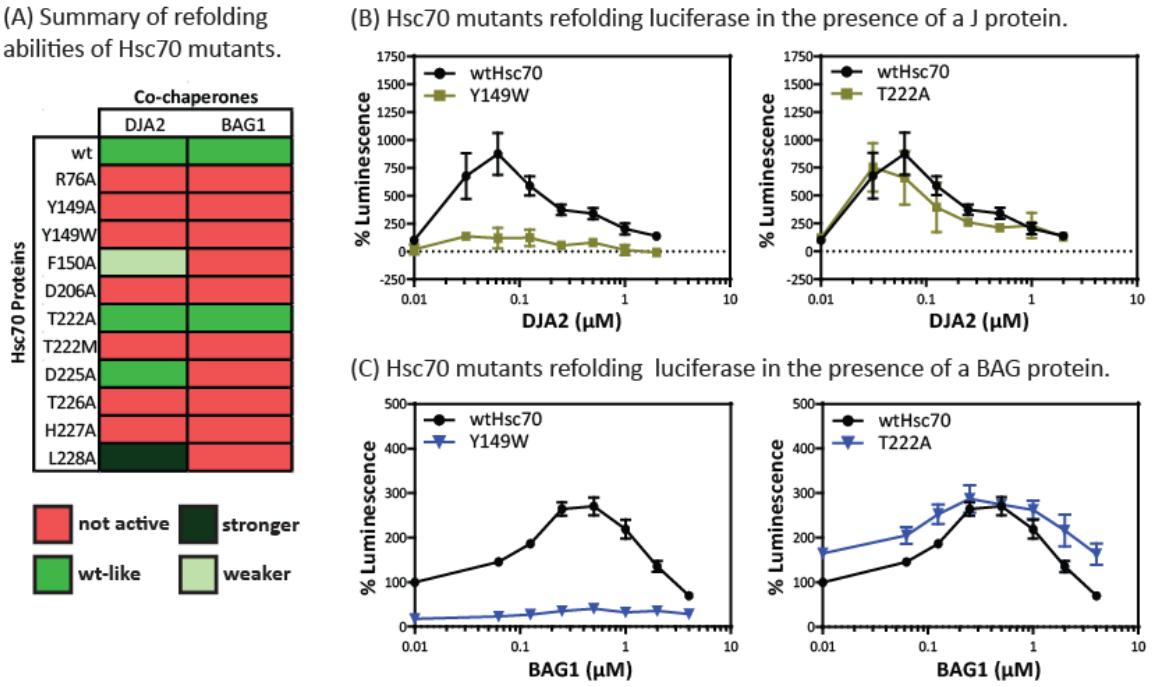

Figure 3.7 Hsc70 mutants are deficient in their ability to refold substrates. (A) Summary of substrate refolding abilities of Hsc70 mutants. (A) Hsc70 mutants refolding denatured luciferase in the presence of a J protein. For this assay, Hsc70 (1 μM) was incubated with DNAJA2 at the concentrations indicated. (B) Hsc70 mutants refolding denatured luciferase in the presence of a BAG protein. For this assay, Hsc70 (1 μM) and DNAJA2 (0.2 μM) were incubated with BAG1 at the concentrations indicated.

BAG1 could stimulate these complexes. At low concentrations of BAG1, the activity of wt Hsc70 and the T222A mutant was indeed enhanced. However, the other ten mutants were not stimulated by the NEF (Figure 3.7B and Appendix 3.6.7). These results suggest that allosteric networks in the NBD and SBD might be decoupled by the mutations.

3.3.7 Many Hsc70 mutants are trapped in an ADP-like conformation

The decoupling of allosteric networks in Hsc70 suggested that the MKT-077 binding pocket might regulate nucleotide-dependent conformational transitions. To test this hypothesis, I utilized a partial proteolysis assay. It has been previously shown that trypsin digestion of Hsp70 results in distinct patterns that are indicative of the chaperone's nucleotide state (ATP-bound *vs.* ADP-bound) [32]. Thus, this platform is a simple way to analyze the gross structure of Hsc70 mutants. For wt Hsc70, the most apparent difference in digestion patterns between nucleotide states was observed around 60 kDa (Figure 3.8). Specifically, there were two bands when Hsc70 was in an ADP-bound state and three bands when the chaperone was in an ATP-bound state.

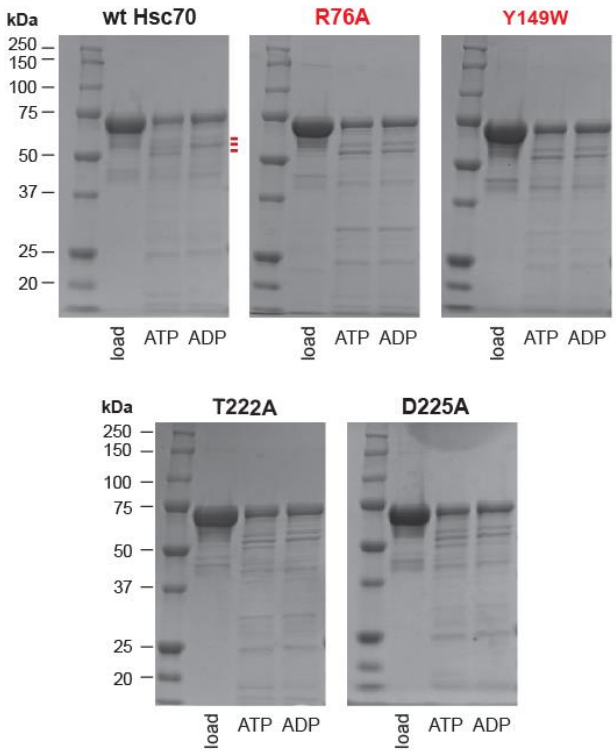

Figure 3.8 Partial proteolysis pattern of Hsc70 mutants. Similar to wt Hsc70, some mutants (T222A and D225A) had a distinct digestion pattern between ATP- and ADP-bound forms. This is clearly seen in the bands around 60 kDa. Other mutants (R76A and Y149W) assumed an ADP-like conformation even with excess ATP. For these experiments, proteolysis was carried out for 20 minutes.

Six of the eleven mutants (Y149A, F150A, T222A, D225A, H227A, and L228A) had similar patterns. All other mutants (R76A, Y149W, D206A, T222M, and T226A) assumed an ADP-bound conformation (two bands around 60 kDa) even in the presence of ATP (Figure 3.8 and Appendix 3.6.8). This observation is consistent with the previous finding that MKT-077 binds exclusively to the ADP-bound state of Hsc70 [25]. Together, these data suggest that this allosteric site in Hsc70 controls nucleotide-dependent communication.

3.4 Conclusions

3.4.1 The MKT-077 binding site controls inter-domain allostery in Hsp70

MKT-077 and its analogs work through Hsp70 to relieve disease phenotypes in models of neurodegeneration [5, 6]. Based on these findings, I set out to understand the mechanism by which these molecules modulate Hsp70's functions. To do this, I performed mutagenesis on MKT-077's binding pocket and studied the effects of these mutations using a host of *in vitro* chaperone assays. The results of these studies are summarized in Figure 3.9. Interestingly, mutations within the MKT-077 binding pocket tended to have little effect on Hsp70's ability to bind, release, and turnover nucleotide. These results suggest that the MKT-077 binding site is not directly linked to the nucleotide-binding cleft. Moreover, most of the Hsc70 mutants responded normally to co-chaperones. For example, their response to DNAJA2 in ATPase assays and BAG proteins in nucleotide release assays was largely normal. Thus, the PPIs with J proteins and NEFs are not strongly coupled to the MKT-077 binding site. However, MKT-077 binding site mutations generally impaired, and in some cases abolished, the ability of Hsp70 to refold luciferase. Luciferase folding requires the

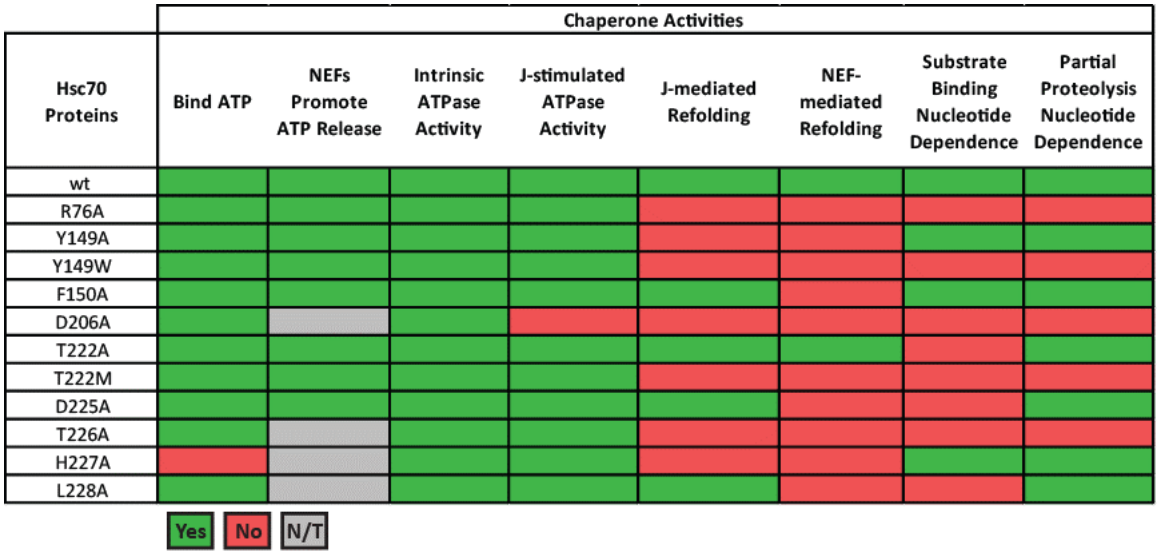

Figure 3.9 Summary of mutations' effects on various Hsp70 activities. Green signifies functional activities, while red indicates broken activities. Gray signifies that the mutant was not tested (N/T) in that assay.

coordination of the NBD and SBD. Further, this process requires stimulation by J proteins and multiple rounds of ATP turnover [31, 33, 34]. Thus, the MKT-077 binding site seems to be selectively coupled with the allosteric networks that allow this activity. In further support of this idea, I observed that these mutations prevented Hsp70 from binding substrates in a nucleotide-dependent manner, another function that requires inter-domain allostery.

3.4.2 The MKT-077 binding site is linked to allosteric hotspots in Hsp70

What specific allosteric networks could be linked to the MKT-077 binding pocket? One clue comes from the location of the site, which is near the proline "switch," a subset of catalytic residues, and the "hinge" region (Figure 3.1). As mentioned in the introduction to this chapter, these three regions are closely linked to inter-domain allostery. For example, residues Y149 and F150 are located in the MKT-077 binding site and they sit adjacent to a small loop that includes the proline "switch" (Hsc70 residues V146-P147-A148-Y149-F150)

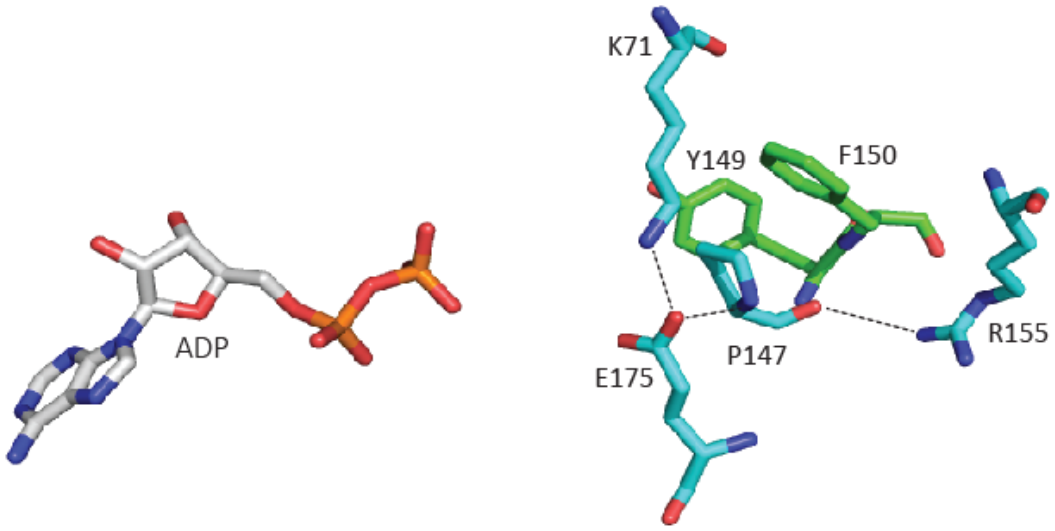

Figure 3.10 The proline "switch" model. In stick representations are shown of nucleotide (gray) and the residues involve in the proline "switch" model of allostery (blue). Additionally, MKT-077 binding site residues, Y149 and F150, are shown (green). Residue numbers correspond to human Hsc70 (PDB = 2QWL). This image was prepared using PyMOL.

in subdomain IA (Figures 3.1 and 3.3). Crystal structures illustrate that the carbonyl oxygen of P147 is stabilized by the guandinium group of R155 through hydrogen bonding. Additionally, P147 is in close proximity (<3.6 Å) to E175 and K71, which are catalytic residues. The catalytic residue K71 positions a water molecule for the nucleophilic attack of the γ-phosphate of ATP (Figure 3.10) [15]. It is suggested that this network responds to the nucleotide state of Hsp70, possibly via proline cis-trans isomerization, to trigger long range conformational changes in the SBD, such as lid opening and closing [15]. My mutagenesis results suggest that residues adjacent to this proline, such as Y149 and F150, are also part of this allosteric network. For example, mutating Y149 to either an alanine or tryptophan impairs Hsc70's ability to refold luciferase. It is important to note that these mutants behaved differently when measuring their binding to a model client. Like wt Hsc70, the Y149A mutant had no appreciable affinity for the client FP tracer in the presence of ATP, but bound it with low micromolar affinity in the presence of ADP. However, the

Y149W mutant bound the tracer probe significantly better in the presence of ATP. My partial proteolysis results indicated that the Y149W mutant is permanently trapped in an ADP-like conformation. Based on the structural analysis described above, the increase in size of the side chain from mutating the Y149 to a tryptophan likely changes the orientation of P147, which in turn disrupts key stabilizing hydrogen bond interactions between residues of the "switch" network. This model suggests that the bulkiness of this mutation triggers the "switch" to be stuck in an "on mode," causing the protein to be no longer responsive to nucleotide and locked in an ADP-like conformation. Future structural studies will attempt to explore this possibility.

In addition to the proline "switch," MKT-077 analogs seem to engage other allosteric hotspots on the NBD of Hsp70, such as the "hinge" region (Figure 3.1). As discussed previously, the nucleotide-dependent rotation of the IIB subdomain is regulated by "hinge" residues at the interface of the IIB and IIA subdomains, such as G229 [14]. Mutating residues adjacent to this glycine, H227 and L228, impairs some Hsp70 functions, such as NEF mediated refolding of substrates. This suggests that MKT-077 molecules engage this allosteric network. Like G229, I suspect that H227 and L228 are involved in properly orientating the IIB subdomain in response to nucleotide. However, mutating these residues to alanine does not engender the same biochemical profile in our chaperone assays (Figure 3.9). For example, the H227A mutant exhibits a nucleotide-dependence when binding substrate, but the L228A mutant does not. This finding supports the idea that networks within the MKT-077 binding pocket are connected and tunable.

These results have important implications for building better MKT-077 analogs. My hypothesis prior to starting these studies is that some of the regions of MKT-077 might be important for triggering allosteric effects, while other regions are more important for binding. Unlike orthosteric inhibitors, not all regions of an allosteric inhibitor are necessarily linked to function and the binding affinity of a compound is not necessarily linked to its potency. Rather, allosteric compounds are defined by their ability to trigger a proper series of conformational changes (*e.g.* side chain swiveling, changes in dynamics, *etc.*) that produces the outcome. Thus, optimizing an allosteric inhibitor can be more challenging. The studies described here are important for building better MKT-077 analogs because they focus attention on the regions of the molecule located near the residues Y149, F150, H227, and L228. With additional structural data, it might be possible to rationally design MKT-077 analogs to act on particular allosteric networks of Hsp70. Moreover, the goal of my thesis is to identify ways of targeting Hsp70 complexes, so this finding is of special importance.

3.5 Experimental procedures

3.5.1 Plasmids

All proteins were expressed from a pMCSG7 vector that contained an N-terminal His-tag and TEV cleavage site. Site-directed mutagenesis for Hsc70 mutants (R76A, Y149A, Y149W, F150A, D206A, T222A, T222M, D225A, T226A, H227A, and L228A) was performed using the Phusion Site-Directed Mutagenesis Kit protocol (New England Biolabs, Ipswich, MA).

3.5.2 Protein expression and purification

Full length Hsc70 proteins, as well as Hsc70 NBD, were expressed, purified, and made apo (nucleotide free) using the same procedure as described for full length wt Hsp72 in chapter 2. Human DNAJA2 was expressed and purified using the same procedure as described for DNAJC7 in chapter 2. Human BAG proteins were expressed and purified using a previously described method [28].

Hsc70 SBD was expressed in *E. coli* BL21 (DE3) cells. Liter cultures of terrific broth were grown at 37 °C until an OD_{600} of 0.6 was reached. Cultures were cooled to 18 °C before induction with IPTG (final concentration of 500 μM) and then grown overnight. Cells were lysed by sonication, pelleted by centrifugation, and the supernatant was applied to Ni-NTA His-Bind Resin (Novagen, Darmstadt, Germany). The resin was washed with His-binding buffer (50 mM TRIS, 10 mM Imidazole, 300 mM NaCl, pH 8), followed by His-washing buffer (50 mM TRIS, 30 mM Imidazole, 300 mM NaCl, pH 8). The protein was then removed from the resin using His-elution buffer (50 mM TRIS, 300 mM Imidazole, 300 mM NaCl, pH 8). The N-terminal His-tag was then removed using TEV protease. The sample was then further purified by size exclusion chromatography using a prep grade XK 16/100 Superdex 75 column (GE Healthcare Life Sciences) in a 25 mM HEPES, 5 mM $MgCl_2$, 10 mM KCl, pH 7.5 buffer.

3.5.3 Fluorescence polarization assays

All experiments were performed in 384-well, black, low volume, round-bottom plates (catalog number = 4511, Corning, NY). Polarization values in millipolarization units (mP) were measured at an excitation wavelength at 485 nm and an emission wavelength at 530 nm using a Molecular Devices Spectramax M5 plate reader (Sunnyvale, CA). For binding experiments, equilibrium-binding isotherms were constructed by plotting FP readings as a function of the protein concentration at a fixed concentration of a tracer. All experiments were performed at least twice in triplicate. Results are shown as the average and SEM. All experimental data were analyzed using GraphPad Prism 6 software. The binding of Hsc70 proteins to the fluorescent ATP analog (Fam-ATP) and the fluorescent substrate peptide (Fam-HLA) was performed using the procedures described for wt Hsp72 in chapter 2. Additionally, I also determined the ability of BAG proteins to promote the release of the Fam-ATP probe from Hsc70 proteins. First, an apo Hsc70 protein was added to each well. The concentration of protein added equals the concentration of Hsc70/mutant at which 50% of the FP probe (Fam-ATP) is bound based on binding experiments. Next, a 2-fold dilution series of a NEF (BAG 1,2, or 3), made using the assay buffer (100 mM TRIS, 20 mM KCl, 6 mM $MgCl_2$, 0.001% Triton X-100, pH 7.4), was added. Final concentrations of the NEF ranged from 0 to 25 µM. Finally, Fam-ATP was added to each well, to give a final concentration of 20 nM and a total assay volume of 20 µL. The plate was covered from light and allowed to incubate at room temperature for 30 minutes in order to reach equilibrium.

3.5.4 ATPase assays

These experiments were performed using previously described methods with minor modifications [1, 22]. Stocks of malachite green (0.081% w/v), polyvinyl alcohol (2.3% w/v), and ammonium heptamolybdate tetrahydrate (5.7% w/v in 6 M HCl) were prepared and mixed with water in a 2:1:1:2 ratio to make the malachite green reagent. All experiments were performed in 96-well clear plates. Intrinsic ATPase rates of Hsc70 proteins were determined in the absence of co-chaperones. A 2-fold dilution series of Hsc70 was added to wells; final concentrations ranged from 0 to 7 µM. For co-chaperone stimulation assays, Hsc70 (final concentration of 1 µM) and various concentrations of DNAJA2 were added to the wells. Next, ATP (final concentration of 1 mM) was added to each well, bringing the reaction volume to 25 µL. Reactions were incubated for 1 h at 37 °C, developed with the addition of 80 µL malachite green reagent, and then immediately quenched with 10 µL of 32% (w/v) sodium citrate. Assays were incubated at 37 °C for 15 minutes and then measured at OD_{620} using a Molecular Devices Spectramax M5 plate reader (Sunnyvale, CA). Additionally, background signal from non-specific ATP hydrolysis in controls was subtracted. A phosphate standard curve of potassium dibasic phosphate was used to calculate pmol P_i/chaperone µM/min. Stimulation curves were fit to a modified Michaelis Menten equation ($y = V_{max} \bullet X/(K_m+x)+b$). All experiments were performed at least twice in triplicate. All experimental data were analyzed using GraphPad Prism 6 software.

3.5.5 Luciferase refolding assays

Experiments were performed as described previously [31]. Briefly, working stocks of denatured luciferase were prepared by mixing 10 µL of 203 µM native luciferase (Promega)

with 30 µL of 8 M GnHCl for 1 h at room temperature. Denatured luciferase stocks were stored at -80 °C until use. To white 96-well plates, was added denatured luciferase (final concentration of 100 nM), Hsc70 (final concentration of 1 µM), and various concentrations of DNAJA2 and/or BAG1 to give a final volume of 25 µL in refolding buffer (23 mM HEPES, 120 mM KAc, 1.2 mM MgAc, 15 mM DTT, 61 mM creatine phosphate, 35 U/mL creatine kinase, 5 ng/µL BSA, pH 7.4). The reaction was initiated by adding 10 µL of 2.5 mM ATP to give a final concentration of 1 mM. Plates were covered and incubated at 37 °C for 1 h. Next, 25 µL of Steady-Glo reagent (Promega) was added to each well and luminescence values were measured immediately using a Molecular Devices Spectramax M5 plate reader (Sunnyvale, CA).

3.5.6 Partial proteolysis

Partial proteolysis experiments were performed using previously described procedures [22]. Samples of 6 µM Hsc70/mutant were prepared in a partial proteolysis buffer (40 mM HEPES, 20 mM NaCl, 8 mM MgCl2, 20 mM KCl, 0.3 mM EDTA, pH 8.0) with either 1 mM ATP or ADP. Samples were allowed to incubate at room temperature for 30 minutes. Next, Trypsin (EC 3.4.21.4, Sigma) was added at 1:4 (Trypsin:Hsc70/mutant) molar ratio, bringing the reaction volume to 50 µL. Proteolysis was carried out over a 40 minute time span. Reactions were quenched at 5, 10, 20, and 40 minute time intervals with 25 µL of SDS loading buffer (240 mM TRIS, 6% (w/v) SDS, 30% (v/v) glycerol, 16% (v/v) β-mercaptoethanol, 0.6 mg/mL bromophenol blue, pH 6.8) and then heated at 95 °C for 3 minutes. Samples were then subjected to SDS-PAGE using 10% Mini-PROTEAN TGX Precast

Gels (cat # =4561036, BioRad). Gels were run for ~40 minutes at 200V and then stained with Coomassie blue.

Notes

Experiments in this chapter were designed by Victoria A. Assimon and Jason E. Gestwicki. Zapporah T. Young conducted ATPase and refolding assays. All other experiments were conducted by Victoria A. Assimon.

3.6 Appendix

3.6.1 Analysis of purified Hsc70 mutants by SDS-PAGE

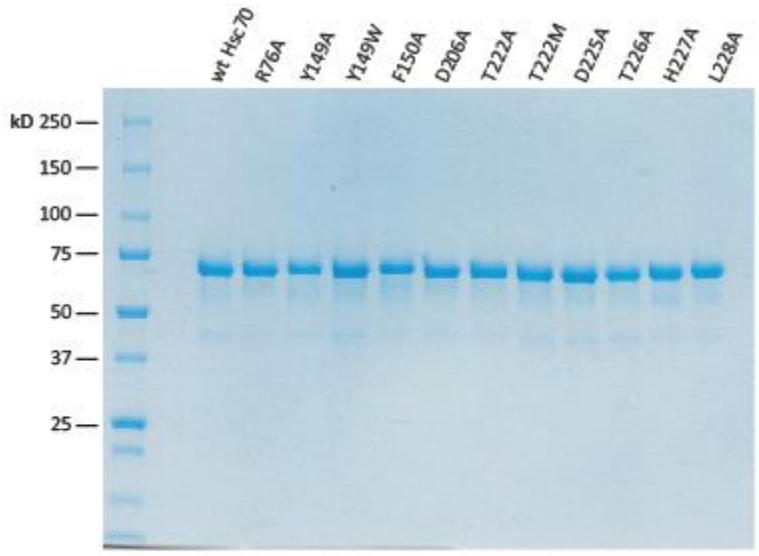

Appendix 3.6.1 Analysis of purified Hsc70 mutants by SDS-PAGE. To a well was loaded 10 µL of a protein sample. Samples were prepared by diluting Hsc70 protein using a 100 mM TRIS buffer (20 mM KCl, 6 mM $MgCl_2$, 0.001% Triton X-100, pH 7.4). The final concentration of the samples was 4 µM after adding loading dye. Gels (10% Mini-PROTEAN TGX) were run for ~40 minutes at 200V and then stained with Coomassie blue.

3.6.2 Hsc70 mutants can engage with nucleotide

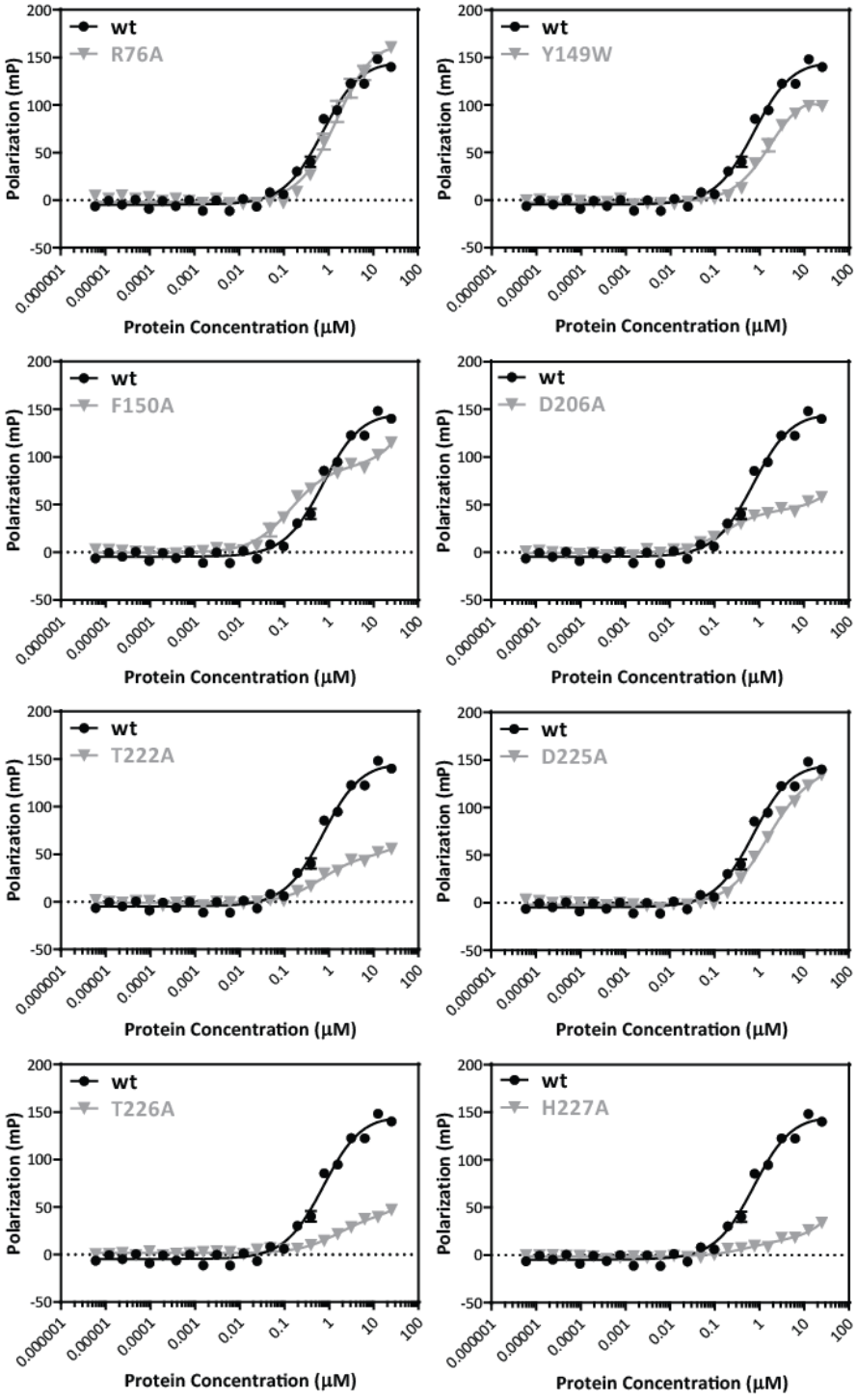

Appendix 3.6.2 Hsc70 MKT-077 binding site mutants can engage with nucleotide. Binding curves are shown for the following Hsc70 mutants: R76A, Y149W, F150A, D206A, T222A, D225A, T226A, and H227A. Affinities were measured by FP using a fluorescently labeled ATP analog (Fam-ATP). These experiments were performed at least twice in triplicate. Results are shown as the average and SEM.

3.6.3 BAG proteins promote the release of nucleotide from Hsc70 mutants

(A) The nucleotide exchange factors BAG2 and BAG3 do not interact with Fam-ATP.

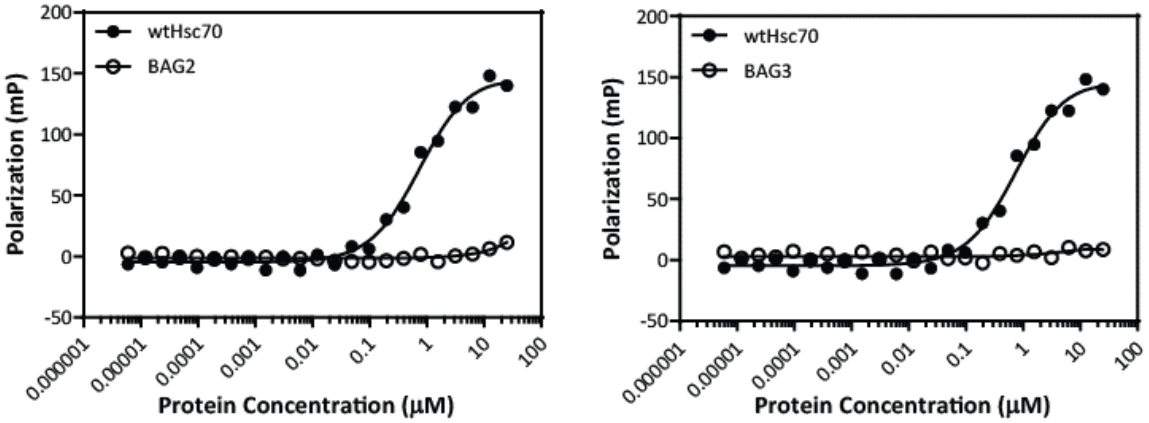

(B) Hsc70 mutants differ in their BAG-mediated release of nucleotide.

Hsc70 Proteins	BAG1		BAG2		BAG3	
	EC_{50} (µM)	95% CI	EC_{50} (µM)	95% CI	EC_{50} (µM)	95% CI
wt	0.69	0.58 - 0.81	0.63	0.58 - 0.69	0.37	0.33 - 0.41
R76A	0.79	0.63 - 1.00	0.62	0.50 - 0.76	0.33	0.27 - 0.41
Y149A	0.20	0.17 - 0.23	0.33	0.24 - 0.47	0.10	0.08 - 0.12
Y149W	0.19	0.14 - 0.25	0.08	0.04 - 0.13	0.05	0.03 - 0.08
F150A	0.10	0.09 - 0.12	0.10	0.08 - 0.13	0.05	0.04 - 0.06
T222A	0.39	0.28 - 0.54	0.38	0.24 - 0.61	0.18	0.11 - 0.28
T222M	0.86	0.68 - 1.10	0.58	0.34 - 0.98	0.37	0.21 - 0.61
D225A	0.84	0.69 - 1.03	0.60	0.46 - 0.78	0.33	0.25 - 0.43

Appendix 3.6.3 BAG proteins promote the release of nucleotide from Hsc70 mutants. (A) The nucleotide exchange factors BAG2 and BAG3, shown in white, do not interact with Fam-ATP by FP. (B) Table summarizing the ability of BAG 1, 2, and 3 to promote the release of nucleotide from Hsc70 mutants. All experiments were performed at least twice in triplicate. Results are shown as the average and SEM.

3.6.4 J proteins stimulate ATP turnover in wt Hsc70 and mutants

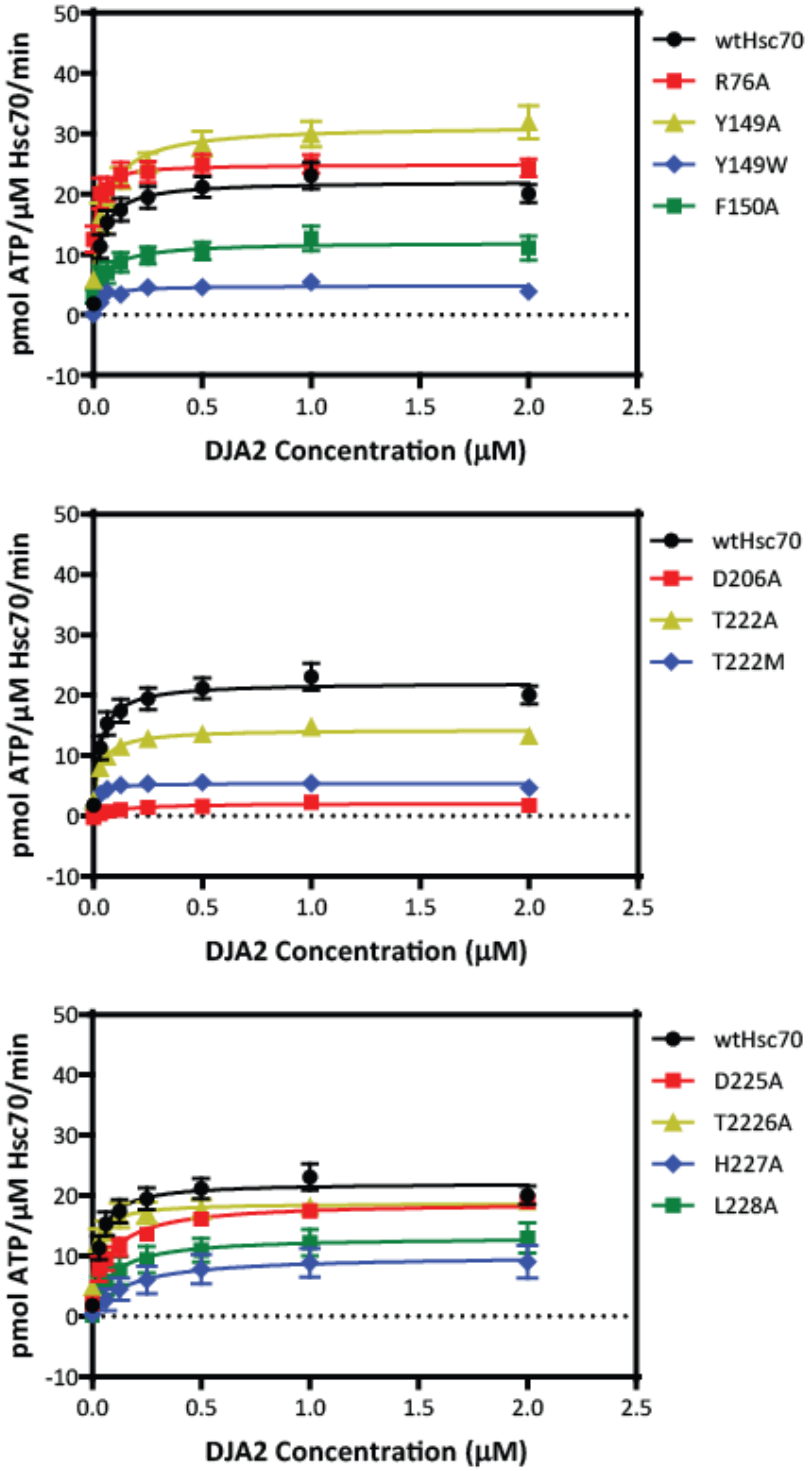

Appendix 3.6.4 Co-chaperones mediated the stimulation of ATP turnover in wt Hsc70 and mutants. An Hsc70 protein (1 µM) was incubated with DNAJA2 at the concentrations indicated. Curves were generated using a nonlinear hyperbolic fit with a non-zero intercept.

3.6.5 Hsc70 mutants do not recognize substrate in a nucleotide-dependent manner

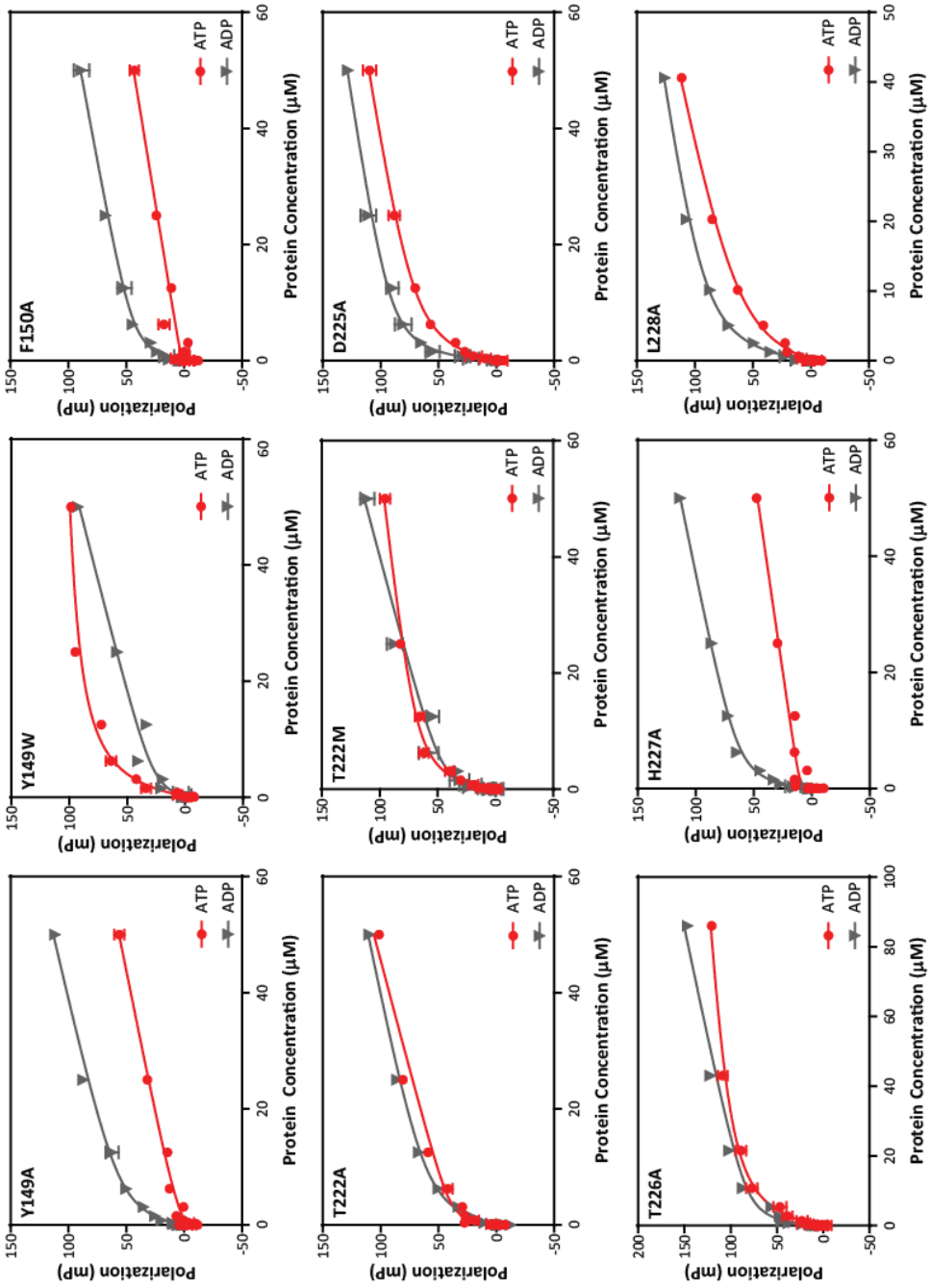

Appendix 3.6.5 Hsc70 mutants do not recognize substrate in a nucleotide dependent manner. The binding of Hsc70 mutants to the FP substrate probe, Fam-HLA, in the presence of ATP (red) or ADP (gray) is shown. Binding curves are shown for the following Hsc70 mutants: Y149A, Y149W, F150A, T222A, T222M, D225A, T226A, H227A, and L228A. These experiments were performed at least twice in triplicate. Results are shown as the average and SEM.

3.6.6 Hsc70 mutants are deficient in their J-mediated refolding of substrates

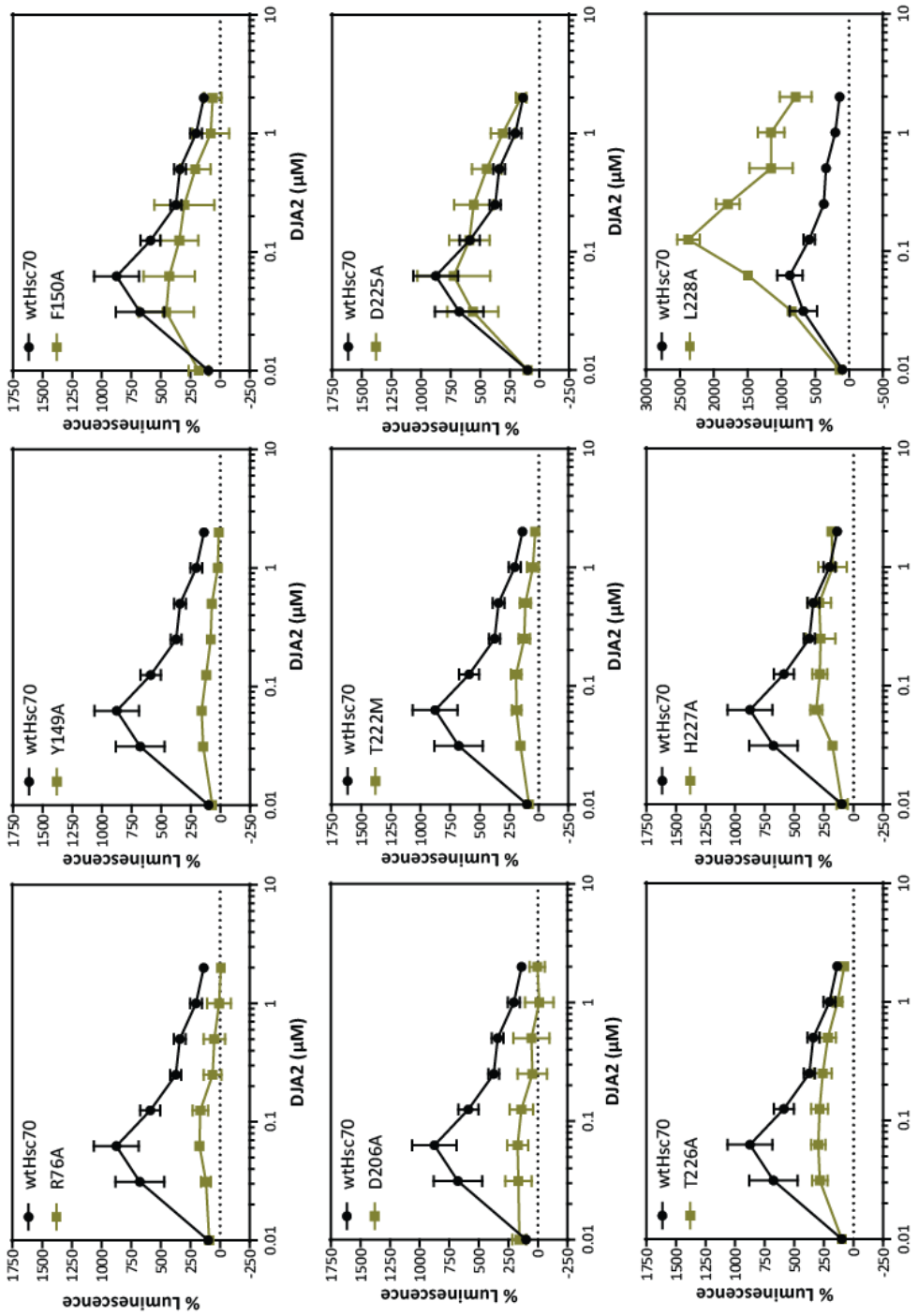

Appendix 3.6.6 Hsc70 mutants are deficient in their ability to refold substrates. Raw data of Hsc70 mutants refolding denatured luciferase in the presence of a J protein. For this assay, Hsc70 (1 μM) was incubated with DNAJA2 at the concentrations indicated.

3.6.7 Hsc70 mutants are deficient in their NEF-mediated refolding of substrates

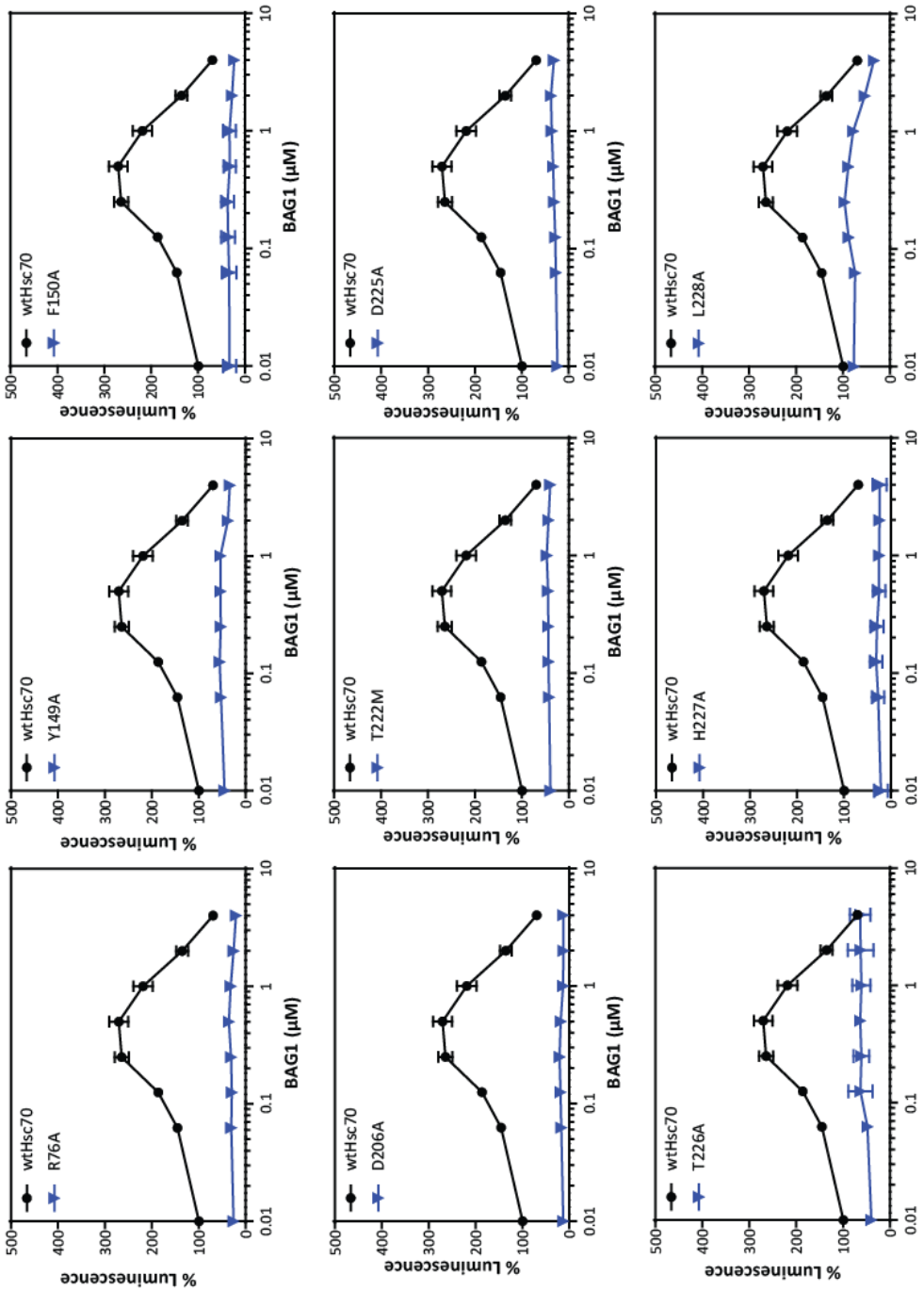

Figure 3.6.7 Hsc70 mutants are deficient in their ability to refold substrates. Raw data of Hsc70 mutants refolding denatured luciferase in the presence of a BAG protein. For this assay, Hsc70 (1 μM) and DNAJA2 (0.2 μM) were incubated with BAG1 at the concentrations indicated.

3.6.8 Partial proteolysis patterns of Hsc70 mutants

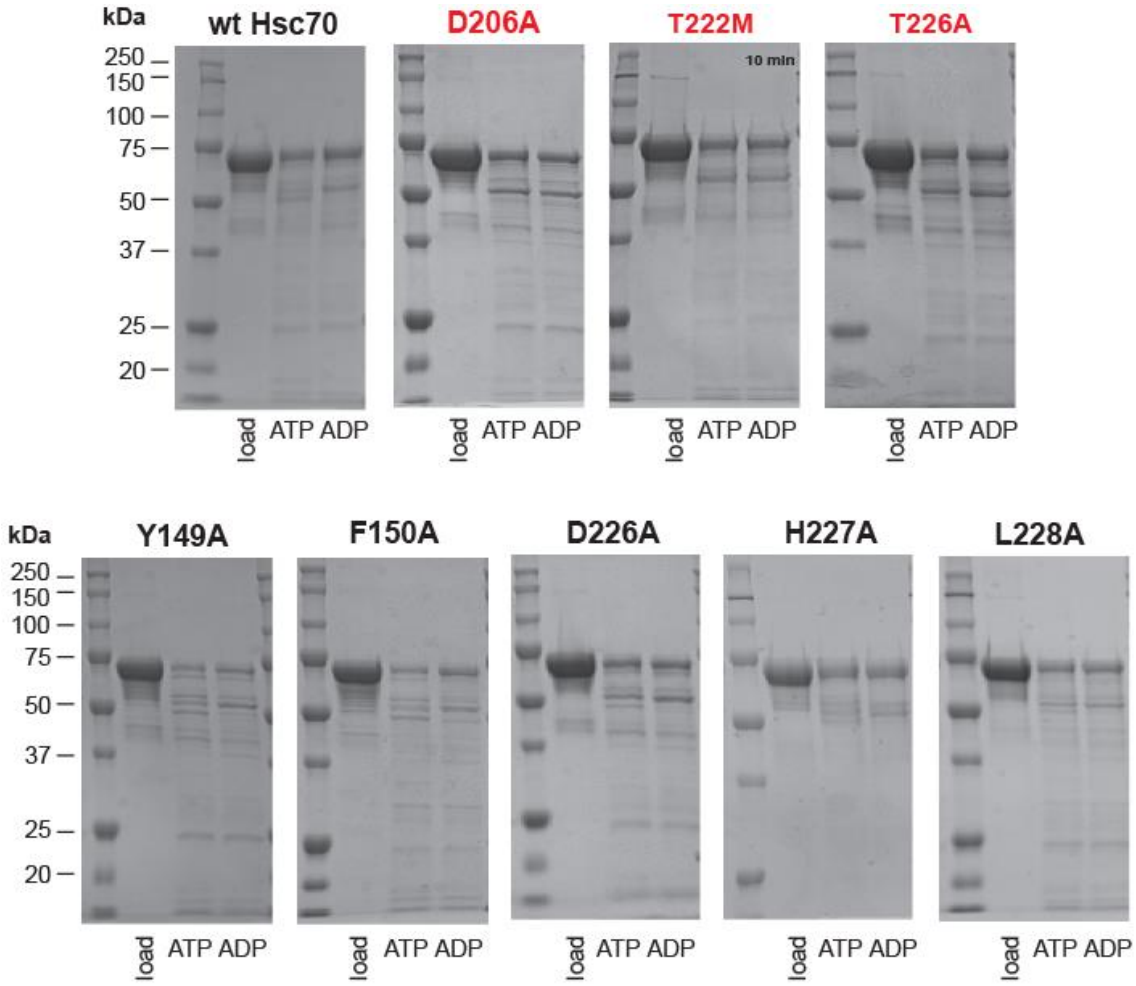

Appendix 3.6.8 Partial proteolysis pattern of Hsc70 mutants. Similar to wt Hsc70, some mutants (Y149A, F150A, D226A, L228A, and H227A) had a distinct digestion pattern between ATP- and ADP-bound forms. This is clearly seen in the bands around 60 kDa. Other mutants (D206A, T222M, and 2226A) assumed an ADP-like conformation even with excess ATP. For these experiments, proteolysis was carried out for 20 minutes unless noted otherwise.

3.7 References

1. Chang, L., et al., *High-throughput screen for small molecules that modulate the ATPase activity of the molecular chaperone DnaK.* Analytical Biochemistry, 2008. **372**(2): p. 167-176.
2. Miyata, Y., et al., *High-Throughput Screen for Escherichia coli Heat Shock Protein 70 (Hsp70/DnaK): ATPase Assay in Low Volume by Exploiting Energy Transfer.* Journal of Biomolecular Screening, 2010. **15**(10): p. 1211-1219.
3. Chang, L., et al., *Chemical Screens against a Reconstituted Multiprotein Complex: Myricetin Blocks DnaJ Regulation of DnaK through an Allosteric Mechanism.* Chemistry & Biology, 2011. **18**(2): p. 210-221.
4. Cesa, L.C., et al., *Inhibitors of Difficult Protein-Protein Interactions Identified by High-Throughput Screening of Multiprotein Complexes.* Acs Chemical Biology, 2013. **8**(9): p. 1988-1997.
5. Abisambra, J., et al., *Allosteric Heat Shock Protein 70 Inhibitors Rapidly Rescue Synaptic Plasticity Deficits by Reducing Aberrant Tau.* Biological Psychiatry, 2013. **74**(5): p. 367-374.
6. Wang, A.M., et al., *Activation of Hsp70 reduces neurotoxicity by promoting polyglutamine protein degradation.* Nature Chemical Biology, 2013. **9**(2): p. 112-118.
7. Miyata, Y., et al., *Synthesis and Initial Evaluation of YM-08, a Blood-Brain Barrier Permeable Derivative of the Heat Shock Protein 70 (Hsp70) Inhibitor MKT-077, Which Reduces Tau Levels.* Acs Chemical Neuroscience, 2013. **4**(6): p. 930-939.
8. Li, X.K., et al., *Analogues of the Allosteric Heat Shock Protein 70 (Hsp70) Inhibitor, MKT-077, As Anti-Cancer Agents.* Acs Medicinal Chemistry Letters, 2013. **4**(11): p. 1042-1047.
9. Bertelsen, E.B., et al., *Solution conformation of wild-type E. coli Hsp70 (DnaK) chaperone complexed with ADP and substrate.* Proc Natl Acad Sci U S A, 2009. **106**(21): p. 8471-6.
10. Zhuravleva, A. and L.M. Gierasch, *Allosteric signal transmission in the nucleotide-binding domain of 70-kDa heat shock protein (Hsp70) molecular chaperones.* Proceedings of the National Academy of Sciences of the United States of America, 2011. **108**(17): p. 6987-6992.
11. Kityk, R., et al., *Structure and Dynamics of the ATP-Bound Open Conformation of Hsp70 Chaperones.* Molecular Cell, 2012. **48**(6): p. 863-874.
12. Bork, P., C. Sander, and A. Valencia, *An ATPase domain common to prokaryotic cell cycle proteins, sugar kinases, actin, and hsp70 heat shock proteins.* Proc Natl Acad Sci U S A, 1992. **89**(16): p. 7290-4.
13. Mayer, M.P., et al., *Multistep mechanism of substrate binding determines chaperone activity of Hsp70.* Nat Struct Biol, 2000. **7**(7): p. 586-93.
14. Ung, P.M.U., et al., *Identification of Key Hinge Residues Important for Nucleotide-Dependent Allostery in E. coli Hsp70/DnaK.* Plos Computational Biology, 2013. **9**(11).

15. Vogel, M., B. Bukau, and M.P. Mayer, *Allosteric regulation of Hsp70 chaperones by a proline switch.* Molecular Cell, 2006. **21**(3): p. 359-367.
16. Johnson, E.R. and D.B. McKay, *Mapping the role of active site residues for transducing an ATP-induced conformational change in the bovine 70-kDa heat shock cognate protein.* Biochemistry, 1999. **38**(33): p. 10823-10830.
17. Fontaine, S.N., et al., *Isoform-selective Genetic Inhibition of Constitutive Cytosolic Hsp70 Activity Promotes Client Tau Degradation Using an Altered Co-chaperone Complement.* Journal of Biological Chemistry, 2015. **290**(21): p. 13115-13127.
18. Zhang, Y.B. and E.R.P. Zuiderweg, *The 70-kDa heat shock protein chaperone nucleotide-binding domain in solution unveiled as a molecular machine that can reorient its functional subdomains.* Proceedings of the National Academy of Sciences of the United States of America, 2004. **101**(28): p. 10272-10277.
19. Bhattacharya, A., et al., *Allostery in Hsp70 Chaperones Is Transduced by Subdomain Rotations.* Journal of Molecular Biology, 2009. **388**(3): p. 475-490.
20. Harrison, C.J., et al., *Crystal structure of the nucleotide exchange factor GrpE bound to the ATPase domain of the molecular chaperone DnaK.* Science, 1997. **276**(5311): p. 431-435.
21. Brehmer, D., et al., *Tuning of chaperone activity of Hsp70 proteins by modulation of nucleotide exchange.* Nature Structural Biology, 2001. **8**(5): p. 427-432.
22. Chang, L., et al., *Mutagenesis Reveals the Complex Relationships between ATPase Rate and the Chaperone Activities of Escherichia coli Heat Shock Protein 70 (Hsp70/DnaK).* Journal of Biological Chemistry, 2010. **285**(28): p. 21282-21291.
23. Wisen, S., et al., *Binding of a Small Molecule at a Protein-Protein Interface Regulates the Chaperone Activity of Hsp70-Hsp40.* Acs Chemical Biology, 2010. **5**(6): p. 611-622.
24. Swain, J.F., et al., *Hsp70 chaperone ligands control domain association via an allosteric mechanism mediated by the interdomain linker.* Molecular Cell, 2007. **26**(1): p. 27-39.
25. Rousaki, A., et al., *Allosteric Drugs: The Interaction of Antitumor Compound MKT-077 with Human Hsp70 Chaperones.* Journal of Molecular Biology, 2011. **411**(3): p. 614-632.
26. Bhattacharya, A., et al., *Allostery in Hsp70 chaperones is transduced by subdomain rotations.* J Mol Biol, 2009. **388**(3): p. 475-90.
27. Cunningham, B.C. and J.A. Wells, *High-Resolution Epitope Mapping of Hgh-Receptor Interactions by Alanine-Scanning Mutagenesis.* Science, 1989. **244**(4908): p. 1081-1085.
28. Rauch, J.N. and J.E. Gestwicki, *Binding of Human Nucleotide Exchange Factors to Heat Shock Protein 70 (Hsp70) Generates Functionally Distinct Complexes in Vitro.* Journal of Biological Chemistry, 2014. **289**(3): p. 1402-1414.
29. Frydman, J., *Folding of newly translated proteins in vivo: The role of molecular chaperones.* Annual Review of Biochemistry, 2001. **70**: p. 603-647.
30. Hartl, F.U., A. Bracher, and M. Hayer-Hartl, *Molecular chaperones in protein folding and proteostasis.* Nature, 2011. **475**(7356): p. 324-332.

31. Wisen, S. and J.E. Gestwicki, *Identification of small molecules that modify the protein folding activity of heat shock protein 70.* Analytical Biochemistry, 2008. **374**(2): p. 371-377.
32. Buchberger, A., et al., *Nucleotide-Induced Conformational-Changes in the Atpase and Substrate-Binding Domains of the Dnak Chaperone Provide Evidence for Interdomain Communication.* Journal of Biological Chemistry, 1995. **270**(28): p. 16903-16910.
33. Szabo, A., et al., *The Atp Hydrolysis-Dependent Reaction Cycle of the Escherichia-Coli Hsp70 System - Dnak, Dnaj, and Grpe.* Proceedings of the National Academy of Sciences of the United States of America, 1994. **91**(22): p. 10345-10349.
34. Barthel, T.K., J.D. Zhang, and G.C. Walker, *ATPase-Defective derivatives of Escherichia coli DnaK that behave differently with respect to ATP-induced conformational change and peptide release.* Journal of Bacteriology, 2001. **183**(19): p. 5482-5490.

Chapter 4

Discovery of antibiotics targeting Hsp70

4.1 Abstract

A rise in antibiotic resistance has created an urgent need for new drug targets. The prokaryotic heat shock protein 70 (Hsp70), DnaK, is a highly conserved molecular chaperone that limits protein aggregation and favors folding. Deletion of *dnaK* produces strains of *Staphylococcus aureus* that have diminished survival in host infection models, suggesting that this chaperone might be a new antibacterial target. However, until recently, few selective inhibitors of Hsp70/DnaK were known, so this hypothesis has been under explored. The Gestwicki laboratory has recently developed potent new Hsp70/DnaK inhibitors based on the rhodacyanine MKT-077. In chapter 3, I described how these compounds bind to an allosteric site in Hsc70 and I used mutagenesis to understand how they inhibit specific chaperone functions. That work suggested that MKT-077 analogs might have antibiotic activity. In this chapter, I first confirmed that this allosteric network is conserved in DnaK and then tested ~300 analogs of MKT-077 for activity against pathogenic Gram-positive and Gram-negative bacterial strains. I found that several MKT-077 derivatives had promising activity against Gram-positive bacteria, with minimum inhibitory concentration (MIC) values ranging from 8 to < 0.125 μg/mL. These results validate Hsp70/DnaK as a possible new antibiotic target for Gram-positive infections.

Moreover, MKT-077 analogs appear to be useful chemical probes for studying the role of DnaK in bacterial pathogenesis.

4.2 Introduction

4.2.1 The prokaryotic Hsp70, DnaK, is a promising antibacterial target

The prokaryotic Hsp70, DnaK, is essential for the survival of bacterial cells under various cellular pressures, such as extreme temperatures and oxidative stress. At times of cellular stress, many proteins are susceptible to unfolding or aggregation. A major function of DnaK is to bind to these misfolding clients and prevent them from aggregating [1-3]. Upon a return to normal conditions, DnaK is also active in the refolding of these proteins [4, 5]. Consistent with these functions, *Escherichia coli* and *Staphylococcus aureus ΔdnaK* strains have reduced viability at intermediate temperatures (30 °C) and are not able to grow under heat shock conditions (>42°C) [6-8]. Similarly, knockdown of DnaK in *Streptococcus mutans* results in cell growth defects at elevated temperatures [9]. In addition to thermal sensitivity, *ΔdnaK* strains have increased susceptibility to antibiotics. For example, *E. coli dnaK* or *dnaJ* null strains are more sensitive to fluoroquinolones [10, 11] and a *ΔdnaK* methicillin-resistant *S. aureus* (MRSA) strain has increased susceptibility to the cell wall active antibiotics oxacillin and methicillin [6]. Intracellular pathogens, such as *Salmonella enterica* and *Listeria monocytogenes*, also require DnaK for growth and proliferation in macrophages [12, 13]. Most importantly, deletion of *dnaK* produces strains of *S. aureus* and *S. enterica* that have diminished survival in host infection models [6, 12]. Taken together, this genetic data illustrates that DnaK is critical for the survival, pathogenicity,

and virulence of bacteria, suggesting that this chaperone might be a new antibacterial target.

4.2.2 DnaK's refolding activity is linked to its ability to promote survival in response to stress

As discussed in the previous chapters, Hsp70/DnaK has many different activities, including ATP turnover, client refolding, and client binding. Which of these activities should be inhibited to create a potent antibiotic? Are they all required? In other words, what does an inhibitor need to block to be an antibiotic? Two previous members of the Gestwicki laboratory, Lyra Chang and Andrea Thompson, explored this question. Specifically, they created a library of point mutants in DnaK, which they introduced into *ΔdnaK E. coli* to understand which ones could complement the loss of function under heat shock conditions. They also measured the activities of the purified mutant proteins in common chaperone assays, such as ATP turnover and luciferase refolding. Interestingly, they found that the capacity of these mutants to refold luciferase was much more predicative of their *in vivo* activity than these mutants' ATPase rates [14]. Specifically, mutants that are deficient in their ability to refold substrates fail to rescue *ΔdnaK E. coli* cells. Based on this finding, I hypothesized that compounds that inhibit DnaK's refolding function might be the best situated to promote bacterial cell death. However, this question had not been addressed, largely because chemical inhibitors were not available.

4.2.3 A chemical biology approach to exploring DnaK's role in bacterial pathogenesis

As discussed throughout this thesis, there has been interest in developing compounds that target Hsp70/DnaK [15-17]. Recent efforts from the Gestwicki laboratory and others have led to discovery of inhibitors that bind to different regions in the NBD and SBD [16-18] (**Figure 4.1**). Because these molecules bind to different regions of the chaperone, it is thought that they might have distinct effects on co-chaperone interactions, ATP turnover, and substrate refolding. However, the mechanisms of only a handful have been studied. Based on my work in chapter 3, I was particularly interested in using MKT-077 analogs to explore the role of DnaK in bacterial survival because I had found that the MKT-077 binding site controlled inter-domain interactions in Hsp70. Indeed, mutants that disrupted this inter-domain allostery had a dramatic effect on chaperone-mediated luciferase refolding

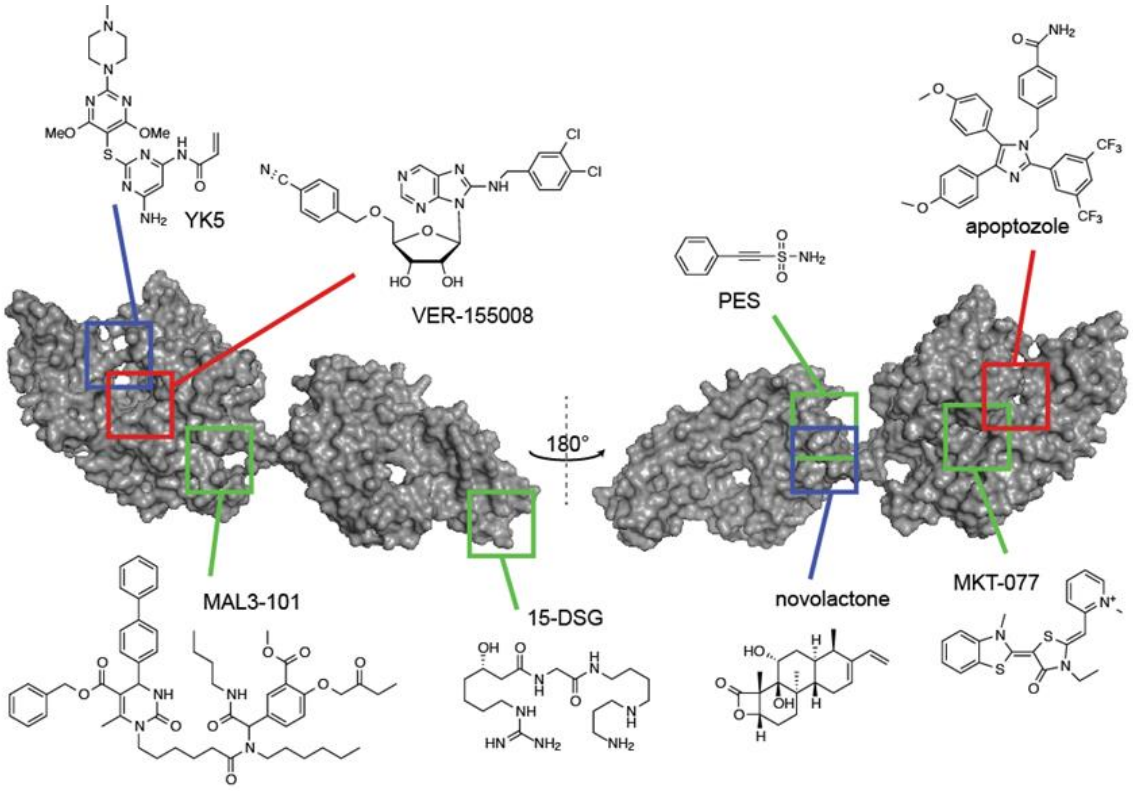

Figure 4.1 Overview of the diversity of inhibitor binding sites on Hsp70/DnaK. Binding sites are distributed throughout the nucleotide and substrate binding domains, including orthosteric molecules (VER-155008 and apoptozole) that compete with nucleotide and other molecules that occupy many other allosteric sites. ATP competitive inhibitors are indicated in red, covalent inhibitors are indicated in blue, and other allosteric inhibitors are shown in green. This image was prepared in PyMOL using PDB code 2KHO.

in vitro. Thus, of all of the available Hsp70 inhibitors, I wanted to focus on MKT-077 analogs as potential antibiotics.

4.3 Results and discussion

4.3.1 Human Hsc70 and *E. coli* DnaK have conserved allosteric networks that are modulated by MKT-077 analogs

There is high sequence conservation between Hsc70 and DnaK, including in the allosteric site I described in chapter 3. However, Hsc70 and DnaK do not always have the same allosteric control mechanisms. For example, client binding stimulates the ATPase activity of DnaK, but not Hsp70. Thus, my first step in this project was to explore whether the MKT-077 binding site and its associated allosteric networks were conserved in *E. coli* DnaK. Accordingly, I made mutations in the analogous residues of full length DnaK: Y145A, Y145K, D201A, T221A, and T225A (**Appendix 4.6.1**). Then, I tested each mutant in the same biochemical assays used to study Hsc70 mutants in chapter 3. The results are summarized in **Figure 4.2** and the raw data can be found in **Appendix 4.6.2-9**. These results showed that these allosteric networks are conserved between the orthologs. For example, $DnaK^{D201A}$ behaved similarly to $Hsc70^{D206A}$: it bound nucleotide, it was not stimulated by a J protein, and it was not able to refold luciferase. Like I found in the human system, mutations within the MKT-077 binding pocket have a minor effect on DnaK's ability to bind, release, or turnover nucleotide (**Figure 4.2** and **Appendix 4.6.2-5**). Instead, they impaired, and in some cases abolished, refolding activity (**Appendix 4.6.6** and **4.6.7**). These results suggest that the allosteric networks controlling inter-domain allostery are conserved. Moreover, these

(A) Human Hsc70 chaperone system.

Hsc70 Proteins	Chaperone Activities							
	Bind ATP	NEFs Promote ATP Release	Intrinsic ATPase Activity	J-stimulated ATPase Activity	J-mediated Refolding	NEF-mediated Refolding	Substrate Binding Nucleotide Dependence	Partial Proteolysis Nucleotide Dependence
wt								
R76A								
Y149A								
Y149W								
F150A								
D206A								
T222A								
T222M								
D225A								
T226A								
H227A								
L228A								

Yes
No
N/T

(B) *E. coli* DnaK chaperone system.

DnaK Proteins	Chaperone Activities							
	Bind ATP	NEFs Promote ATP Release	Intrinsic ATPase Activity	J-stimulated ATPase Activity	J-mediated Refolding	NEF-mediated Refolding	Substrate Binding Nucleotide Dependence	Partial Proteolysis Nucleotide Dependence
wt								
Y145A (Y149)								
Y145K (Y149)								
Y145W (Y149)								
D201A (D206)								
T221A (T222)								
T225A (T226)								

Yes
No
N/T

Figure 4.2 Summary of MKT-077 binding site mutations' effects on various Hsc70 and DnaK activities. Green signifies functional activities, while red indicates broken activities. Gray signifies that the mutant was not tested (N/T) in that assay. (A) Mutational analysis of the human Hsc70 chaperone system. (B) Mutational analysis of *E. coli* Hsp70 (DnaK) system. Corresponding residue numbers for Hsc70 are indicated in parentheses.

results suggest that MKT-077 and its analogs might block the essential chaperone function of DnaK in pathogens.

4.3.2 Screening MKT-077 analog library for antibacterial activity

A focused library of 124 MKT-077 analogs was synthesized by a former postdoctoral scholar in the Gestwicki laboratory, Xiaokai Li. He designed these molecules to have improved metabolic stability (Figure 4.3C), which was a significant liability of the parent molecule. Each compound was screened using a 96-well plate OD_{600} turbidity platform at

a single concentration (16 µg/mL) in triplicate against six bacterial strains, including two Gram-negatives (*E. coli* and *Haemophilus influenzae*) and four Gram-positives (*Bacillus anthracis*, *Bacillus cereus*, *Bacillus subtilis*, and *S. aureus*) (Figure 4.3A). I defined the

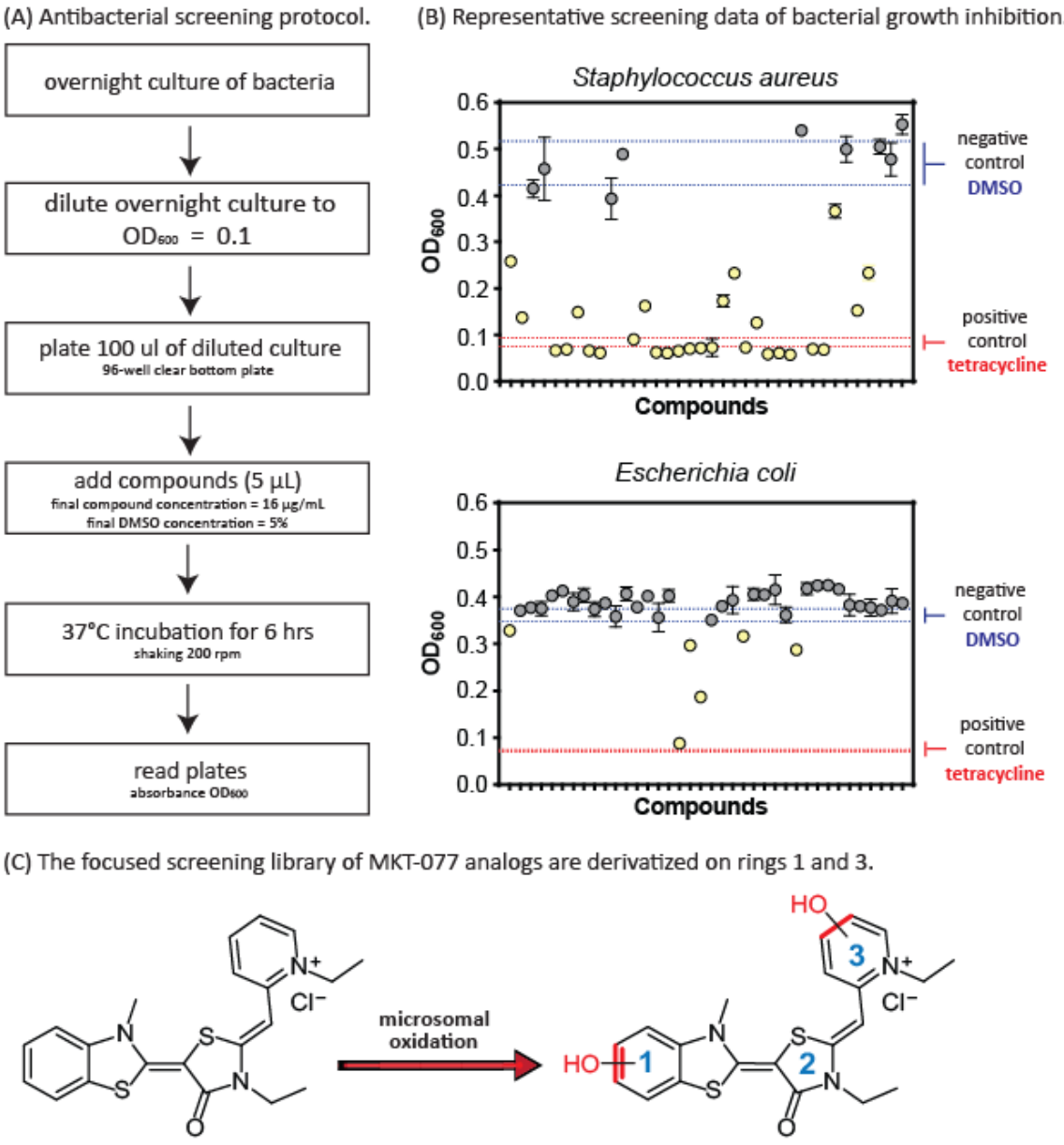

Figure 4.3 Identification of MKT-077 analogs with antibacterial activity. (A) Detailed protocol of antibacterial screening method. (B) Representative screening data of compounds against *S. aureus* and *E. coli* in a bacterial growth assay. Dotted lines represent the average growth and standard deviations in presence of the controls. Results are the average of triplicates and the error bars represent SEM. Gray data points indicate inactive compounds, while yellow data points represent active (hit) compounds. (C) The focused screening library of MKT-077 analogs are derivatized on rings 1 and 3 to help reduce microsomal oxidation of compounds.

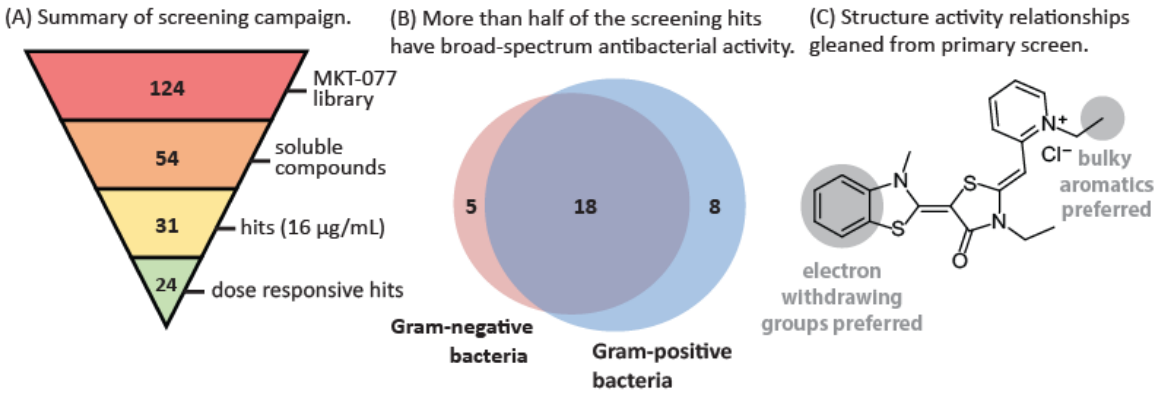

Figure 4.4 Summary of primary screening results. (A) Summary of the screening campaign. (B) Venn diagram depicting the distribution of screening hits amongst Gram-negative and Gram-positive bacteria. (C) Structure activity relationships gleaned from primary screen.

negative control as the growth of each bacterial strain in the presence of 5% DMSO. The positive control was bacterial growth in the presence of 16 µg/mL tetracycline. Compounds that significantly decreased turbidity relative to DMSO were considered "active" (Figure 4.3B and Appendix 4.6.10). Of the 124 molecules in the MKT-077 library, only 54 compounds were sufficiently soluble in this screening format. From these soluble compounds, 31 were active against at least one of the six bacterial strains (Figure 4.4A). Additionally, 18 molecules were active against both Gram-negatives and Gram-positives (Figure 4.4B). Compounds that were active tended to have electron withdrawing groups on the benzothiazole and bulky aromatics appended to the pyridine (Figure 4.4C).

4.3.3 MKT-077 analog, JG97, has antibacterial activity in liquid and solid media

The 31 compounds that were active against at least one of the six bacterial strains were then subjected to confirmatory retesting to determine their minimum inhibitory concentration (MIC) values (Table 4.1). Interestingly, none of the compounds tested were active against *E. coli* (MIC > 16 µg/mL) upon retesting. Five compounds (JG43, JG70, JG73,

Table 4.1 Minimum inhibitory concentrations of hit compounds from primary screening.

	MIC (μg/mL)					
Compound	***B. subtilis***	***B. anthracis***	***B. cereus***	***S. aureus***	***E. coli***	***H. influenzae***
MKT-077	**NT**	**NT**	**>16**	**>16**	**NT**	**16**
YM1	NT	>16	NT	>16	NT	16
YM9	NT	NT	NT	NT	NT	>16
YM21	NT	NT	NT	NT	NT	>16
JG12	>16	>16	NT	>16	NT	16
JG18	NT	>16	NT	NT	NT	>16
JG31	NT	>16	NT	NT	NT	16
JG33	>16	16	16	16	NT	8
JG35	NT	>16	NT	16	NT	16
JG37	NT	NT	NT	NT	NT	>16
JG38	NT	>16	>16	NT	NT	16
JG41	NT	16	>16	16	NT	8
JG43	16	8	8	8	NT	8
JG44	NT	NT	NT	NT	NT	NT
JG58	NT	NT	NT	NT	NT	>16
JG60	NT	>16	>16	>16	NT	16
JG66	NT	>16	NT	>16	NT	NT
JG70	8	8	8	8	NT	16
JG71	>16	NT	NT	NT	>16	NT
JG73	16	8	16	16	>16	8
JG74	NT	8	8	8	>16	4
JG78	NT	4	8	4	NT	8
JG81	>16	>16	>16	>16	NT	16
JG83	8	4	16	8	NT	4
JG86	NT	16	NT	>16	NT	8
JG91	>16	16	>16	16	NT	4
JG96	>16	8	8	8	NT	16
JG97	16	4	8	8	NT	16
JG98	2	NT	NT	NT	NT	NT
JG110	NT	NT	NT	NT	NT	NT
JG111	NT	16	NT	>16	NT	NT
JG121	>16	>16	NT	NT	NT	16
JG123	NT	NT	NT	NT	NT	>16
Tetracycline	**2**	**0.25**	**0.5**	**1**	**4**	**1**
DMSO	**>16**	**>16**	**>16**	**>16**	**>16**	**>16**

Molecules were only tested against bacterial strains in which they showed activity against in the primary screen. Gray boxes indicate that the compound was not tested (N/T) against that bacterial strain.

JG83, and JG97) had MIC values < 16 μg/mL against five of the six bacterial strains. The best of these compounds, JG83 and JG97, had MIC values between 4 and 16 μg/mL (Table 4.1). JG97 has better solubility properties than JG83, so it was chosen for further study.

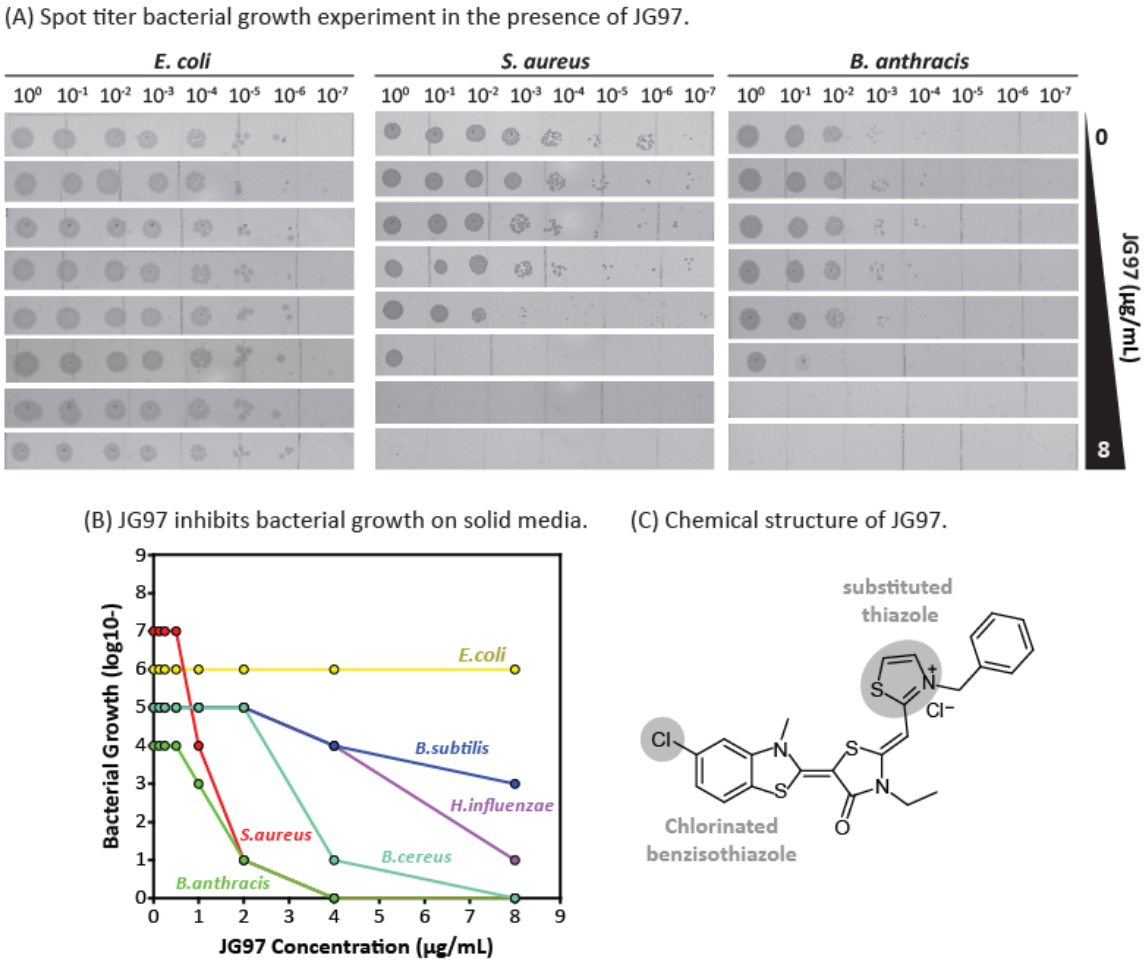

Figure 4.5 JG97 inhibits the growth of bacteria on solid media. (A) Solid media spot titers of bacterial growth in the presence of JG97. Representative data are shown for the *E. coli*, *S. aureus*, and *B. anthracis*. (B) Quantification of solid media spot titer assay. (C) Chemical structure of JG97.

This compound was resynthesized and its activity was reconfirmed in the MIC assay. Next, I tested JG97 activity in solid agar and found that it dose-dependently inhibited the growth of all strains, except *E. coli* (Figure 4.5 and Appendix 4.6.11). Thus, this screening effort yielded JG97 as a particularly promising lead.

4.3.4 Second generation JG97 analogs have potent antibacterial activity

With this promising result, I wanted to explore the structure activity relationships (SAR) around compound JG97. Together, with Xiaokai Li, I assembled a collection of 197 analogs

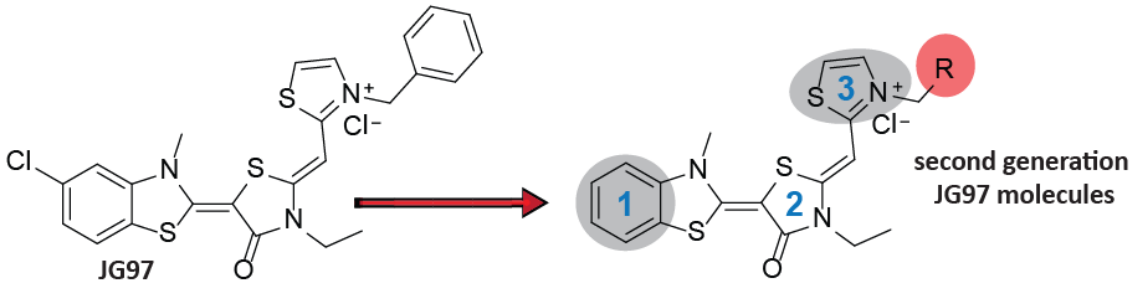

Figure 4.6 Second generation JG97 molecules were designed to have improved solubility and potency. Specifically, the thiazole moiety of JG97 was functionalized, which is highlighted in red.

of JG97. This library was designed with the intention of improving both compound solubility and potency. Specifically, we largely focused on functionalizing the thiazole group (ring 3) (Figure 4.6). Each library member was tested in the MIC assay against *S. aureus*. Only seven molecules (4% of the library) exhibited poor solubility in this assay, which was a substantial improvement on the primary screen. Of ~200 compounds tested, 13 had MIC values < 2 µg/mL and thus were chosen for further study. The structures of these compounds can be seen in Appendix 4.6.12. Next, I tested these compounds in liquid broth cultures and found that they all dose-dependently inhibited the growth of *S. aureus* (Appendix 4.6.13). Additionally, using this assay, I identified four compounds (JG220, JG296, JG319, and JG314) that dose-dependently increased the lag time of *E. coli* growth (Figure 4.7), a sign that they had some bioactivity in this model. These compounds were especially aliphatic, suggesting that physical properties might be used to enhance broad-spectrum antibacterial activity in the future.

Finally, I wanted to test the activity of our lead molecules against a wider panel of bacterial strains. In collaboration with the Sylvie Garneau-Tsodikova laboratory (University of

Kentucky), we determined the MICs of thirteen compounds against pathogenic bacterial strains, including clinical isolates of MRSA and vancomycin-resistant enteroccoci (VRE). At the same time, we tested JG-237, which is a structurally related negative control molecule that does not interact with Hsp70/DnaK (Appendix 4.6.12 and 4.6.14). As expected JG237

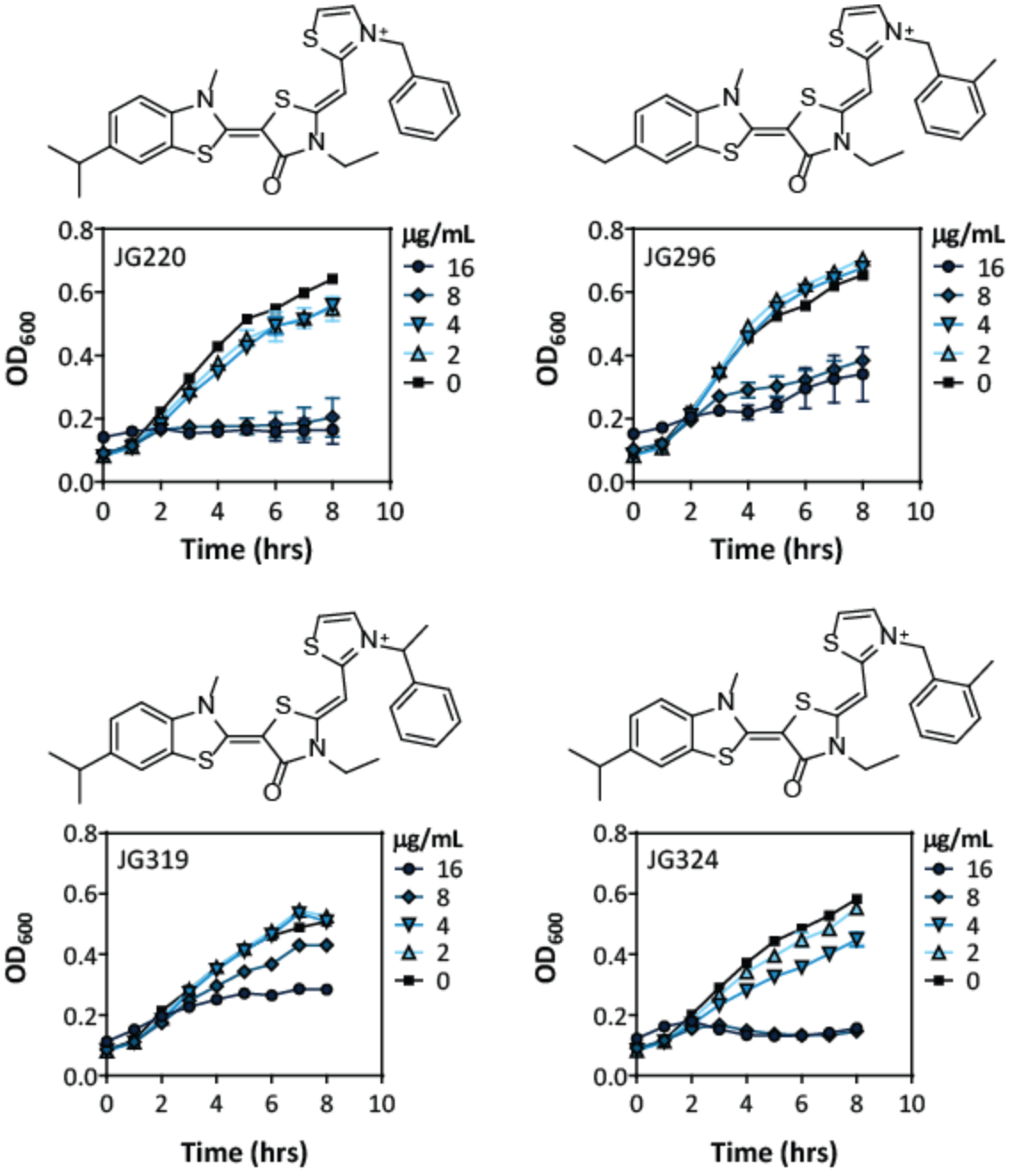

Figure 4.7 Aliphatic JG97 analogs dose-dependently increase of lag time ***E. coli*** **growth in liquid culture.** Growth curve experiment were performed twice in triplicate. Representative graphs are shown.

did not exhibit any antibacterial activity (MIC > 64 μg/mL). Additionally, with few exceptions, JG97 analogs were not active against the Gram-negative bacteria, such as *S. enterica* or *Pseudomonas aeruginosa* (MIC > 64 μg/mL). Instead, Gram-positive bacteria were much more susceptible to compound treatment. The activity against MRSA (MIC values ranging between ~0.125 and 1 μg/mL) and VRE (MIC values ranging between 0.25 and 16 μg/mL) was particularly promising (Appendix 4.6.14). These MIC values are comparable to those of newly approved antibiotics linezolid (MIC = 0.25 – 1 μg/mL) and daptomycin (MIC = 0.064 – 1.5 1 μg/mL) against MRSA [19]. This finding is particularly important, because the increasing frequency of resistant pathogens, such as MRSA and VRE, is presenting a therapeutic problem due to limited drug options [20, 21]. Based on these results, MKT-077 analogs appear to be useful chemical probes for studying the role of Hsp70/DnaK in bacterial pathogenesis. Further, these compounds might serve as leads for the development of antibiotics with a new target and a new mechanism of action.

4.4 Conclusions

4.4.1 DnaK is an antibacterial drug target

A wealth of genetic data strongly suggests that DnaK could be an antibacterial drug target. However, it was not clear what activity of DnaK should be inhibited to achieve the same result with a small molecule. Previous work from our group had suggested that inter-domain allostery and luciferase refolding might be especially important to bacterial survival. This observation, combined with my work on MKT-077 in chapter 3, suggested that these molecules might be particularly attractive as antibiotics. In this chapter, I first

used mutagenesis to show that the MKT-077 binding site controls a conserved allosteric networks in both human and prokaryotic Hsc70/DnaK. I found that interruption of these networks impairs refolding of luciferase, suggesting that MKT-077 analogs might indeed be antibiotics. Next, I tested analogs of MKT-077 for activity against pathogenic Gram-positive and Gram-negative strains. I found that several MKT-077 derivatives had promising activity against Gram-positive strains, including drug resistant pathogens, with MIC values ranging from 8 to < 0.125 μg/mL. These results validate DnaK as an antibacterial target. More specifically, these results clarify that the refolding activity of DnaK is a key function required for bacterial growth.

We found that some of the most dangerous pathogenic strains, such as MRSA and VRE, were especially susceptible to MKT-077 analogs. This observation raises the interesting possibility that DnaK might be especially important in pathogens, which often express virulence factors. Existing in this heightened pathogenic state might create a stress on the bacteria that creates an "addiction" to DnaK, analogous to what has been observed in human cancers and Hsp70 (as discussed in chapter 1). Thus, one interesting future direction for this project is to use MKT-077 analogs as chemical probes to better understand the relationships between DnaK and virulence factors.

4.5 Experimental procedures

4.5.1 Plasmids

All proteins were expressed from a pMCSG7 vector that contained an N-terminal His-tag and TEV cleavage site. Site-directed mutagenesis for DnaK mutants (Y145A, Y145K, Y145W, D201A) was performed using the Phusion Site-Directed Mutagenesis Kit protocol (New England Biolabs, Ipswich, MA).

4.5.2 Protein expression and purification

Full length DnaK proteins were expressed, purified, and made apo (nucleotide free) using the same procedure as described for full length wt Hsp72 in chapter 2. *E.coli* GrpE was expressed in *E. coli* BL21 (DE3) cells. Liter cultures of terrific broth were grown at 25 °C until an OD_{600} of 0.6 was reached. Cultures were cooled to 18 °C before induction with IPTG (final concentration of 200 µM) and then grown overnight. Cells were lysed by sonication, pelleted by centrifugation, and the supernatant was applied to Ni-NTA His-Bind Resin (Novagen, Darmstadt, Germany). The resin was washed with His-binding buffer (50 mM TRIS, 10 mM Imidazole, 500 mM NaCl, pH 8), followed by His-washing buffer (50 mM TRIS, 30 mM Imidazole, 300 mM NaCl, pH 8). The protein was then removed from the resin using His-elution buffer (50 mM TRIS, 300 mM Imidazole, 300 mM NaCl, pH 8). The N-terminal His-tag was then removed using TEV protease. Next, the protein was dialyzed in His-binding buffer and the remaining cleaved His-tag was removed by a second Ni-NTA column. The purified protein was dialyzed into 25 mM HEPES, 5 mM $MgCl_2$, 10 mM KCl, pH 7.5 buffer before storage.

E.coli, DnaJ was expressed in *E. coli* BL21 (DE3) cells. Liter cultures of terrific broth were grown at 37°C until an OD_{600} of 0.6. Cultures were cooled to 18 °C before induction with IPTG (final concentration of 200 µM) and then grown overnight. Cell pellets were re-suspended in DnaJ His-binding buffer (25 mM TRIS, 10 mM Imidazole, 500 mM NaCl, pH 8) supplemented with protease inhibitors. Cells were lysed by sonication, subjected to centrifugation, and the supernatant was then applied to Ni-NTA His-Bind Resin (Novagen, Darmstadt, Germany). The resin was washed with the DnaJ His-binding buffer, followed by an extensive wash with DnaJ His-washing buffer 1 (25 mM TRIS, 30 mM Imidazole, 500 mM NaCl, 3% ethanol, pH 8). The resin was washed a third time with DnaJ His-washing buffer 2 (25 mM TRIS, 30 mM Imidazole, 100 mM NaCl, 3% ethanol, pH 8). Finally, the protein was then removed from the resin with the His-elution buffer (25 mM TRIS, 300 mM Imidazole, 300 mM NaCl, pH 8). The purified protein was concentrated and exchanged into a 25 mM HEPES, 5 mM $MgCl_2$, 150 mM KCl pH 7.4 buffer for storage. Note that the N-terminal His-tag was not removed.

4.5.3 Fluorescence polarization assays

All experiments were performed in 384-well, black, low volume, round-bottom plates (catalog number = 4511, Corning, NY). Polarization values in millipolarization units (mP) were measured at an excitation wavelength at 485 nm and an emission wavelength at 530 nm using a Molecular Devices Spectramax M5 plate reader (Sunnyvale, CA). For binding experiments, equilibrium-binding isotherms were constructed by plotting FP readings as a function of the protein concentration at a fixed concentration of a tracer. All

experiments were performed at least twice in triplicate. Results are shown as the average and SEM. All experimental data were analyzed using GraphPad Prism 6 software. The binding of DnaK proteins to the fluorescent ATP analog (Fam-ATP) and the fluorescent substrate peptide (Fam-HLA) was performed using the procedures described for wt Hsp72 in chapter 2. Additionally, we also determined the ability of GrpE to promote the release of the Fam-ATP probe from DnaK proteins. First, an apo DnaK protein was added to each well. The concentration of protein added equals the concentration of DnaK at which 50% of the FP probe (Fam-ATP) is bound based on binding experiments. Next, a 2-fold dilution series of GrpE made using the assay buffer (100 mM TRIS, 20 mM KCl, 6 mM $MgCl_2$, 0.001% Triton X-100, pH 7.4), was added. Final concentrations of GrpE ranged from 0 to 15 µM. Finally, Fam-ATP was added to each well, to give a final concentration of 20 nM and a total assay volume of 20 µL. The plate was covered from light and allowed to incubate at room temperature for 30 minutes in order to reach equilibrium.

4.5.4 ATPase assays

These experiments were performed using previously described methods with minor modifications [14, 22]. Stocks of malachite green (0.081% w/v), polyvinyl alcohol (2.3% w/v), and ammonium heptamolybdate tetrahydrate (5.7% w/v in 6 M HCl) were prepared and mixed with water in a 2:1:1:2 ratio to make the malachite green reagent. All experiments were performed in 96-well, clear plates. Intrinsic ATPase rates of DnaK proteins were determined in the absence of co-chaperones. A 2-fold dilution series of Hsc70 was added to wells and final concentrations ranged from 0 to 7 µM. For co-

chaperone stimulation assays, DnaK (final concentration of 1 µM) and various concentrations of DnaJ and/or GrpE was added to the wells. Next, ATP (final concentration of 1 mM) was added to each well, bringing the reaction volume to 25 µL. Reactions were incubated for 1 h at 37 °C, developed with the addition of 80 µL malachite green reagent, and then immediately quenched with 10 µL of 32% (w/v) sodium citrate. Assays were incubated at 37 °C for 15 minutes and then measured at OD_{620} using a Molecular Devices Spectramax M5 plate reader (Sunnyvale, CA). Additionally, background signal from non-specific ATP hydrolysis in controls was subtracted. Phosphate standard curve of potassium dibasic phosphate was used to calculate pmol P_i/chaperone µg/min. Stimulation curves were fit to a modified Michaelis Menten equation ($y = V_{max} \bullet X/(K_m+x)+b$). All experiments were performed at least twice in triplicate. All experimental data were analyzed using GraphPad Prism 6 software.

4.5.5 Luciferase refolding assays

Experiments were performed as described previously [23]. Briefly, working stocks of denatured luciferase were prepared by mixing 10 µL of 203 µM native luciferase (Promega) with 30 µL of 8 M GnHCl for 1 h at room temperature. Denatured luciferase stocks were stored at -80 °C until use. To white 96-well plates, was added denatured luciferase (final concentration of 100 nM), DnaK (final concentration of 1 µM), and various concentrations of DnaJ and/or GrpE to give a final volume of 25 µL in refolding buffer (23 mM HEPES, 120 mM KAc, 1.2 mM MgAc, 15 mM DTT, 61 mM creatine phosphate, 35 U/mL creatine kinase, 5 ng/µL BSA, pH 7.4). The reaction was initiated by adding 10 uL of 2.5 mM ATP to give a

final concentration of 1 mM. Plates were covered and incubated at 37 °C for 1 h. Next, 25 uL of Steady-Glo reagent (Promega) was added to each well and luminescence values were measured immediately using a Molecular Devices Spectramax M5 plate reader (Sunnyvale, CA).

4.5.6 Partial proteolysis

Partial proteolysis experiments were performed using previously described procedures [14]. Samples of 6 µM DnaK were prepared in a partial proteolysis buffer (40 mM HEPES, 20 mM NaCl, 8 mM MgCl2, 20 mM KCl, 0.3 mM EDTA, pH 8.0) with either 1 mM ATP or ADP. Samples were allowed to incubate at room temperature for 30 minutes. Next, Trypsin (EC 3.4.21.4, Sigma) was added at 1:4 (Trypsin:Hsc70) molar ratio, bringing the reaction volume to 50 µL. Proteolysis was carried out over a 40 minute time span. Reactions were quenched at 5, 10, 20, and 40 minute time intervals with 25 µL of SDS loading buffer (240 mM TRIS, 6% (w/v) SDS, 30% (v/v) glycerol, 16% (v/v) β-mercaptoethanol, 0.6 mg/mL bromophenol blue, pH 6.8) and then heated at 95 °C for 3 minutes. Samples were then subjected to SDS-PAGE using 10% Mini-PROTEAN TGX Precast Gels (cat # =4561036, BioRad). Gels were run for ~40 minutes at 200V and then stained with Coomassie blue.

4.5.7 Growth and maintenance of laboratory bacterial strains

The following bacterial strains were used in the primary screen: *Bacillus anthracis* 34F2 Sterne, *Bacillus cereus* ATCC 11778, *Bacillus subtilis* 168, *Escherichia coli* K-12 (MG1655), *Haemophilus influenzae* ATCC 51907, and *Staphylococcus aureus* RN4220. *H. influenzae*

was grown in Brain Heart Infusion (BHI) media supplemented with hemin and β-nicotinamide adenine dinucleotide hydrate [24]. Broth cultures of *H. influenzae* were prepared by scraping bacteria from agar plates and suspending into fresh supplemented BHI medium to the desired OD_{600}. *B. anthracis* 34F2 Sterne, *B. cereus* ATCC 11778, *B. subtilis* 168, and *E.coli* K-12 (MG1655) were grown in Luria–Bertani (LB) medium. Inoculum for liquid culture assays was prepared by diluting an overnight LB broth culture, grown at 37 °C with shaking (200 rpm), into fresh liquid medium to the desired OD_{600}. All other bacterial strains were maintained by the Sylvie Garneau-Tsodikova laboratory according to procedures defined by the Clinical & Laboratory Standards Institute [25].

4.5.8 Antibacterial screening assay

Bacterial inoculum of each strain was prepared to an OD_{600} of 0.1 as described above. Next, 100 µL of each dilute culture was added in triplicate to a sterile non-treated CytoOne 96-well clear bottom plate. To each well, was added 5 µL of either compound in DMSO or DMSO alone. The final concentration of compound was 16 µg/mL and the concentration of DMSO was 5%. The plates were covered and incubated at 37 °C with shaking (200 rpm) for 6 hours. Afterwards, bacterial growth was recorded by measuring OD_{600} using a SpectraMax M5 plate reader.

4.5.9 Minimum inhibitory concentration assay

MIC experiments were performed using the double dilution method. Briefly, inoculum of *B. anthracis* 34F2 Sterne, *B. cereus* ATCC 11778, *B. subtilis* 168, *E. coli* K-12 (MG1655), *H.*

influenzae ATCC 51907 or *S. aureus* RN4220 was prepared to an OD_{600} of 0.1 as described above and 200 µL of each dilute culture was added to a sterile non-treated CytoOne 96-well clear bottom plate. To the plated dilute cultures, was added 10 µL of compound from a 2-fold dilution series. The final concentrations of the compounds were in the range of 16 to 0.25 µg/mL. Plates were covered and incubated at 37 °C with shaking (200 rpm) for 24 hours before MIC values were determined. These experiments were performed at least twice in triplicate. For all other bacterial strains, MIC experiments were performed by the Sylvie Garneau-Tsodikova laboratory according to procedures defined by the Clinical & Laboratory Standards Institute[25].

4.5.10 Bacterial growth assay in liquid culture

Bacterial cultures were prepared to an OD_{600} of 0.1 as described above and 200 µL of each dilute culture was added to the wells of sterile non-treated CytoOne 96-well clear bottom plates. Compounds (10 µL) from a 2-fold dilution series were then added to a final concentration between 32 and 1 µg/mL. Plates were covered and incubated at 37 °C with shaking (200 rpm). Bacterial growth was recorded every ~30 minutes by measuring OD_{600} using a SpectraMax M5 plate reader.

4.5.11 Spot titer assays

Bacterial cultures were prepared to an OD_{600} of 0.5 as described above. These cultures were then serially diluted 10-fold in sterile phosphate buffered saline and spotted (1 µL)

on pre-warmed LB agar plates containing various concentrations of JG97. Finally, colonies were counted after incubation for 24 hours at 37 °C.

Notes

Experiments in this chapter were designed by Victoria A. Assimon and Jason E. Gestwicki. Isabelle R. Taylor performed ATPase and refolding assays. Daniel Nguyen assisted with the primary antibacterial screen. Xiaokai Li synthesized all MKT-077 analogs. MIC experiments against pathogenic bacterial strains were performed in collaboration with the Sylvie Garneau-Tsodikova laboratory (University of Kentucky). All other experiments were performed by Victoria A. Assimon.

4.6 Appendix

4.6.1 Analysis of purified DnaK mutants by SDS-PAGE.

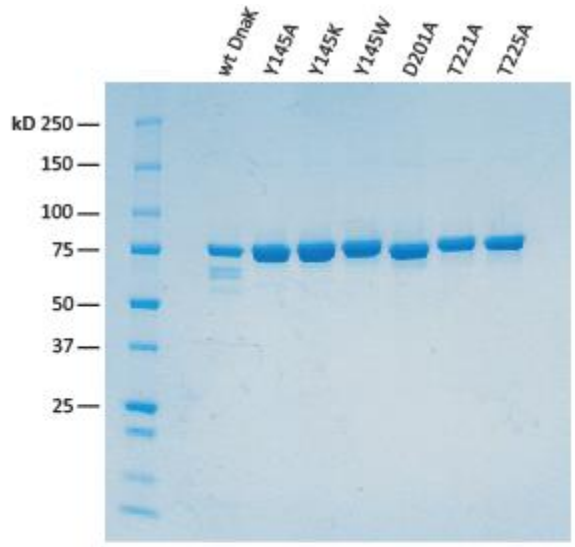

Appendix 4.6.1 Analysis of purified DnaK mutants by SDS-PAGE. To a well was loaded 10 µL of a protein sample. Samples were prepared by diluting DnaK protein using a 100 mM TRIS buffer (20 mM KCl, 6 mM $MgCl_2$, 0.001% Triton X-100, pH 7.4). The final concentration of the samples was 4 µM after adding loading dye. Gels (10% Mini-PROTEAN TGX) were run for ~40 minutes at 200V and then stained with Coomassie blue.

4.6.2 DnaK mutants can engage with nucleotide

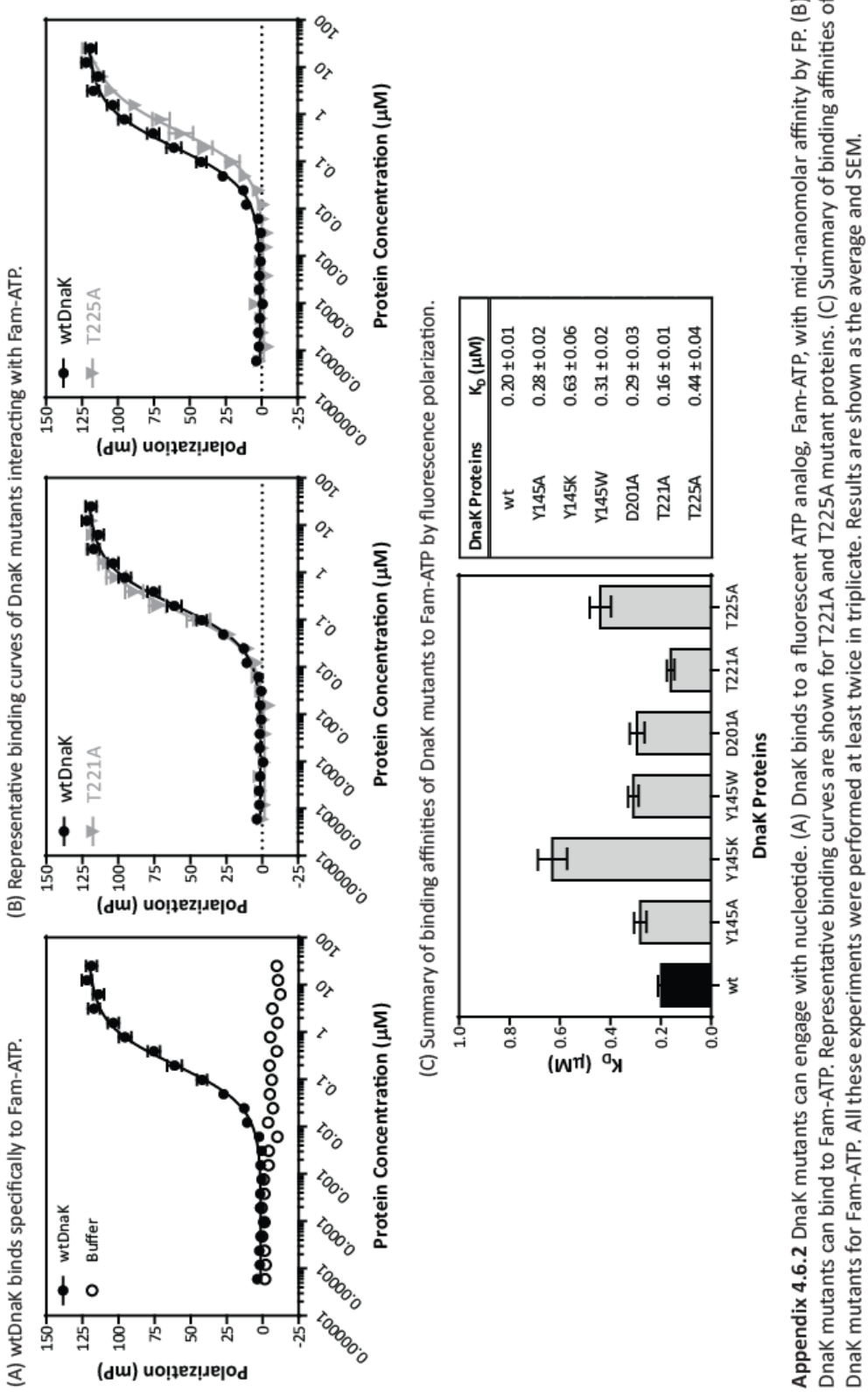

Appendix 4.6.2 DnaK mutants can engage with nucleotide. (A) DnaK binds to a fluorescent ATP analog, Fam-ATP, with mid-nanomolar affinity by FP. (B) DnaK mutants can bind to Fam-ATP. Representative binding curves are shown for T221A and T225A mutant proteins. (C) Summary of binding affinities of DnaK mutants for Fam-ATP. All these experiments were performed at least twice in triplicate. Results are shown as the average and SEM.

4.6.3 GrpE promotes the release of nucleotide from DnaK mutants

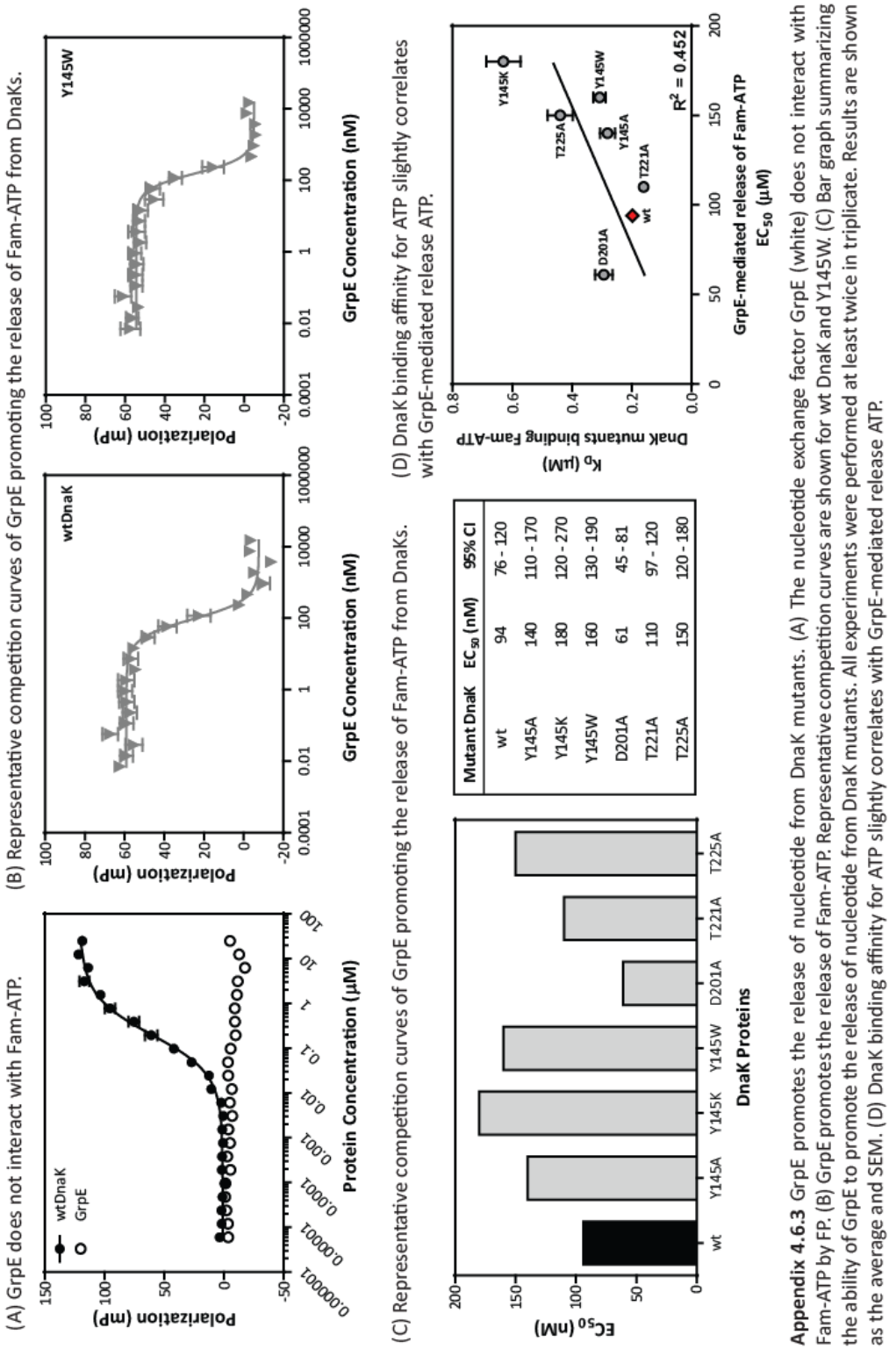

Mutant DnaK	EC_{50} (nM)	95% CI
wt	94	76 - 120
Y145A	140	110 - 170
Y145K	180	120 - 270
Y145W	160	130 - 190
D201A	61	45 - 81
T221A	110	97 - 120
T225A	150	120 - 180

Appendix 4.6.3 GrpE promotes the release of nucleotide from DnaK mutants. (A) The nucleotide exchange factor GrpE (white) does not interact with Fam-ATP by FP. (B) GrpE promotes the release of Fam-ATP. Representative competition curves are shown for wt DnaK and Y145W. (C) Bar graph summarizing the ability of GrpE to promote the release of nucleotide from DnaK mutants. All experiments were performed at least twice in triplicate. Results are shown as the average and SEM. (D) DnaK binding affinity for ATP slightly correlates with GrpE-mediated release ATP.

4.6.4 The ATPase activity of DnaK mutants

DnaK Protein	Intrinsic ATPase Rate	DnaJ Stimulation		GrpE Stimulation		Substrate Stimulation	
	$pmolP_i/\mu g/min$	$Vmax_J$ $pmolP_i/\mu g/min$	Km_J μM	$Vmax_E$ $pmolP_i/\mu g/min$	Km_E nM	$Vmax_{NR}$ $pmolP_i/\mu g/min$	Km_{NR} μM
WT	**1.7 ± 0.1**	**19.5 ± 0.8**	**0.19 ± 0.03**	**23.4 ± 1.58**	**58.4 ± 15.7**	**10.1 ± 5.4**	**44.9 ± 62.4**
Y145A	6.5 ± 0.3	25.7 ± 2.2	0.18 ± 0.06	40.3 ± 4.3	75.5 ± 30.9	37.3 ± 7.9	59.0 ± 28.9
Y145W	3.0 ± 0.2	13.1 ± 1.8	0.16 ± 0.08	38.2 ± 6.0	139.9 ± 70.1	NF	NF
Y145K	20.4 ± 0.9	5.3 ± 1.6	0.03 ± 0.04	128.0 ± 8.8	170.0 ± 34.7	17.1 ± 4.9	16.6 ± 18.0
D201A	0.6 ± 0.1	NF	NF	NF	NF	NF	NF
T221A	4.0 ± 0.1	22.5 ± 2.5	0.71 ± 0.29	NF	NF	4.2 ± 3.5	26.6 ± 71.9
T225A	8.4 ± 0.3	16.4 ± 2.7	0.13 ± 0.08	49.5 ± 7.4	135.5 ± 65.9	11.2 ± 1.2	12.3 ± 5.0

Gray boxes indicate that either the ATPase rate was not stimulated, as defined by a mutant in which the SEM of the K_m or V_{max} encompassed zero, or when a non-linear fit could not be obtained. Such proteins were deemed nonfunctional (NF). The V_{max} value (calculated by the equation described in Experimental Procedures) represents the increase in ATPase rate compared to a solvent control. All these experiments were performed at least twice in triplicate. Results are shown as the average and standard error of the mean. Raw data can be found in Appendix 4.6.5.

4.6.5 Co-chaperones mediate the stimulation of ATP turnover in wt DnaK and mutants

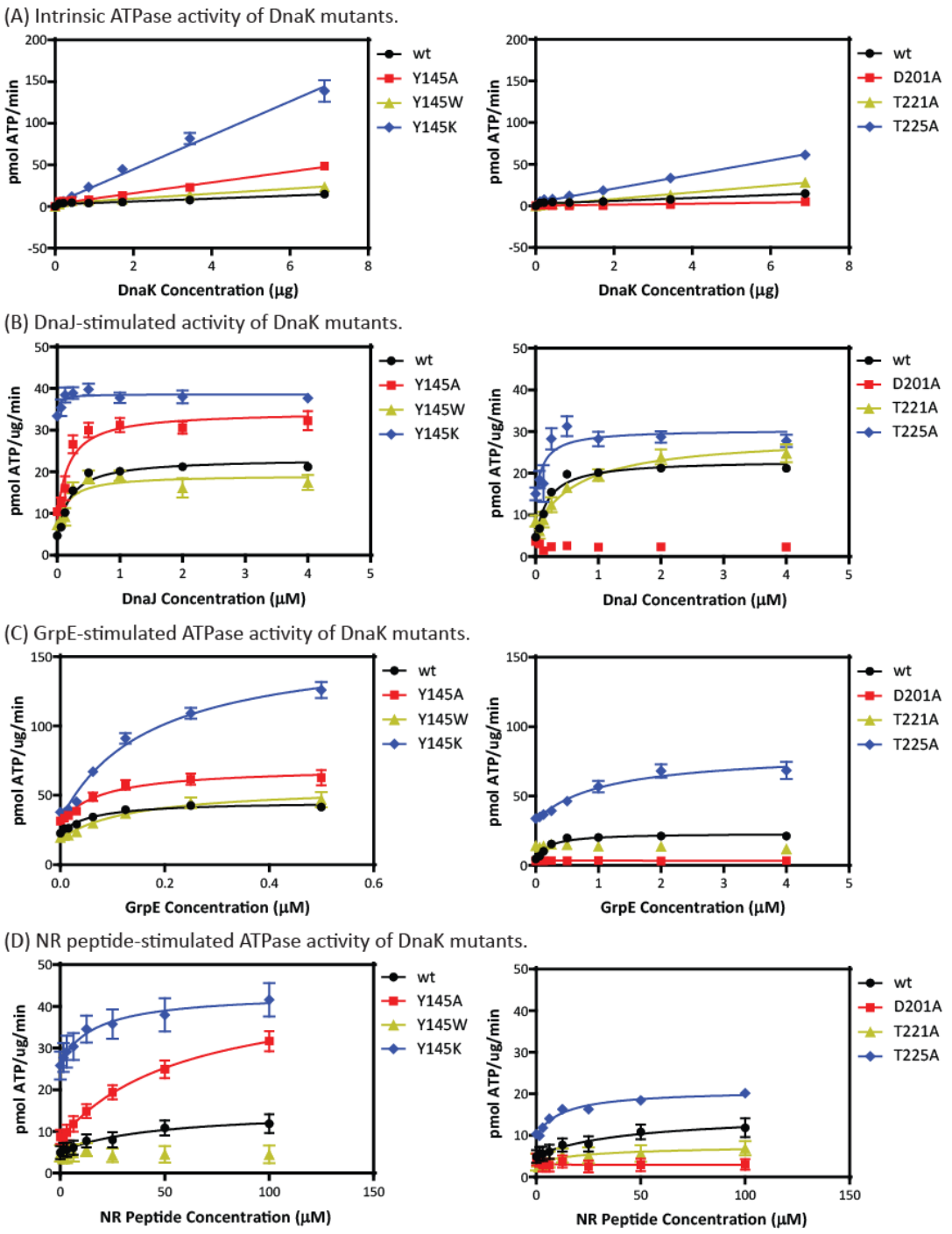

Appendix 4.6.5 Co-chaperones mediate the stimulation of ATP turnover in wt DnaK and mutants. (A) Intrinsic ATPase activity of DnaK mutants. (B) DnaJ-stimulated ATPase activity of DnaK mutants. A DnaK protein (1 µM) was incubated with DnaJ at the concentrations indicated. (C) GrpE-stimulated ATPase activity of DnaK mutants. Constant concentrations of a DnaK (1 µM) protein and DnaJ (0.25 µM) were incubated with increasing concentration of GrpE. (D) NR peptide-stimulated ATPase activity of DnaK mutants. A DnaK protein (1 µM) was incubated with NR-peptide at the concentrations indicated.

4.6.6 DnaK mutants are deficient in their DnaJ-mediated refolding of substrates

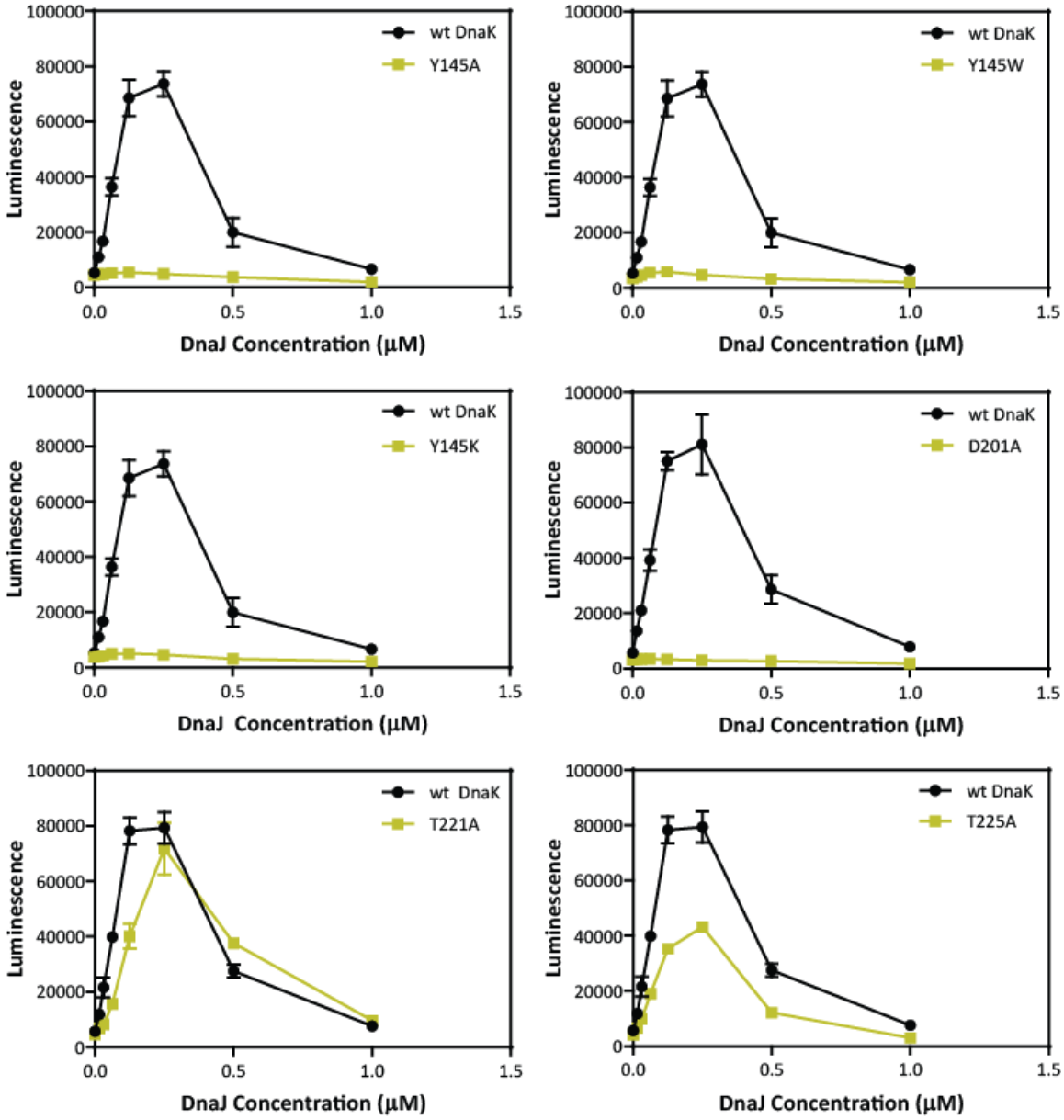

Appendix 4.6.6 DnaK mutants are deficient in their ability to refold substrates. Raw data of DnaK mutants refolding denatured luciferase in the presence of DnaJ. For this assay, DnaK (1 µM) and GrpE (0.1 µM) were incubated with DnaJ at the concentrations indicated.

4.6.7 DnaK mutants are deficient in their GrpE-mediated refolding of substrates

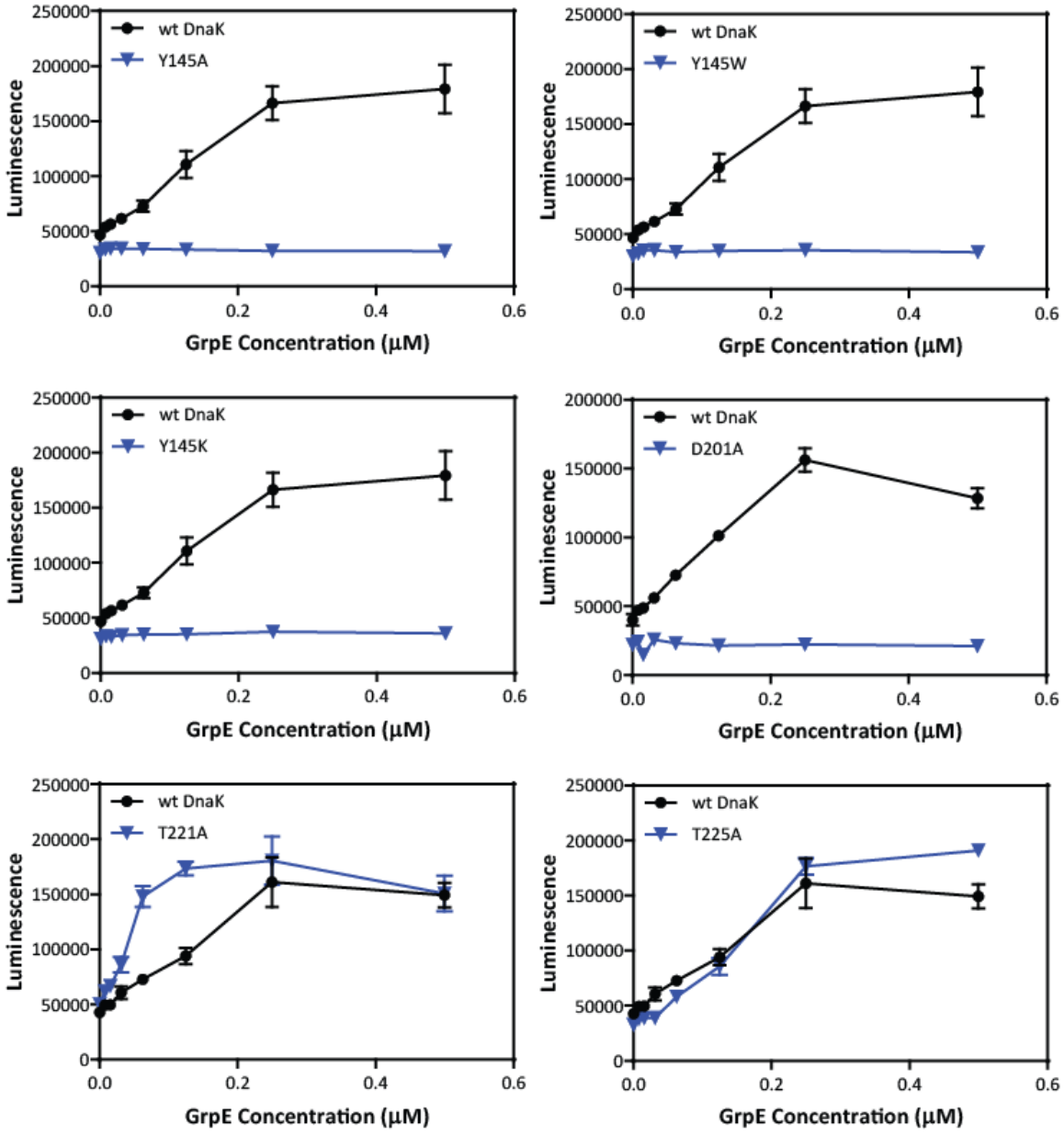

Figure 4.6.7 DnaK mutants are deficient in their ability to refold substrates. Raw data of DnaK mutants refolding denatured luciferase in the presence of GrpE. For this assay, DnaK (1 µM) and DnaJ (0.125 µM) were incubated with GrpE at the concentrations indicated.

4.6.8 DnaK mutants do not bind substrate in a nucleotide-dependent manner

(A) DnaK binds to Fam-HLA probe in a nucleotide dependent manner.

(B) The substrate peptide NRLLLTG can compete with Fam-HLA for binding to DnaK.

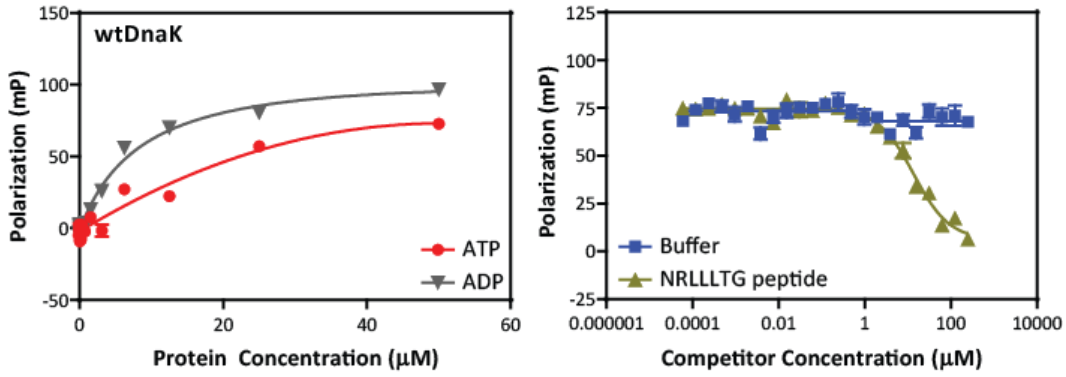

(C) Multiple DnaK mutants do not exhibit a nucleotide dependence when binding Fam-HLA.

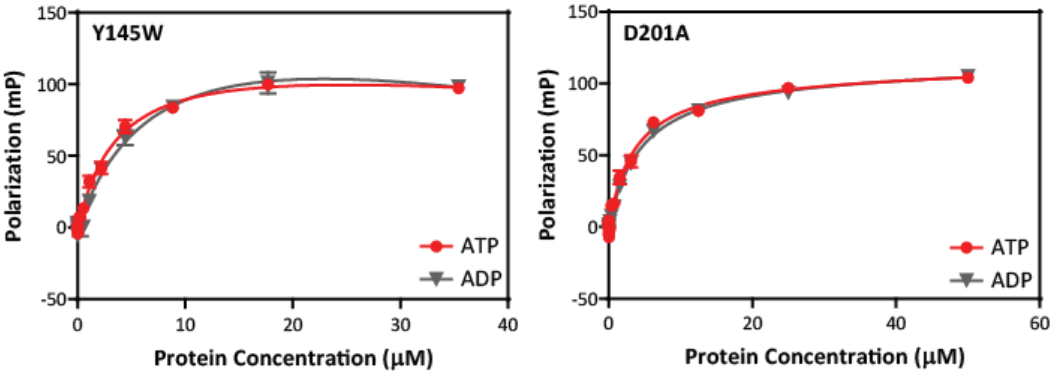

(D) Summary of binding affinities of DnaK mutants to Fam-HLA in the presence of ATP or ADP.

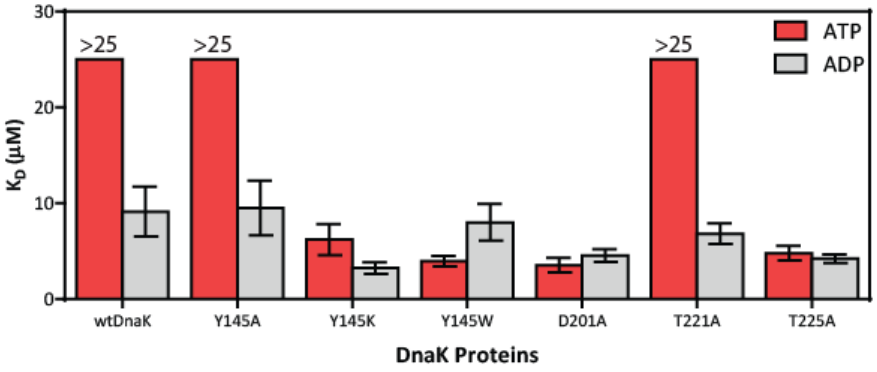

Appendix 4.6.8 DnaK mutants do not bind substrate in a nucleotide dependent manner. (A) Wt DnaK has low micromolar affinity for the substrate peptide probe, Fam-HLA, in presence of ADP (gray). In the presence of ATP, wt DnaK does not have appreciable affinity from Fam-HLA. (B) The model substrate peptide NRLLLTG can compete with Fam-HLA for binding to DnaK. (C) Multiple DnaK mutants do not exhibit a nucleotide dependence when binding Fam-HLA. Representative binding curves are shown for Y145W and D201A. (D) Summary of binding affinities of DnaK mutants to Fam-HLA in the presence of ATP (red) or ADP (gray).

4.6.9 Partial proteolysis pattern of DnaK mutants

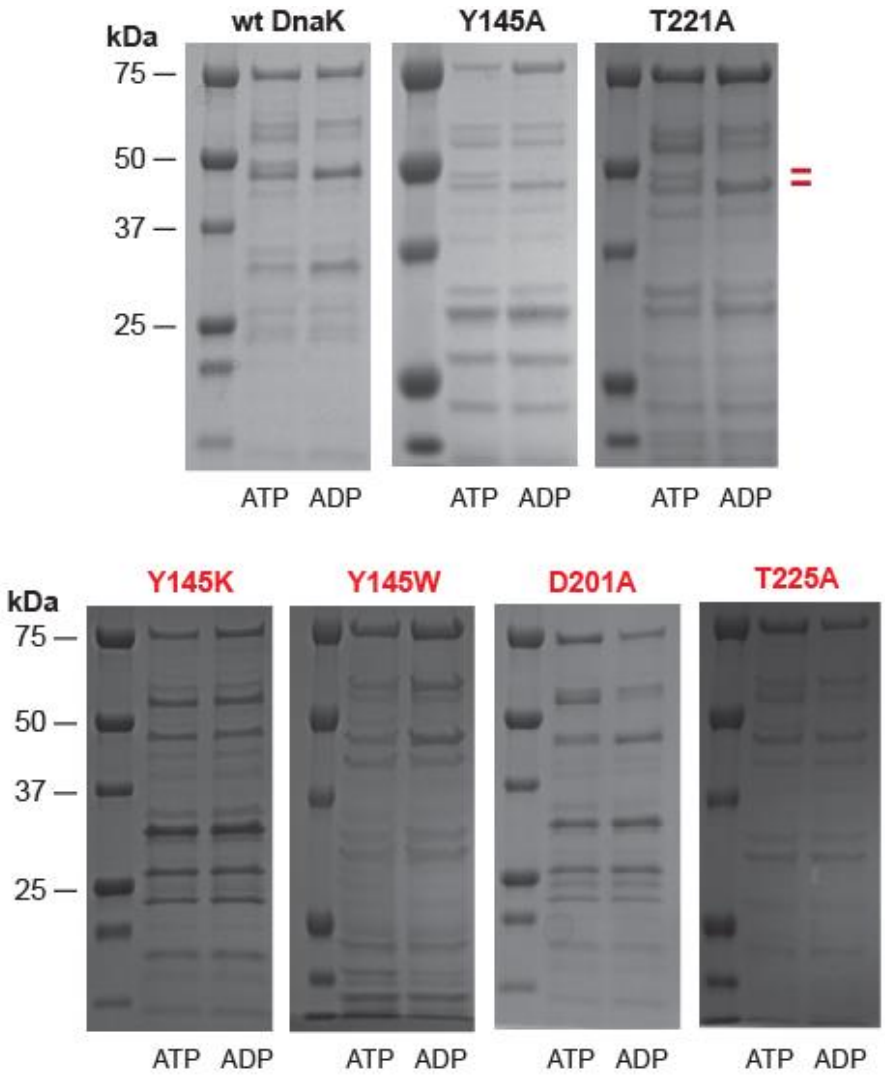

Appendix 4.6.9 Partial proteolysis pattern of DnaK mutants. Similar to wt DnaK, some mutants (Y145A and T221A) had a distinct digestion pattern between ATP- and ADP-bound forms. This is clearly seen in the bands around 48 kDa. Specifically, there were two bands when wt DnaK was in an ATP-bound state and one band when the chaperone was in an ADP-bound state. Other mutants (Y145K, Y145W, D201A, and T225A) assumed an ADP-like conformation even with excess ATP. For these experiments, proteolysis was carried out for 20 minutes.

4.6.10 Bacterial growth inhibition screens

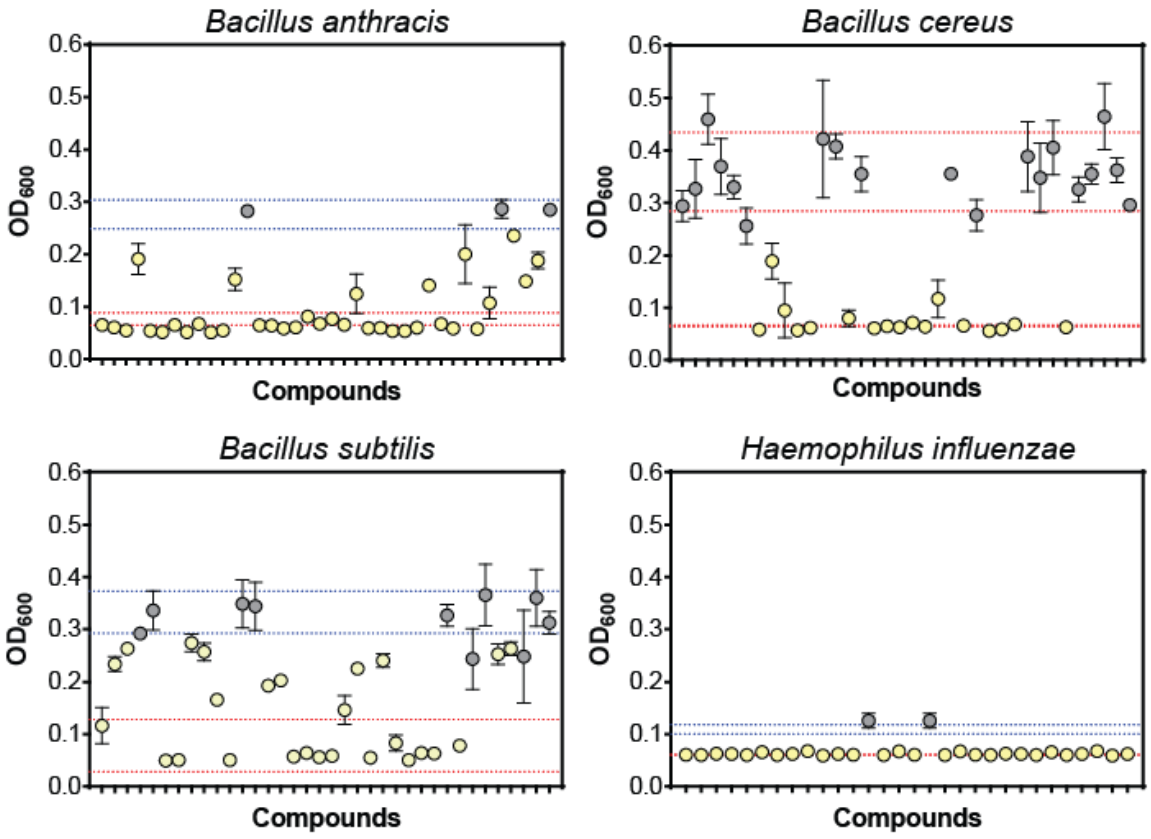

Appendix 4.6.10 Screening data of compounds against *B. anthracis*, *B. cereus*, *B. subtilis*, and *H. influenzae* in a bacterial growth assay. Dotted lines represent the average growth and standard deviations in presence of the controls. The blue lines represent the negative control (DMSO). The red lines represent the positive control (tetracycline). Results are the average of triplicates and the error bars represent SEM. Gray data points indicate inactive compounds, while yellow data points represent active (hit) compounds.

4.6.11 JG97 inhibits the growth of bacteria on solid media

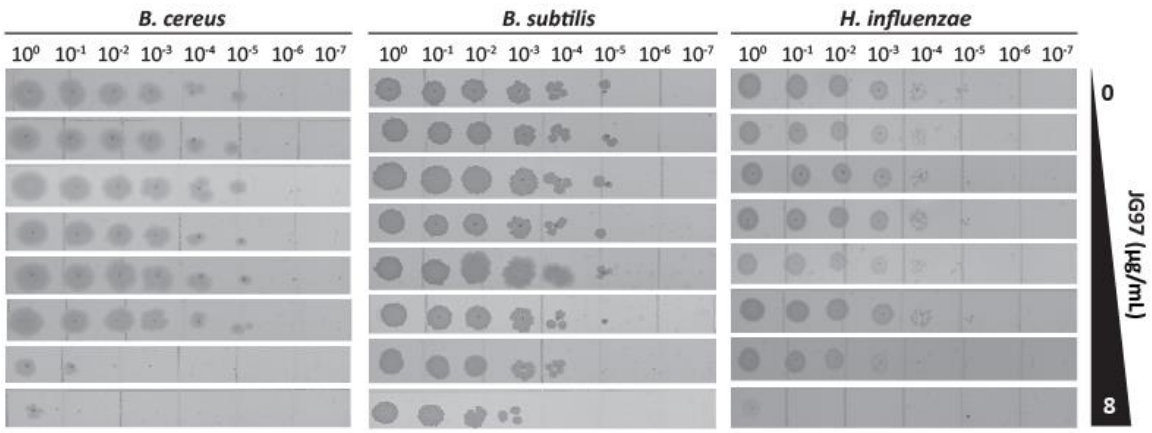

Appendix 4.6.11 JG97 inhibits the growth of bacteria on solid media. Solid media spot titers of bacterial growth in the presence of JG97. Representative data are shown for the *B. cereus*, *B. subtilis*, and *H. influenzae*.

4.6.12 The structures of JG97 analogs with potent antibacterial activity

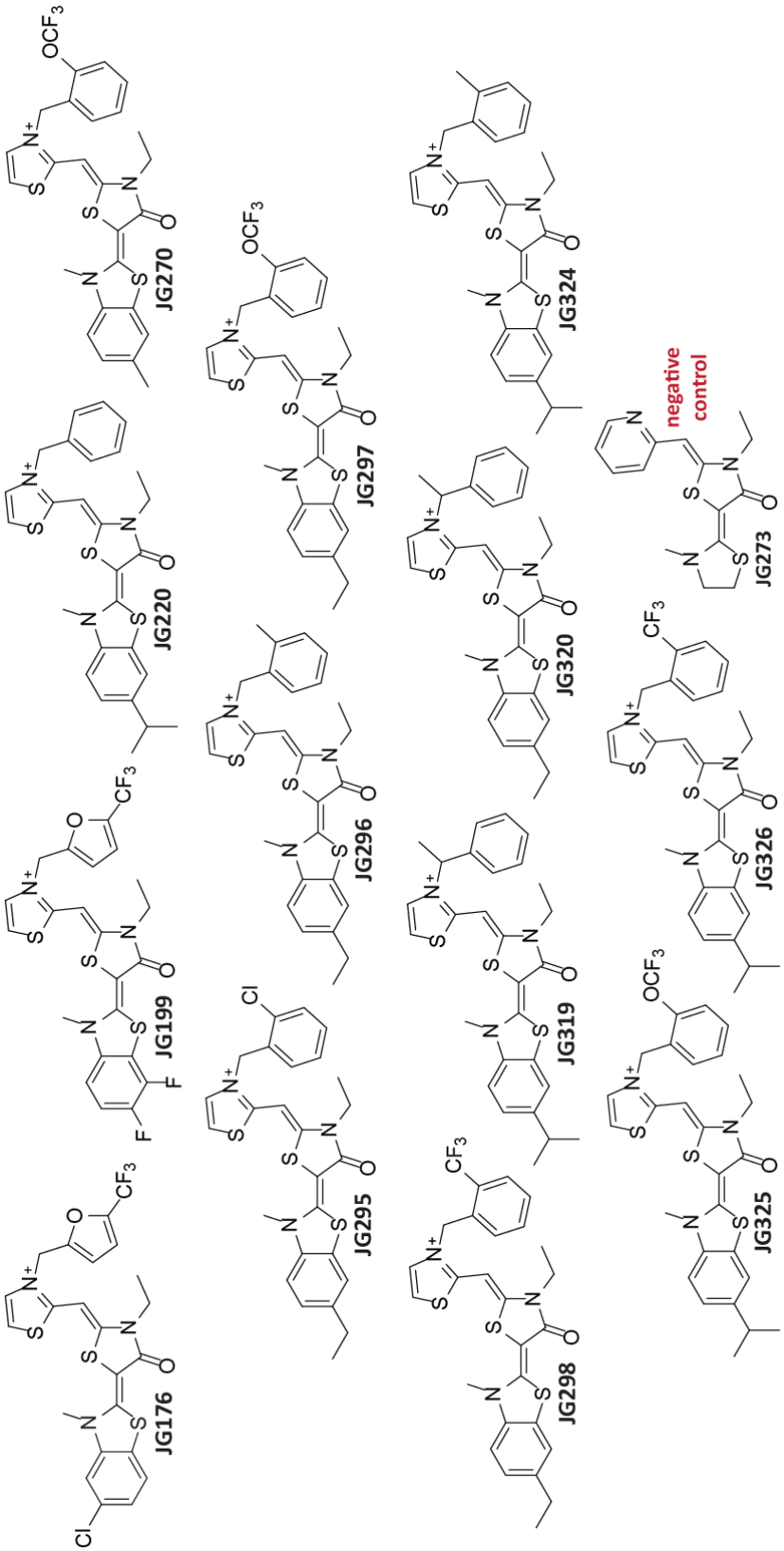

Appendix 4.6.12 Structures of JG97 analogs with potent antibacterial activity.

4.6.13 JG97 analogs exhibit a dose-dependent inhibition of *S. aureus* growth

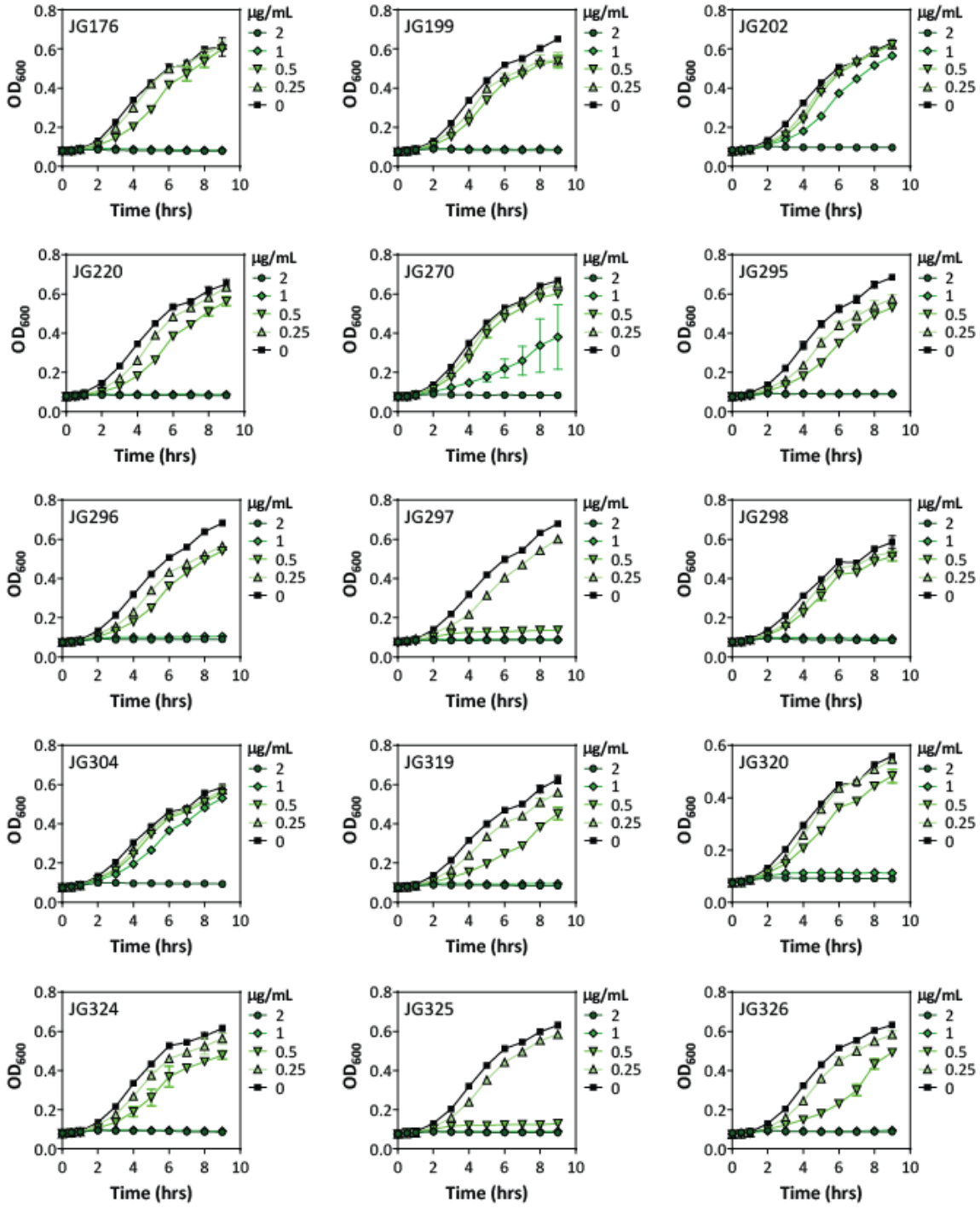

Appendix 4.6.13 JG97 analogs show a dose-dependent inhibition of bacterial growth against *S. aureus*. Growth curve experiments were performed twice in triplicate. Representative graphs are shown.

4.6.14 Minimum inhibitory concentrations of JG97 analogs against pathogenic bacteria

Appendix 4.6.14 Minimum inhibitory concentration of top JG97 analogs against pathogenic bacteria.

Compound	MIC (μg/mL)															
	MRSA	*M. smegmatis* MC122	*P. aeruginosa* ATCC 27853	*S. enterica* ATCC 14028	*S. epidermidis* ATCC 12228	VRE	*S. aureus* USA100	*S. aureus* USA200	*S. aureus* USA300	*S. aureus* USA600	*S. aureus ATCC 29213*	MRSA2	*E. faecium* BM4105-RF	*E. faecium* U275	*E. faecium* S51	*E. faecium* C21190	*E. faecium* S1152
JG176	≤0.125	8-32	> 64	> 64	> 128	8-16	2	2-4	2	4	0.25-1	0.25-1	> 64	0.5-1	1	> 64	> 64
JG199	≤0.125	4	> 64	> 64	> 128	0.5	0.5-1	1	2	1	0.25-0.5	≤0.25	> 64	0.5	0.25-0.5	> 64	> 64
JG220	≤0.125	2	> 64	> 64	> 128	0.5	0.5	1	1	0.5	0.25-0.5	0.25	4	0.25	0.25-0.5	> 64	> 64
JG270	≤0.125	32	> 64	> 64	> 128	1-2	1 - 2	2	2	2	0.25	≤0.25	> 64	0.5	0.5	> 64	> 64
JG295	≤0.125	16	8	> 64	> 128	1	4	4	2	4	0.25	0.25	> 64	1	2	> 64	> 64
JG296	≤0.125	1	> 64	> 64	> 128	0.25	0.5	0.5-1	1	1	0.25-0.5	0.25	4	0.5	0.25-0.5	> 64	> 64
JG297	≤0.125	1	> 64	> 64	> 128	0.5	1	0.5	1	0.5	≤0.25	≤0.25	32	0.25	0.2	> 64	> 64
JG298	≤0.125	> 64	> 64	> 64	> 128	2	8	4	2	1	1	≤0.5	> 64	2	2	> 64	> 64
JG319	≤0.25	1-2	> 128	> 128	> 128	0.5	0.5-1	1	1	1	≤0.25	≤0.125	4	0.5	0.25	8	8
JG320	≤0.25	2	> 128	> 128	> 128	0.5	1	1	1	1	≤0.125	≤0.125	4	0.25	0.25	32	32
JG324	≤0.25	1-2	> 128	> 128	> 128	≤0.25	1	1	1	1	0.25-0.5	0.5	2	0.25	0.25-0.5	32	32
JG325	≤0.25	> 128	> 128	> 128	> 128	0.5	1	1	1	0.5	0.25	0.25	64	0.25	0.5	> 64	> 64
JG326	≤0.125	> 64	> 64	> 64	> 128	0.5	0.5	1	1-2	1	0.25-0.5	0.5	> 64	0.5	0.5	> 64	> 64
JG237	> 64	> 64	NT	NT	NT	> 64	> 64	> 64	> 64	> 64	> 64	> 64	> 64	> 64	> 64	> 64	1-2

Gram-positive bacteria are highlighted in blue, while Gram-negative bacteria are highlighted in red. The following is a list of bacterial strain abbreviations: Methicillin-resistant *Staphylococcus aureus* (MRSA), *Mycobacterium smegmatis*, *Pseudomonas aeruginosa*, *Salmonella enterica*, *Staphylococcus epidermidis*, Vancomycin-resistant *Enterococcus* (VRE), *Staphylococcus aureus, and Enterococcus faecium*. Compounds that were not tested (NT) are indicated by a gray box.

4.7 References

1. Hesterkamp, T. and B. Bukau, *Role of the DnaK and HscA homologs of Hsp70 chaperones in protein folding in E-coli.* Embo Journal, 1998. **17**(16): p. 4818-4828.
2. Gragerov, A., et al., *Cooperation of Groel/Groes and Dnak/Dnaj Heat-Shock Proteins in Preventing Protein Misfolding in Escherichia-Coli.* Proceedings of the National Academy of Sciences of the United States of America, 1992. **89**(21): p. 10341-10344.
3. Mogk, A., et al., *Identification of thermolabile Escherichia coli proteins: prevention and reversion of aggregation by DnaK and ClpB.* Embo Journal, 1999. **18**(24): p. 6934-6949.
4. Groemping, Y. and J. Reinstein, *Folding properties of the nucleotide exchange factor GrpE from Thermus thermophilus: GrpE is a thermosensor that mediates heat shock response.* Journal of Molecular Biology, 2001. **314**(1): p. 167-178.
5. Grimshaw, J.P.A., et al., *Thermosensor action of GrpE - The DnaK chaperone system at heat shock temperatures.* Journal of Biological Chemistry, 2003. **278**(21): p. 19048-19053.
6. Singh, V.K., et al., *Role for dnaK locus in tolerance of multiple stresses in Staphylococcus aureus.* Microbiology-Sgm, 2007. **153**: p. 3162-3173.
7. Itikawa, H. and J.I. Ryu, *Isolation and Characterization of a Temperature-Sensitive Dnak Mutant of Escherichia-Coli-B.* Journal of Bacteriology, 1979. **138**(2): p. 339-344.
8. Bukau, B. and G.C. Walker, *Cellular Defects Caused by Deletion of the Escherichia-Coli Dnak Gene Indicate Roles for Heat-Shock Protein in Normal Metabolism.* Journal of Bacteriology, 1989. **171**(5): p. 2337-2346.
9. Lemos, J.A., Y. Luzardo, and R.A. Burne, *Physiologic effects of forced down-regulation of dnaK and groEL expression in Streptococcus mutans.* Journal of Bacteriology, 2007. **189**(5): p. 1582-1588.
10. Yamaguchi, Y., et al., *Effects of disruption of heat shock genes on susceptibility of Escherichia coli to fluoroquinolones.* Bmc Microbiology, 2003. **3**.
11. Sell, S.M., et al., *Isolation and Characterization of Dnaj Null Mutants of Escherichia-Coli.* Journal of Bacteriology, 1990. **172**(9): p. 4827-4835.
12. Takaya, A., et al., *The DnaK/DnaJ chaperone machinery of Salmonella enterica serovar typhimurium is essential for invasion of epithelial cells and survival within macrophages, leading to systemic infection.* Infection and Immunity, 2004. **72**(3): p. 1364-1373.
13. Hanawa, T., et al., *The Listeria monocytogenes DnaK chaperone is required for stress tolerance and efficient phagocytosis with macrophages.* Cell Stress & Chaperones, 1999. **4**(2): p. 118-128.
14. Chang, L., et al., *Mutagenesis Reveals the Complex Relationships between ATPase Rate and the Chaperone Activities of Escherichia coli Heat Shock Protein 70 (Hsp70/DnaK).* Journal of Biological Chemistry, 2010. **285**(28): p. 21282-21291.
15. Brodsky, J.L. and G. Chiosis, *Hsp70 molecular chaperones: Emerging roles in human disease and identification of small molecule modulators.* Current Topics in Medicinal Chemistry, 2006. **6**(11): p. 1215-1225.
16. Evans, C.G., L. Chang, and J.E. Gestwicki, *Heat Shock Protein 70 (Hsp70) as an Emerging Drug Target.* Journal of Medicinal Chemistry, 2010. **53**(12): p. 4585-4602.
17. Patury, S., Y. Miyata, and J.E. Gestwicki, *Pharmacological Targeting of the Hsp70 Chaperone.* Current Topics in Medicinal Chemistry, 2009. **9**(15): p. 1337-1351.
18. Srinivasan, S., et al., *Allosteric Inhibitors of Hsp70: Drugging the Second Chaperone of Tumorigenesis*. 2015, Springer Berlin Heidelberg. p. 1-32.

19. Chitnis, S., et al., *In vitro activity of daptomycin & linezolid against methicillin resistant Staphylococcus aureus & vancomycin resistant enterococci isolated from hospitalized cases in Central India.* Indian Journal of Medical Research, 2013. **137**: p. 191-196.
20. Boucher, H.W., et al., *Bad Bugs, No Drugs: No ESKAPE! An Update from the Infectious Diseases Society of America.* Clinical Infectious Diseases, 2009. **48**(1): p. 1-12.
21. Rossolini, G.M., et al., *Update on the antibiotic resistance crisis.* Current Opinion in Pharmacology, 2014. **18**: p. 56-60.
22. Chang, L., et al., *High-throughput screen for small molecules that modulate the ATPase activity of the molecular chaperone DnaK.* Analytical Biochemistry, 2008. **372**(2): p. 167-176.
23. Wisen, S. and J.E. Gestwicki, *Identification of small molecules that modify the protein folding activity of heat shock protein 70.* Analytical Biochemistry, 2008. **374**(2): p. 371-377.
24. Johnston, J.W., *Laboratory growth and maintenance of Haemophilus influenzae.* Current protocols in microbiology, 2010. **Chapter 6**: p. Unit 6D.1-Unit 6D.1.
25. Shrestha, S.K., et al., *Amphiphilic Tobramycin Analogues as Antibacterial and Antifungal Agents.* Antimicrobial agents and chemotherapy, 2015. **59**(8): p. 4861-9.

Chapter 5

Conclusions and future directions: Progress towards understanding how to modulate the Hsp70 chaperone system

5.1 Abstract

The Hsp70 system is a model for the next generation of difficult drug targets. It is composed of multiple protein components and it conducts many different biochemical and cellular activities, making it challenging to understand the best way of turning this chaperone system "on" or "off" with small molecules. Throughout this thesis, I developed an approach to this problem that involved comprehensive measurement of Hsp70's functions, such as ATPase rate, substrate binding, and co-chaperone interactions. Indeed, this systematic probing has enriched our understanding of allostery and protein-protein interactions (PPIs) within the Hsp70 system and revealed ways of interrupting function. Additionally, this work has been particularly important in connecting Hsp70's *in vitro* biochemical activities to its cellular chaperone functions. Together, these findings have led to new insights on how to safely target Hsp70. In this chapter, I discuss some of the remaining challenges associated with targeting Hsp70 and I speculate about how new approaches can be employed to modulate this chaperone. In addition, I also discuss how my thesis work might be leveraged in order to develop even more informative *in vitro*

screening strategies. These concepts might have broader relevance to other multi-protein complexes.

5.2 Conclusions

Hsp70 is a central triage chaperone that binds to protein substrates to assist with their folding, degradation, transport, and solubility [1-6]. Therefore, Hsp70 is considered to be an essential regulator of protein homeostasis and its dysregulation is thought to be associated with diseases of protein misfolding. By understanding how Hsp70 makes these triage "decisions," previous and current members of the Gestwicki laboratory have made progress towards learning how to best leverage Hsp70 as a therapeutic drug target. The major goal of my thesis was to gain a better understanding of what factors within the Hsp70 system direct this chaperone's cellular functions and how such factors could be chemically modulated (Figure 5.1).

When I joined the Gestwicki laboratory in 2010, Lyra Chang and Yoshi Miyata had performed the first high-throughput screen (HTS) against the ATPase activity of Hsp70/co-chaperone complexes [7, 8]. These screens led to the identification of new chemical tools, which the laboratory has used to probe different aspects of Hsp70's biology. However, many important co-chaperones, such as TPR proteins, do not alter Hsp70's ATPase activity (V. A. Assimon and J. E. Gestwicki unpublished results). Thus, an alternative approach was needed to study these Hsp70 complexes. Based on this finding, I was interested in developing a new assay that would permit the discovery of compounds that modulate the

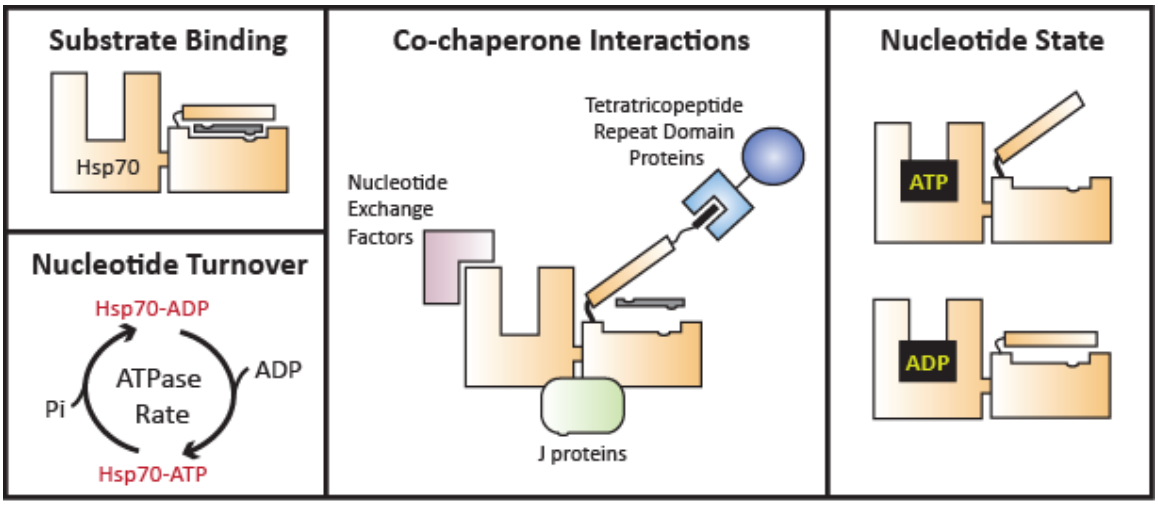

Figure 5.1 Exploring the distinct aspects of Hsp70's various functions.

physical interaction between Hsp70 and a TPR co-chaperone. Thus, in chapter 2, I developed a fluorescence polarization (FP) platform that allowed me to characterize the how various TPR co-chaperones (CHIP, Hop, DNAJC7, FKBP51, and FKBP52) bind the C-termini of cytosolic human Hsp70s and Hsp90s *in vitro*. Using this FP platform, I found that TPR co-chaperones do not display a clear hierarchy of affinity constants for chaperones. Instead, with a few exceptions (*i.e.* FKBP51/52 binding exclusively to Hsp90s), I found limited differences between the observed affinity constants of various Hsp70/90-TPR complexes. Based on these findings, I concluded that it would be very challenging to directly interfere with a specific Hsp70-TPR co-chaperone complex using small molecules (*e.g.* orthosteric inhibitors) without inhibiting all of them. Instead, a HTS using this platform would likely lead to the discovery of pan-specific TPR inhibitors. This work, and evidence from PPI inhibitor discovery programs [9-11], suggests that compounds that are able to bind to allosteric sites might be the best option to target the Hsp70 system in a specific manner.

Next, my focus shifted to understanding how to identify and tune allosteric networks within the Hsp70 system in order to manipulate this chaperone's various functions in a specific manner. As discussed above, the Gestwicki laboratory has performed multiple unbiased chemical screens to identify inhibitors of Hsp70 complexes, leading to the identification of many molecules that appear to act at allosteric sites [7, 8, 12, 13]. Additionally, Yoshi Miyata and Xiaokai Li have validated and optimized compounds that are based on the rhodacyanine dye MKT-077, which are known to interact with an allosteric site on Hsp70 [14-16]. I became particular interested in this class of molecules because in multiple models of neurodegeneration, such as Spinal-Bulbar Muscular Atrophy (SBMA), MKT-077 and its analogs have been shown to bind selectively to an allosteric pocket on Hsp70 and relieve disease phenotypes [15]. However, the molecular mechanism by which these molecules modulate Hsp70's functions had not been fully elucidated. In part, this was because the fluorescent properties of MKT-077 analogs precluded their use in most biochemical assays. To circumvent this problem, I performed point mutagenesis on MKT-077's binding pocket and studied the effects of these mutations using a host of *in vitro* chaperone assays. Mutations within the MKT-077 binding pocket tended to have little effect on Hsp70's ability to bind, release, and turnover nucleotide. These results suggest that the MKT-077 binding site is not directly linked to the nucleotide-binding cleft. I found that mutations within the MKT-077 binding pocket of Hsp70 dysregulate key allosteric networks, which ultimately leads to the trapping of Hsp70 in an ADP-like conformation where it can no longer refold substrates. Thus, in chapter 3, I described how MKT-077

analogs bind to a conserved allosteric site in Hsp70/DnaK and used mutagenesis to understand how they inhibit specific chaperone functions.

My findings from chapter 3 provided new strategies for how to tune Hsp70's functions (Figure 5.1). I next wanted to see if these strategies could be employed to treat bacterial infections. A wealth of genetic data strongly suggests that Hsp70/DnaK could be an antibacterial drug target. I became particularly interested in using MKT-077 analogs to explore the role of Hsp70/DnaK in bacterial survival. In addition to my work, this interest was based on previous studies from Lyra Chang and Andrea Thompson. They illustrated that Hsp70/DnaK mutants that are deficient in their ability to refold substrates fail to rescue *ΔdnaK E. coli* cells [17]. Thus, it seemed likely that compounds that inhibited Hsp70/DnaK's refolding function, such as MKT-077 analogs, would promote bacterial cell death. I tested ~300 analogs of MKT-077 for activity against pathogenic Gram-positive and Gram-negative strains. I found that several MKT-077 derivatives had promising activity against Gram-positive strains, including the drug resistant pathogens MRSA and VRE, with MIC values ranging from 8 to < 0.125 μg/mL. Thus, my results in chapter 4 validated Hsp70/DnaK as an antibacterial target and further illustrated that the refolding activity of Hsp70/DnaK is a key function required for bacterial growth.

5.3 Future directions

5.3.1 The prospectus of MKT-077 analogs for therapeutic development

As discussed throughout this these thesis, Hsp70 is a potential drug target for many diseases. However, it is not clear how to safely achieve this goal. It also is not clear if the same Hsp70 inhibitor would be safe and effective in all disease settings. In chapter 4, I used MKT-077 analogs to confirm Hsp70/DnaK as an antibacterial drug target. While this was an important first step, more work needs to be done to validate these compounds as potential leads for therapeutic development. One major concern is the high sequence conservation between different orthologs of Hsp70. For example, the *E. coli* Hsp70 (DnaK) and the constitutively expressed human Hsp70 (Hsc70/HSPA8) are ~46% identical to each other at the amino acid level. Moreover, nearly every residue involved in the binding of MKT-077 analogs to these proteins is conserved. Thus, it unclear if MKT-077 analogs could be used to treat bacterial infections in humans without deleterious side-effects. A postdoctoral scholar in the Gestwicki laboratory, Hao Shao, has collected initial safety data for our most potent MKT-077 analogs. Initial results of solubility, metabolic stability, and toxicity studies have focused our attention on the MKT-077 analog JG199 (Appendix 4.6.12). JG199 has MIC values of 0.125 μg/mL (210 nM) against MRSA, a relatively long lifetime in liver microsomes ($t_{1/2}$ > 60 min), and minimal toxicity in human fibroblasts (EC_{50} ~ 2.3 μM in MTT viability assays). Maximum tolerated dose and pharmacokinetics studies on JG199 and other promising MKT-077 analogs in adult CD1 mice are ongoing. Regardless of the results of these experiments, I anticipate that MKT-077 analogs will be, at the very least, useful chemical probes for studying the role of DnaK in bacterial pathogenesis.

5.3.2 The substrate binding domain has the potential to be leveraged for specific inhibition of bacterial DnaK

In addition to MKT-077 molecules, numerous other scaffolds have been used to pharmacologically manipulate Hsp70 functions (**Figure 4.1**). These molecules have different binding sites and are likely to have different mechanisms. It is unclear whether some of these compounds might be safer than others in normal human cells. Because Hsp70 is a core mediator of protein homeostasis, one major concern is how the global proteome will respond to inhibitors of this chaperone. Inhibitors of other "housekeeping" factors in the proteostasis network, such as the proteasome and Hsp90, have had clinical success [18, 19], suggesting that at least some of the inhibitors of Hsp70 might also be tolerated. However, an even safer approach towards antibacterials might be to create molecules that target locations on Hsp70 homologs (*i.e.* DnaK *vs.* human Hsp70) that are not well conserved. Recent computational studies have identified hot spot residues in the substrate binding domain (SBD) that might fit this criteria [20]. In order to properly exploit these differences, it will be necessary to understand these how hot spot residues regulate the structure and function of the Hsp70 system. A protein engineering strategy, such as the one I employed in chapter 3, might be a powerful way to elucidate the roles of these residues. Specifically, each hot spot residue should be mutated and effects of these mutations should be evaluated using *in vitro* chaperone assays. This strategy, in combination with site-directed ligand discovery methodology [21], could result in the discovery of chemical modulators that are specific to bacterial DnaK. Such molecules could be exciting new antibiotic candidates.

5.3.4 Developing new screening strategies for Hsp70

My thesis work suggests new strategies for high-throughput screening of Hsp70. Previous screening efforts have focused on the discovery of molecules that inhibit Hsp70's ATPase activity, but my work suggests that other biochemical measures might be more appropriate. For example, my work in chapter 3 suggests that substrate binding might be an even better surrogate of important chaperone functions. As discussed previously, ATP binding in the NBD triggers conformational changes that weaken the SBD's affinity for client peptides. My studies suggest that preventing Hsp70 from binding to its substrates in a nucleotide-dependent manner would result is bacterial cell death (chapter 4). In chapter 3, I used a FP platform to monitor the binding of a fluorescently labeled substrate to Hsp70. This platform seems ideally suited for the discovery of inhibitors. The assay could even be optimized to allow for the discovery of molecules that enhance Hsp70's ability to bind substrate in the presence of high concentrations of ATP (Figure 5.2A). This particular screening strategy would be expected to select for molecules that dysregulate Hsp70's inter-domain allostery, perhaps increasing the likelihood of discovering Hsp70 modulators with antibacterial activity. Alternatively, a Förster resonance energy transfer (FRET) assay could be developed. Previously, FRET pairs have been used to detect structural changes in *E. coli* DnaK under different nucleotide states [22]. I would design a FRET pair between the lid and the SBD of DnaK and screen for molecules that stabilize ADP-like (lid-closed) conformation under high concentrations of ATP (Figure 5.2B). Together, these new

(A) Fluorescence polarization assay.

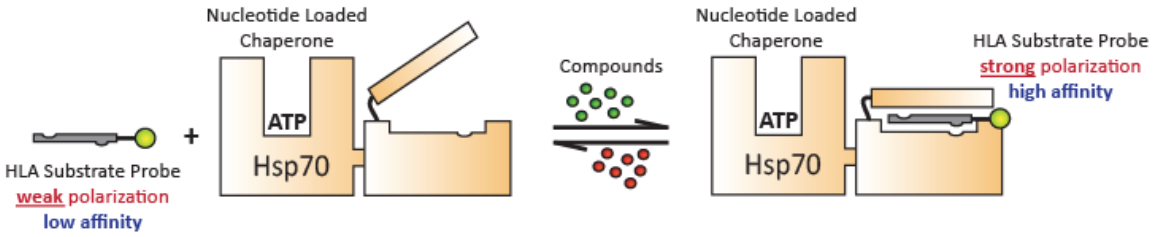

(B) FRET-based assay.

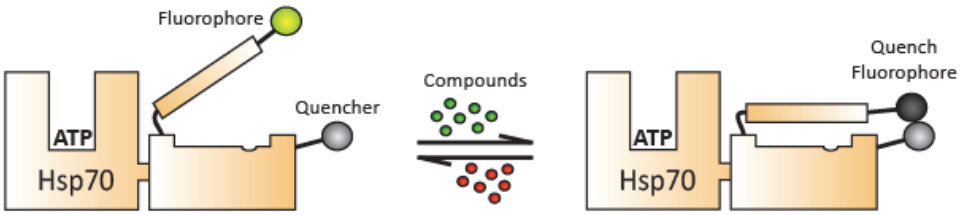

Figure 5.2 Design of new Hsp70 screening assays. (A) Fluorescence polarization assay. FP platforms have been used to monitor the binding of fluorescently labeled substrates to Hsp70. This type of platform could be used to identity molecules that dysregulate Hsp70's inter-domain allostery by screening for compounds that enhance Hsp70's affinity for substrate in the presence of ATP. (B) FRET-based assay. A fluorophore donor and an acceptor chromophore would be place on lid and SBD of Hsp70, respectively. This assay would be used to screen for compounds the lock Hsp70 in distinct conformations.

screening strategies have the potential to uncover new Hsp70 modulators with greater mechanistic specificity.

5.4 Broader implications

The Hsp70 system is only one of many multi-protein systems that control important biology. Despite the prevalence of multi-protein complexes, very few inhibitors specifically target them. In this thesis, I have used the Hsp70 system as a model for tackling such problems. As expected, I found that multi-protein complexes are much more complex than individual targets. For example, inhibition of a kinase is relatively straightforward (at least in concept): one develops a molecule that competes for binding to the natural enzyme substrate. However, in multi-protein complexes the possible scenarios for inhibition is

much larger. For example, in the Hsp70 system, a small molecule might change enzyme turnover, but it might also impact allostery and/or PPIs. In part, my thesis work provides a possible template on for how this complexity might be categorized and systematically addressed. I found that a comprehensive strategy was needed, in which many biochemical assays were assessed in parallel before conclusions could be drawn. In addition, I found that a combination of small molecules and point mutants could be used to help clarify mechanisms. The small molecules were helpful because they can be used in both *in vitro* and cellular experimental platforms. Point mutants were helpful because they have high selectivity in cellular systems. I hope that these studies are helpful to others in thinking about their programs.

5.5 Final thoughts

In this chapter, I have briefly summarized my progress towards understanding allostery and PPIs in the Hsp70 system and outlined possible ways to target this chaperone in a safe manner. In this effort, I used both mutagenesis and small molecules to probe Hsp70 biology. This approach required me to, at times, assume the role of a synthetic chemist, generating new organic molecules (see thesis appendix). I also took on the role of a protein biochemist, understanding the interactions between components of the chaperone sub-network *in vitro* (chapters 2 and 3). Finally, I had to incorporate the tools of the drug discovery scientist, using chemical probes to validate a drug target and understand its mechanism of action (chapter 4). I am proud of the integration of these skills, which was critical to the success of my doctoral studies. I strongly believe that an interdisciplinary

approach to science, integrating synthetic chemistry and molecular biology, will aid in the discovery of the mechanisms of disease and permit innovative ways to treat or cure disease.

5.6 References

1. Kundrat, L. and L. Regan, *Balance between folding and degradation for Hsp90-dependent client proteins: a key role for CHIP.* Biochemistry, 2010. **49**(35): p. 7428-38.
2. Chiang, H.L., et al., *A Role for a 70-Kilodaton Heat-Shock Protein in Lysosomal Degradation of Intracellular Proteins.* Science, 1989. **246**(4928): p. 382-385.
3. Bercovich, B., et al., *Ubiquitin-dependent degradation of certain protein substrates in vitro requires the molecular chaperone Hsc70.* Journal of Biological Chemistry, 1997. **272**(14): p. 9002-9010.
4. Bukau, B., J. Weissman, and A. Horwich, *Molecular chaperones and protein quality control.* Cell, 2006. **125**(3): p. 443-51.
5. Hartl, F.U. and M. Hayer-Hartl, *Protein folding - Molecular chaperones in the cytosol: from nascent chain to folded protein.* Science, 2002. **295**(5561): p. 1852-1858.
6. Young, J.C., et al., *Pathways of chaperone-mediated protein folding in the cytosol.* Nature Reviews Molecular Cell Biology, 2004. **5**(10): p. 781-791.
7. Chang, L., et al., *High-throughput screen for small molecules that modulate the ATPase activity of the molecular chaperone DnaK.* Analytical Biochemistry, 2008. **372**(2): p. 167-176.
8. Miyata, Y., et al., *High-Throughput Screen for Escherichia coli Heat Shock Protein 70 (Hsp70/DnaK): ATPase Assay in Low Volume by Exploiting Energy Transfer.* Journal of Biomolecular Screening, 2010. **15**(10): p. 1211-1219.
9. Gestwicki, J.E. and P.S. Marinec, *Chemical control over protein-protein interactions: beyond inhibitors.* Comb Chem High Throughput Screen, 2007. **10**(8): p. 667-75.
10. Berg, T., *Modulation of protein-protein interactions with small organic molecules.* Angew Chem Int Ed Engl, 2003. **42**(22): p. 2462-81.
11. Arkin, M.R. and J.A. Wells, *Small-molecule inhibitors of protein-protein interactions: progressing towards the dream.* Nat Rev Drug Discov, 2004. **3**(4): p. 301-17.
12. Chang, L., et al., *Chemical Screens against a Reconstituted Multiprotein Complex: Myricetin Blocks DnaJ Regulation of DnaK through an Allosteric Mechanism.* Chemistry & Biology, 2011. **18**(2): p. 210-221.
13. Cesa, L.C., et al., *Inhibitors of Difficult Protein-Protein Interactions Identified by High-Throughput Screening of Multiprotein Complexes.* Acs Chemical Biology, 2013. **8**(9): p. 1988-1997.
14. Rousaki, A., et al., *Allosteric Drugs: The Interaction of Antitumor Compound MKT-077 with Human Hsp70 Chaperones.* Journal of Molecular Biology, 2011. **411**(3): p. 614-632.
15. Wang, A.M., et al., *Activation of Hsp70 reduces neurotoxicity by promoting polyglutamine protein degradation.* Nature Chemical Biology, 2013. **9**(2): p. 112-118.

16. Li, X.K., et al., *Analogues of the Allosteric Heat Shock Protein 70 (Hsp70) Inhibitor, MKT-077, As Anti-Cancer Agents.* Acs Medicinal Chemistry Letters, 2013. **4**(11): p. 1042-1047.
17. Chang, L., et al., *Mutagenesis Reveals the Complex Relationships between ATPase Rate and the Chaperone Activities of Escherichia coli Heat Shock Protein 70 (Hsp70/DnaK).* Journal of Biological Chemistry, 2010. **285**(28): p. 21282-21291.
18. Zhang, J.K., P. Wu, and Y.Z. Hu, *Clinical and Marketed Proteasome Inhibitors for Cancer Treatment.* Current Medicinal Chemistry, 2013. **20**(20): p. 2537-2551.
19. Kim, Y.S., et al., *Update on Hsp90 Inhibitors in Clinical Trial.* Current Topics in Medicinal Chemistry, 2009. **9**(15): p. 1479-1492.
20. Chiappori, F., et al., *DnaK as Antibiotic Target: Hot Spot Residues Analysis for Differential Inhibition of the Bacterial Protein in Comparison with the Human HSP70.* Plos One, 2015. **10**(4).
21. Erlanson, D.A., et al., *Site-directed ligand discovery.* Proceedings of the National Academy of Sciences of the United States of America, 2000. **97**(17): p. 9367-9372.
22. Mapa, K., et al., *The conformational dynamics of the mitochondrial Hsp70 chaperone.* Mol Cell, 2010. **38**(1): p. 89-100.

Appendix

Concise synthesis of spergualin-inspired molecules with antibiotic activity

A.1 Abstract

The molecular chaperone Hsp70 is an essential regulator of cellular protein quality control. For example, Hsp70 has roles in primary folding, the stabilization of proteins under stress conditions, and the clearance of misfolded proteins. As discussed in chapters 1 and 2, it is thought that complexes formed between Hsp70 and TPR co-chaperones direct Hsp70's various activities during protein quality control. However, the molecular mechanisms that influence which TPR co-chaperone will bind with Hsp70 remain uncharacterized. This is an important question because the "choice" of bound TPR co-chaperone is thought to be critical in regulating cellular quality control decisions.

My original goal was to understand how the combinatorial assembly of TPR co-chaperones with Hsp70 drives protein quality control decisions. It has been suggested that a derivative of the natural product spergualin may bind to the C-terminal EEVD motif of Hsp70 [1]. As discussed in chapter 2, the C-terminal EEVD motif of Hsp70/90 is the major binding epitope for TPR co-chaperones. Based on these observations, I postulated that spergualin analogs could serve as useful chemical tools for tuning the formation of Hsp70 complexes with TPR

co-chaperones. Using the Ugi multicomponent reaction, I assembled spergualin-inspired molecules in a single step, dramatically improving the overall yield in comparison to previous synthetic schemes. Using this strategy, I generated 43 new analogs. Preliminary data suggested that these molecules did indeed block interactions between TPR co-chaperones and Hsp70. However, the binding of TPR co-chaperones to Hsp70 is dominated by electrostatic interactions between conserved lysine residues of TPR domains and the C-terminal EEVD motif of Hsp70/90. Due to the conserved and concise nature (small surface area) of Hsp70-TPR co-chaperone binding interfaces (Chapter 2), I was not able to engender selectivity from these molecules. Thus, these molecules where pan-specific and not useful tools for tuning the formation of specific Hsp70-TPR co-chaperone complexes.

Despite this result, I was able to repurpose these compounds. The natural product spergualin was previously shown to have promising antibacterial activity. But, its challenging synthesis had limited further exploration. I tested my small library of spergualin-inspired molecules for antibacterial activity against two Gram-negative and four Gram-positive bacterial strains. I found that the most potent analog, compound 6, had MIC values between 4 and 32 μg/mL against the six strains. This study serendipitously provided a concise route to a broad-spectrum antibiotic with a novel chemical scaffold.

A.2 The natural product spergualin has antibacterial activity and is difficult to synthesize

Spergualin was first isolated from culture broths of *Bacillus laterosprus* in 1981 and was

shown to have broad-spectrum antibacterial activity. This compound has a modular structure consisting of a guanidino group and a spermidine-like polyamine linked through a peptoid (Figure A.1) [2]. Spergualin is structurally distinct from other antibiotics used in the clinic, which prompted my interest in revisiting this privileged scaffold [3-5]. Moreover, there has been limited exploration of this molecule since the 1990s [6]. One of the major reasons is that the synthesis of spergualin is protracted. Typical routes produce spergualin and its analogs in low yield (0.3 to 18%) over at least 10 steps [7, 8]. Additionally, spergualin has poor stability. It hydrolyzes in aqueous buffers and consequently has a short lifetime *in vivo* [9].

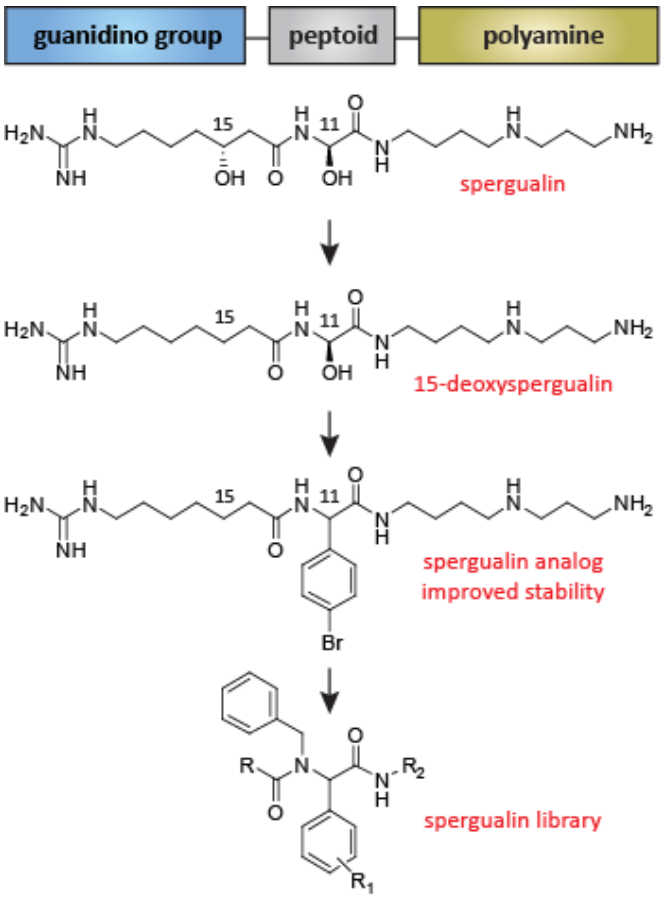

Figure A.1 Chemical structure of spergualin and its derivatives. Spergualin has a modular structure consisting of a guanidino group and a spermidine-like polyamine linked through a peptoid.

A.3 The Ugi multicomponent reaction is an efficient way to assemble spergualin analogs

The Gestwicki laboratory recently reported an improved synthetic approach that features the Ugi multicomponent reaction [10]. This route increased the overall yield of spergualin

derivatives, reduced the number of synthetic transformations (by 4 or 5 steps), and expanded the scope of accessible analogs. The stability issue has previously been overcome through removing the hydroxyl at position 15, to produce 15-deoxyspergualin (15-DSG) and installing a bulky group at position 11 (Figure A.1) [7, 8, 10]. While these initial efforts were informative, I hoped to support the creation of a greater number of analogs by further reducing the number of synthetic transformations.

A.4 Results

A.4.1 Synthesis of spergualin-inspired library using the Ugi multicomponent reaction

The overall yields of spergualin analogs were not optimized, with the major losses coming during purification and workup setups. I envisioned a route to spergualin-like analogs that might improve access through the use of the Ugi multicomponent reaction (Table A.1). Early studies showed that benzyl protection of the amine at position 12 dramatically improved the ease of purification without negatively impacting biological activity (data not shown). Thus, I designed the library to include this feature. Specifically, the Ugi reaction proceeded through the condensation of benzylamine with a variety of isocyanides, carboxylic acids, and aldehydes to probe the requirements in the guanidine (R–), 11 position aromatic (R1–) and polyamine (R2–) regions (Table A.1). Most of the components were commercially available or accessible in a single step.

Table A.1 Synthesis of spergualin-inspired peptoid library using the Ugi multicomponent reaction. In total, 43 unique peptoids were synthesized by varying the functionality of the carboxylic acid, the aldehyde, and the isocyanide starting materials.

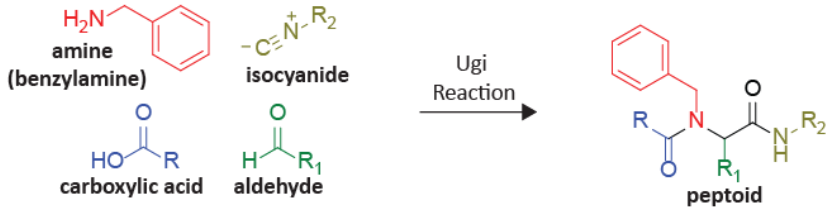

Compound	R	R_1	R_2
1		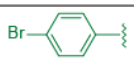	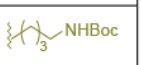
2	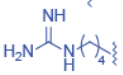	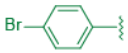	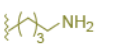
3		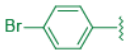	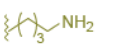
4	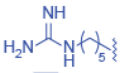	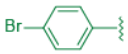	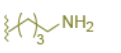
5		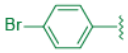	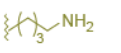
6		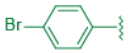	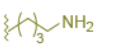
7		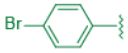	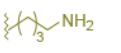
8		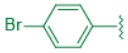	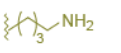
9	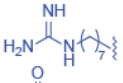	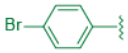	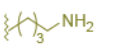
10		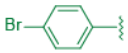	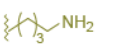
11	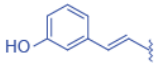	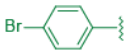	
12		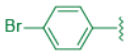	
13		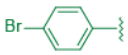	
14			
15			
16			
17			
18			
19			
20			
21			
22			

Compound	R	R_1	R_2
23			
24			
25			
26			
27			
28			
29			
30			
31			
32			
33			
34			
35			
36			
37			
38			
39			
40			
41			
42			
43			

The individual components were combinatorially assembled to generate a library of 43 molecules (Table A.1). Briefly, benzylamine (1 equivalent) and an aldehyde (1 equivalent) were mixed in methanol at room temperature until imine formation was detected by thin layer chromatography (~30 minutes). The reaction was then purified by column chromatography on silica gel using a hexane and ethyl acetate gradient, resulting in compounds 1 and 13–43. Compounds 2–12, which were derived from *tert*-butyl (4-isocyanobutyl) carbamate [11], were first subjected to a boc deprotection prior to purification by column chromatography on basic alumina oxide using an ethyl acetate gradient and methanol gradient. The final purified yields ranged from 20 to 96% (see Appendix A.7.5 and A.7.6 for synthesis and characterization), representing a dramatic increase in overall yield compared to previous reports.

A.4.2 Screening spergualin analog library for antibacterial activity

To explore the antibacterial activity of these compounds, I tested them for the ability to suppress bacterial growth using a 96-well OD_{600} turbidity platform. Each library member was initially screened at a single concentration (200 μM) in triplicate against six bacterial strains, including two Gram-negatives (*Escherichia coli* and *Haemophilus influenzae*) and four Gram-positives (*Bacillus anthracis*, *Bacillus cereus*, *Bacillus subtilis*, and *Staphylococcus aureus*) (Figure A.2A). I defined the negative control as the growth of each bacterial strain in the presence of 5% DMSO. The positive control was bacterial growth in the presence of 200 μM ampicillin. Compounds that decreased turbidity relative to DMSO

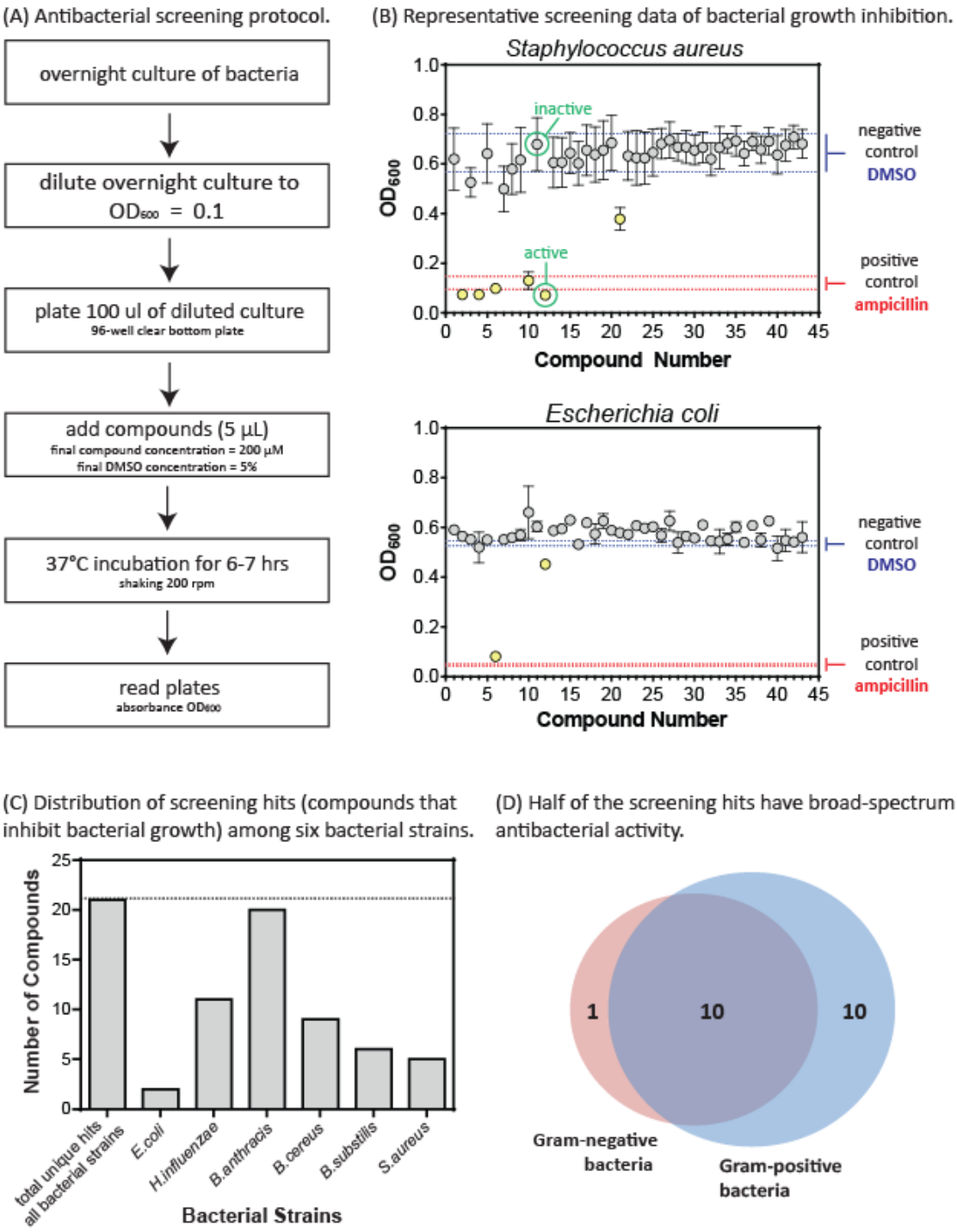

Figure A.2 Identification of spergualin-inspired analogs with antibacterial activity. (A) Detailed protocol of antibacterial screening method. (B) Representative screening data of compounds against *S. aureus* and *E. coli* in a bacterial growth assay. Dotted lines represent the average growth and standard deviations in presence of the controls. Results are the average of triplicates and the error bars represent SEM. Gray data points indicate inactive compounds, while yellow data points represent active (hit) compounds. (C) Distribution of screening hits among the six different bacteria tested. (D) Venn diagram depicting the distribution of screening hits amongst Gram-negative and Gram-positive bacteria.

were considered "active" (Figure A.2B and Appendix A.7.1). I found that 21 molecules were active against at least one of the six bacterial strains. *B. anthracis* was the most susceptible, while only two compounds were active against *E. coli* (Figure A.2C and A.2D).

A.4.3 Compound 6 has potent broad-spectrum antibacterial activity

The ten molecules with activity against both Gram-negatives and Gram-positives (Figure A.2D) were then subject to confirmatory retesting to determine their minimum inhibitory concentration (MIC) values. Only two compounds (6 and 12) had MIC values < 256 µg/mL against all six bacterial strains (Figure A.3A and A.3B). The best of these, compound 6, had MIC values between 4 and 32 µg/mL. These MIC values are even better than those of

(A) Summary of screening campaign.

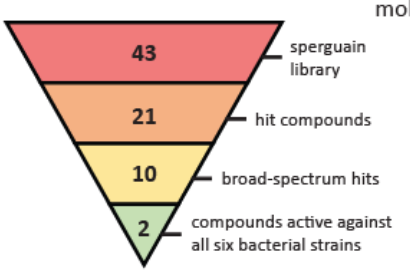

(B) Chemical structures of active molecules.

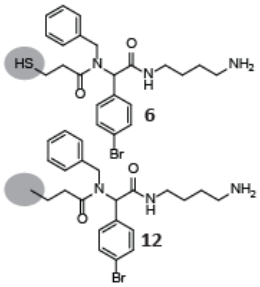

(C) Compound 6 has potent antibacterial and broad-spectrum activity.

Bacterial Strains	MIC (µg/mL)			
	Compd 6	Compd 12	Spergualin	Tetracycline
E. coli	32	256	50	<2
H. influenzae	16	64	N/T	<2
B. anthracis	4	32	12.5	<2
B. cereus	8	32	50	<2
B. subtilis	4	16	6.25-25	<2
S. aureus	8	32	6.25-50	<2

N/A = data not available

(D) Compound 6 inhibits bacterial growth.

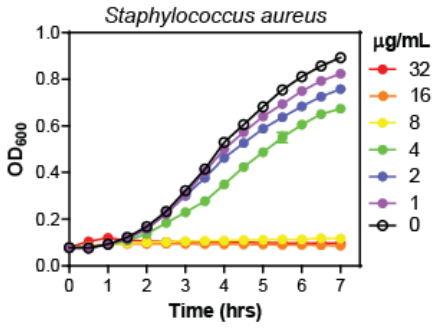

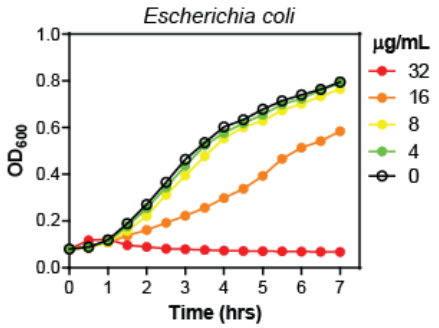

Figure A.3 Compound 6 has broad-spectrum antibacterial activity. (A) Summary of the screening campaign. (B) Chemical structures of lead compounds 6 and 12. (C) Minimum inhibitory concentrations (MICs) of compounds 6 and 12 against six bacterial strains, compared to the natural product spergualin. MIC assays were performed at least twice in triplicate. (D) Compound 6 shows a dose-dependent inhibition of bacterial growth. Growth curve experiments were performed twice in triplicate. Representative graphs are shown.

spergualin (MIC values between 6.25 and 50 μg/mL), so compound 6 was chosen for further study (Figure A.3C). This compound was first resynthesized and its activity confirmed in the MIC assay. Next, I tested compound 6 in liquid broth cultures (Figure A.3D) and found that it also dose-dependently inhibited bacterial growth of all six strains in that platform (Appendix A.7.2). In control experiments, we confirmed that none of the synthetic precursors to compound 6 (*i.e.* benzylamine, 3-mercaptopropionic acid, 4-bromobenzaldehyde or spermidine, an alkyl polyamine) were active (Appendix A.7.3), suggesting that the functionalized peptoid is the relevant pharmacophore.

A.4.4 The peptoid region of compound 6 appears to be the pharmacophore

To explore the potential structure activity relationships (SAR) around compound 6, I purchased structurally similar molecules (compounds 6a–d) (Appendix A.7.7) and tested their activity against the six strains. None of these analogs were significantly active (MIC >128 μg/mL) (Appendix A.7.7). However, this information in combination with the previous results, helped to refine my understanding of compound 6's pharmacophore. Specifically, the minimal pharmacophore appears to be the peptoid region with pendant aromatic groups at the C11 and N12 positions (Figure A.1). Short, flexible alkyl chains terminated with electron rich groups, such as thiols and amines, were preferred at either end. Future work should explore the SAR in more detail. For example, it would be interesting to specifically explore the effects of stereochemistry at position 11 on potency, as all the molecules reported here are racemic mixtures. Previous work suggested that the

stereochemistry at this position has modest effects on anti-tumor activity [12], but this issue needs to be resolved for antibacterial activity.

A.4.5 Compound 6 has a bactericidal mode-of-action

Finally, I wanted to explore whether compound 6 was bactericidal or bacteriostatic. *S. aureus* cultures were treated for 24 hours at the MIC value (8 µg/mL) or 2x the MIC value (16 µg/mL) and the resulting samples were plated on solid agar to count colony forming units (CFUs). At both concentrations, compound 6 was clearly bactericidal (>3 $\log_{10}$ decrease in CFUs) (Figure A.4). Taken together, these results suggest that compound 6 is a promising scaffold for further development.

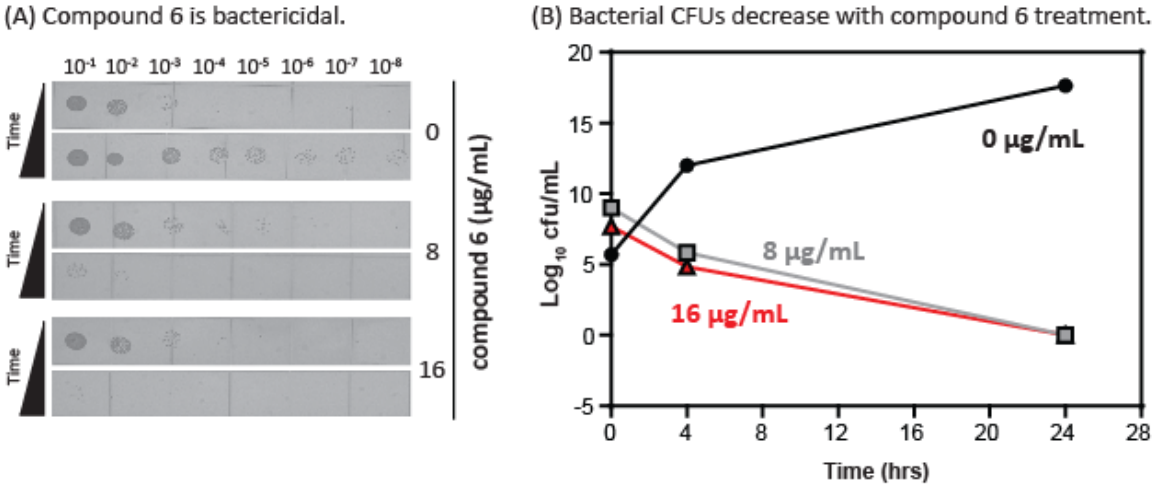

Figure A.4 Compound 6 has a bactericidal mode-of-action. (A) Representative time-kill spot titer plates of *S. aureus* in the presence of compound 6 (0, 8, and 16 µg/mL) over time (0 and 4 hours). (B) Representative time-kill curves of *S. aureus* in the presence of 0, 8, and 16 µg/mL of compound 6.

A.5 Discussion

A.5.1 The concise assembly of compound 6 could prompt the discovery of antibacterials

The natural product spergualin has promising antibacterial activity, but its cumbersome synthesis and limited stability have hindered its use. Using a synthetic route that features the Ugi multicomponent reaction, I generated a small library of synthetically tractable analogs and tested them for antibacterial activity. The results showed that short and flexible alkyl chains terminated with electron rich groups at either end of the peptoid pharmacophore were necessary for activity. Most notably, I found that compound 6 had particularly promising broad-spectrum antibacterial activity. The concise and convergent assembly of compound 6 is expected to accelerate discovery of new antibacterial molecules.

A.5.2 Compound 6 warrants further exploration

The mechanism of action (MoA) of spergualin is not yet known and its targets in bacteria are unclear. Thus, the spergualin-inspired analogs reported here could additionally serve as useful chemical probes. To this point, MoA studies with spergualin have not been practical because of its poor stability and its tendency to rapidly hydrolyze. Compound 6 represents a chance to possibly identify the target responsible for broad-spectrum bactericidal activity. This next step will be particularly powerful because the structure of compound 6 has significantly diverged from that of the natural product. After the MOA and target are identified, it will be essential to explore whether compound 6 and its analogs share the same profile as spergualin. Finally, although the activity of compound 6 is promising, the potency of this series needs to be further improved. Because MIC values of

4 μg/mL were obtained using a relatively small library of ~40 analogs, I am optimistic about the possibility of improving the potency of this scaffold with more medicinal chemistry. However, the relatively narrow scope of the SAR suggests that dramatic changes to the pharmacophore may not be tolerated. Regardless, the improved route and preliminary SAR provided here warrant further exploration.

A.6 Materials and methods

A.6.1 Synthesis of *tert*-butyl(4-isocyanobutyl)carbamate

The preparation of this isocyanide was based on literature precedent [11]. Specifically, to a 500 mL 3-necked RBF equipped with an addition funnel and purged with N_2(g) was added 1,4-diaminobutane (15 g, 170.2 mmol) dissolved in 60 mL of dioxane. Using the addition funnel, boc anhydride (3.7 g, 17.02 mmol) dissolved in 60 mL of dioxane was added dropwise over 1.5 hours. The addition of boc anhydride resulted in the formation of a white precipitate. The reaction was allowed to stir overnight at RT. The next morning, the solvent was removed under vacuum resulting in a white solid to which 100 mL of water was added. The resulting insoluble material was removed by gravity filtration. The filtrate was then extracted with DCM (3 × 100 mL). The organic layers were dried with anhydrous sodium sulfate and concentrated to give *N*-boc-1,4-diaminobutane, a light yellow oil, in 80–89% yield. Next, to a 100 mL RBF purged with N_2(g) was added *N*-boc-1,4-diaminobutane (2.8 g, 14.9 mmol) diluted in 25 mL of DCM. The reaction was then cooled using an ice bath. Once cooled, DIC (2.3 mL, 14.9 mmol) was added dropwise and the resulting white mixture

was allowed to stir overnight at RT. The next morning, the reaction was subjected to gravity filtration. The resulting filtrate was washed with 2 × 50 mL of saturated sodium bicarbonate. The organic layers were pooled, dried with anhydrous sodium sulfate, and concentrated to give the intermediate *tert*-butyl(4-formamidobutyl)carbamate. Next, in a 100 mL RBF purged with N_2(g) was added *tert*-butyl(4-formamidobutyl)carbamate (1 g, 4.6 mmol) dissolved in 10 mL of DCM and TEA (1.9 mL,13.8 mmol). This reaction was cooled using an ice bath. Once cooled, phosphoryl chloride (0.44 mL, 4.6 mmol) was added dropwise, causing the reaction mixture to turn orange. This mixture was allowed to stir at RT for 30 minutes. Afterwards, potassium carbonate (6.4 g, 4.6 mmol) dissolved in water was added dropwise and the reaction was allowed to stir for an additional 30 minutes. The reaction was then transferred to a separatory funnel, the organic layer was removed and saved. The remaining aqueous layer was extracted with 5 × 20 mL of DCM. The combined organic layers were dried with anhydrous sodium sulfate and then concentrated under vacuum. This crude product was purified by column chromatography on silica gel using a hexane:ethyl acetate gradient. The purified product eluted at 50:50 hexane:ethyl acetate. Solvent removal resulted in a yellow oil in 20–43% yield. ^{1}H NMR (500 MHz, chloroform-*d*) δ 4.65 (s, 1H), 3.42 (t, J = 6.5 Hz, 1H), 3.16–3.13 (m, 2H), 1.74–1.68 (m, 2H), 1.65–1.59 (m, 2H), 1.43 (s, 9H).

A.6.2 General synthesis for guanidylated acids

The preparation of guanidylated acids was based on literature precedent [13]. To a 3-necked RBF equipped with a condenser and N_2(g) inlet, was added either pentanoic, hexanoic, or octanoic acid (1 mmol). The flask was purged with N_2(g). Afterwards, 8 mL of anhydrous DCM was added and the flask was heated to 55–60 °C using an oil bath. Once heated, *N*-methyl-*N*-(trimethylsilyl)trifluoroacetamide (0.4 mL, 2.2 mmol) was added dropwise. The resulting cloudy mixture was allowed to reflux for 2 hours. Afterwards, the reaction was removed from heat and was allowed to cool to RT. TEA (0.15 mL, 1.1 mmol) was added, followed by 1,3-di-boc-2-(trifluoromethylsulfonyl)guanidine (0.430 g, 1.1 mmol) and an additional 2 mL of DCM. The reaction flask was re-purged with N_2(g) and allowed to stir for 4–5 hours at RT. During this time the reaction mixture clarified. Afterwards, the reaction was washed in the following manner: 2 × 8 mL brine, 1 × 8 mL water, and 1 × 8 mL 10% citric acid. The combined organic layers were dried with anhydrous sodium sulfate and then concentrated under vacuum. This crude product was purified by column chromatography on silica gel using a hexane:ethyl acetate gradient. The purified product eluted at 50:50 hexane:ethyl acetate. (*Z*)-5-(2,3-bis(*tert*-butoxycarbonyl)guanidino) pentanoic acid. White solid in 48.3% yield. ^{1}H NMR (400 MHz, chloroform-*d*) δ 8.48 (s, 1H), 3.48 (s, 2H), 2.41 (t, J = 6.9 Hz, 2H), 1.75–1.59 (m, 4H), 1.49 (s, 18H). (*Z*)-6-(2,3-bis(*tert*-butoxycarbonyl)guanidino)hexanoic acid. White solid in 41% yield. ^{1}H NMR (400 MHz, chloroform-*d*) δ 8.36 (s, 1H), 3.41 (q, J = 8.0 Hz, 2H), 2.34 (t, J = 7.4 Hz, 2H), 1.71–1.61 (m, 2H), 1.61–1.54 (m, 2H), 1.48 (d, J = 2.7 Hz, 18H), 1.44–1.34 (m, 2H). (*Z*)-8-(2,3-bis(*tert*-butoxycarbonyl)guanidine)octanoic acid. White solid in 63% yield.

^{1}H NMR (400 MHz, chloroform-*d*) δ 8.28 (s, 1H), 3.36 (q, *J* = 7.2 Hz, 2H), 2.31 (t, *J* = 7.5 Hz, 2H), 1.65–1.57 (m, 2H), 1.56–1.50 (m, 2H), 1.47 (d, *J* = 2.4 Hz, 18H), 1.31 (s, 6H).

A.6.3 General synthesis of spergualin-inspired analogs

In a 50 mL RBF, benzylamine (1 mmol), an aldehyde (1 mmol), and 5 mL of methanol were mixed at RT until imine formation was detected by thin layer chromatography (~30 minutes). Next, a carboxylic acid (1 mmol) and an isocyanide (1 mmol) were added and allowed to react overnight. This reaction was then purified by column chromatography on silica gel using a hexane and ethyl acetate gradient, resulting in compounds 1 and 13–43. Molecules 2–12, compounds that contained the *tert*-butyl(4-isocyanobutyl) carbamate starting material, were then subjected to a boc deprotection before purification. Briefly, the boc protected peptoid was dissolved in DCM (10 mL) and treated with 85% phosphoric acid (3 equivalents). This mixture was allowed to stir overnight at RT. Afterwards, 10 mL of water was added and then the reaction mixture's pH was neutralized using 10% NaOH. This mixture was quenched with saturated sodium bicarbonate and then extracted with 3 × 10 mL of ethyl acetate. The combined organic layers were dried, concentrated, and the subjected to column chromatography on basic alumina oxide using an ethyl acetate and methanol gradient. Compound yields ranged from 20–96%. See the Appendix A.7.4 – A.7.6 for additional details and characterization.

A.6.4 Growth and maintenance of laboratory bacterial strains

The following bacterial strains were used: *Bacillus anthracis* 34F2 Sterne, *Bacillus cereus* ATCC 11778, *Bacillus subtilis* 168, *Escherichia coli* K-12 (MG1655), *Haemophilus influenzae* ATCC 51907, and *Staphylococcus aureus* RN4220. *H. influenzae* was grown in Brain Heart Infusion (BHI) media supplemented with hemin and β-nicotinamide adenine dinucleotide hydrate [14]. Broth cultures of *H. influenzae* were prepared by scraping bacteria from agar plates and suspending into fresh supplemented BHI medium to the desired OD_{600}. All other bacterial strains were grown in Luria–Bertani (LB) medium. Inoculum for liquid culture assays was prepared by diluting an overnight LB broth culture, grown at 37 °C with shaking (200 rpm), into fresh liquid medium to the desired OD_{600}.

A.6.5 Antibacterial screening assay

Bacterial inoculum of each strain was prepared to an OD_{600} of 0.1 as described above. Next, 100 µL of each dilute culture was added in triplicate to a sterile non-treated CytoOne 96-well clear bottom plate. To each well, was added 5 µL of either compound in DMSO or DMSO alone. The final concentration of compound was 200 µM and the concentration of DMSO was 5%. The plates were covered and incubated at 37 °C with shaking (200 rpm) for 6 to 7 hours. Afterwards, bacterial growth was recorded by measuring OD_{600} using a SpectraMax M5 plate reader.

A.6.6 Minimum inhibitory concentration assay

MIC experiments were performed using the double dilution method. Briefly, inoculum of each strain was prepared to an OD_{600} of 0.1 and 200 µL of each dilute culture was added to a sterile non-treated CytoOne 96-well clear bottom plate. To the plated dilute cultures, was added 10 µL of compound from a 2-fold dilution series. The final concentrations of the compounds were in the range of 256 to 2 µg/mL. Plates were covered and incubated at 37 °C with shaking (200 rpm) for 24 hours before MIC values were determined. All experiments were performed at least twice in triplicate.

A.6.7 Bacterial growth assay in liquid culture

Bacterial cultures were prepared to an OD_{600} of 0.1 and 200 µL of each dilute culture was added to the wells of sterile non-treated CytoOne 96-well clear bottom plates. Compounds (10 µL) from a 2-fold dilution series were then added to a final concentration between 32 and 1 µg/mL. Plates were covered and incubated at 37 °C with shaking (200 rpm). Bacterial growth was recorded every 30 minutes by measuring OD_{600} using a SpectraMax M5 plate reader. All experiments were performed at least twice in triplicate.

A.6.8 Assay of bactericidal/bacteriostatic activity

Time-kill studies were performed using 5 mL cultures of *S. aureus* (OD_{600} = 0.1) treated with either 250 µL of compound 6 or DMSO. Final compound concentrations were 8 to 16 µg/mL. Samples (100 µL) of each culture were removed after 0, 4, and 24 hours, serially

diluted 10-fold in sterile phosphate buffered saline and spotted (2 µL) on LB agar plates. Finally, colonies were counted after incubation for 24 hours at 37 °C.

A.6.9 Compound 6 analogs

Compound 6a (4-cyano-*N*-2-oxo-2-(piperazin-1-yl)ethyl-*N*-(3-phenylpropyl)benzamide) was purchased from ChemDiv. Compound 6b (*N*-(2-(benzylamino)-2-oxoethyl)-4-isopropylcyclohexane-1-carboxamide) was purchased from Vitas-M Laboratory. Compound 6c (*N*-benzyl-2-(2-(isopropylthio)acetamido)acetamide) and compound 6d (*N*-(2-(4-benzylpiperazin-1-yl)-2-oxoethyl)-methylbutanamide) were purchased from Enamine. Mass spectrometry was used to validate the identity of each purchased compound (Appendix A.7.7).

Notes

This work was published as "Concise synthesis of spergualin-inspired molecules with broad-spectrum antibiotic activity" 2015 *MedChemComm* 6: 912-918. Victoria A. Assimon and Jason E. Gestwicki designed experiments. Victoria A. Assimon conducted the experiments. In this study, Hao Shao resynthesized the lead compound. The *Bacillus anthracis* strain was a generous gift from Dr. Phil Hanna (University of Michigan). The *Bacillus cereus* and *Haemophilus influenzae* strains were kind gifts from Dr. Sylvie Garneau-Tsodikova (University of Kentucky).

A.7 Appendix

A.7.1 Bacterial growth inhibition screens

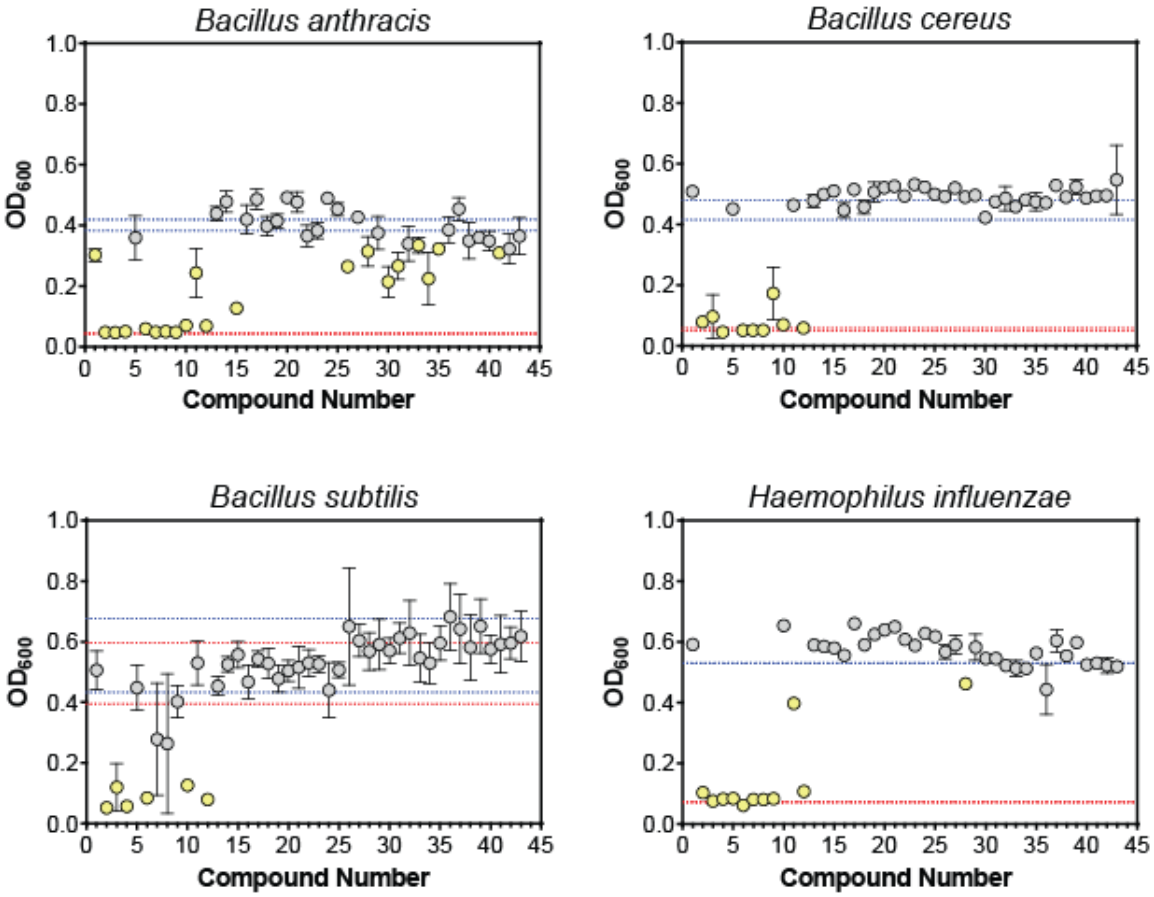

Appendix A.7.1 Screening data of compounds against *B. anthracis*, *B. cereus*, *B. subtilis*, and *H. influenzae* in a bacterial growth assay. Dotted lines represent the average growth and standard deviations in presence of the controls. The blue lines represent the negative control (DMSO). The red lines represent the positive control (ampicillin). Results are the average of triplicates and the error bars represent SEM. Gray data points indicate inactive compounds, while yellow data points represent active (hit) compounds.

A.7.2 Compound 6 shows a dose-dependent inhibition of bacterial growth

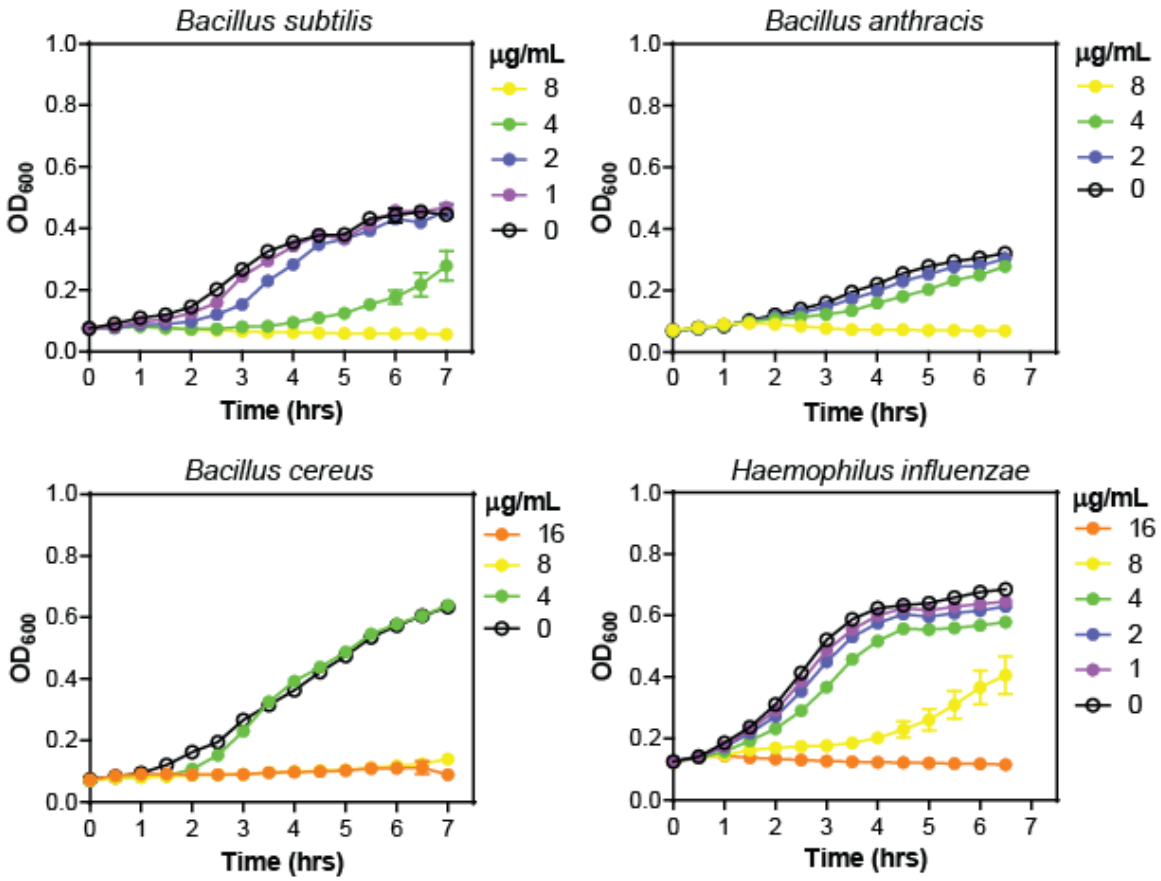

Appendix A.7.2 Compound 6 shows a dose-dependent inhibition of bacterial growth against *B. anthracis*, *B. cereus*, *B. subtilis*, and *H. influenzae*. Growth curve experiments were performed twice in triplicate. Representative graphs are shown.

A.7.3 The peptoid region of compound 6 appears to be pharmacophore of this molecule

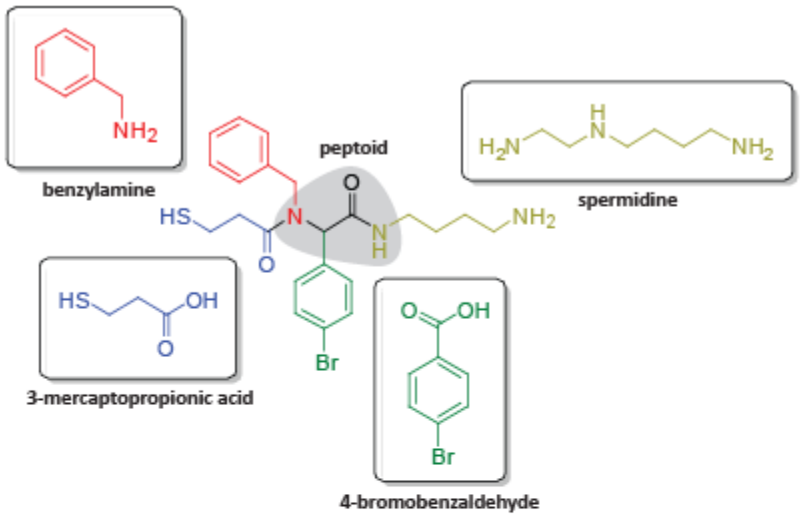

	MIC (µg/mL)					
Compound	*E. coli*	*H. Influenzae*	*B. anthracis*	*B. cereus*	*B. subtilis*	*S. aureus*
6	32	16	4	8	4	8
benzylamine	> 256	> 256	> 256	> 256	> 256	> 256
3-mercaptopropionic acid	> 256	> 256	> 256	> 256	> 256	> 256
4-bromobenzaldehyde	> 256	> 256	> 256	> 256	> 256	> 256
spermidine	> 256	> 256	> 256	> 256	> 256	> 256

Appendix A.7.3 Four chemical moieties (benyzlamine, 3-mercaptopropionic acid, spermidine, and 4-bromobenzyaldehyd) represented in the structure of compound 6 were tested for antibacterial activity in a MIC assay.

A.7.4 Exploration of the structure activity relationships around compound 6

(A) Chemical structures of commercially purchased compound 6 analogs.

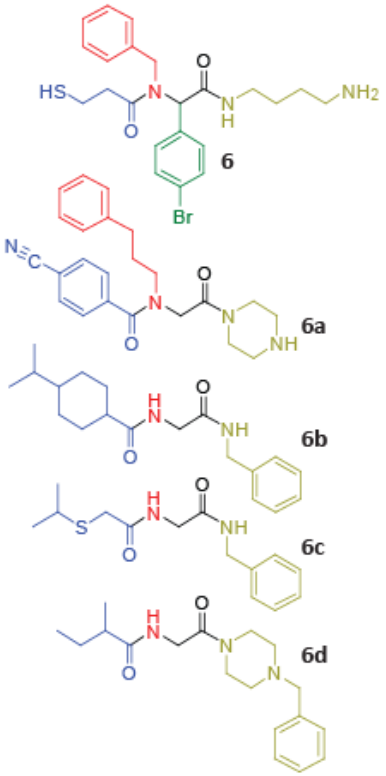

(B) Commercial compound 6 analogs do not have antibacterial activity in MIC assay.

	MIC (μg/mL)				
Bacterial Strain	Compd 6	Compd 6a	Compd 6b	Compd 6c	Compd 6d
E. coli	32	>128	>128	>128	>128
H. Influenzae	16	>128	>128	>128	>128
B. anthracis	4	>128	>128	>128	>128
B. cereus	8	>128	>128	>128	>128
B. subtilis	4	>128	>128	>128	>128
S. aureus	8	>128	>128	>128	>128

(C) Structure activity relationships gleaned from antibacterial screen and MIC assays with compound 6 analogs.

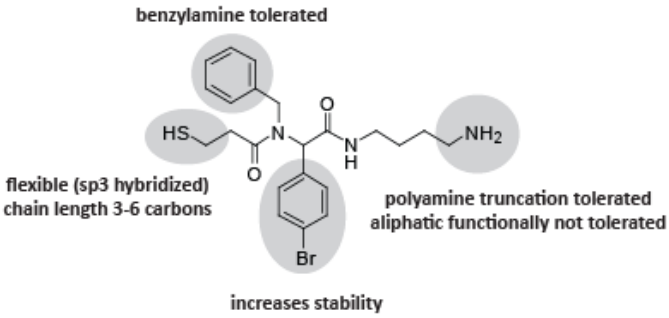

Appendix A.7.4 (A) Chemical structure of commercially purchased compound 6 analogs. (B) Commercial compound 6 analogs do not have antibacterial activity by MIC assays. MIC assays were performed at least twice in triplicate. (C) Summary of structure activity relationships gleaned from antibacterial assays.

A.7.5 Resynthesis and characterization of compound 6

In a 50 mL RBF, benzylamine (1 mmol), 4-bromobenzaldehyde (1 mmol), and 5 mL of methanol were mixed at RT until imine formation was detected by thin layer chromatography (~30 minutes). Next, 3-mercaptopropionic acid (1 mmol) and *tert*-butyl (4-isocyanobutyl)carbamate (1 mmol) were added and allowed to react overnight. This reaction was then purified by column chromatography on silica gel using a hexane and ethyl acetate gradient. Next, a solution of HCl (3M, 0.3 mL) was added to this intermediated in 3 mL of methanol. This mixture was stirred at 80 °C for 3 hr. The mixture was purified using prepared HPLC to yeild the desired product. White solid (20%). ^{1}H NMR (400 MHz, Methanol-d_4) δ 7.34 (d, *J* = 8.4 Hz, 2H), 7.28 – 7.02 (m, 5H), 6.94 (d, *J* = 6.4 Hz, 2H), 5.90 (s, 1H), 4.76 (d, *J* = 17.8 Hz, 1H), 4.49 (d, *J* = 17.8 Hz, 1H), 3.26 – 3.05 (m, 2H), 3.05 – 2.47 (m, 6H), 1.70 – 1.44 (m, 4H). ^{13}C NMR (100Hz, Chloroform-*d*) δ 173.68, 170.13, 136.24, 131.81, 128.60, 127.38, 126.00, 123.17, 63.59, 39.59, 38.65, 33.73, 33.23, 25.54, 24.23. LCMS (ESI$^+$): *m/z* $[M + H]^+$ calculated for $C_{22}H_{29}BrN_3O_2S$, 478.11, find 478.10.

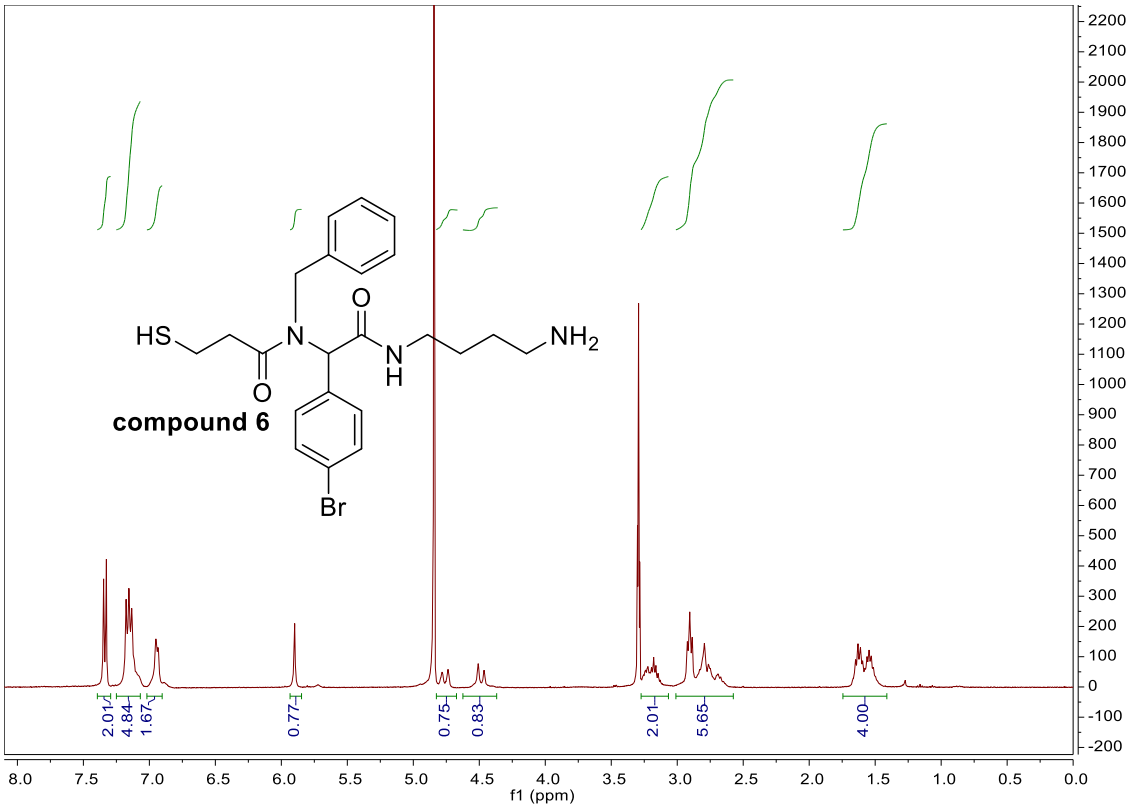
HS
N
O
O
N
H
NH2
compound 6
Br
2.01
4.84
1.67
0.77
0.75
0.83
2.01
5.65
4.00
f1 (ppm)

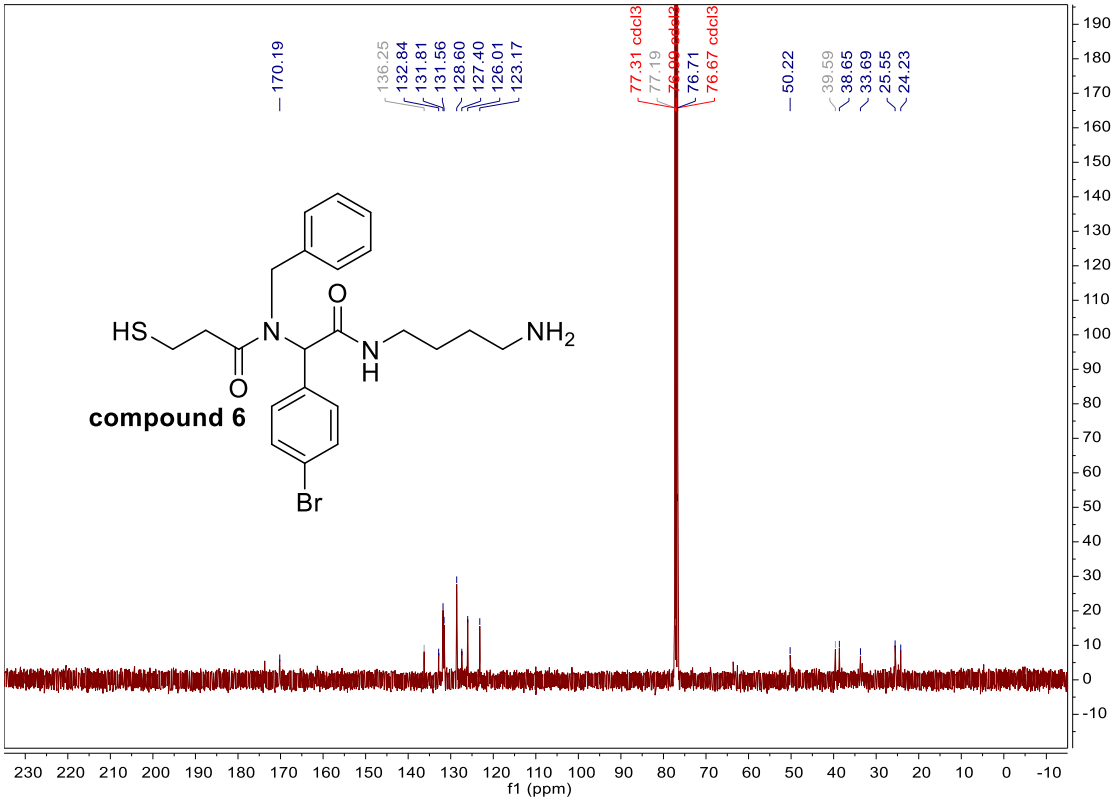
170.19
136.25
132.84
131.81
131.56
128.60
127.40
126.01
123.17
77.31 cdcl3
77.19
76.71
76.67 cdcl3
50.22
39.59
38.65
33.69
25.55
24.23
HS
N
O
O
N
H
NH2
compound 6
Br
f1 (ppm)

A.7.6 Compound characterization of spergualin-inspired library

Compound 1. ^{1}H NMR (400 MHz, Chloroform-*d*) δ 7.24 (d, *J* = 8.4 Hz, 2H), 7.16 – 7.04 (m, 5H), 6.89 (d, *J* = 7.1 Hz, 2H), 6.66 (s, 1H), 5.86 (s, 1H), 4.87 (s, 1H), 4.72 – 4.41 (m, 2H), 3.23 – 3.04 (m, 2H), 2.97 (s, 2H), 2.37 – 2.09 (m, 2H), 1.58 – 1.49 (m, 2H), 1.34 (s, 9) 1.18 – 1.14 (m, 4H), 0.745 (t, *J* = 7.2 Hz, 3H).

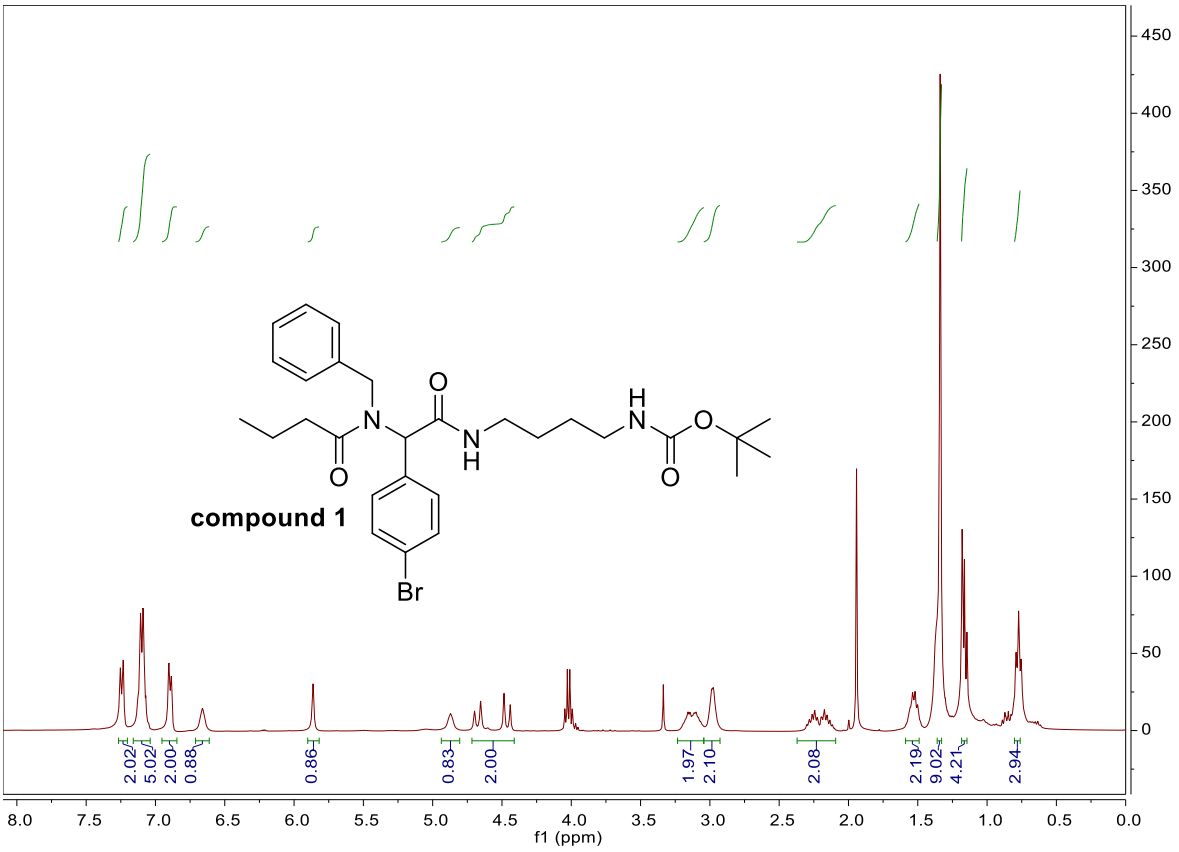

Compound 2. ^{1}H NMR (400 MHz, Chloroform-*d*) δ 7.33 (d, *J* = 8.0 Hz, 2H), 7.21 – 7.08 (m, 5H), 6.97 (d, *J* = 7.4 Hz, 2H), 6.37 (s, 1H), 5.62 (s, 1H) 4.78 (s, 1H), 4.67 (d, *J* = 17.5 Hz, 1H), 4.42 (d, *J* = 17.6 Hz, 1H), 3.26 – 2.95 (m, 5H), 2.57 – 2.19 (m, 2H), 1.76 – 1.61 (m, 2H), 1.63 – 1.50 (m, 2H), 1.31 – 1.11 (m, 4H).

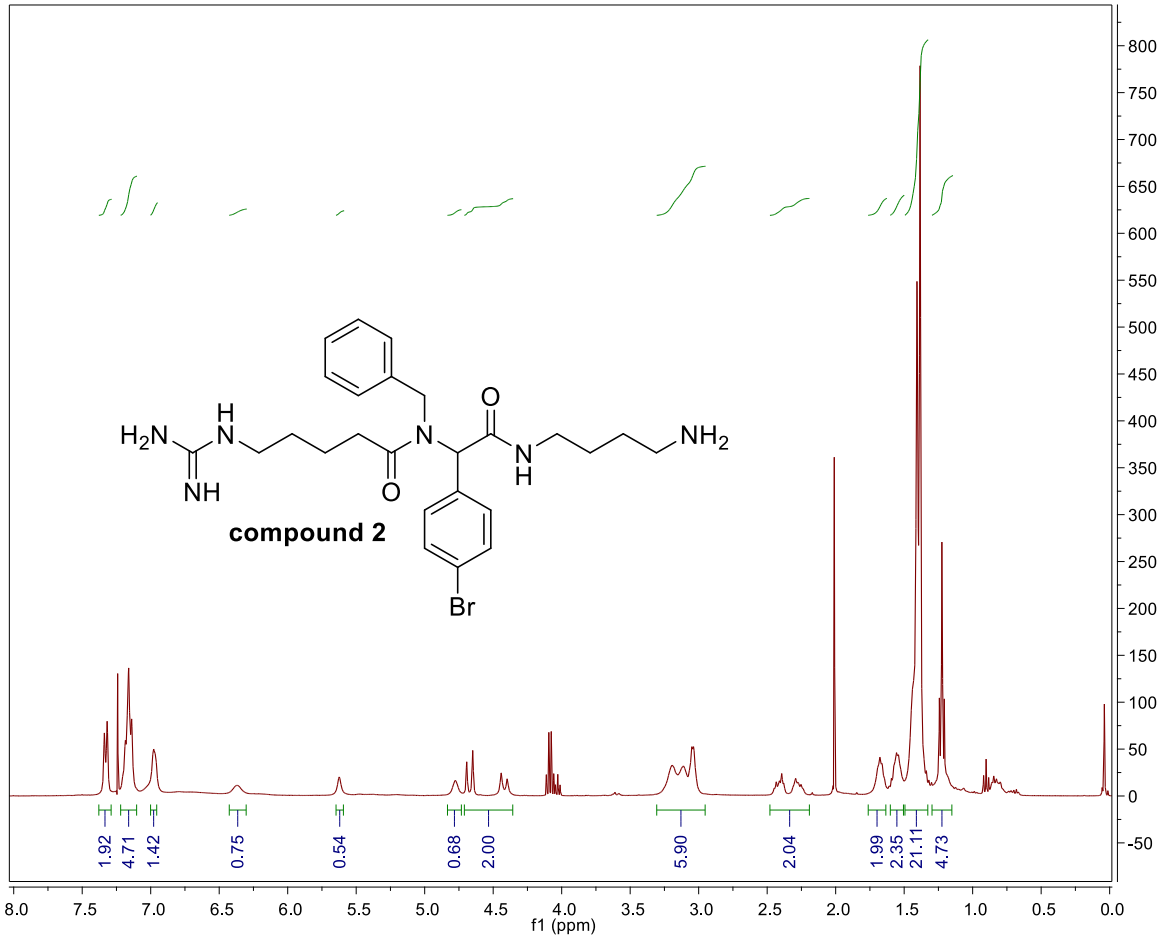

Compound 3. ^{1}H NMR (500 MHz, Chloroform-*d*) δ 7.31 (d, *J* = 8.1 Hz, 2H), 7.24 – 7.07 (m, 5H), 6.95 (d, *J* = 7.3 Hz, 2H), 4.72 (d, *J* = 17.7 Hz, 2H), 4.53 (d, *J* = 17.7 Hz, 1H), 3.85 (s, 2H), 3.30 – 3.08 (m, 2H), 2.79 – 2.56 (m, 2H), 2.28 (ddt, *J* = 52.7, 15.6, 7.6 Hz, 2H), 1.65 – 1.42 (m, 6H), 1.31 – 1.10 (m, 4H), 0.82 (t, *J* = 6.8 Hz, 3H).

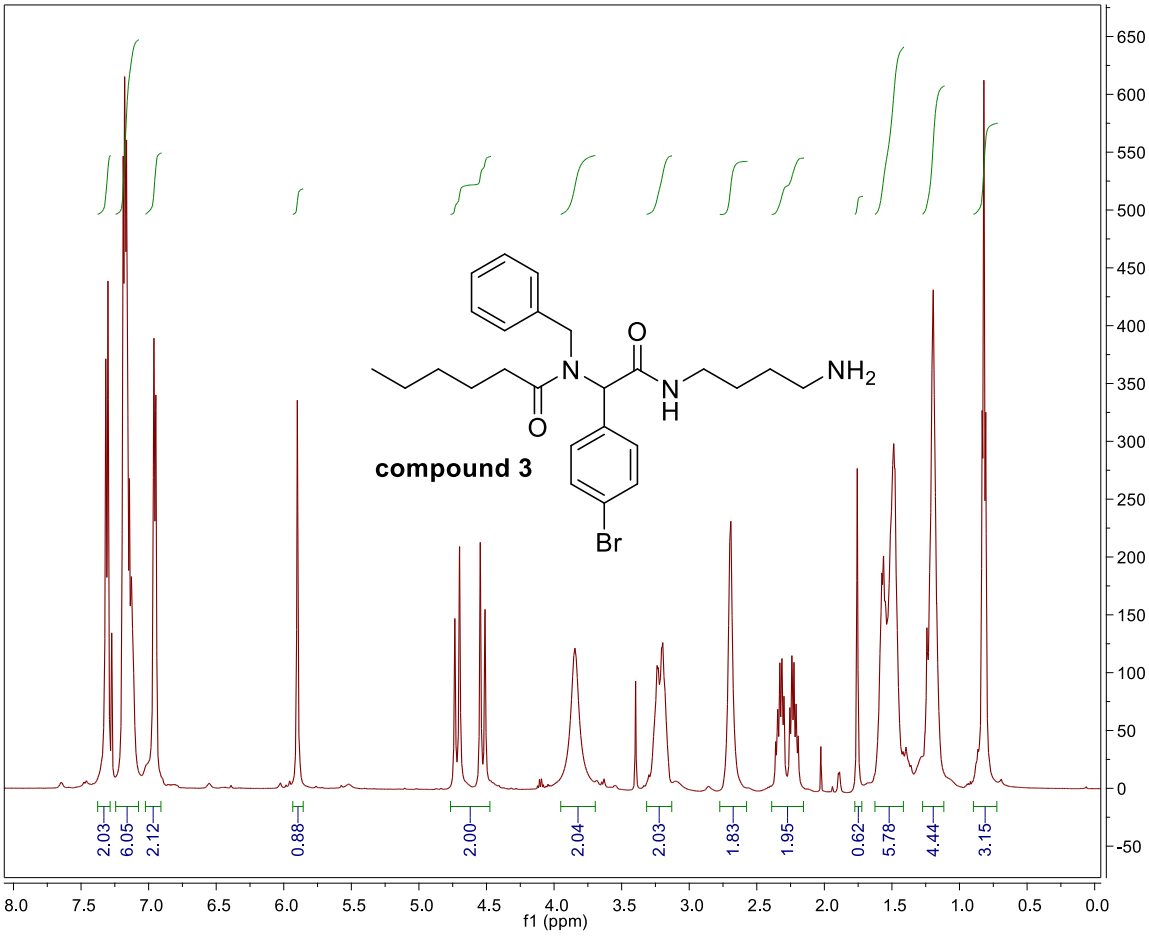

Compound 4. ^{1}H NMR (500 MHz, Chloroform-*d*) δ 7.34 (dd, *J* = 18.1, 7.7 Hz, 2H), 7.26 – 7.10 (m, 5H), 7.01 (s, 2H), 4.81 – 4.63 (m, 2H), 4.46 (d, *J* = 17.6 Hz, 2H), 3.50 – 2.95 (m, 5H), 2.61 -2.14 (m, 2H), 1.79 – 1.07 (m, 14H).

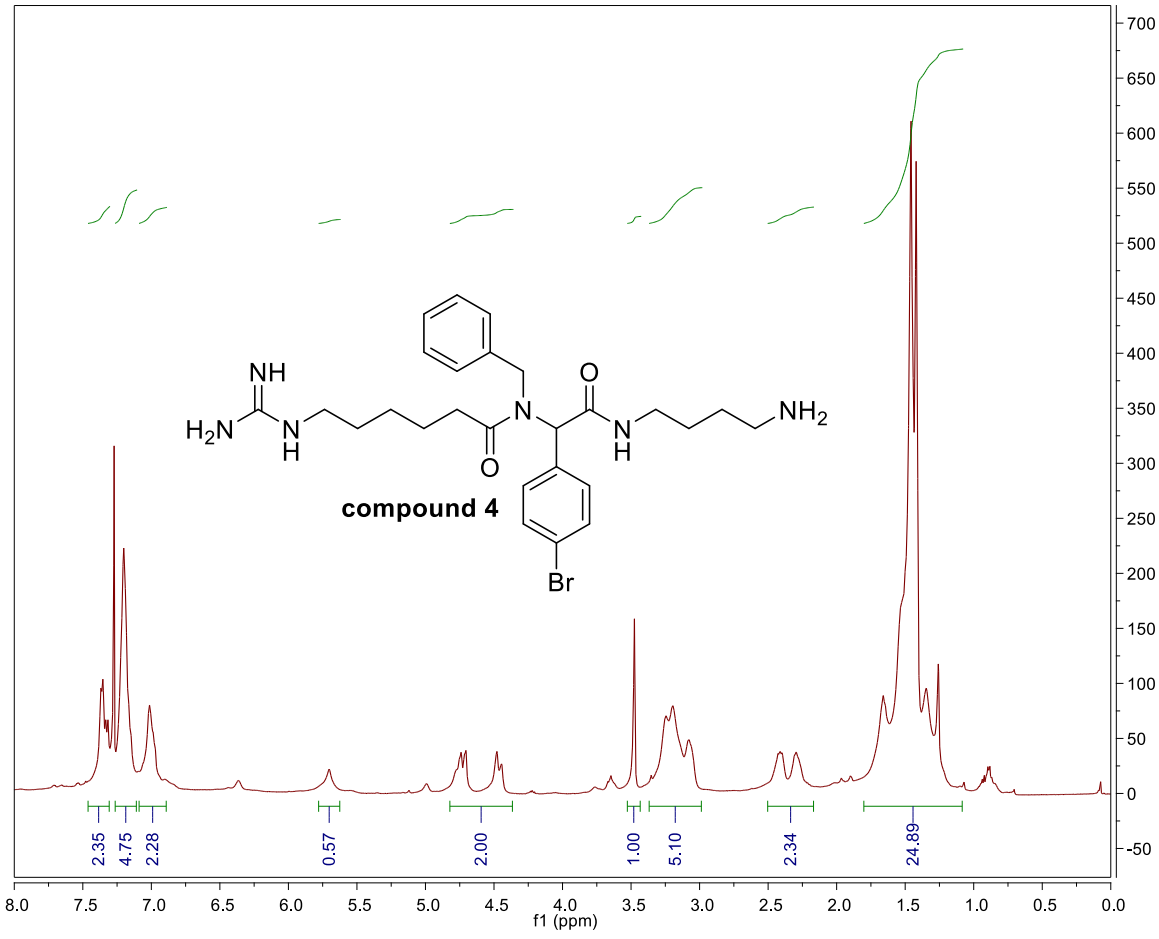

Compound 5. ^{1}H NMR (500 MHz, Methanol-d_4) δ 7.53 – 7.49 (m, 3H), 7.45 (s, 4H), 7.36 (d, J = 8.1 Hz, 4H), 7.22 (s, 2H), 7.13 – 7.07 (m, 5H), 6.88 (s, 2H), 4.40 (d, J = 16.7 Hz, 1H), 3.25 – 3.15 (m, 3H), 2.76 (s, 2H), 1.53 (s, 6H).

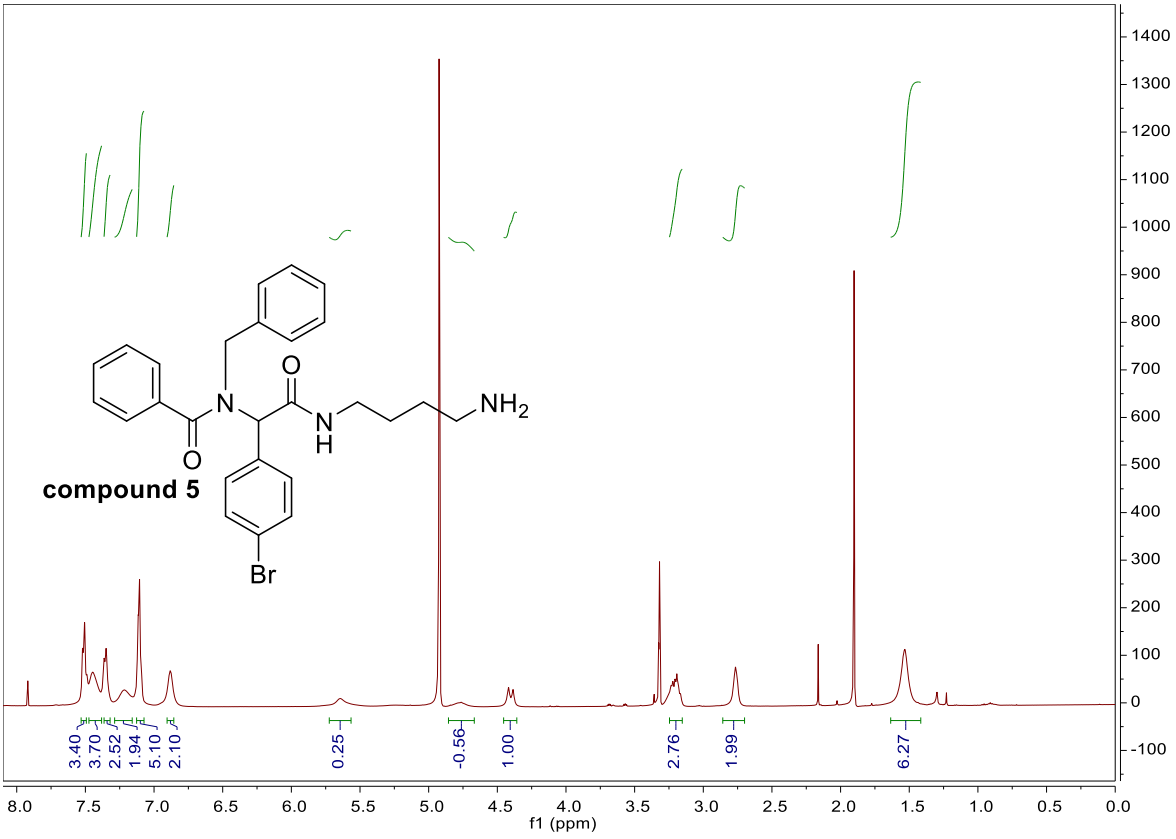

Compound 6. ^{1}H NMR (400 MHz, Methanol-d_4) δ) δ 7.34 (d, J = 8.4 Hz, 2H), 7.28 – 7.02 (m, 5H), 6.94 (d, J = 6.4 Hz, 2H), 5.90 (s, 1H), 4.76 (d, J = 17.8 Hz, 1H), 4.49 (d, J = 17.8 Hz, 1H), 3.26 – 3.05 (m, 2H), 3.05 – 2.47 (m, 6H), 1.70 – 1.44 (m, 4H).

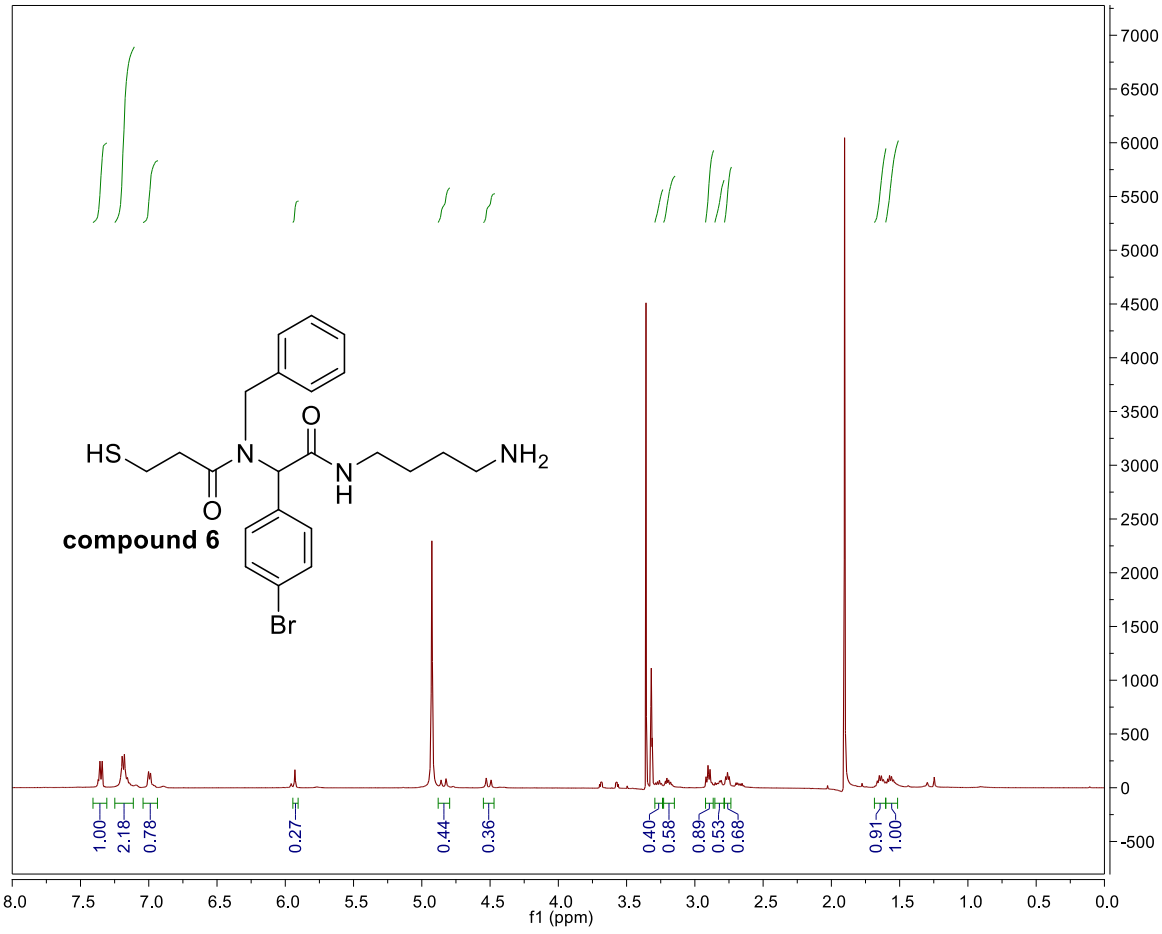

Compound 7. ^{1}H NMR (500 MHz, Methanol-d_4) δ 7.36 (d, J = 8.5 Hz, 2H), 7.22 – 7.06 (m, 5H), 6.95 (d, J = 7.2 Hz, 2H), 6.01 (s, 1H), 4.82 (d, J = 17.9 Hz, 1H), 4.54 (d, J = 18.0 Hz, 1H), 3.32 (p, J = 1.6 Hz, 3H), 3.26 – 3.09 (m, 3H), 2.63 (t, J = 6.9 Hz, 3H), 2.53 – 2.28 (m, 2H), 2.20 – 2.16 (m, 2H), 2.11 (td, J = 7.1, 2.6 Hz, 2H), 1.81 – 1.65 (m, 3H), 1.55 – 1.41 (m, 10H).

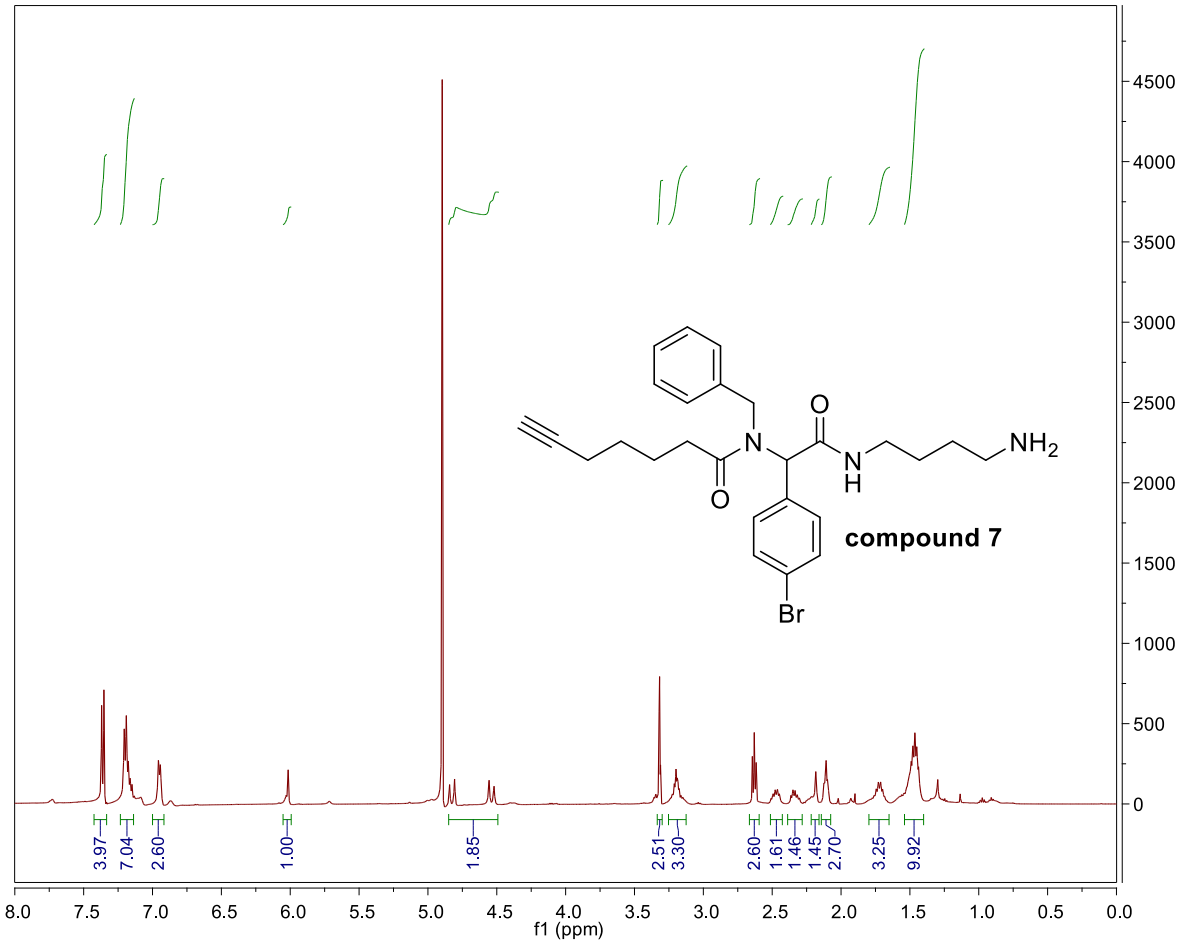

Compound 8. ^{1}H NMR (500 MHz, Methanol-d_4) δ 7.38 – 7.33 (m, 2H), 7.23 – 7.06 (m, 5H), 6.94 (d, *J* = 7.2 Hz, 2H), 6.03 (d, *J* = 4.4 Hz, 1H), 5.77 – 5.66 (m, 1H), 4.96 (d, *J* = 15.1 Hz, 2H), 4.81 (d, *J* = 17.9 Hz, 1H), 4.53 (d, *J* = 18.0 Hz, 1H), 3.19 (hept, *J* = 6.8 Hz, 3H), 2.62 (t, *J* = 6.9 Hz, 2H), 2.50 – 2.24 (m, 2H), 2.02 (q, *J* = 7.5 Hz, 3H), 1.80 – 1.63 (m, *J* = 6.7 Hz, 3H), 1.57 – 1.38 (m, 7H).

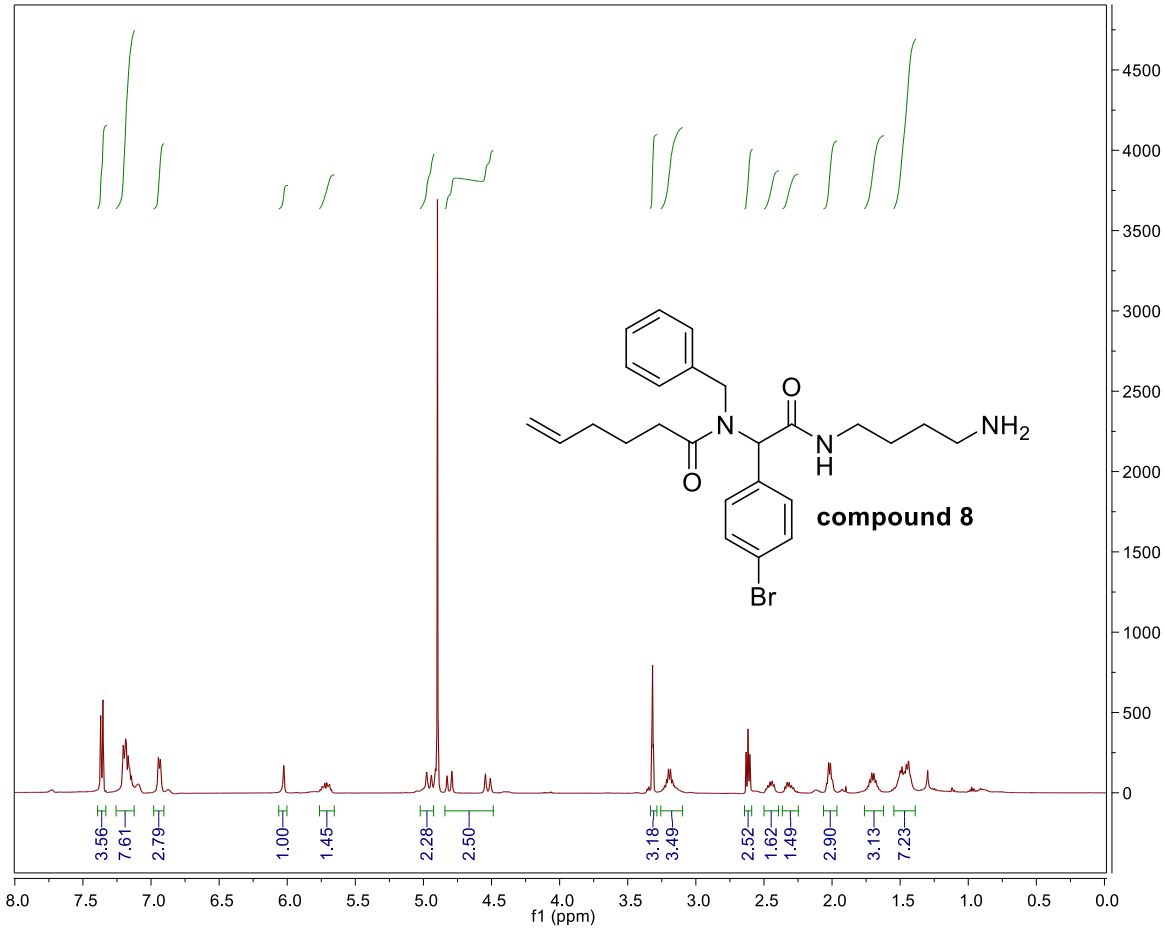

Compound 9. ^{1}H NMR (500 MHz, Methanol-d_4) δ 7.36 (d, J = 8.5 Hz, 2H), 7.24 – 7.05 (m, 5H), 6.94 (d, J = 7.2 Hz, 2H), 4.83 (d, J = 18.0 Hz, 1H), 4.54 (d, J = 18.0 Hz, 1H), 3.18 (dp, J = 12.7, 6.7 Hz, 4H), 2.62 (t, J = 6.9 Hz, 2H), 2.49 – 2.20 (m, 2H), 1.70 – 1.57 (m, 4H), 1.56 – 1.37 (m, 6H), 1.25 (t, J = 7.1 Hz, 2H), 1.02 – 0.92 (m, 2H), 0.89 (t, J = 7.4 Hz, 4H).

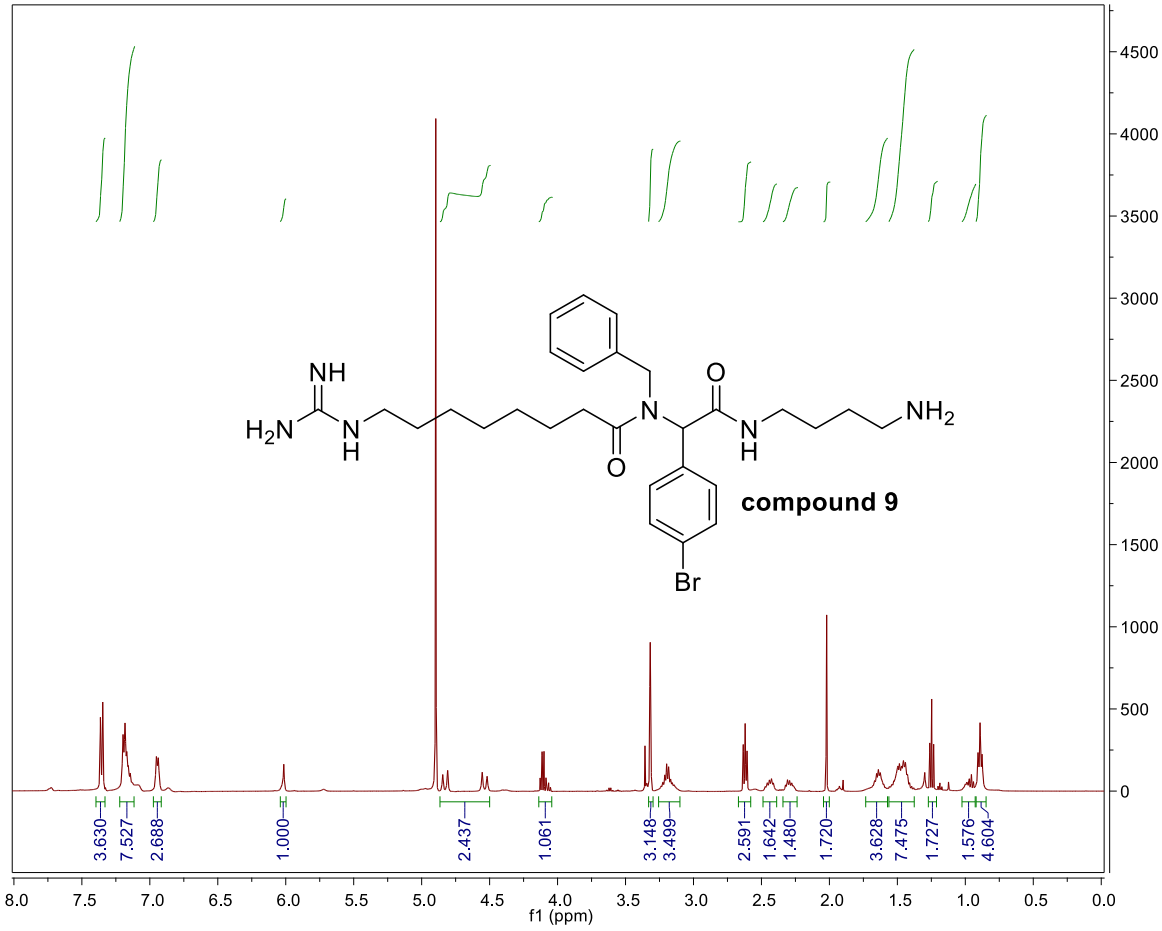

Compound 10. ^{1}H NMR (500 MHz, Methanol-d_4) δ 7.36 (d, J = 8.2 Hz, 2H), 7.23 – 7.05 (m, 5H), 6.95 (d, J = 6.5 Hz, 2H), 6.09 -5.3 (m, 2H), 4.82 (d, J = 17.9 Hz, 1H), 4.53 (d, J = 18.0 Hz, 1H), 3.28 – 3.17 (m, 2H), 3.14 (t, J = 6.5 Hz, 2H), 2.81 (t, J = 7.3 Hz, 1H), 2.71 – 2.65 (m, 1H), 2.44 (t, J = 7.1 Hz, 3H), 1.93 (s, 3H), 1.69 – 1.56 (m, 4H), 1.56 – 1.41 (m, 8H), 1.41 – 1.27 (m, 4H), 1.00 – 0.87 (m, 1H).

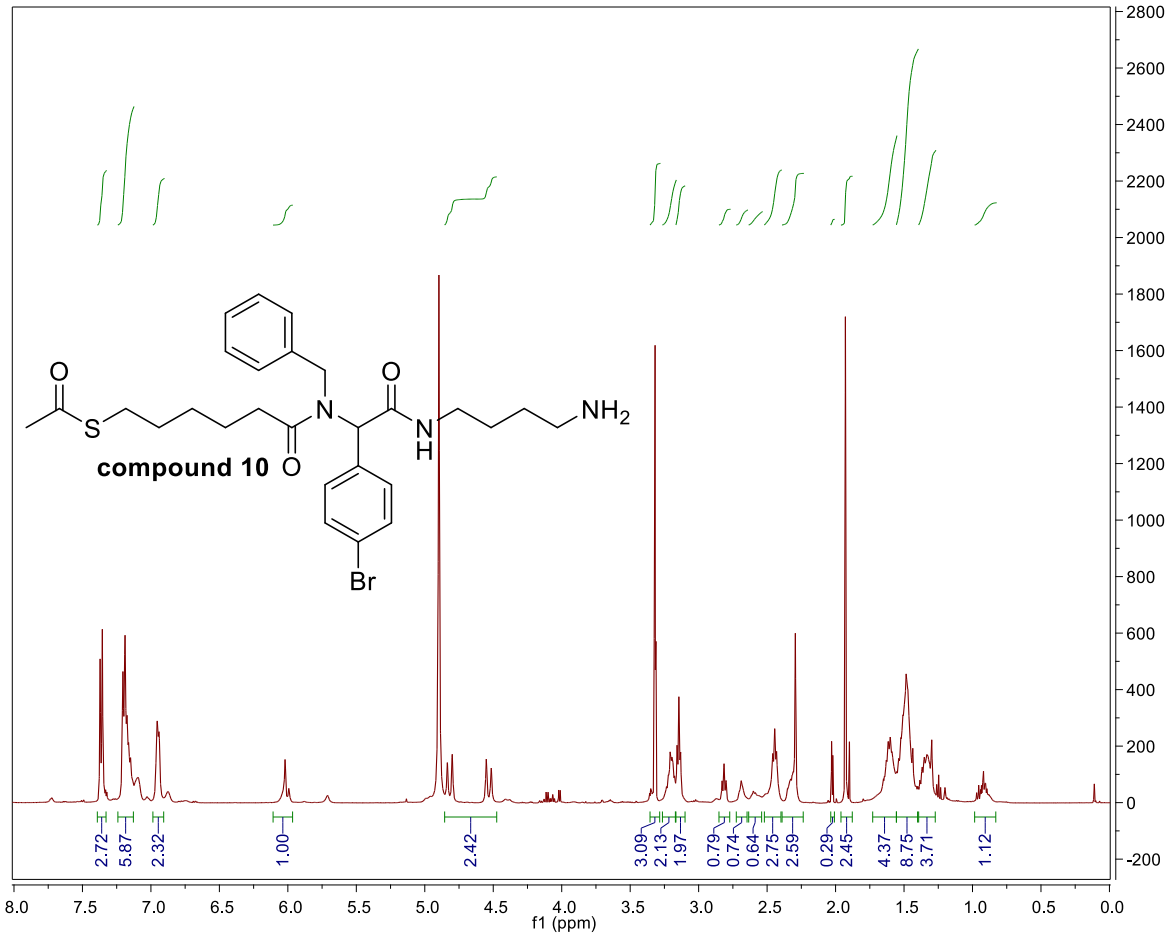

Compound 11. ^{1}H NMR (500 MHz, Methanol-d_4) δ 7.60 (d, J = 15.4 Hz, 1H), 7.37 (d, J = 8.1 Hz, 3H), 7.29 – 7.09 (m, 10H), 7.00 (d, J = 7.4 Hz, 3H), 6.92 – 6.73 (m, 5H), 6.17 (s, 1H), 5.01 (d, J = 18.1 Hz, 1H), 4.65 (d, J = 18.1 Hz, 1H), 3.28 – 3.14 (m, 2H), 3.04 (t, J = 6.6 Hz, 2H), 1.36 – 1.21 (m, 3H), 1.00 – 0.85 (m, 2H).

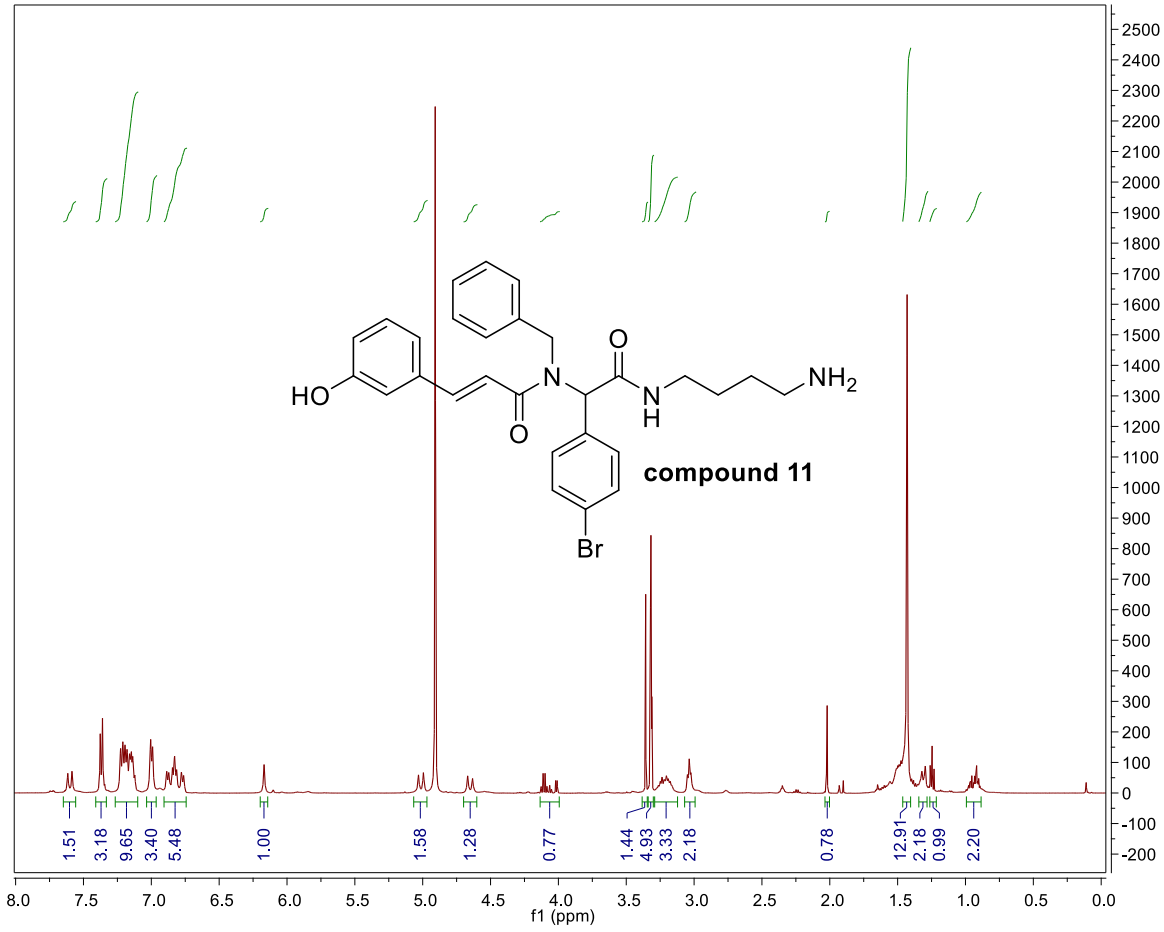

Compound 12. ^{1}H NMR (400 MHz, Methanol-d_4) δ 7.50 – 7.27 (d, J = 8.0 Hz, 2H), 7.27-7.02 (m, 5H), 6.94 (d, J = 8.0 Hz, 2H), 5.84 (s, 1H), 4.78 (d, J = 18.0 Hz, 1H), 4.47 (d, J = 18.0 Hz, 1H), 3.28 – 3.06 (m, 2H), 2.91 (t, J = 7.2 Hz, 2H), 2.50 – 2.25 (m, 2H), 1.71 – 1.48 (m, 6H), 0.88 (t, J = 7.2 Hz, 3H).

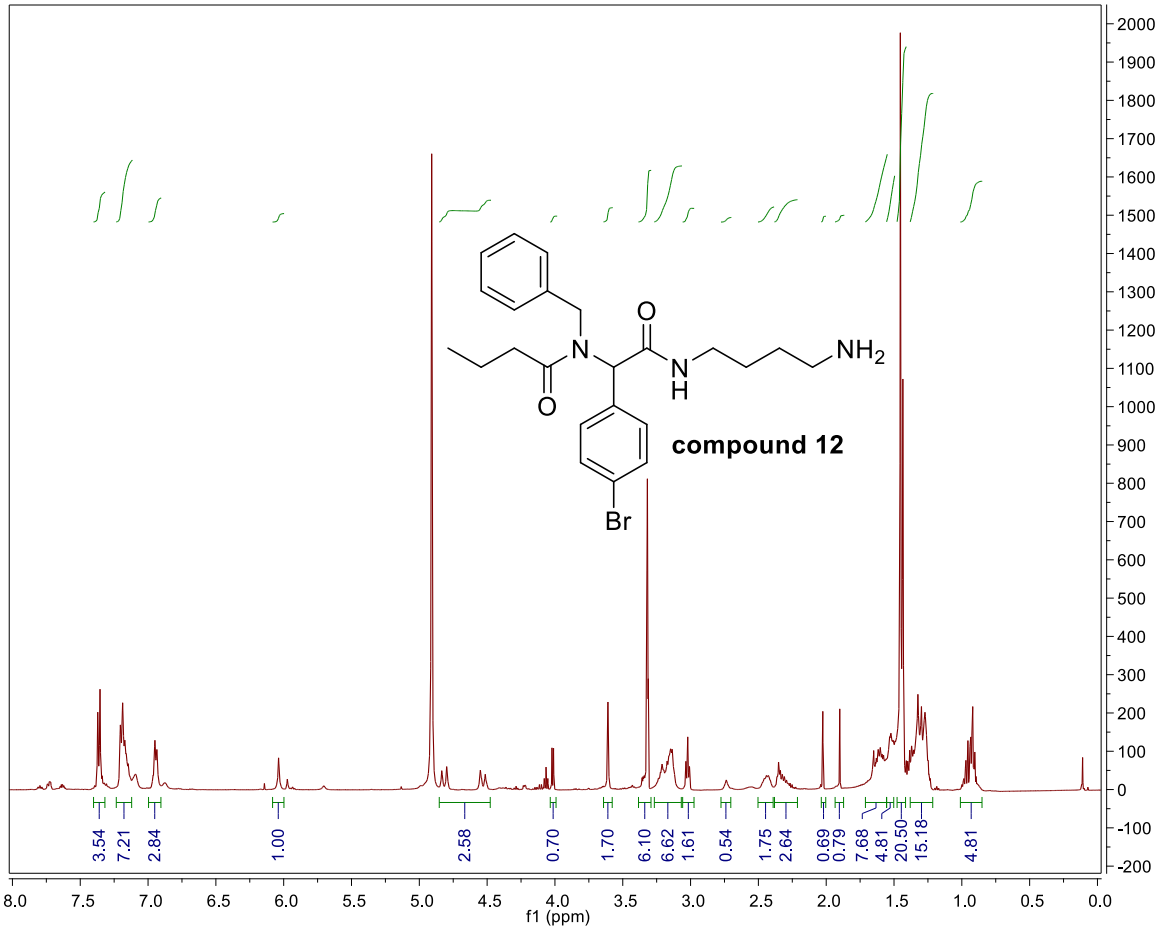

Compound 13. ^{1}H NMR (400 MHz, Chloroform-*d*) δ 7.33 (d, *J* = 8.1 Hz, 2H), 7.21 – 7.06 (m, 5H), 6.99 (d, *J* = 7.6 Hz, 2H), 5.86 (s, 1H), 5.78 (s, 1H), 4.71 (d, *J* = 17.6 Hz, 1H), 4.52 (d, *J* = 17.4 Hz, 1H), 3.23 (tt, *J* = 12.9, 6.6 Hz, 2H), 2.39 – 2.29 (m, 1H), 2.28 – 2.19 (m, 1H), 1.65 (d, *J* = 7.4 Hz, 2H), 1.42 (p, *J* = 7.3 Hz, 2H), 1.26 (dd, *J* = 15.3, 7.7 Hz, 2H), 0.87 (t, *J* = 7.3 Hz, 6H).

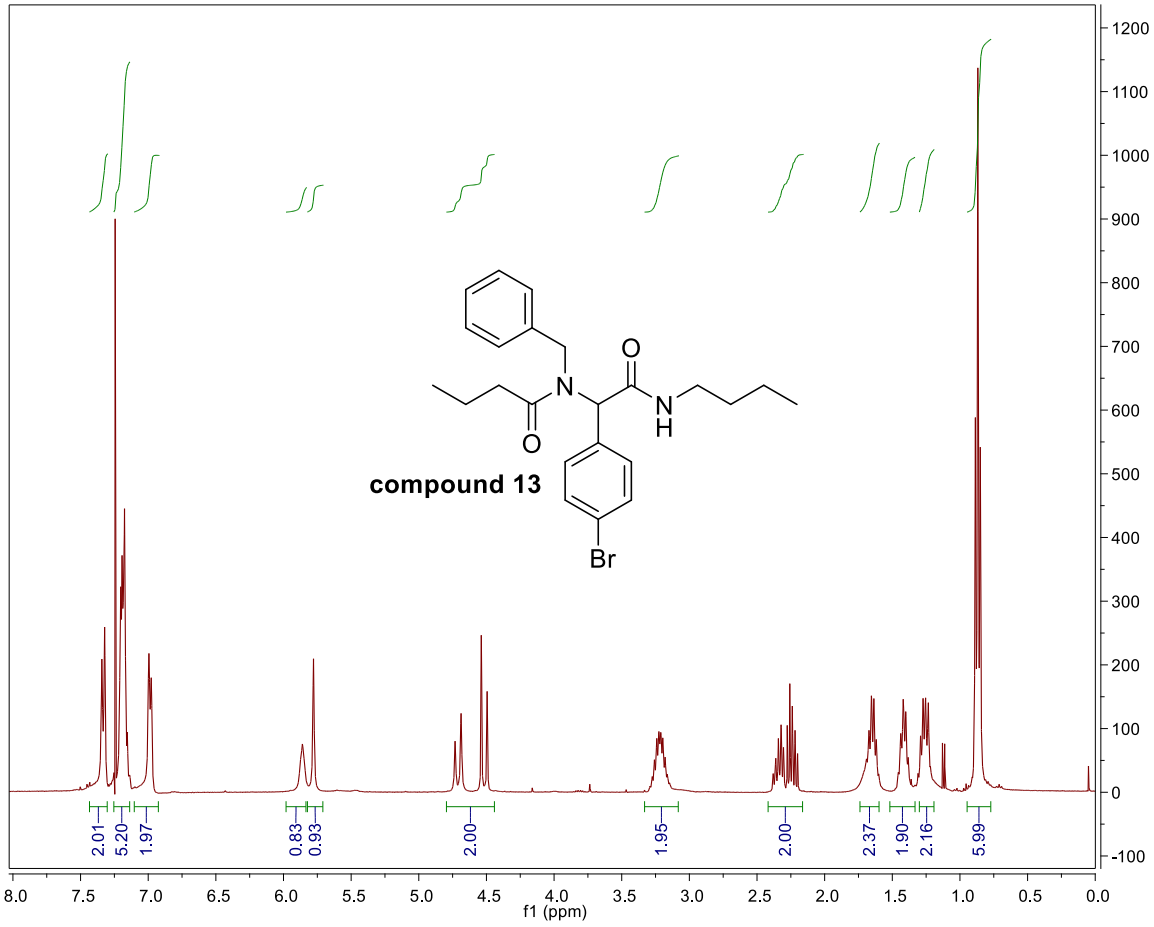

Compound 14. ^{1}H NMR (400 MHz, Chloroform-*d*) δ 7.34 (d, *J* = 8.1 Hz, 2H), 7.24 – 7.14 (m, 5H), 6.99 (d, *J* = 7.3 Hz, 2H), 5.79 (s, 1H), 4.71 (d, *J* = 17.6 Hz, 1H), 4.52 (d, *J* = 17.4 Hz, 1H), 3.31 – 3.12 (m, 2H), 2.40 – 2.21 (m, 2H), 1.66 – 1.57 (m, 2H), 1.42 (q, *J* = 7.2 Hz, 2H), 1.32 – 1.18 (m, 6H), 0.90 – 0.81 (m, 6H).

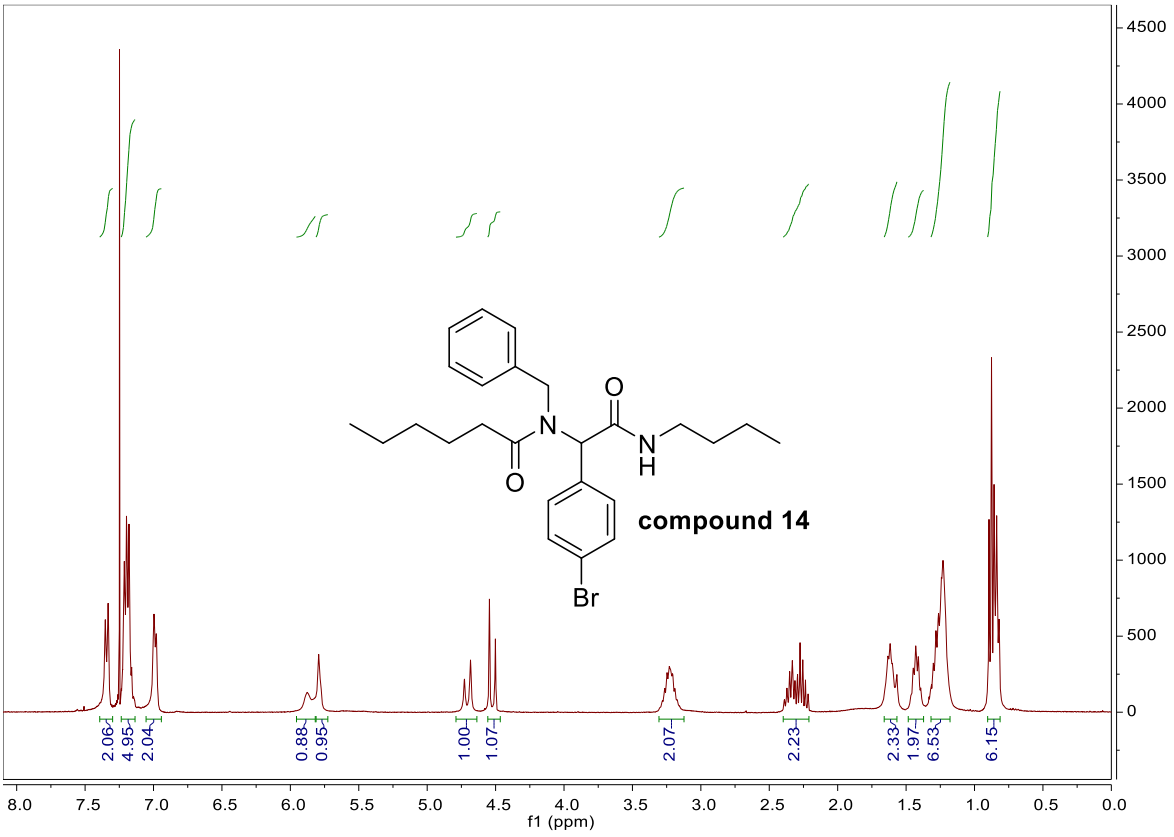

Compound 15. ^{1}H NMR (400 MHz, Chloroform-*d*) δ 7.40 (d, *J* = 8.4 Hz, 2H), 7.28 – 7.18 (m, 5H), 7.03 (d, *J* = 7.5 Hz, 2H), 5.88 (s, 1H), 5.85 (s, 1H), 4.76 (d, *J* = 17.6 Hz, 1H), 4.57 (d, *J* = 17.4 Hz, 1H), 3.39 (t, *J* = 6.8 Hz, 2H), 3.36 – 3.19 (m, 3H), 2.49 – 2.37 (m, 1H), 2.37 – 2.24 (m, 1H), 1.84 (q, *J* = 7.2 Hz, 2H), 1.67 (q, *J* = 7.1, 6.6 Hz, 3H), 1.53 – 1.39 (m, 4H), 1.32 (q, *J* = 7.4 Hz, 2H), 0.93 (t, *J* = 7.3 Hz, 3H).

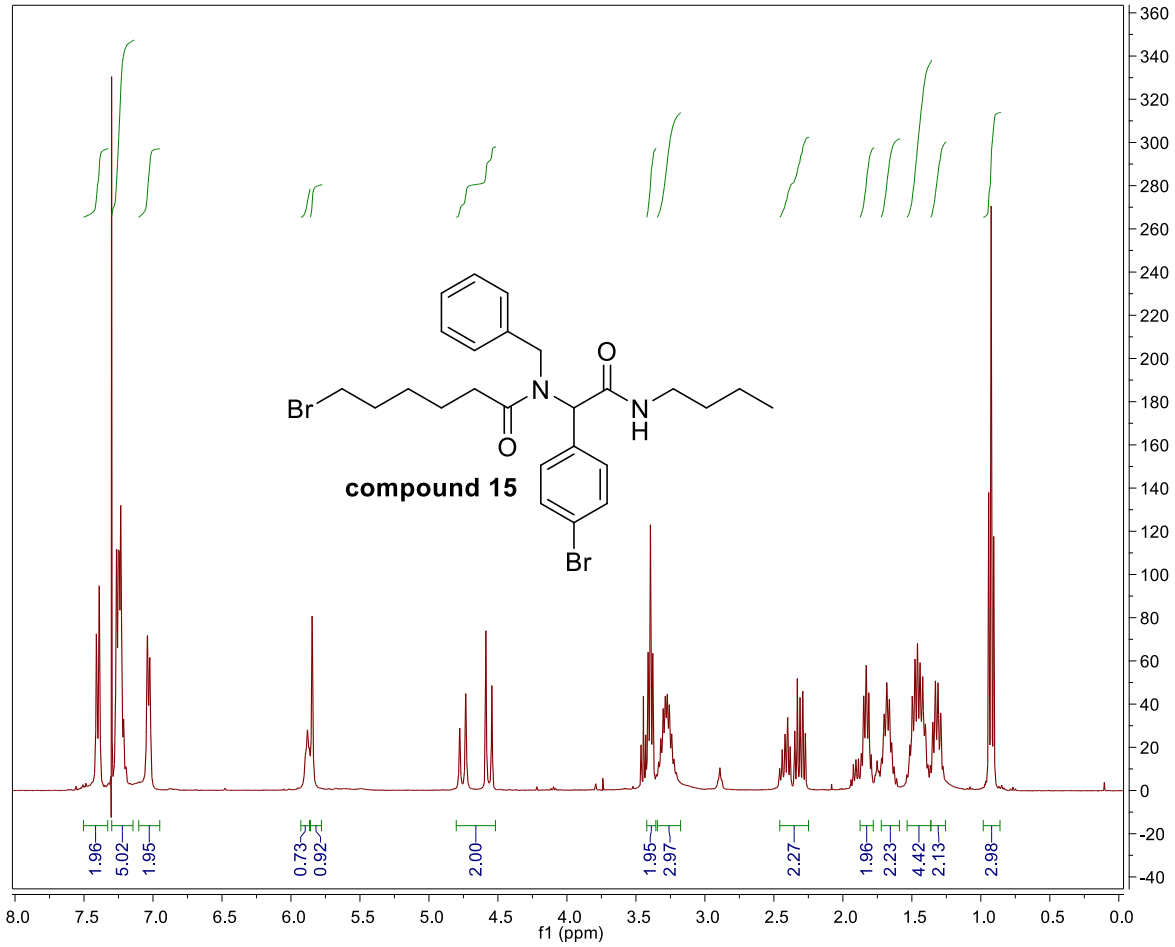

Compound 16. ^{1}H NMR (400 MHz, Chloroform-*d*) δ 7.34 (d, *J* = 8.4 Hz, 2H), 7.27 – 7.12 (m, 5H), 6.99 (d, *J* = 8.0 Hz, 2H), 5.86 (s, 1H), 5.82 (s, 1H), 4.73 (d, *J* = 17.7 Hz, 1H), 4.52 (d, *J* = 17.6 Hz, 1H), 3.30 – 3.18 (m, 2H), 2.82 – 2.71 (m, 3H), 2.71 – 2.67 (m, 1H), 2.62 – 2.55 (m, 1H),1.65 (t, *J* = 8.3 Hz, 1H), 1.42 (q, *J* = 7.5 Hz, 2H), 1.30 – 1.20 (m, 3H), 0.87 (t, *J* = 7.3 Hz, 3H).

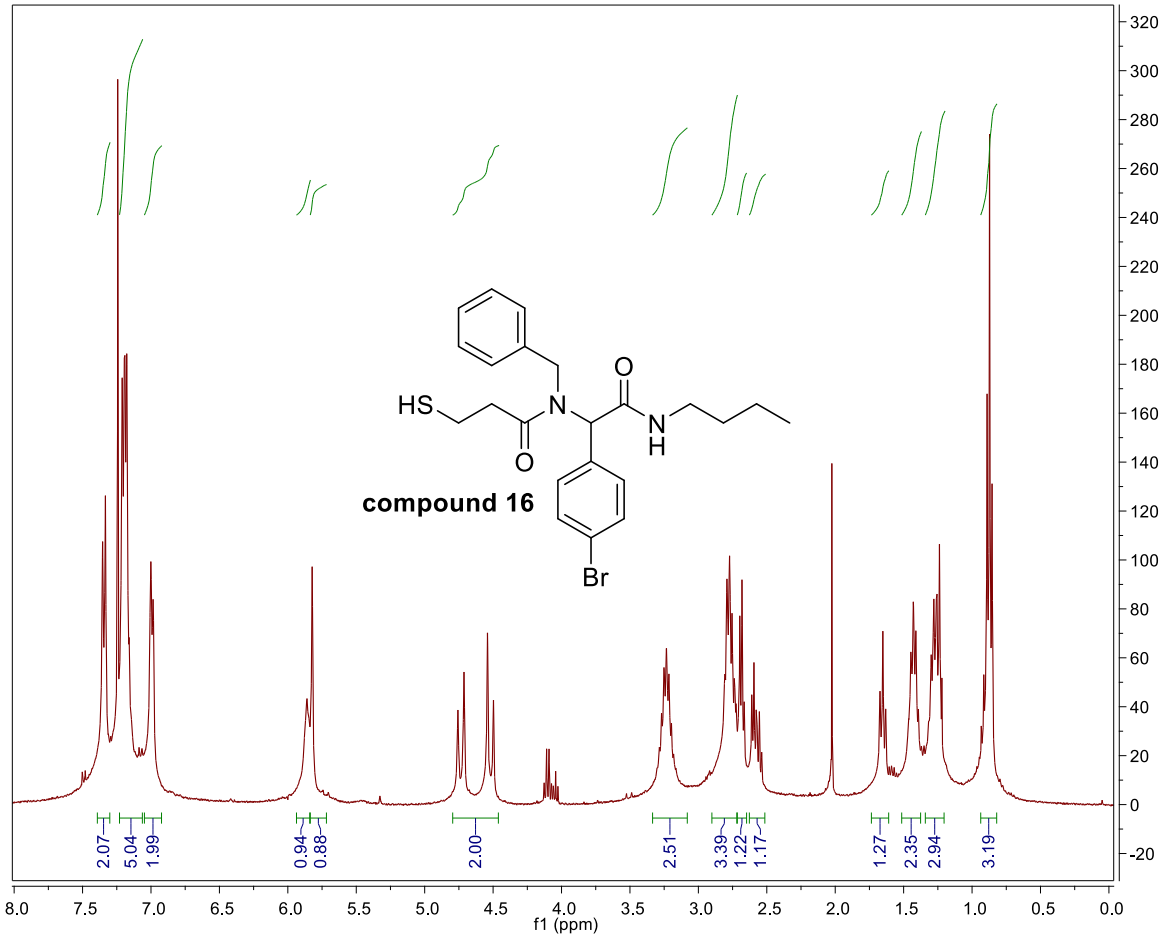

Compound 17. ^{1}H NMR (400 MHz, Chloroform-*d*) δ 7.35 (d, *J* = 8.1 Hz, 2H), 7.22 – 7.13 (m, 5H), 6.98 (d, *J* = 7.1 Hz, 2H), 5.81 (s, 1H), 5.65 (d, *J* = 8.1 Hz, 1H), 4.70 (d, *J* = 17.7 Hz, 1H), 4.50 (d, *J* = 17.6 Hz, 1H), 3.80 – 3.71 (m, 1H), 3.34 (t, *J* = 6.8 Hz, 2H), 2.40 – 2.30 (m, 1H), 2.30 – 2.19 (m, 1H), 1.91 – 1.82 (m, 3H), 1.78 (t, *J* = 7.3 Hz, 3H), 1.72 – 1.52 (m, 7H), 1.44 – 1.22 (m, 5H), 1.09 (p, *J* = 12.0 Hz, 3H).

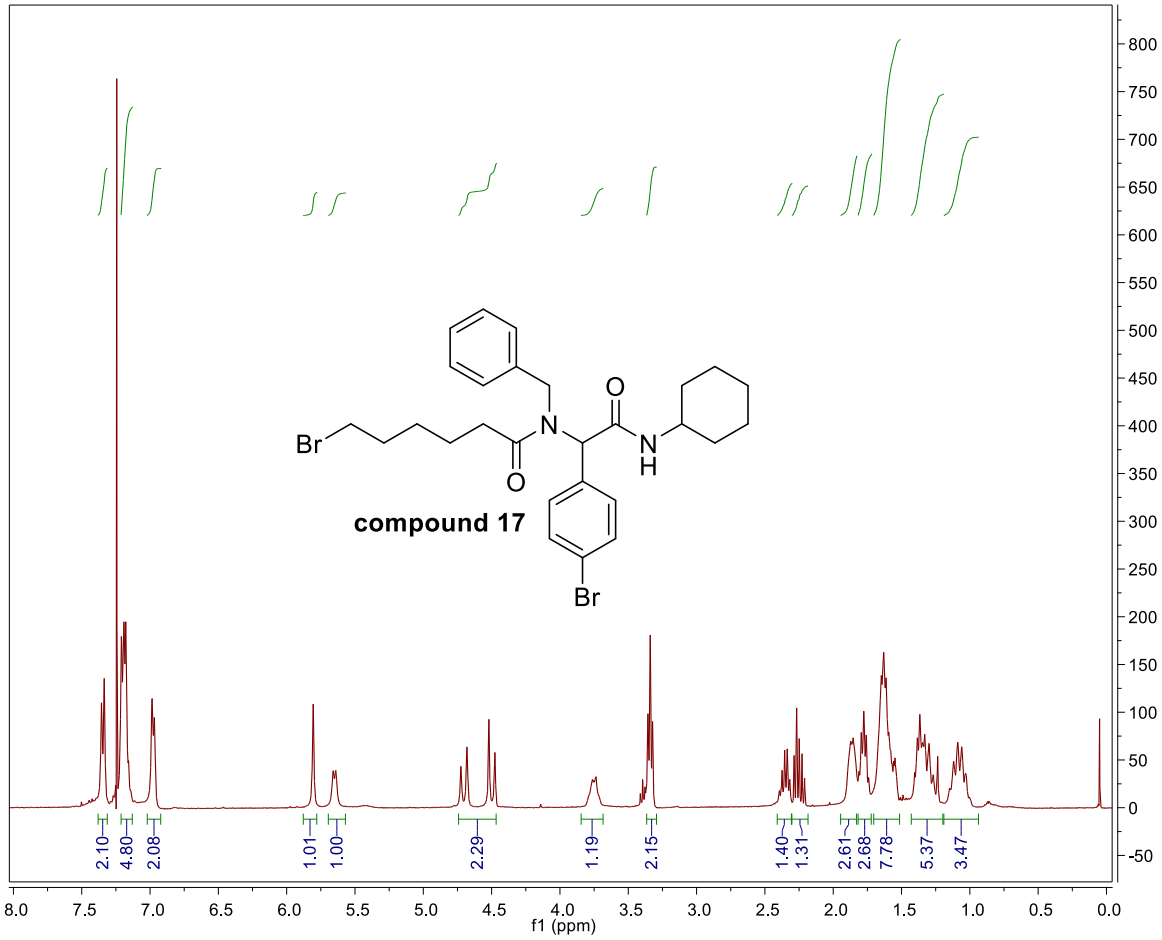

Compound 18. ^{1}H NMR (400 MHz, Chloroform-*d*) δ 7.35 (d, *J* = 8.1 Hz, 2H), 7.21 – 7.13 (m, 5H), 7.00 (d, *J* = 7.0 Hz, 2H), 5.83 (s, 1H), 5.65 (d, *J* = 8.1 Hz, 1H), 4.74 (d, *J* = 17.7 Hz, 1H), 4.50 (d, *J* = 17.7 Hz, 1H), 3.81 – 3.71 (m, 1H), 2.80 (q, *J* = 6.8, 2H), 2.74 – 2.64 (m, 1H), 2.61 – 2.52 (m, 1H), 1.87 (d, *J* = 12.1 Hz, 2H), 1.66 (t, *J* = 8.4 Hz, 2H), 1.58 (s, 4H), 1.37 – 1.23 (m, 4H), 1.08 (q, *J* = 11.8 Hz, 3H).

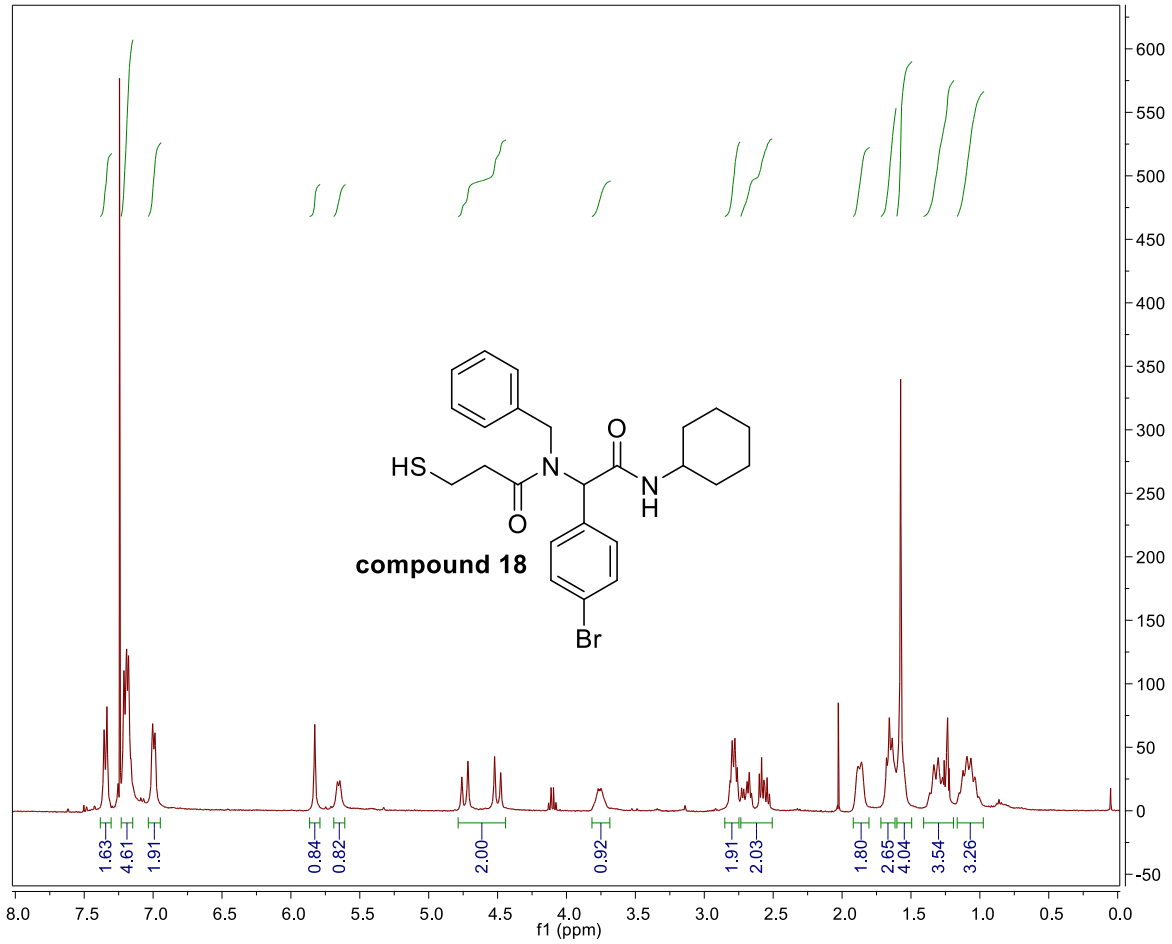

Compound 19. ^{1}H NMR (400 MHz, Chloroform-*d*) δ 7.33 (d, *J* = 8.1 Hz, 2H), 7.23 – 7.10 (m, 5H), 6.99 (d, *J* = 7.0 Hz, 2H), 5.78 (s, 1H), 5.68 (d, *J* = 7.1 Hz, 1H), 4.71 (d, *J* = 17.5 Hz, 1H), 4.50 (d, *J* = 17.4 Hz, 1H), 3.86 – 3.65 (m, 1H), 2.44 – 2.29 (m, 1H), 2.29 – 2.17 (m, 1H), 1.86 (s, 2H), 1.72 – 1.50 (m, 7H), 1.41 – 1.21 (m, 3H), 1.07 (q, *J* = 12.0 Hz, 3H), 0.87 (t, *J* = 7.4 Hz, 3H).

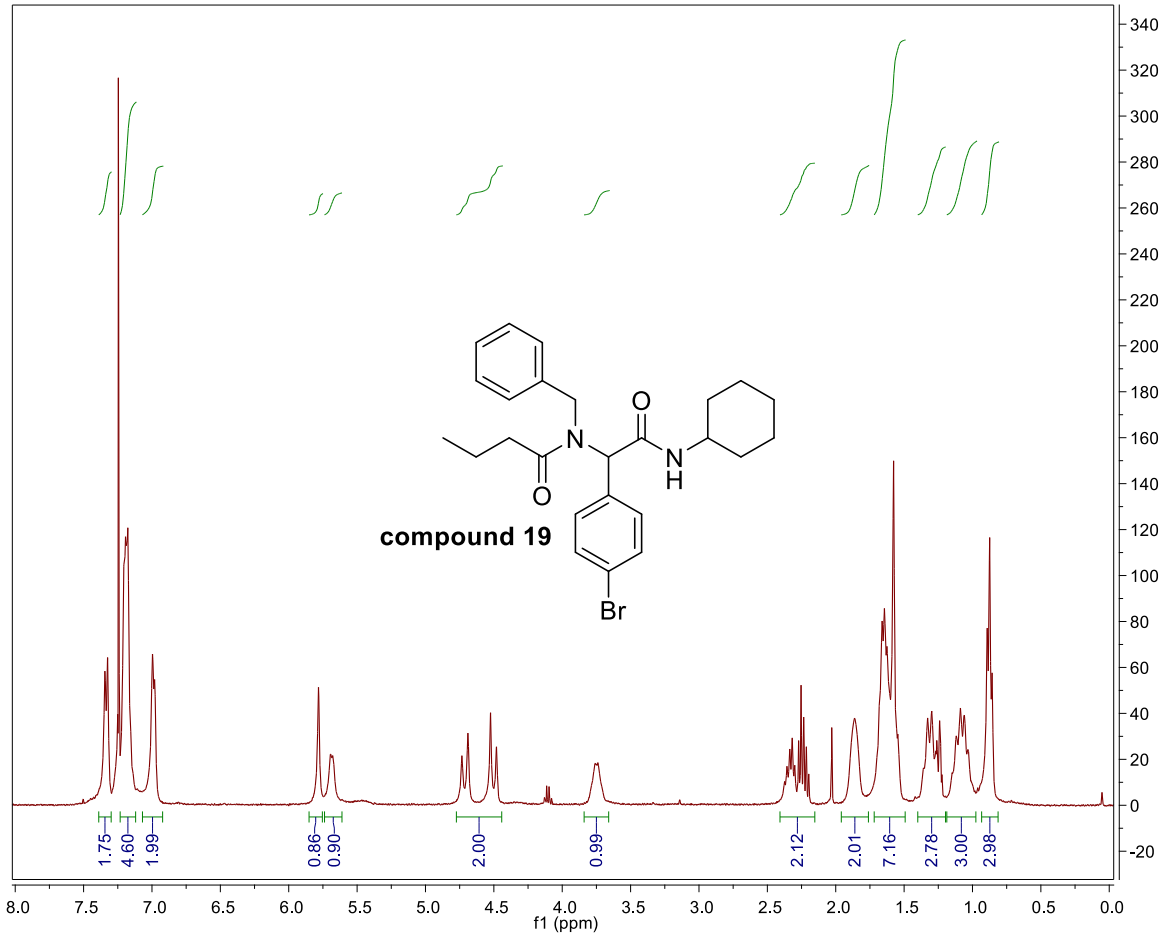

Compound 20. ^{1}H NMR (400 MHz, Chloroform-*d*) δ 7.33 (d, *J* = 8.1 Hz, 2H), 7.23 – 7.15 (m, 5H), 6.98 (d, *J* = 7.1 Hz, 2H), 5.79 (s, 1H), 5.74 – 5.66 (m, 1H), 4.71 (d, *J* = 17.6 Hz, 1H), 4.50 (d, *J* = 17.6 Hz, 1H), 3.94 – 3.52 (m, 1H), 2.34 (dt, *J* = 15.3, 7.6 Hz, 1H), 2.29 – 2.21 (m, 1H), 1.86 (s, 2H), 1.68 – 1.53 (m, 7H), 1.38 – 1.16 (m, 7H), 1.08 (q, *J* = 12.4 Hz, 3H), 0.83 (t, *J* = 6.7 Hz, 3H).

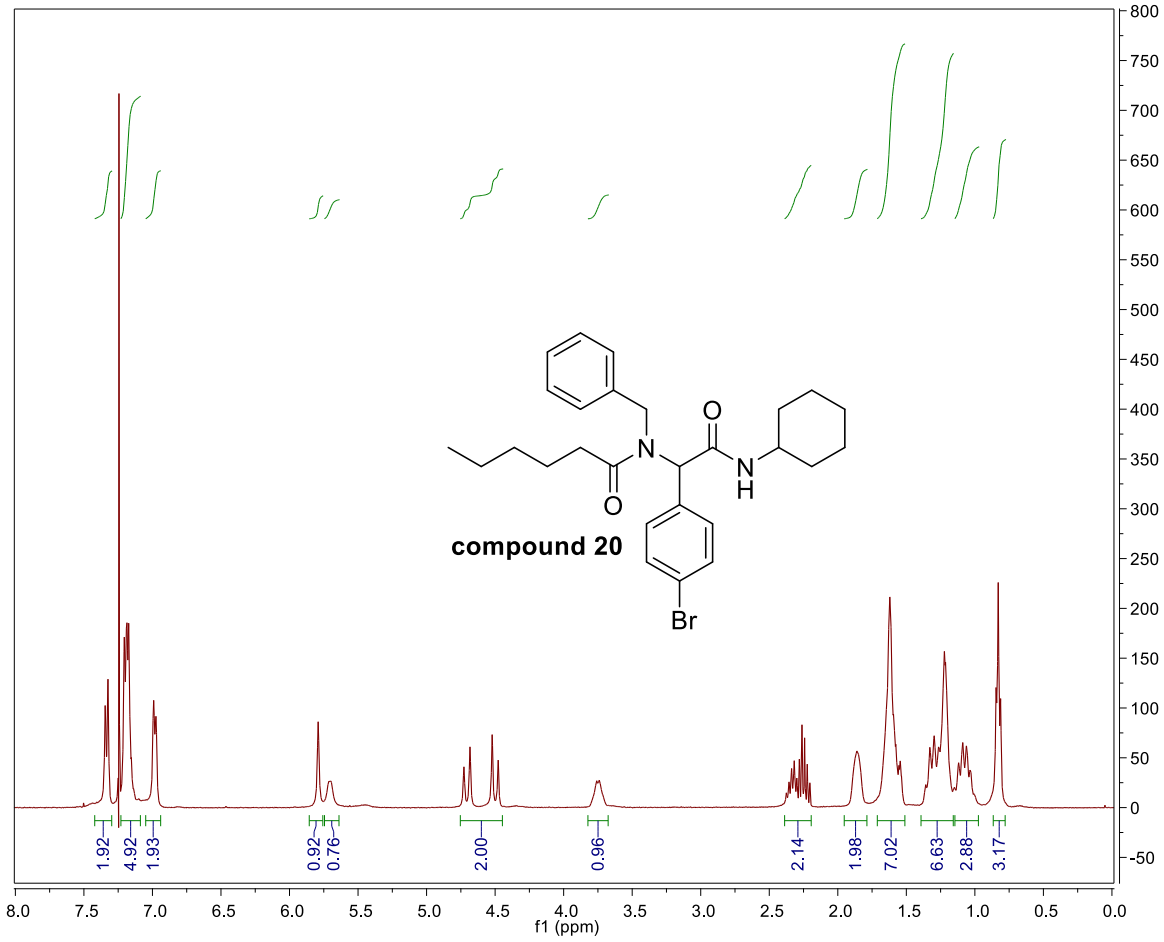

Compound 21. ^{1}H NMR (400 MHz, Chloroform-*d*) δ 7.45 (d, *J* = 8.0 Hz, 2H), 7.40 (d, *J* = 8.4 Hz, 2H), 7.32 (d, *J* = 8.4 Hz, 2H), 7.27 – 7.12 (m, 3H), 7.07 – 6.99 (m, 2H), 5.59 (s, 1H), 5.37 (s, 1H), 4.67 (d, *J* = 16.6 Hz, 1H), 4.41 (d, *J* = 16.9 Hz, 1H), 3.86 – 3.71 (m, 1H), 1.85 (dd, *J* = 26.1, 12.0 Hz, 2H), 1.72 (s, 1H), 1.68 – 1.50 (m, 3H), 1.41 – 1.17 (m, 3H), 1.17 – 0.77 (m, 4H).

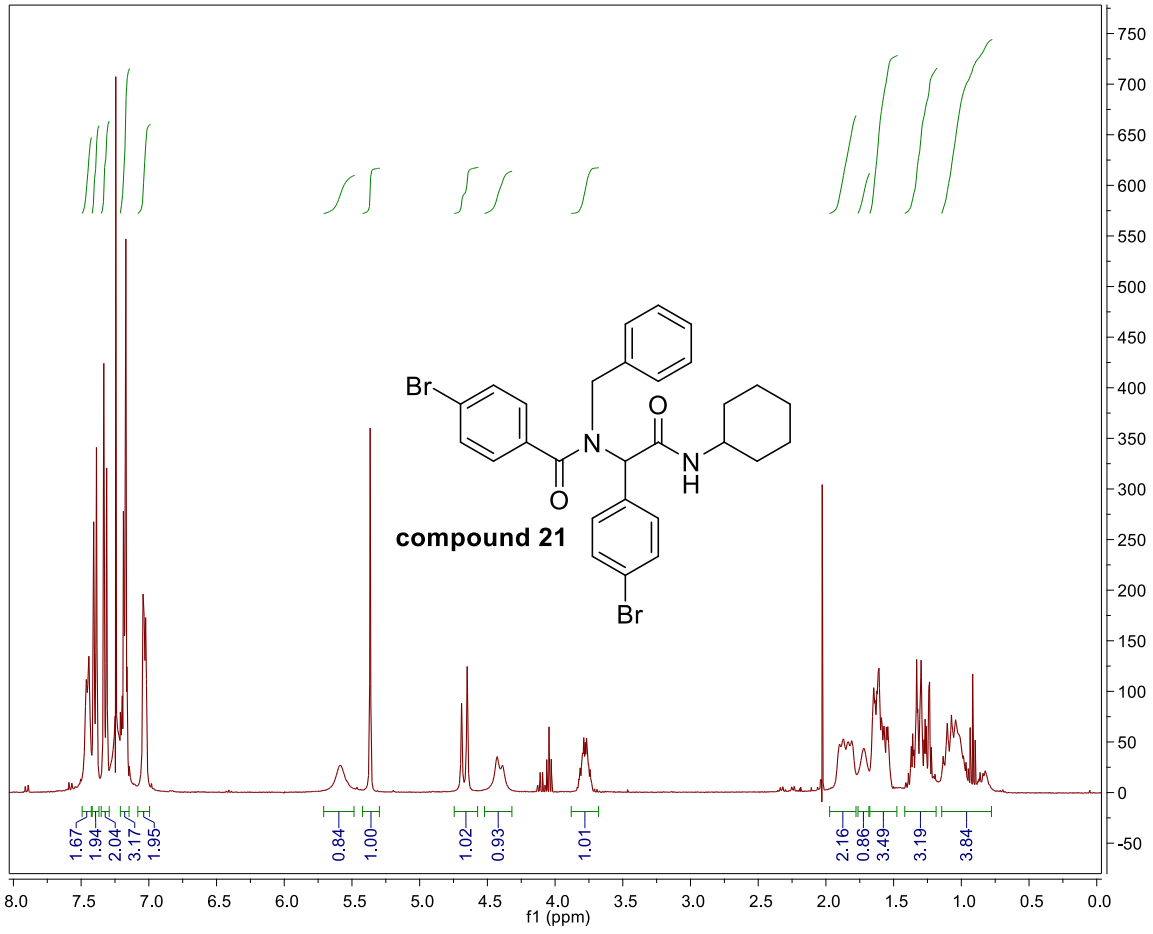

Compound 22. ^{1}H NMR (400 MHz, Chloroform-*d*) δ 7.35 (d, *J* = 8.1 Hz, 2H), 7.23 – 7.12 (m, 5H), 6.98 (d, *J* = 7.0 Hz, 2H), 5.82 (s, 1H), 5.65 (s, 1H), 4.71 (d, *J* = 17.7 Hz, 1H), 4.50 (d, *J* = 17.4 Hz, 1H), 3.75 (s, 1H), 3.31 (t, *J* = 6.3 Hz, 2H), 2.46 – 2.19 (m, 2H), 1.96 – 1.51 (m, 12H), 1.43 – 1.20 (m, 2H), 1.08 (q, *J* = 12.0 Hz, 3H), 0.81 (s, 1H).

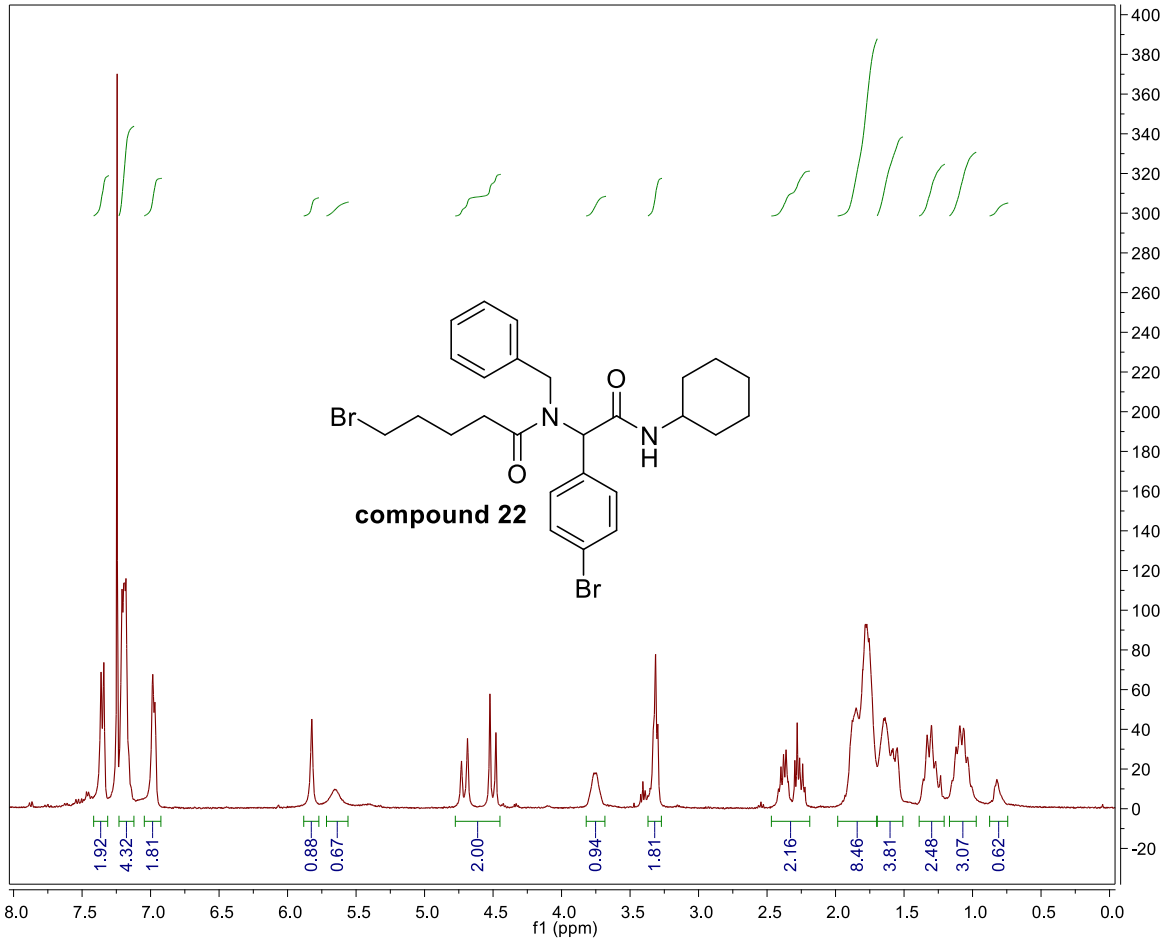

Compound 23. ^{1}H NMR (400 MHz, Chloroform-*d*) δ 7.34 (d, *J* = 8.2 Hz, 2H), 7.24 – 7.12 (m, 5H), 6.98 (d, *J* = 7.0 Hz, 2H), 5.84 (s, 1H), 5.80 (s, 1H), 4.70 (d, *J* = 17.6 Hz, 1H), 4.51 (d, *J* = 17.4 Hz, 1H), 3.22 (dp, *J* = 19.4, 6.6 Hz, 2H), 2.32 (ddt, *J* = 45.1, 15.4, 7.4 Hz, 2H), 2.11 (td, *J* = 7.1, 2.7 Hz, 2H), 1.89 (s, 1H), 1.72 (p, *J* = 7.9, 7.5 Hz, 2H), 1.56 – 1.36 (m, 4H), 1.26 (q, *J* = 7.5 Hz, 2H), 0.87 (t, *J* = 7.3 Hz, 3H).

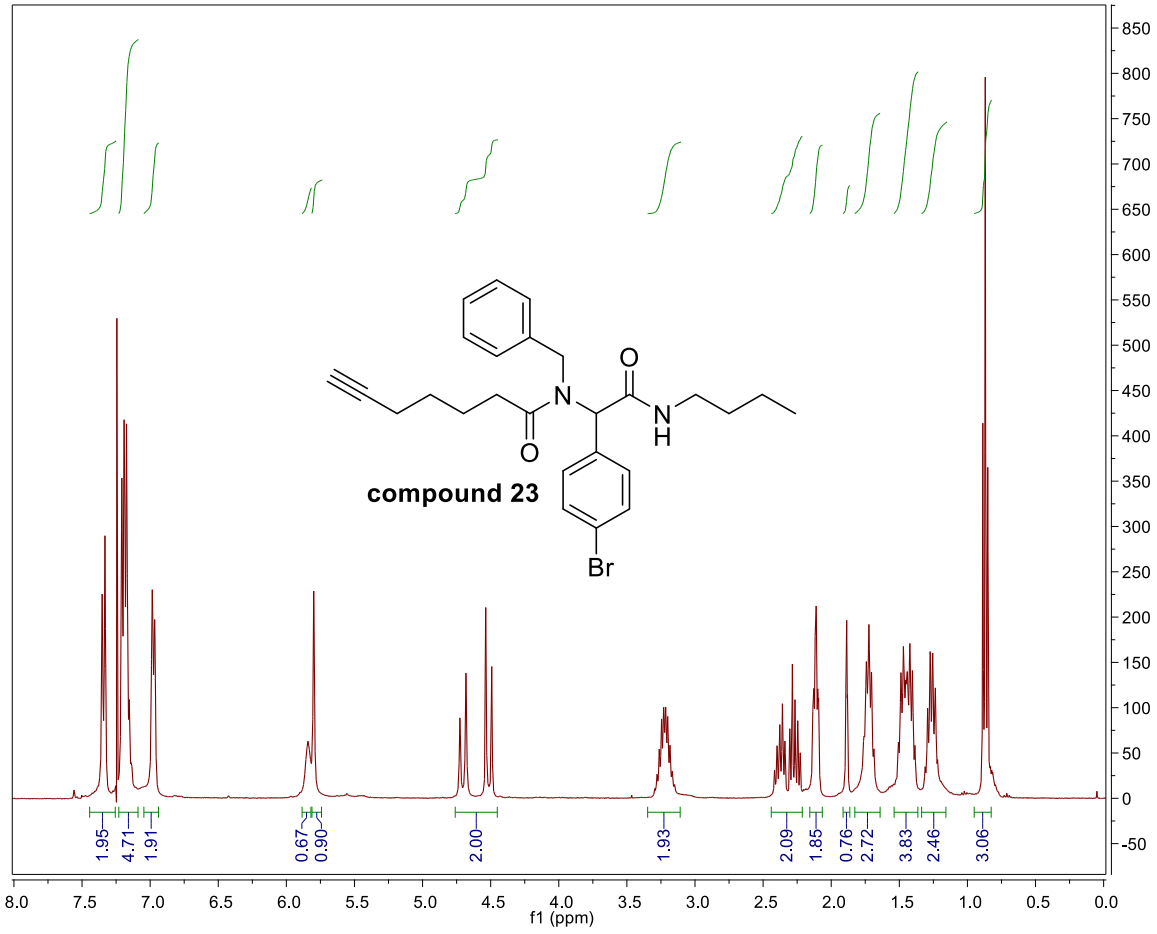

Compound 24. ^{1}H NMR (400 MHz, Chloroform-*d*) δ 7.34 (d, *J* = 8.2 Hz, 1H), 7.23 – 7.12 (m, 5H), 6.97 (d, *J* = 5.4 Hz, 2H), 5.88 (s, 1H), 5.80 (s, 1H), 5.68 (ddt, *J* = 16.9, 10.2, 6.7 Hz, 1H), 4.99 – 4.86 (m, 1H), 4.70 (d, *J* = 17.6 Hz, 1H), 4.51 (d, *J* = 17.4 Hz, 1H), 3.22 (qq, *J* = 13.3, 6.8 Hz, 2H), 2.30 (ddt, *J* = 42.9, 15.6, 7.5 Hz, 2H), 2.00 (q, *J* = 7.2 Hz, 2H), 1.80 – 1.62 (m, 2H), 1.41 (q, *J* = 7.4 Hz, 2H), 1.32 – 1.19 (m, 2H), 0.87 (t, *J* = 7.3 Hz, 3H).

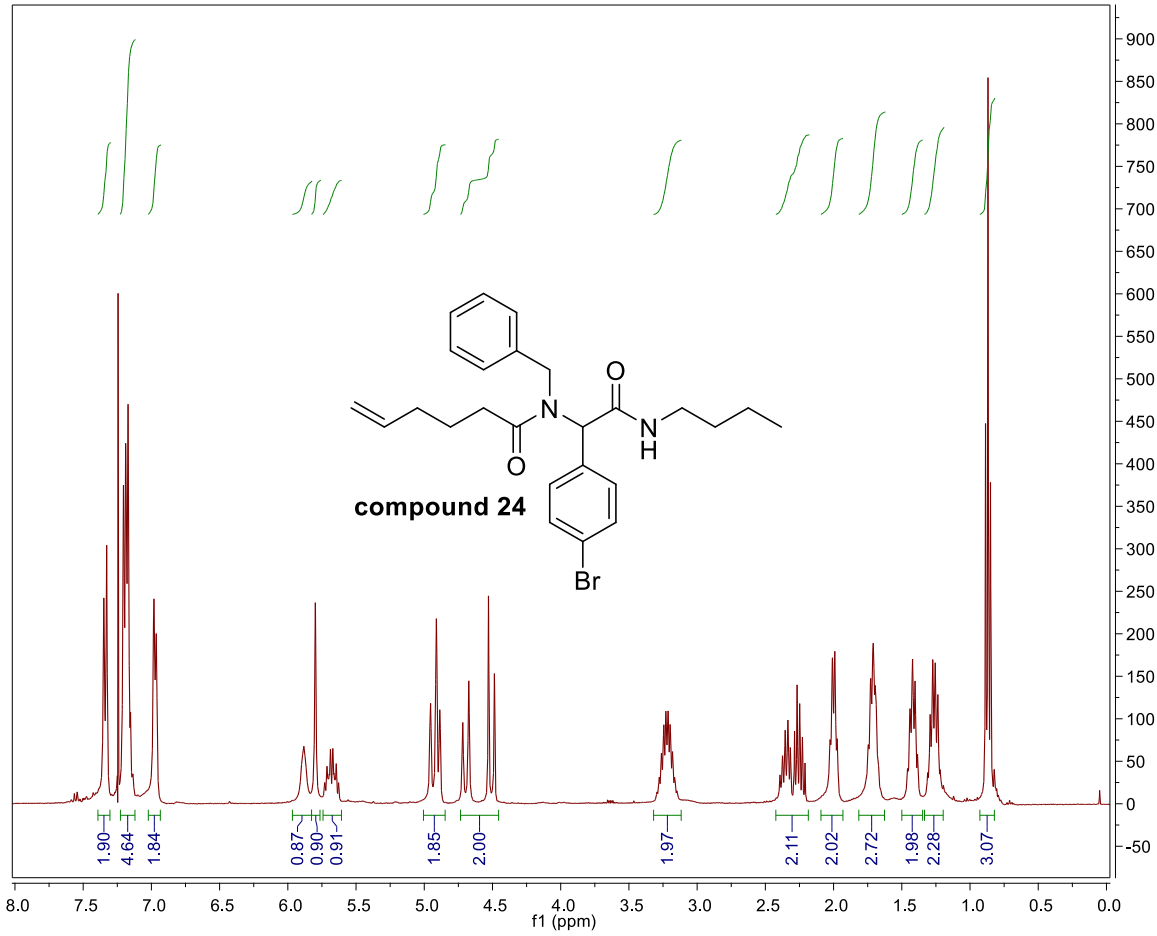

Compound 25. ^{1}H NMR (400 MHz, Chloroform-*d*) δ 7.45 (s, 1H), 7.32 (d, *J* = 8.0 Hz, 1H), 7.26 (d, *J* = 7.3 Hz, 1H), 7.23 – 7.10 (m, 3H), 7.07 (t, *J* = 7.9 Hz, 1H), 6.99 (d, *J* = 7.2 Hz, 2H), 5.95 (s, 1H), 5.85 (s, 1H), 4.73 (d, *J* = 17.6 Hz, 1H), 4.55 (d, *J* = 17.5 Hz, 1H), 3.23 (qq, *J* = 13.3, 6.7 Hz, 2H), 2.31 (ddq, *J* = 30.8, 15.4, 7.5 Hz, 2H), 1.62 (t, *J* = 7.4 Hz, 2H), 1.43 (p, *J* = 7.2 Hz, 2H), 1.35 – 1.15 (m, 6H), 0.95 – 0.75 (m, 6H).

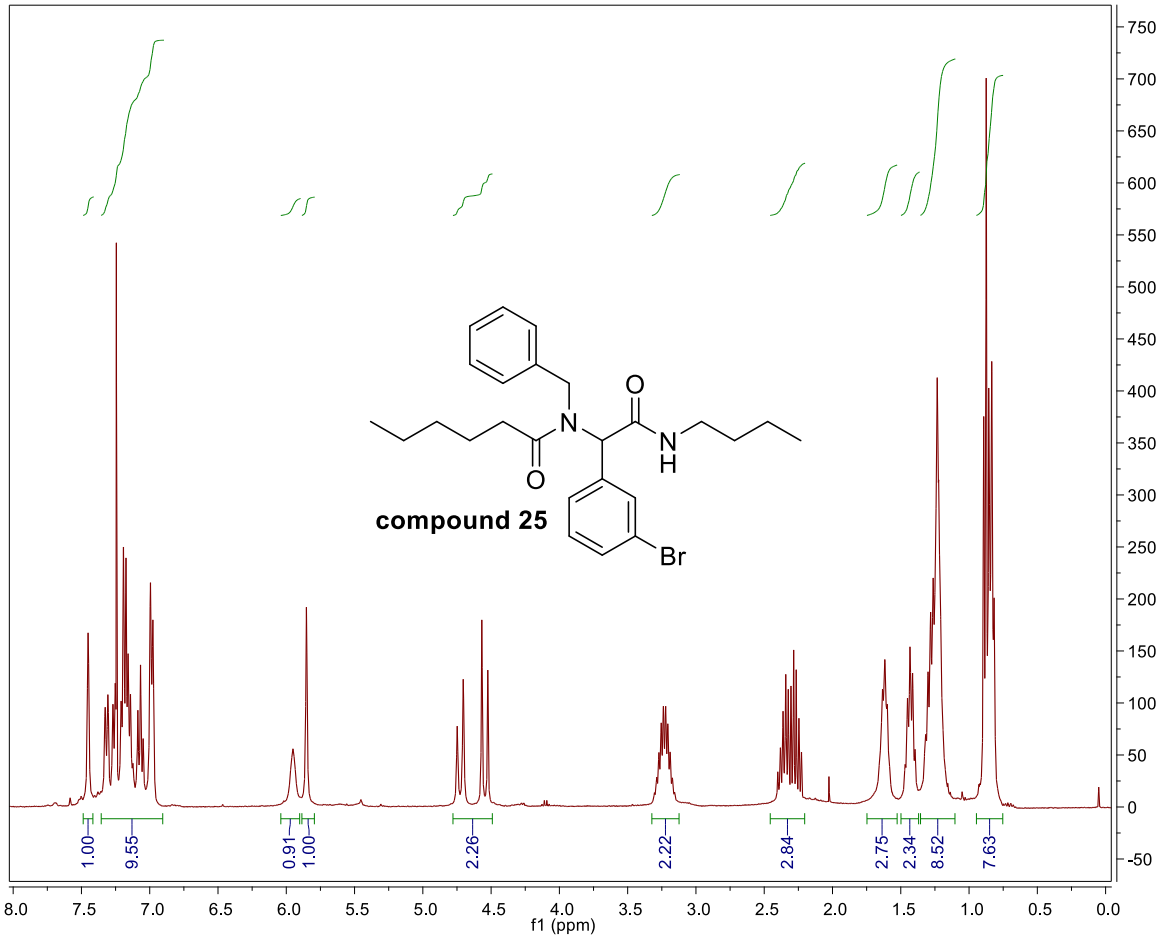

Compound 26. ^{1}H NMR (400 MHz, Chloroform-*d*) δ 7.44 (s, 1H), 7.31 (d, *J* = 8.0 Hz, 1H), 7.26 (d, *J* = 6.0 Hz, 1H), 7.23 – 7.10 (m, 4H), 7.06 (t, *J* = 7.9 Hz, 1H), 6.98 (d, *J* = 7.2 Hz, 2H), 6.02 (s, 1H), 5.87 (s, 1H), 4.74 (d, *J* = 17.6 Hz, 1H), 4.55 (d, *J* = 17.6 Hz, 1H), 3.22 (th, *J* = 13.3, 6.7 Hz, 2H), 2.30 (ddq, *J* = 30.3, 15.4, 7.7 Hz, 2H), 1.65 (h, *J* = 7.7, 7.3 Hz, 2H), 1.43 (p, *J* = 7.2 Hz, 2H), 1.34 – 1.18 (m, 3H), 0.95 (t, *J* = 7.4 Hz, 1H), 0.87 (t, *J* = 7.3 Hz, 6H).

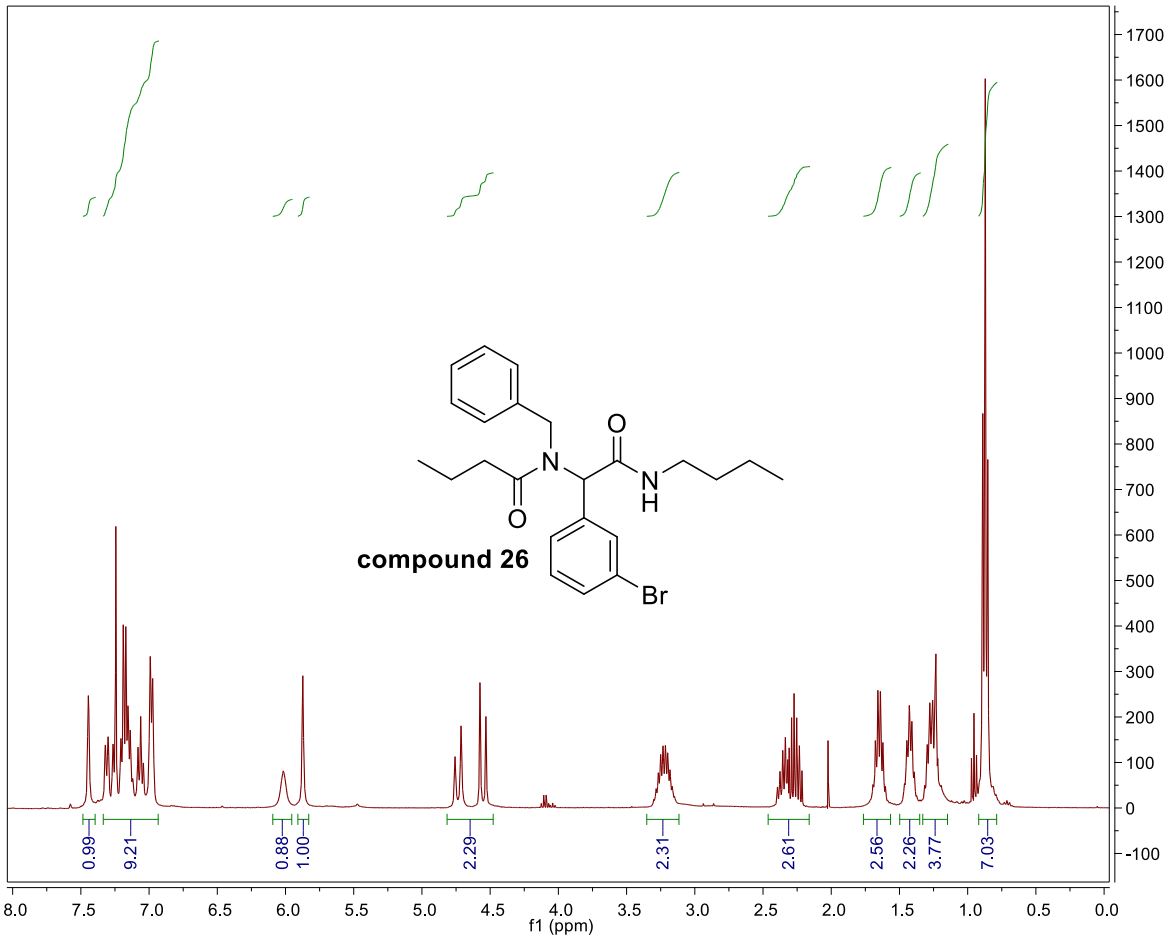

Compound 27. ^{1}H NMR (400 MHz, Chloroform-*d*) δ 7.45 (s, 1H), 7.33 (d, *J* = 8.0 Hz, 1H), 7.26 (d, *J* = 7.7 Hz, 1H), 7.23 – 7.12 (m, 3H), 7.08 (t, *J* = 7.9 Hz, 1H), 6.98 (d, *J* = 7.3 Hz, 2H), 5.85 (s, 1H), 4.72 (d, *J* = 17.7 Hz, 1H), 4.54 (d, *J* = 17.5 Hz, 1H), 3.34 (t, *J* = 6.8 Hz, 2H), 3.23 (tp, *J* = 13.3, 6.6 Hz, 2H), 2.44 – 2.22 (m, 2H), 1.78 (p, *J* = 6.9 Hz, 2H), 1.64 (p, *J* = 7.2 Hz, 2H), 1.40 (dp, *J* = 23.2, 7.4 Hz, 4H), 1.31 – 1.18 (m, 3H), 0.87 (t, *J* = 7.3 Hz, 3H).

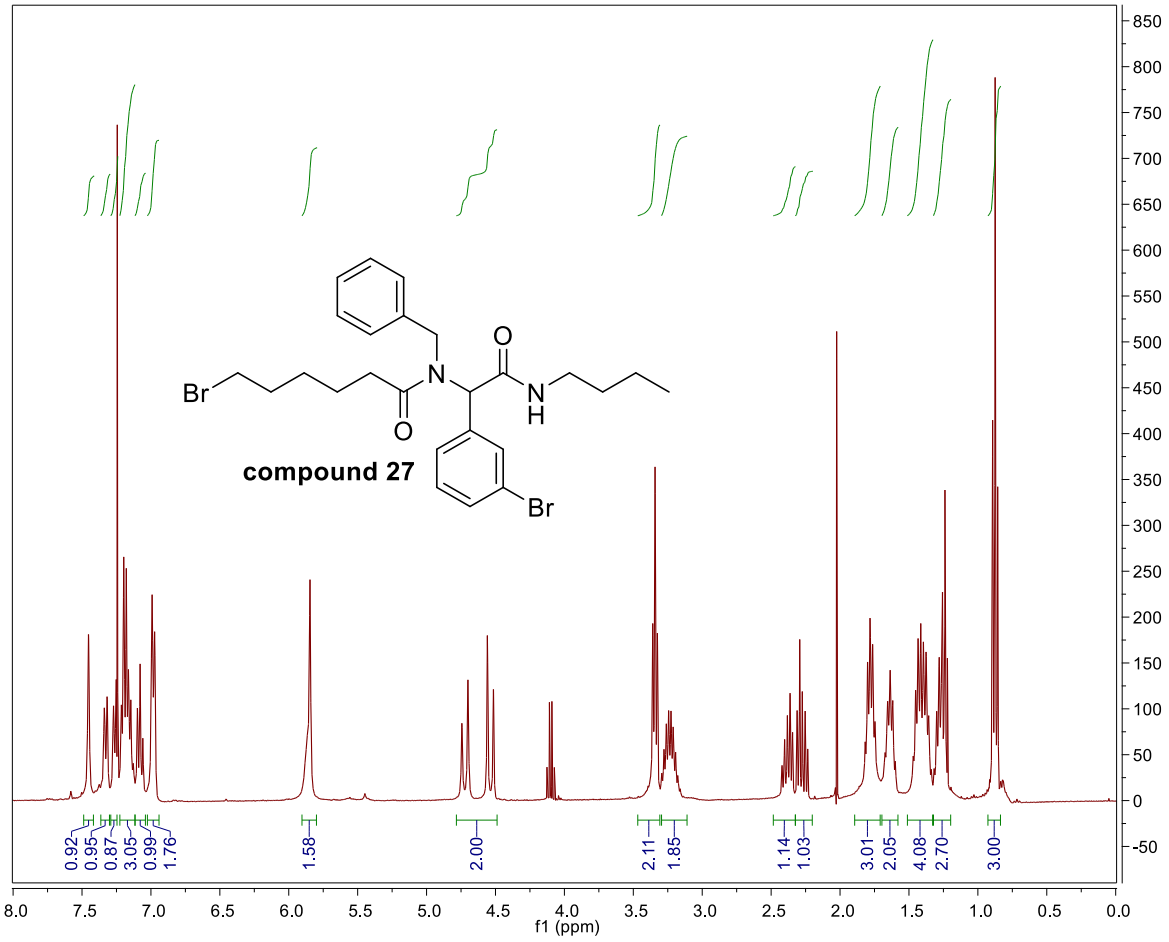

Compound 28. ^{1}H NMR (400 MHz, Chloroform-*d*) δ 7.44 (s, 1H), 7.31 (d, *J* = 8.3 Hz, 1H), 7.25 (d, *J* = 7.3 Hz, 1H), 7.22 – 7.10 (m, 3H), 7.06 (t, *J* = 7.9 Hz, 1H), 6.99 (d, *J* = 7.4 Hz, 2H), 5.83 (s, 1H), 4.73 (d, *J* = 17.7 Hz, 1H), 4.52 (d, *J* = 17.6 Hz, 1H), 3.23 (qq, *J* = 13.3, 6.8 Hz, 2H), 2.86 – 2.72 (m, 2H), 2.71 – 2.64 (m, 1H), 2.63 – 2.51 (m, 1H), 1.76 – 1.59 (m, 2H), 1.42 (p, *J* = 7.2 Hz, 1H), 1.31 – 1.15 (m, 2H), 0.86 (t, *J* = 7.3 Hz, 3H).

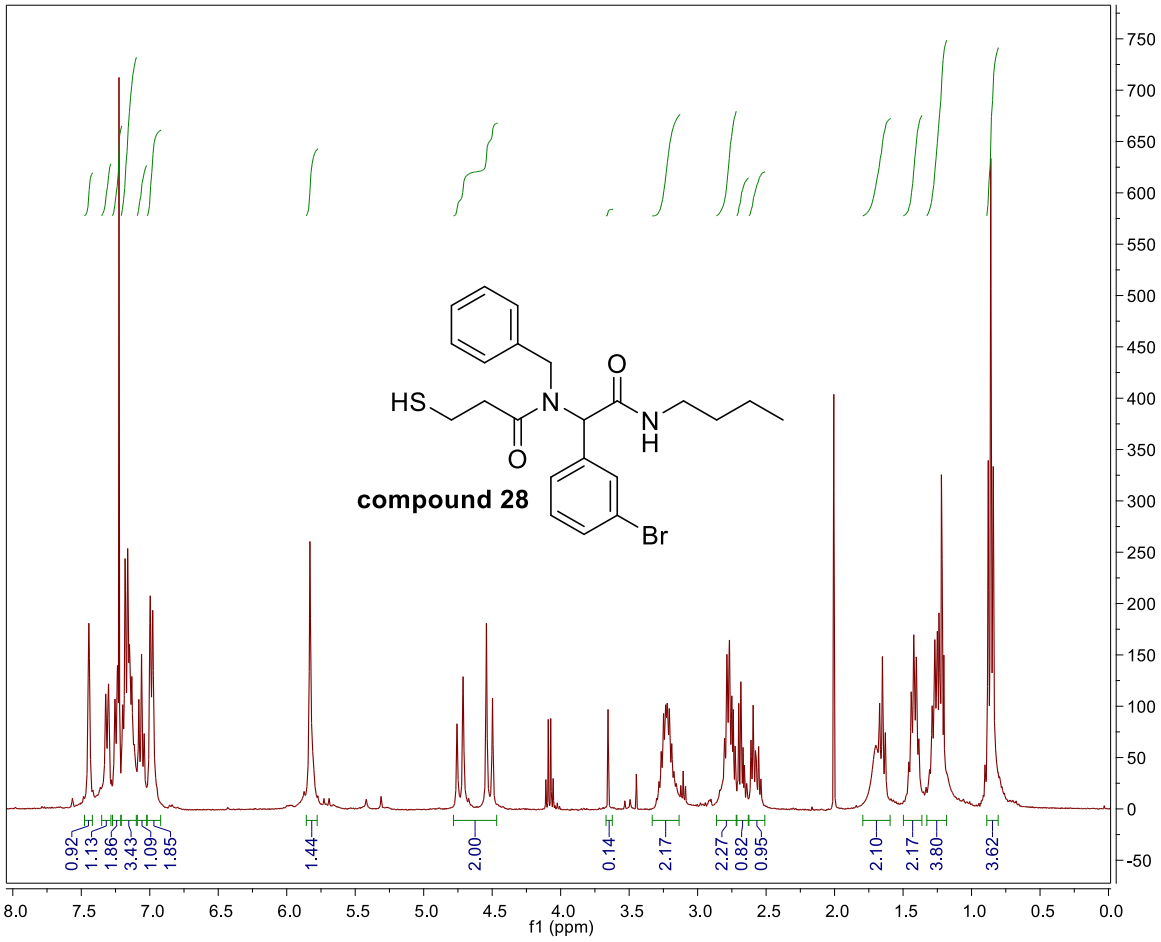

Compound 29. ^{1}H NMR (400 MHz, Chloroform-*d*) δ 7.34 – 7.26 (m, 2H), 7.21 – 7.08 (m, 3H), 6.94 (d, *J* = 7.1 Hz, 2H), 6.88 (t, *J* = 8.5 Hz, 2H), 6.02 (s, 1H), 5.92 (s, 1H), 4.71 (d, *J* = 17.8 Hz, 1H), 4.55 (d, *J* = 17.7 Hz, 1H), 3.22 (dp, *J* = 19.3, 6.7 Hz, 2H), 2.32 (t, *J* = 7.5 Hz, 2H), 2.23 (dt, *J* = 15.5, 7.6 Hz, 1H), 1.68 – 1.54 (m, 4H), 1.42 (p, *J* = 7.3 Hz, 2H), 1.34 – 1.15 (m, 12H), 0.91 – 0.78 (m, 9H).

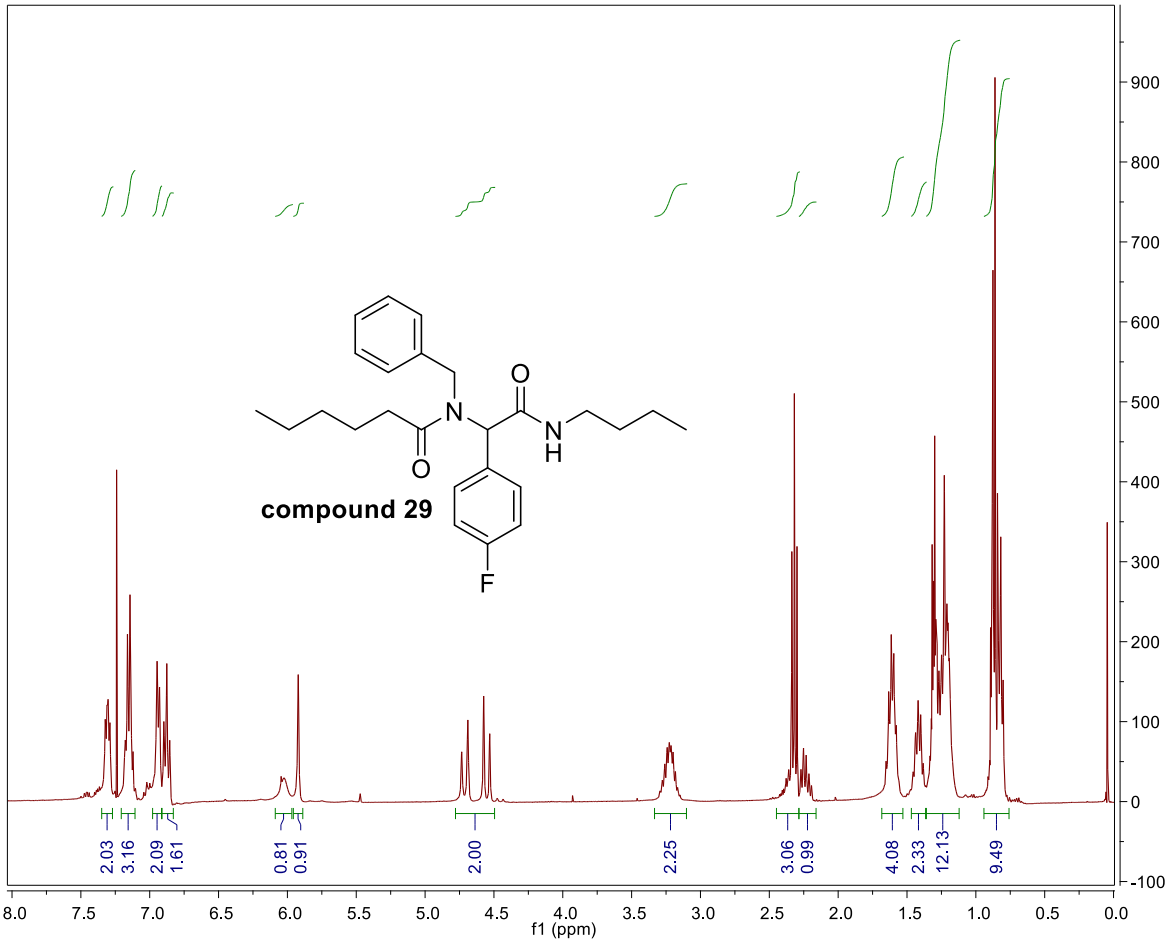

Compound 30. ^{1}H NMR (500 MHz, Chloroform-*d*) δ 7.33 (dd, *J* = 8.4, 5.3 Hz, 2H), 7.22 – 7.13 (m, 3H), 6.98 (d, *J* = 7.4 Hz, 2H), 6.91 (t, *J* = 8.4 Hz, 2H), 5.88 (s, 1H), 4.74 (d, *J* = 17.6 Hz, 1H), 4.56 (d, *J* = 17.5 Hz, 1H), 3.34 – 3.17 (m, 2H), 2.44 – 2.19 (m, 2H), 1.85 (s, 1H), 1.74 – 1.61 (m, 2H), 1.45 (p, *J* = 7.0 Hz, 2H), 1.35 – 1.22 (m, 2H), 0.89 (t, *J* = 7.3 Hz, 6H).

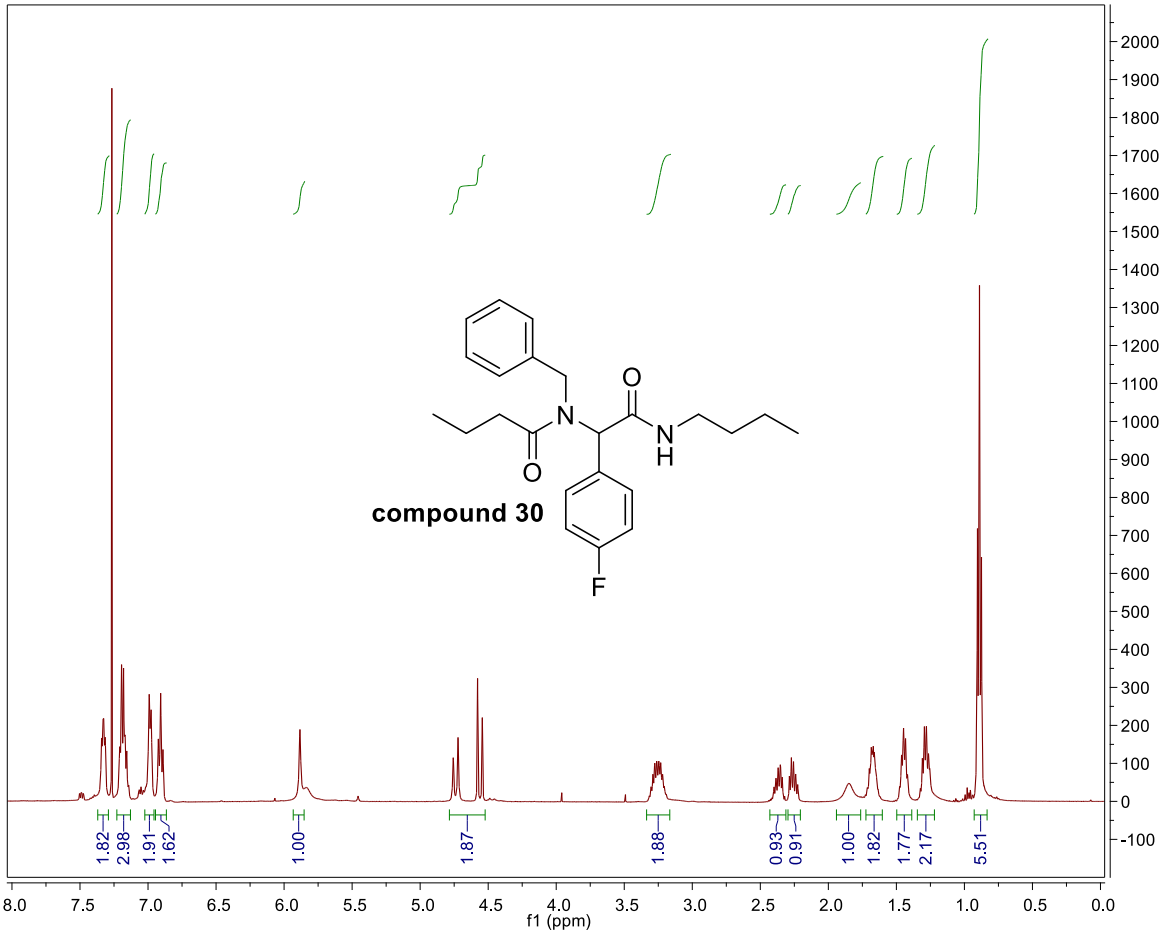

Compound 31. ^{1}H NMR (400 MHz, Chloroform-*d*) δ 7.31 (dd, *J* = 8.5, 5.3 Hz, 2H), 7.21 – 7.10 (m, 3H), 6.95 (d, *J* = 7.3 Hz, 2H), 6.89 (t, *J* = 8.5 Hz, 2H), 5.87 (s, 1H), 5.80 (s, 1H), 4.70 (d, *J* = 17.8 Hz, 1H), 4.53 (d, *J* = 17.5 Hz, 1H), 3.34 (t, *J* = 6.8 Hz, 2H), 3.22 (tp, *J* = 13.1, 6.4 Hz, 2H), 2.45 – 2.19 (m, 2H), 1.82 – 1.71 (m, 2H), 1.70 – 1.56 (m, 2H), 1.52 – 1.32 (m, 4H), 1.31 – 1.18 (m, 2H), 0.86 (t, *J* = 7.3 Hz, 3H).

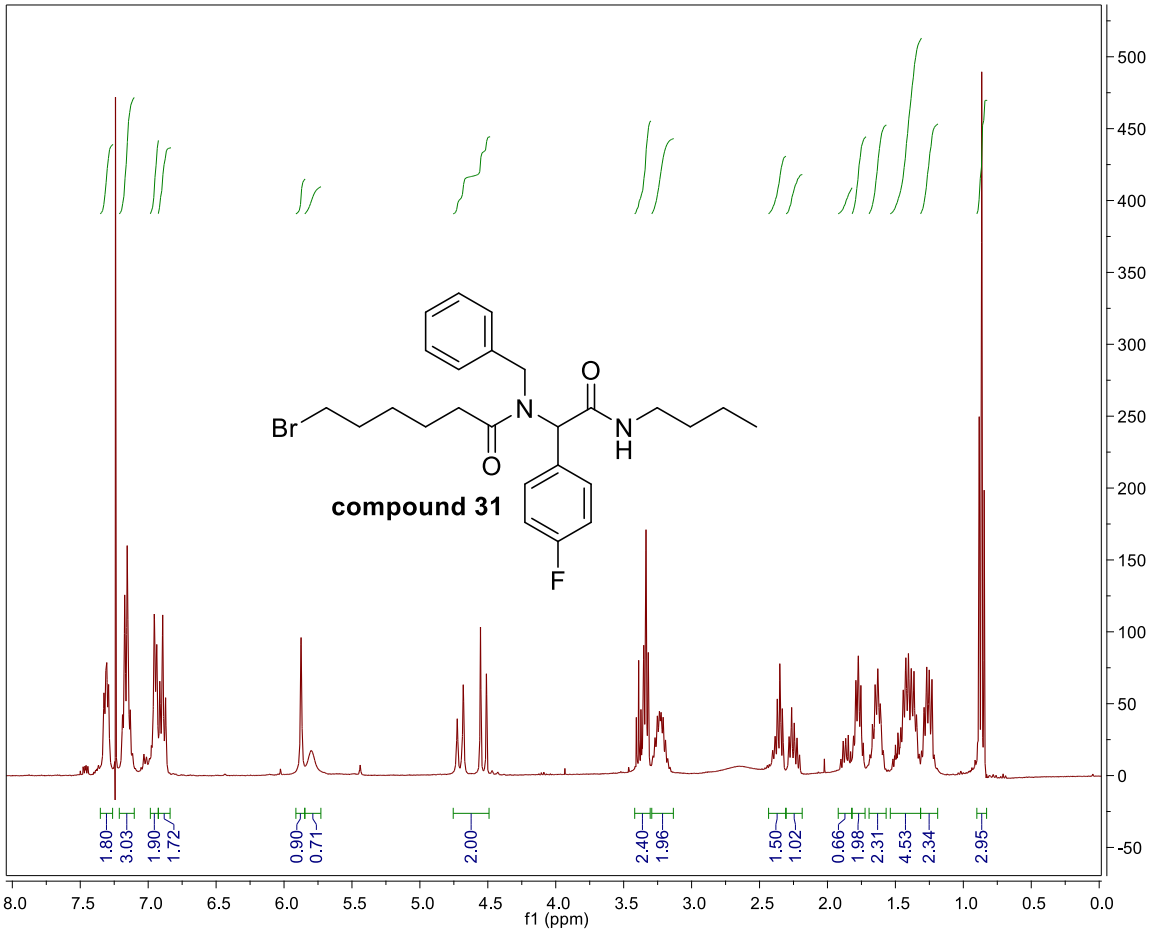

Compound 32. ^{1}H NMR (500 MHz, Chloroform-*d*) δ 7.38 – 7.30 (m, 2H), 7.23 – 7.13 (m, 3H), 7.00 (d, *J* = 7.4 Hz, 2H), 6.92 (t, *J* = 8.6 Hz, 2H), 5.90 (s, 1H), 5.78 (s, 1H), 4.76 (d, *J* = 17.8 Hz, 1H), 4.55 (d, *J* = 17.8 Hz, 1H), 3.27 (qq, *J* = 13.4, 6.8 Hz, 2H), 2.82 (p, *J* = 7.5, 7.1 Hz, 2H), 2.73 (dt, *J* = 16.3, 6.3 Hz, 1H), 2.63 – 2.55 (m, 1H), 1.69 (t, *J* = 8.1 Hz, 2H), 1.46 (p, *J* = 7.2 Hz, 2H), 1.34 – 1.23 (m, 2H), 0.90 (t, *J* = 7.3 Hz, 3H).

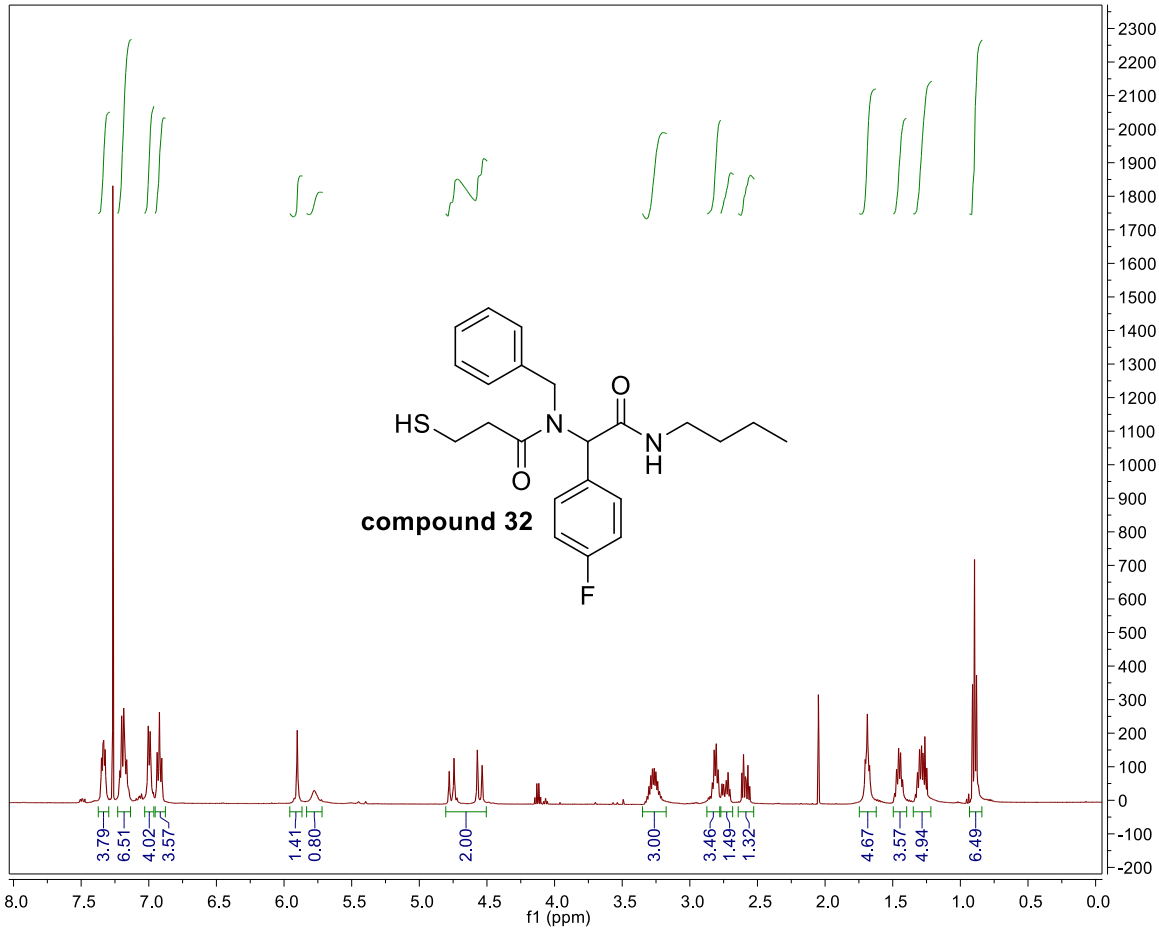

Compound 33. ^{1}H NMR (500 MHz, Chloroform-*d*) δ 7.24 – 7.14 (m, 5H), 7.14 – 7.06 (m, 2H), 7.02 (d, *J* = 7.5 Hz, 2H), 6.93 (t, *J* = 8.3 Hz, 1H), 5.97 (s, 1H), 5.88 (s, 1H), 4.75 (d, *J* = 17.6 Hz, 1H), 4.59 (d, *J* = 17.4 Hz, 1H), 3.34 – 3.17 (m, 2H), 2.43 – 2.22 (m, 3H), 1.70 – 1.59 (m, 2H), 1.53 – 1.41 (m, 2H), 1.36 – 1.17 (m, 7H), 0.87 (dt, *J* = 19.7, 7.2 Hz, 6H).

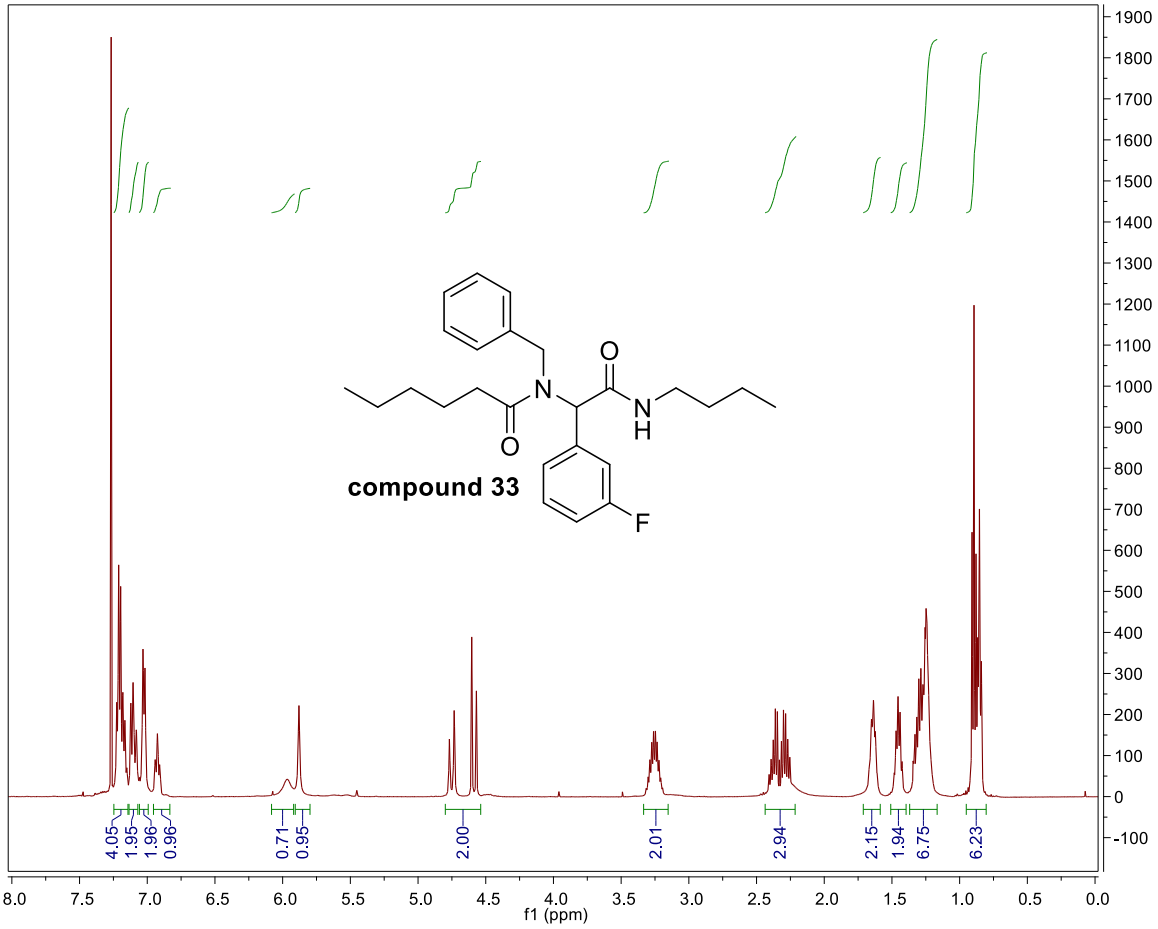

Compound 34. ^{1}H NMR (500 MHz, Chloroform-*d*) δ 7.25 – 7.14 (m, 4H), 7.13 – 7.06 (m, 2H), 7.03 (d, *J* = 7.4 Hz, 2H), 6.92 (t, *J* = 7.6 Hz, 1H), 5.91 (s, 1H), 5.86 (s, 1H), 4.76 (d, *J* = 17.7 Hz, 1H), 4.58 (d, *J* = 17.4 Hz, 1H), 3.39 – 3.16 (m, 2H), 2.45 – 2.20 (m, 2H), 1.79 (s, 1H), 1.68 (dq, *J* = 15.8, 8.0 Hz, 2H), 1.45 (p, *J* = 7.4 Hz, 2H), 1.29 (h, *J* = 7.4 Hz, 2H), 0.90 (td, *J* = 7.4, 3.9 Hz, 6H).

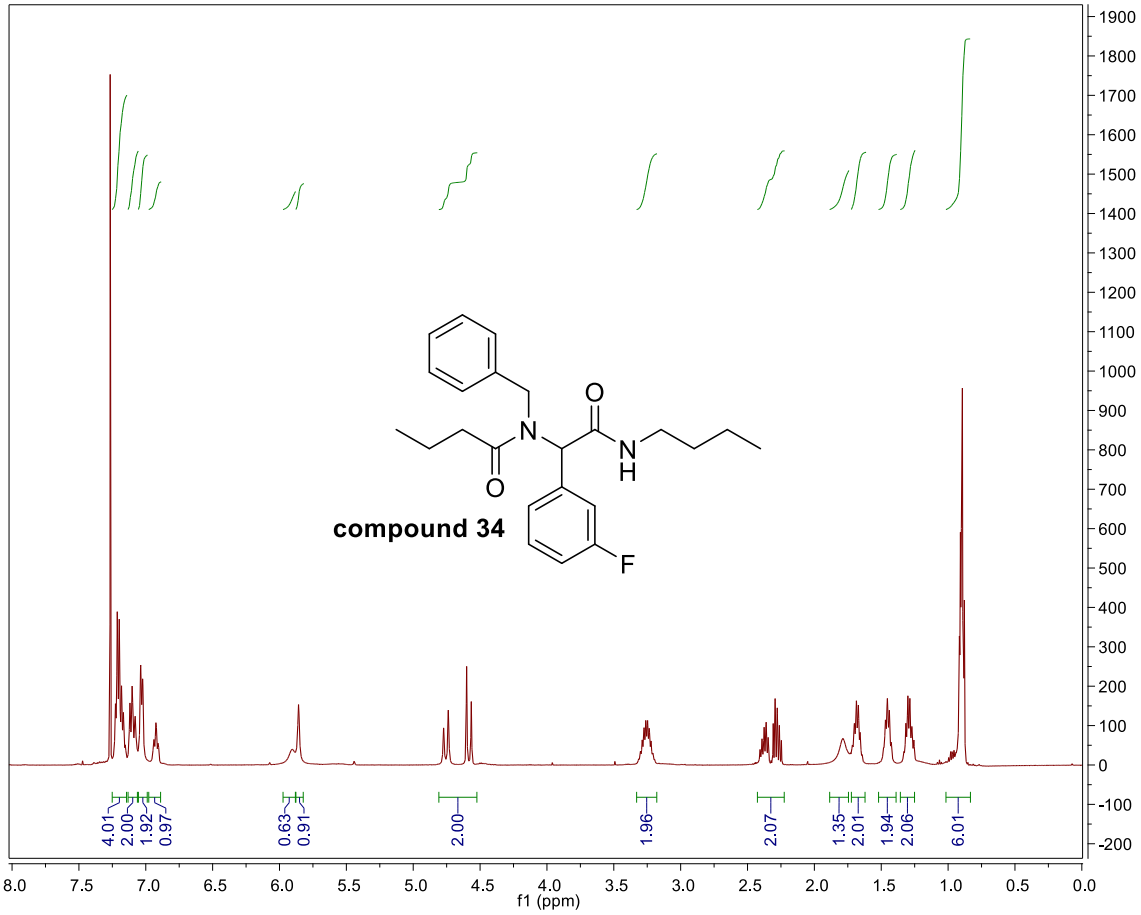

Compound 35. ^{1}H NMR (400 MHz, Chloroform-*d*) δ 7.24 – 7.13 (m, 4H), 7.08 (t, *J* = 9.3 Hz, 2H), 7.00 (d, *J* = 7.3 Hz, 2H), 6.91 (t, *J* = 8.6 Hz, 1H), 5.84 (s, 1H), 4.72 (d, *J* = 17.6 Hz, 1H), 4.55 (d, *J* = 17.3 Hz, 1H), 3.34 (t, *J* = 6.0 Hz, 2H), 3.25 (td, *J* = 14.5, 13.9, 6.6 Hz, 2H), 2.44 – 2.22 (m, 2H), 1.78 (p, *J* = 7.1 Hz, 2H), 1.74 – 1.58 (m, 4H), 1.40 (dp, *J* = 23.6, 7.7, 7.3 Hz, 4H), 1.28 (p, *J* = 8.3, 7.8 Hz, 2H), 0.87 (t, *J* = 7.3 Hz, 3H).

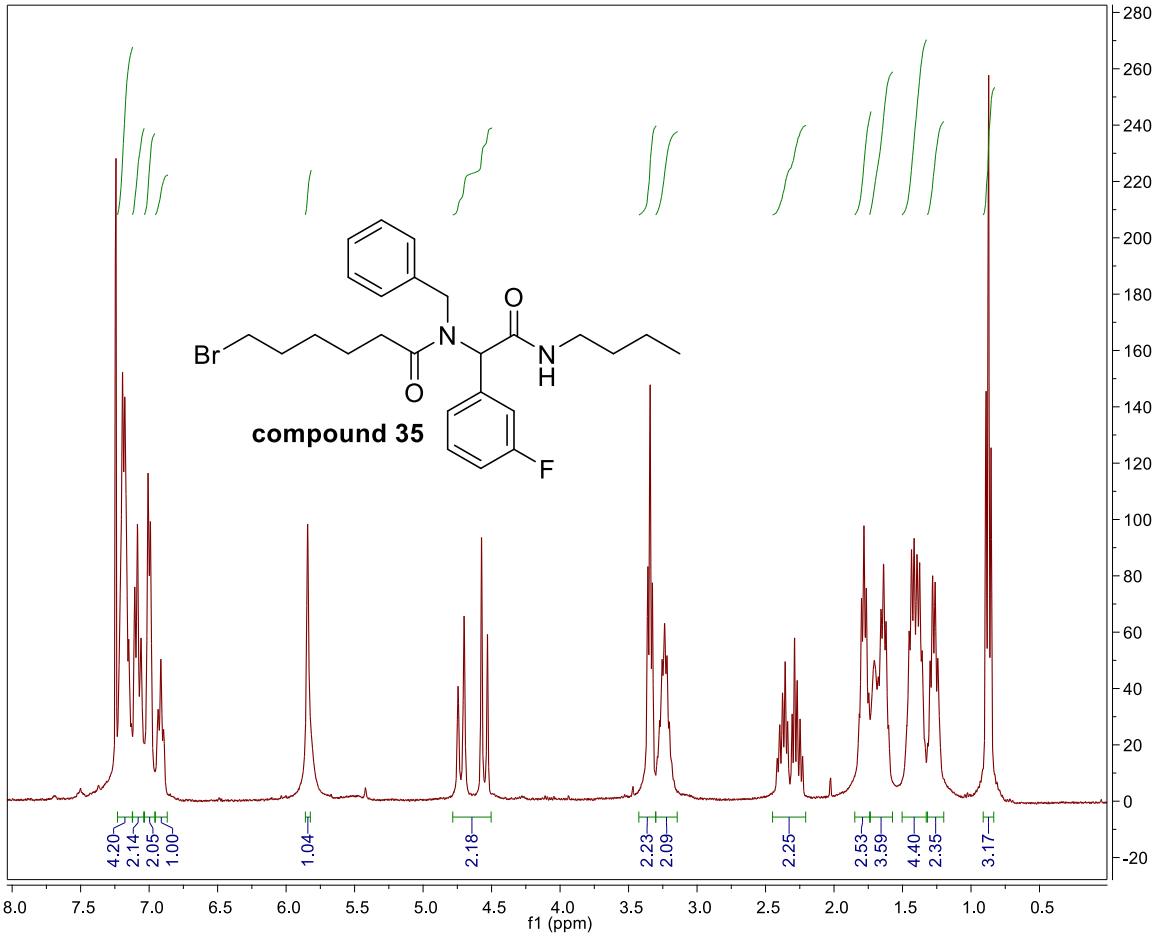

Compound 36. ^{1}H NMR (400 MHz, Chloroform-*d*) δ 7.23 – 7.12 (m, 4H), 7.09 (t, *J* = 9.2 Hz, 2H), 7.02 (d, *J* = 7.6 Hz, 2H), 6.92 (t, *J* = 8.4 Hz, 1H), 5.86 (s, 1H), 4.75 (d, *J* = 17.7 Hz, 1H), 4.55 (d, *J* = 17.6 Hz, 1H), 3.25 (p, *J* = 7.1 Hz, 2H), 2.78 (p, *J* = 7.2 Hz, 2H), 2.73 – 2.67 (m, 1H), 2.64 – 2.52 (m, 1H), 1.67 (s, 2H), 1.43 (q, *J* = 7.4 Hz, 2H), 1.35 – 1.19 (m, 2H), 0.88 (t, *J* = 6.4 Hz, 3H).

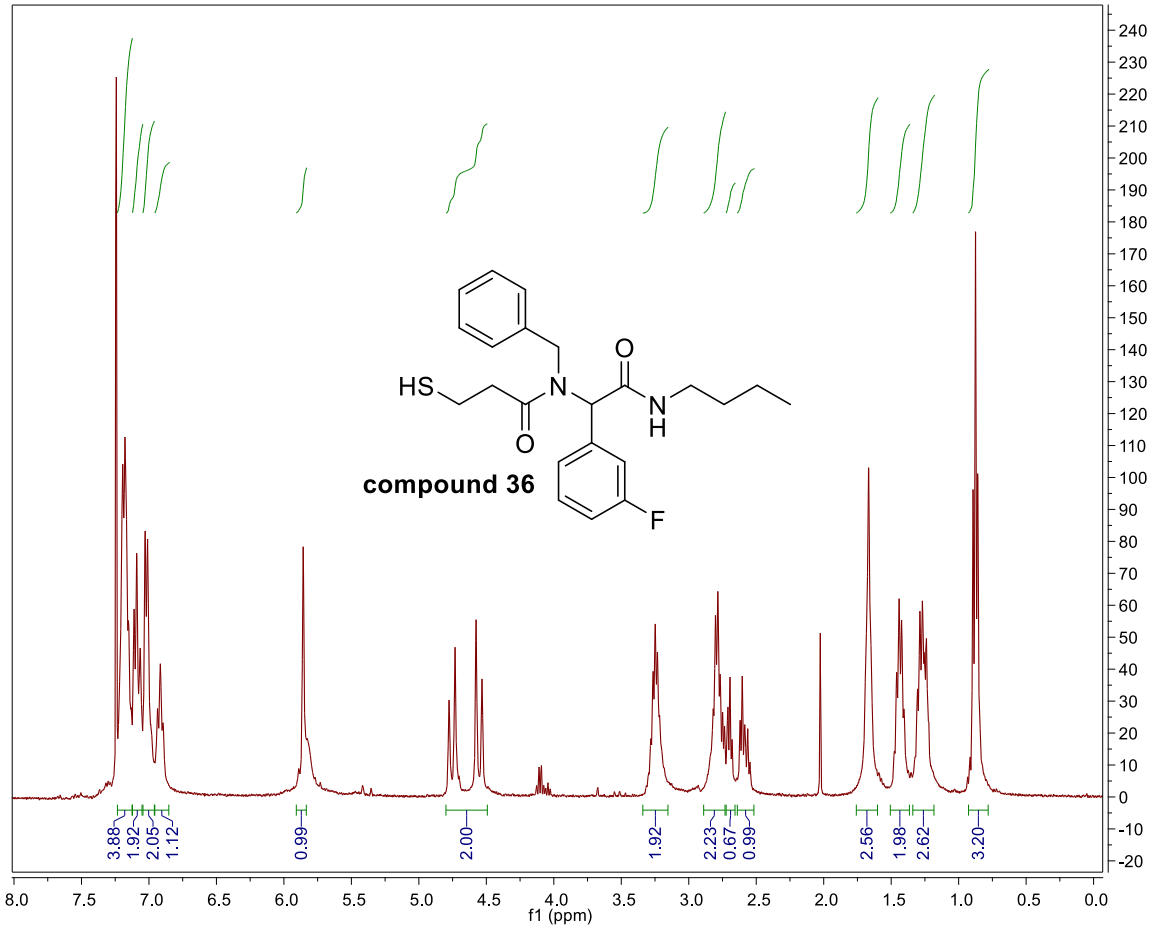

Compound 37. ^{1}H NMR (500 MHz, Chloroform-*d*) δ 7.31 (d, *J* = 8.2 Hz, 2H), 7.27 – 7.18 (m, 5H), 7.03 (d, *J* = 7.2 Hz, 2H), 5.89 (s, 1H), 5.86 (s, 1H), 4.76 (d, *J* = 17.6 Hz, 1H), 4.57 (d, *J* = 17.4 Hz, 1H), 3.28 (dhept, *J* = 20.1, 6.8 Hz, 2H), 2.47 – 2.25 (m, 2H), 1.66 (q, *J* = 5.8, 5.3 Hz, 2H), 1.48 (p, *J* = 7.4 Hz, 2H), 1.40 – 1.17 (m, 6H), 0.90 (dt, *J* = 19.3, 7.2 Hz, 6H).

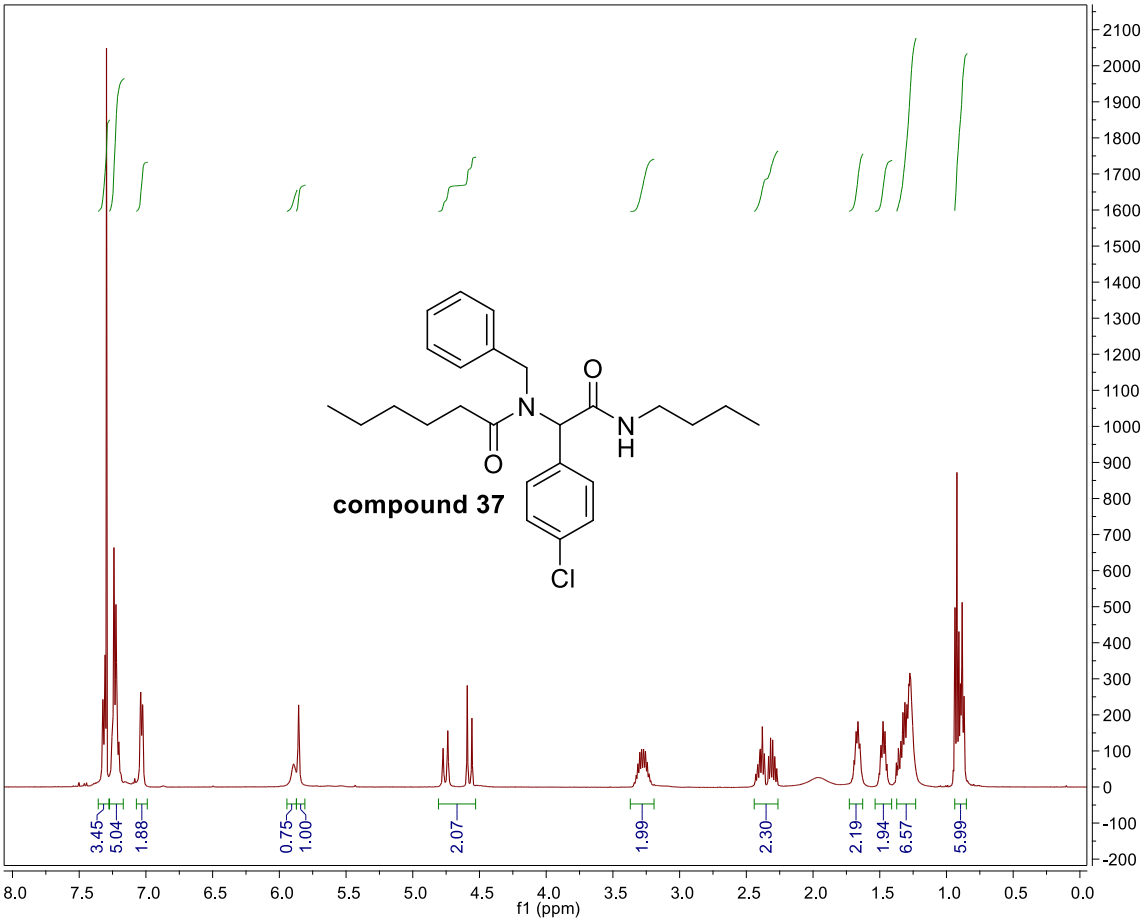

Compound 38. ^{1}H NMR (400 MHz, Chloroform-*d*) δ 7.26 (d, *J* = 6.8 Hz, 2H), 7.22 – 7.12 (m, 5H), 6.98 (d, *J* = 7.0 Hz, 2H), 5.89 (s, 1H), 5.82 (s, 1H), 4.71 (d, *J* = 17.7 Hz, 1H), 4.53 (d, *J* = 17.3 Hz, 1H), 3.22 (tq, *J* = 13.3, 6.7 Hz, 2H), 2.45 – 2.18 (m, 2H), 1.65 (h, *J* = 7.7 Hz, 2H), 1.42 (p, *J* = 7.3 Hz, 2H), 1.27 (h, *J* = 7.3 Hz, 2H), 0.87 (t, *J* = 7.3 Hz, 6H).

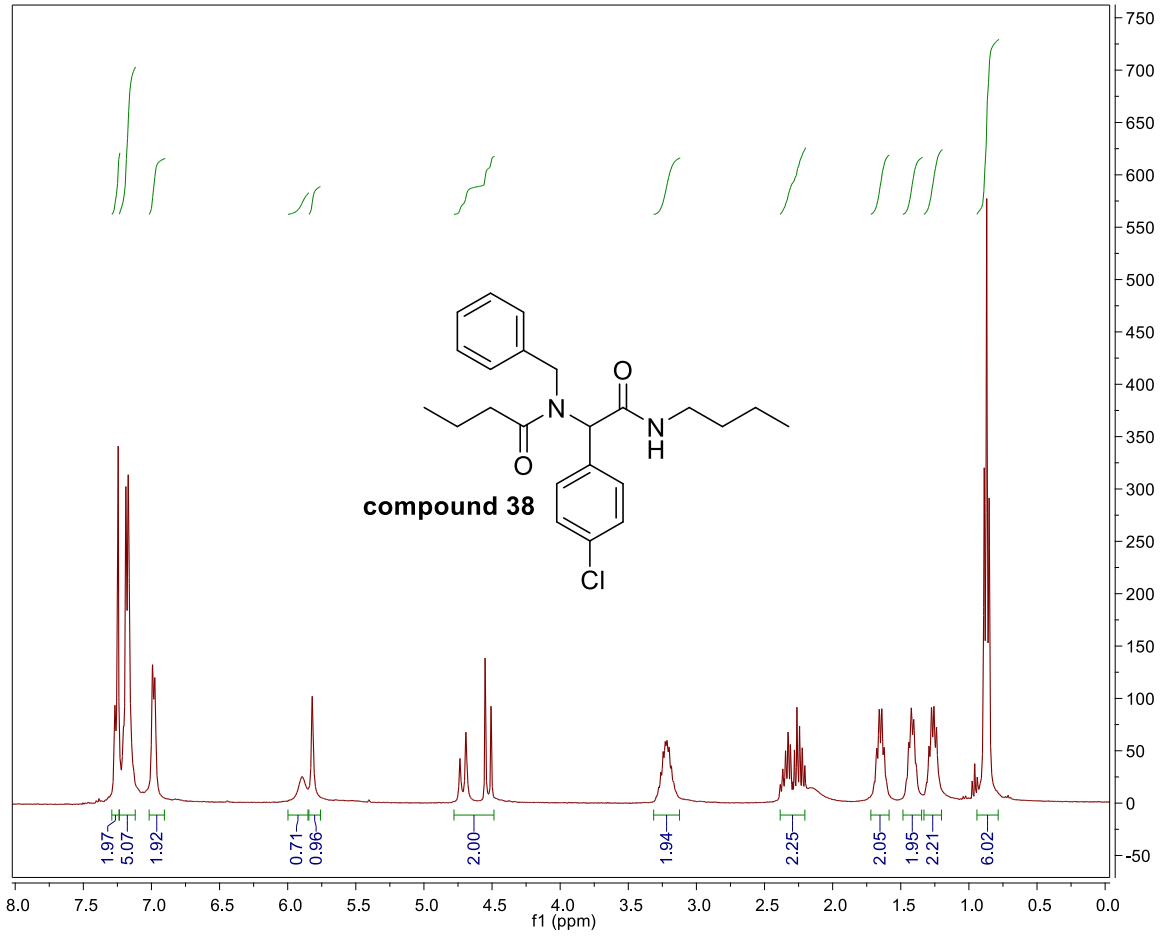

Compound 39. ^{1}H NMR (400 MHz, Chloroform-*d*) δ 7.26 (d, *J* = 8.1 Hz, 2H), 7.22 – 7.12 (m, 5H), 6.97 (d, *J* = 7.1 Hz, 2H), 5.82 (s, 1H), 4.70 (d, *J* = 17.7 Hz, 1H), 4.52 (d, *J* = 17.4 Hz, 1H), 3.33 (t, *J* = 6.8 Hz, 2H), 3.29 – 3.15 (m, 2H), 2.47 – 2.18 (m, 2H), 1.77 (p, *J* = 7.0 Hz, 2H), 1.62 (p, *J* = 7.7 Hz, 2H), 1.39 (dp, *J* = 23.1, 7.6 Hz, 4H), 1.26 (q, *J* = 7.6 Hz, 2H), 0.87 (t, *J* = 7.3 Hz, 3H).

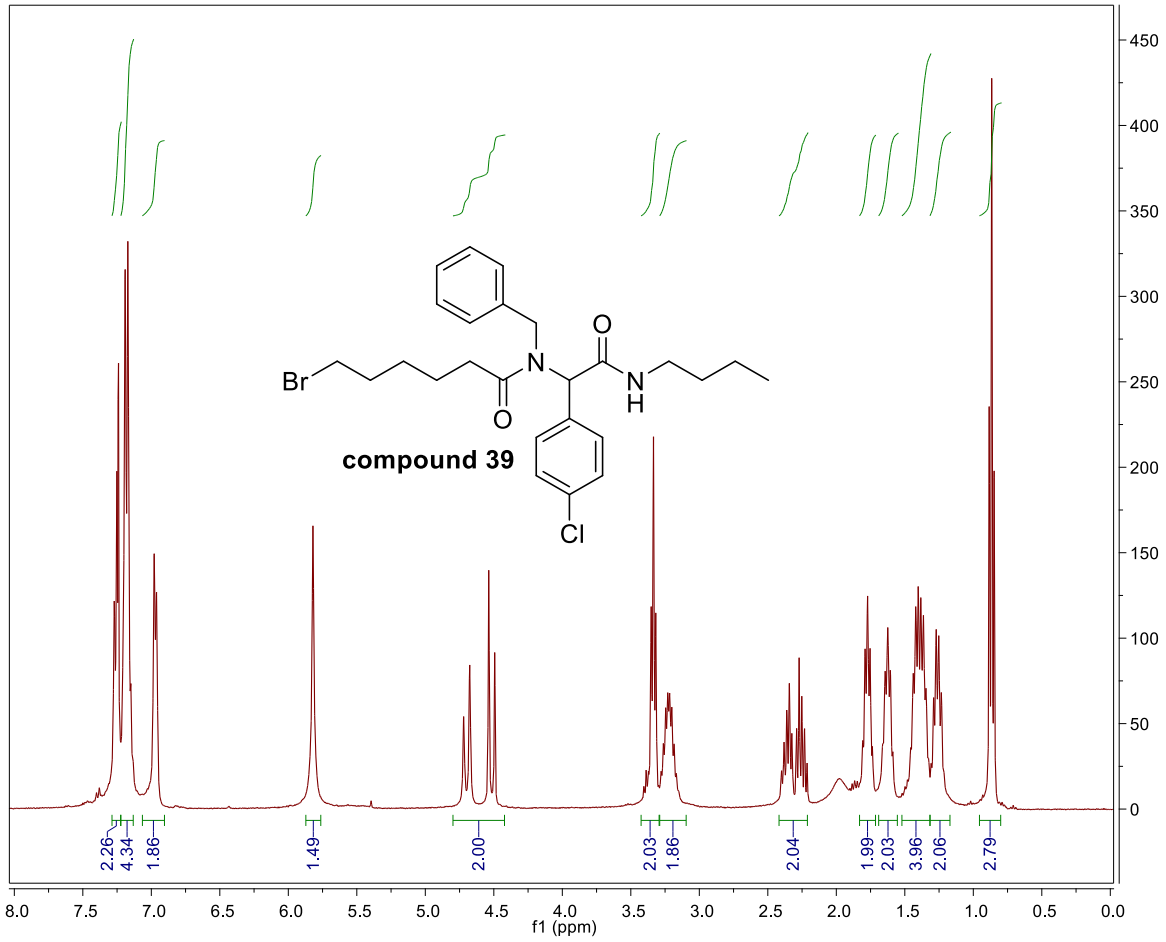

Compound 40. ^{1}H NMR (500 MHz, Chloroform-*d*) δ 7.30 (d, *J* = 8.5 Hz, 2H), 7.26 – 7.16 (m, 5H), 7.03 (d, *J* = 6.6 Hz, 2H), 5.87 (s, 1H), 5.83 (s, 1H), 4.77 (d, *J* = 17.7 Hz, 1H), 4.55 (d, *J* = 17.7 Hz, 1H), 3.28 (qq, *J* = 13.4, 6.9 Hz, 2H), 2.89 – 2.79 (m, 2H), 2.79 – 2.70 (m, 1H), 2.61 (dt, *J* = 16.2, 6.6 Hz, 1H), 1.70 (t, *J* = 8.4 Hz, 1H), 1.52 – 1.40 (m, 2H), 1.34 – 1.22 (m, 2H), 0.91 (t, *J* = 7.3 Hz, 3H).

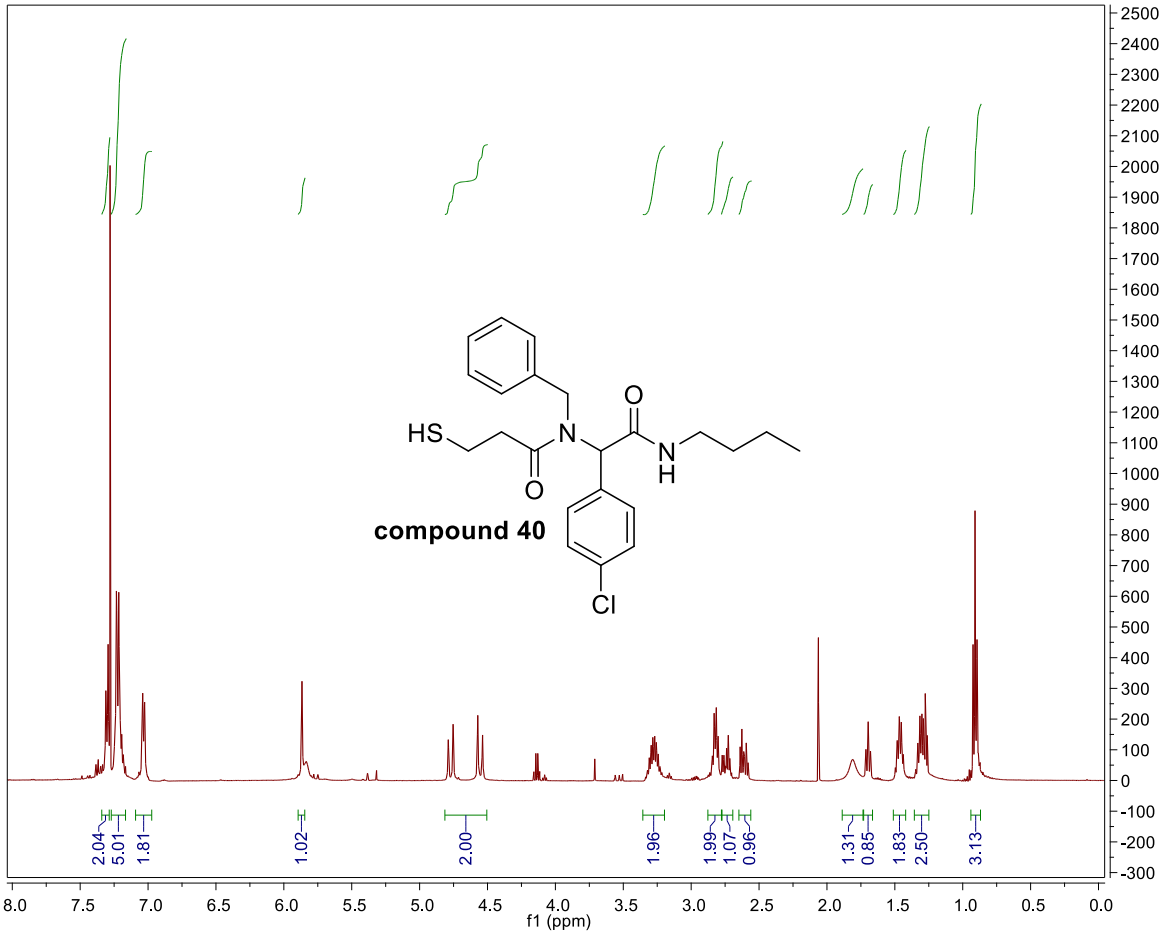

Compound 41. ^{1}H NMR (500 MHz, Chloroform-*d*) δ 7.41 – 7.35 (m, 2H), 7.31 – 7.12 (m, 6H), 7.02 (d, *J* = 7.3 Hz, 2H), 5.94 (s, 1H), 5.83 (s, 1H), 4.76 (d, *J* = 17.7 Hz, 1H), 4.58 (d, *J* = 17.7 Hz, 1H), 3.38 – 3.18 (m, 2H), 2.43 – 2.34 (m, 1H), 2.30 – 2.21 (m, 1H), 1.72 – 1.60 (m, 2H), 1.47 (p, *J* = 8.3, 7.3 Hz, 2H), 1.37 – 1.17 (m, 6H), 0.89 (dt, *J* = 19.1, 7.2 Hz, 6H).

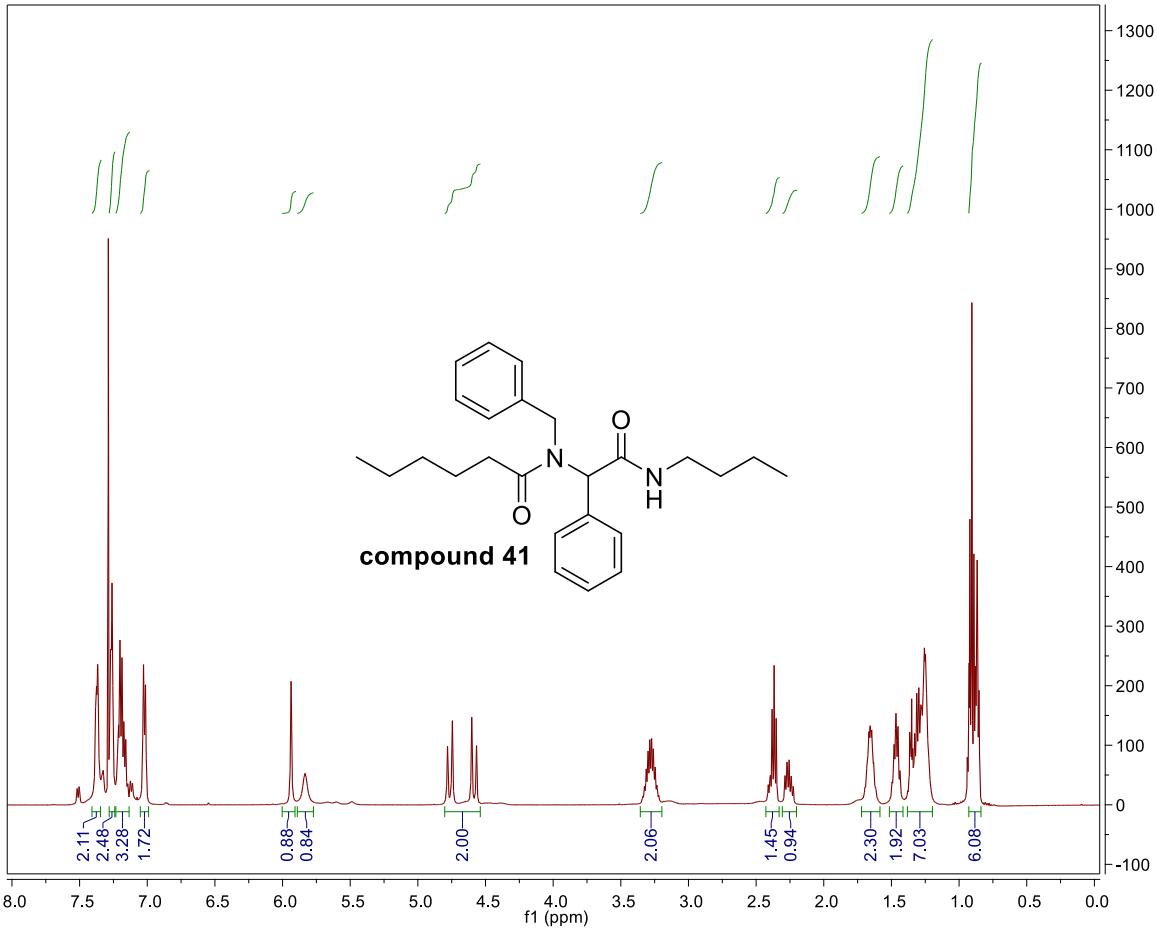

Compound 42. ^{1}H NMR (500 MHz, Chloroform-*d*) δ 7.40 – 7.32 (m, 2H), 7.29 – 7.11 (m, 6H), 7.03 (d, *J* = 7.3 Hz, 2H), 5.91 (s, 1H), 5.76 (s, 1H), 4.77 (d, *J* = 17.7 Hz, 1H), 4.58 (d, *J* = 17.7 Hz, 1H), 3.28 (qq, *J* = 13.4, 6.9 Hz, 2H), 2.49 – 2.11 (m, 2H), 1.84 – 1.63 (m, 2H), 1.47 (p, *J* = 7.5 Hz, 2H), 1.31 (h, *J* = 7.4 Hz, 2H), 0.91 (t, *J* = 7.4 Hz, 6H).

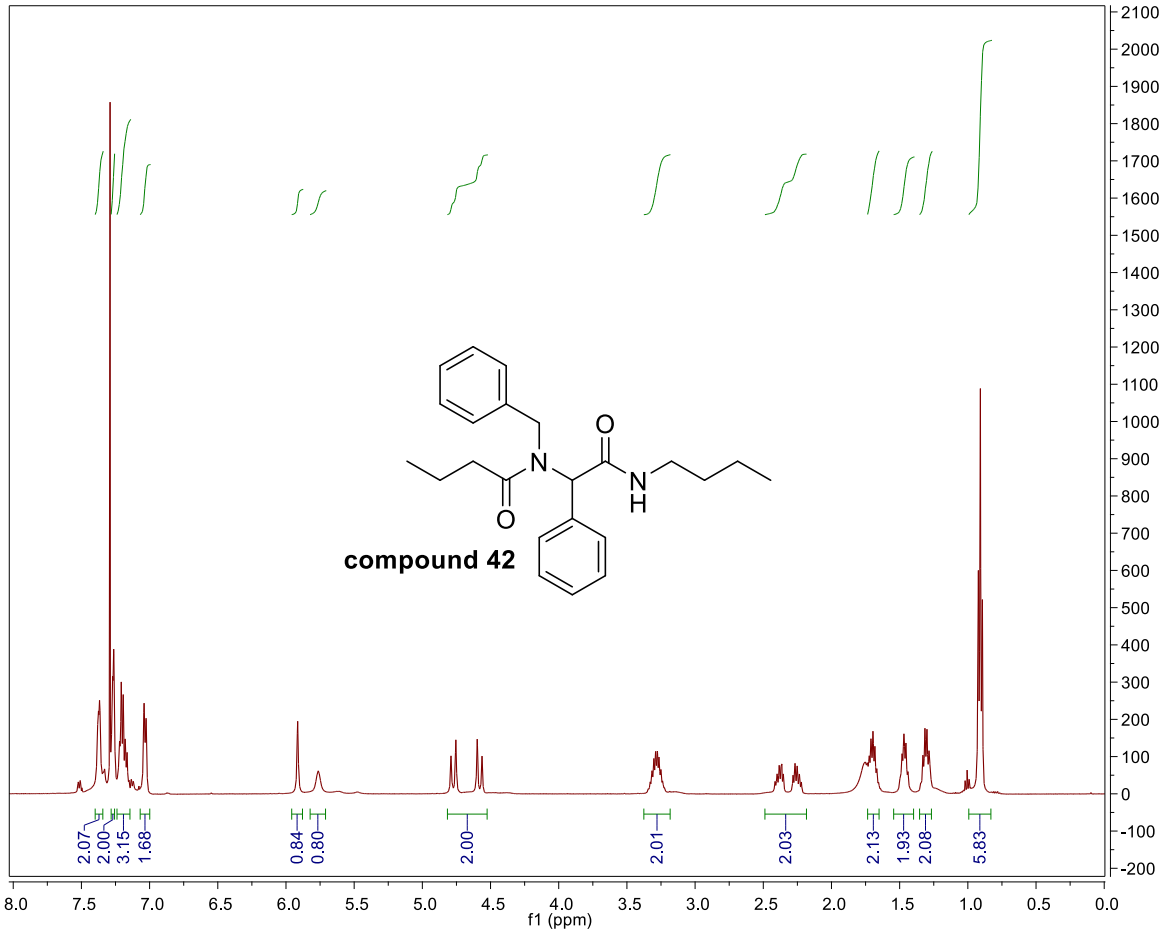

Compund 43. ^{1}H NMR (401 MHz, Chloroform-*d*) δ 7.37 – 7.26 (m, 2H), 7.26 – 7.07 (m, 6H), 6.97 (d, *J* = 7.2 Hz, 2H), 5.91 (s, 1H), 5.77 (s, 1H), 4.71 (d, *J* = 17.8 Hz, 1H), 4.54 (d, *J* = 17.7 Hz, 1H), 3.32 (t, *J* = 6.8 Hz, 2H), 3.28 – 3.14 (m, 2H), 2.42 – 2.13 (m, 2H), 1.76 (p, *J* = 7.0 Hz, 2H), 1.69 – 1.54 (m, 2H), 1.51 – 1.30 (m, 4H), 1.30 – 1.17 (m, 2H), 0.86 (t, *J* = 7.3 Hz, 3H).

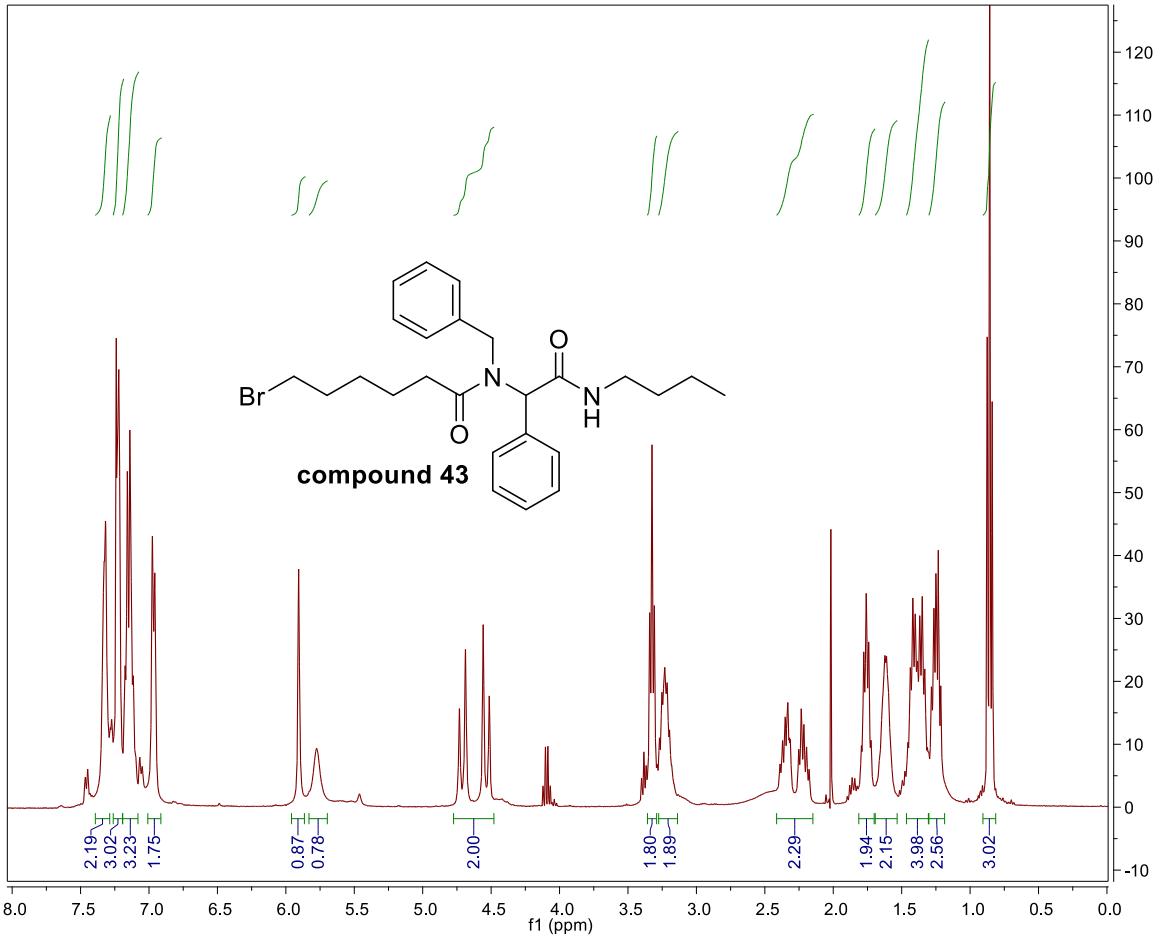

A.7.6 Characterization starting materials

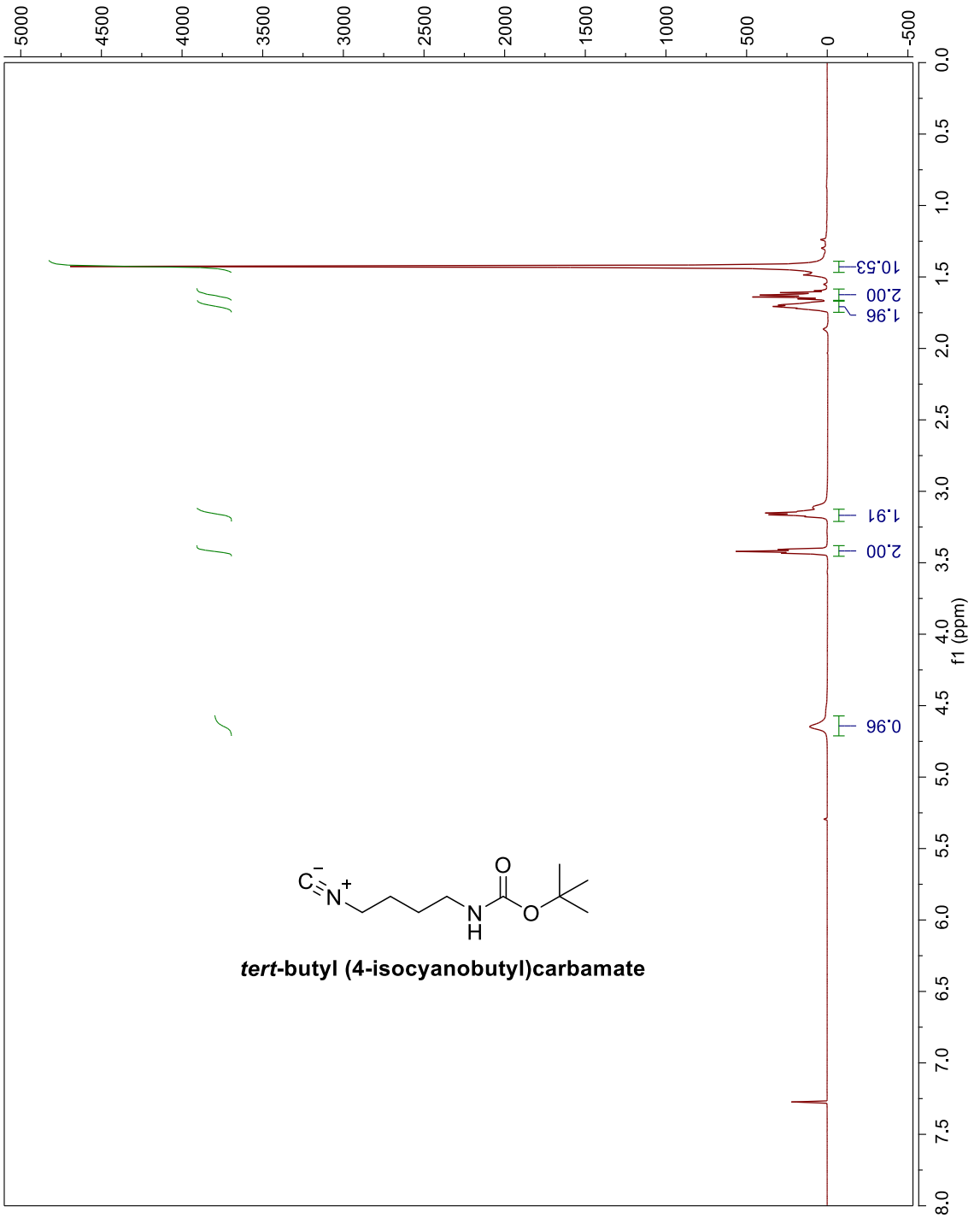

***tert*-butyl (4-isocyanobutyl)carbamate**

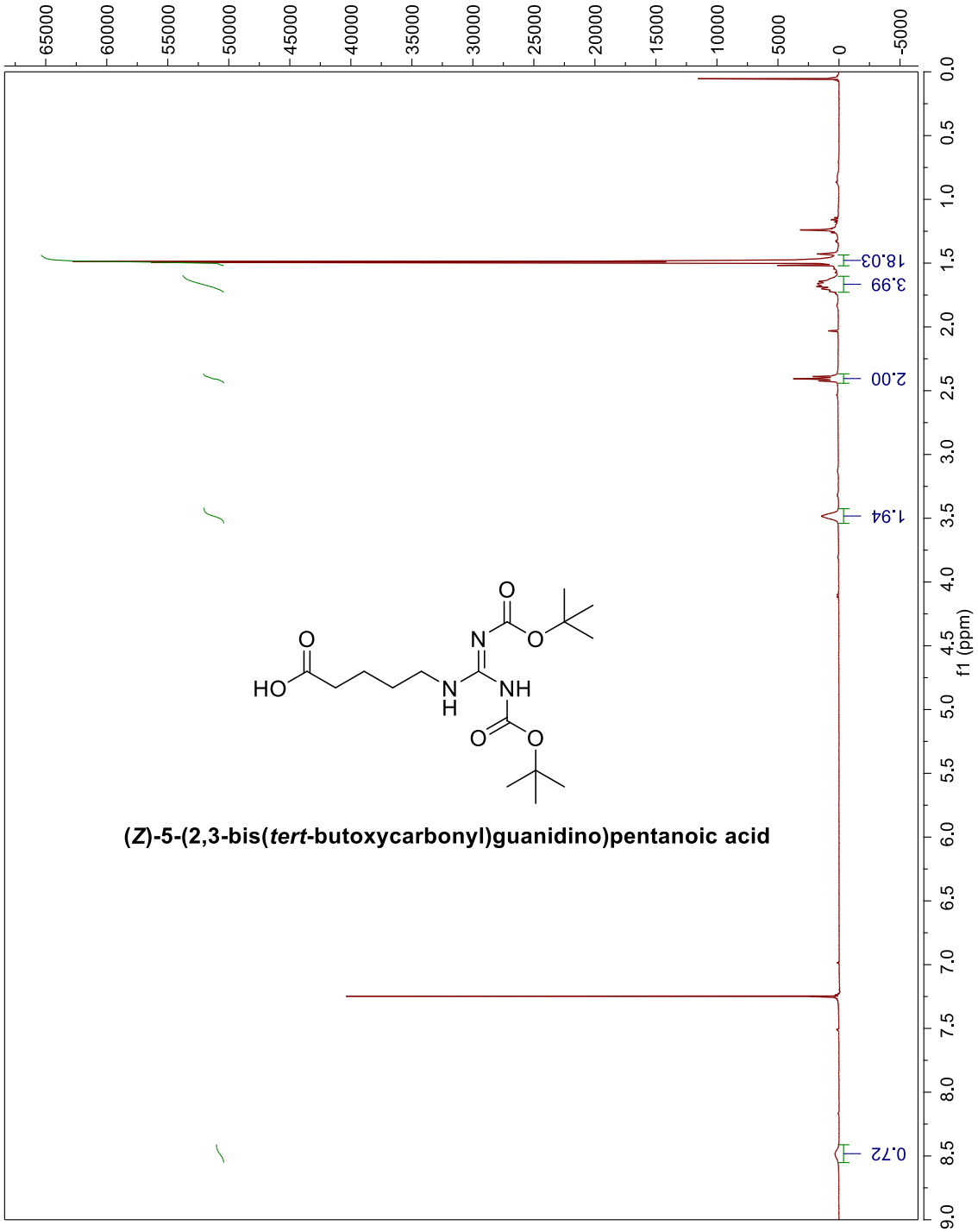

(*Z*)-5-(2,3-bis(*tert*-butoxycarbonyl)guanidino)pentanoic acid

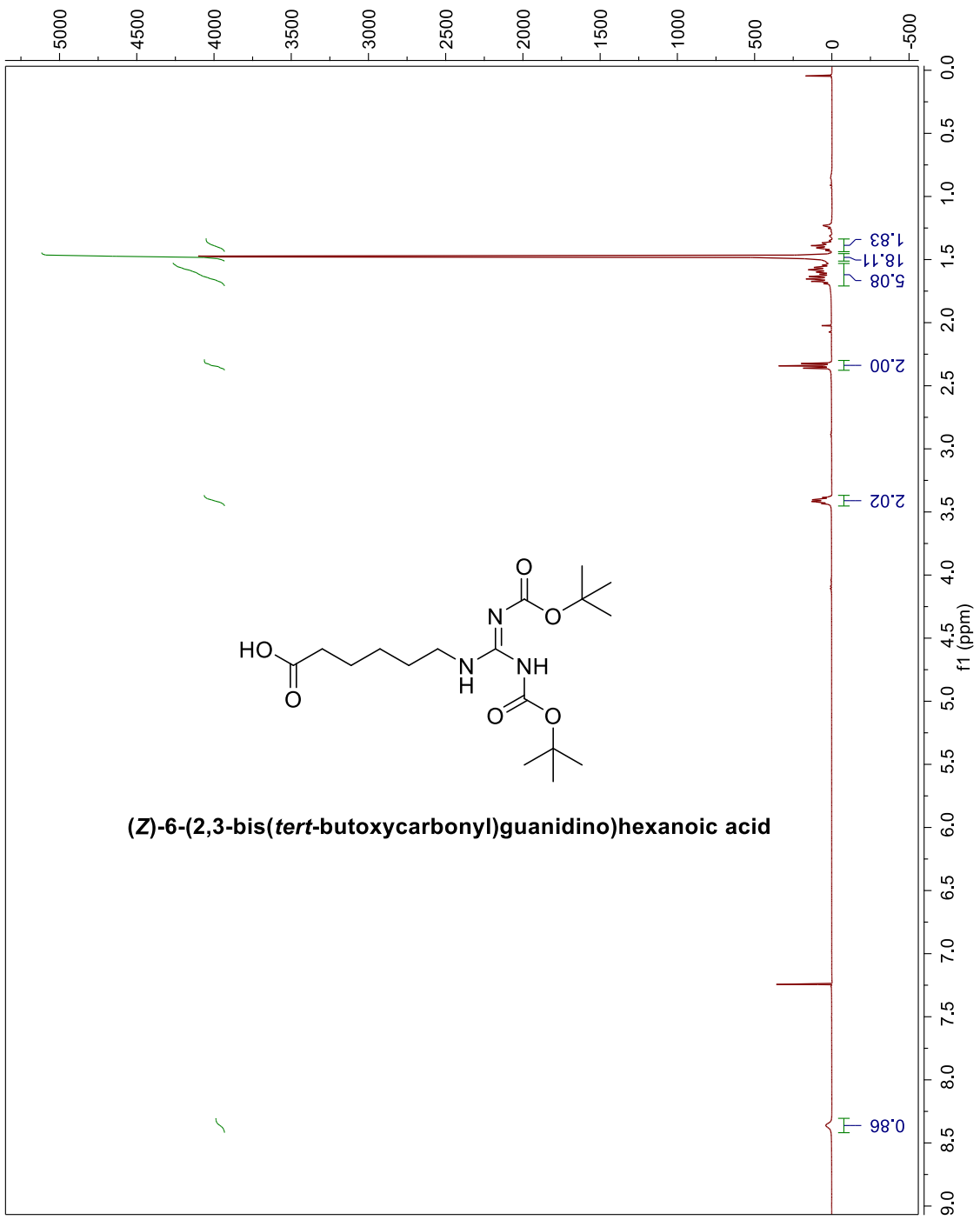

(*Z*)-6-(2,3-bis(*tert*-butoxycarbonyl)guanidino)hexanoic acid

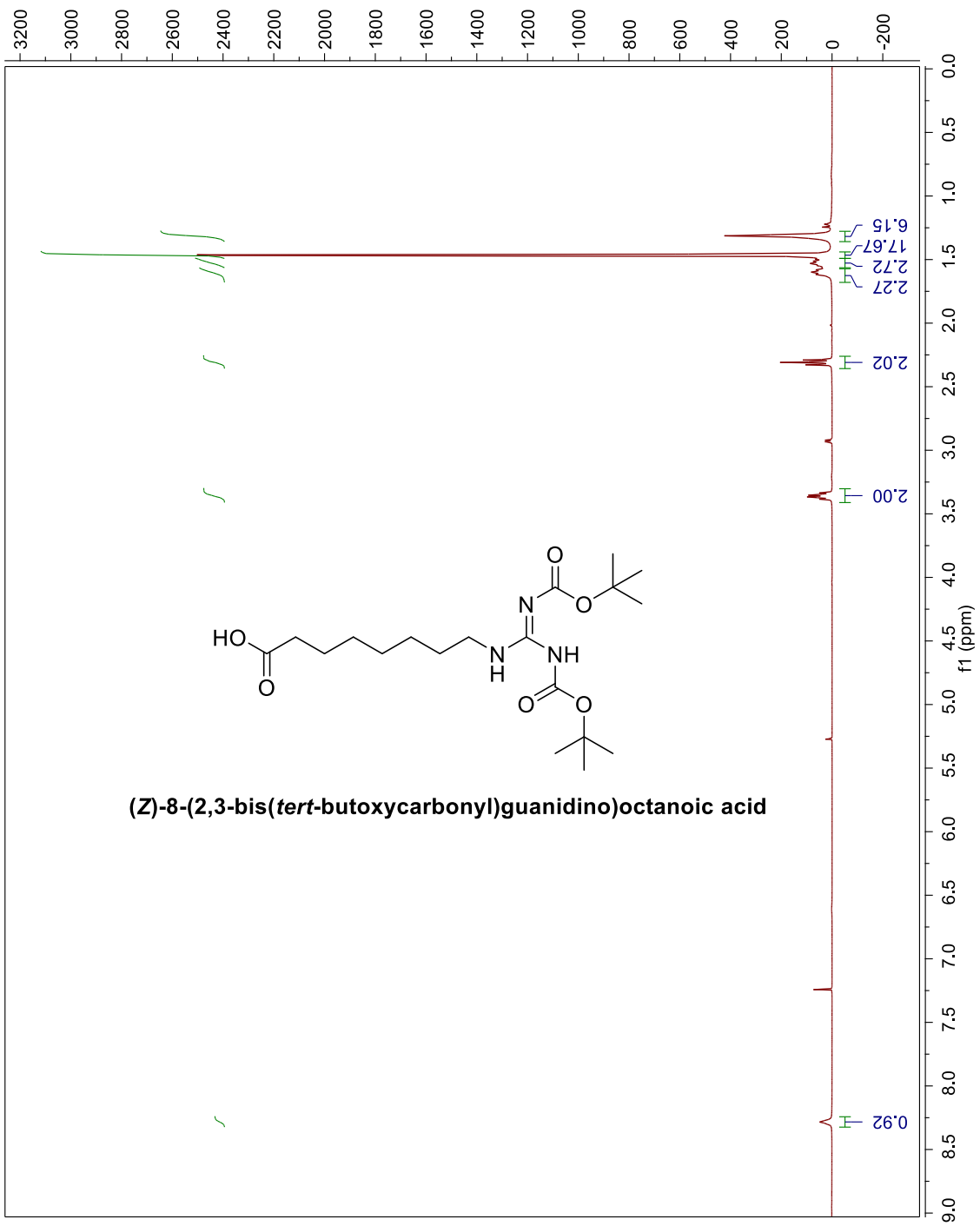

(*Z*)-8-(2,3-bis(*tert*-butoxycarbonyl)guanidino)octanoic acid

A.7.4 Mass spectrometry to validate the identity of purchased compound 6 analogs

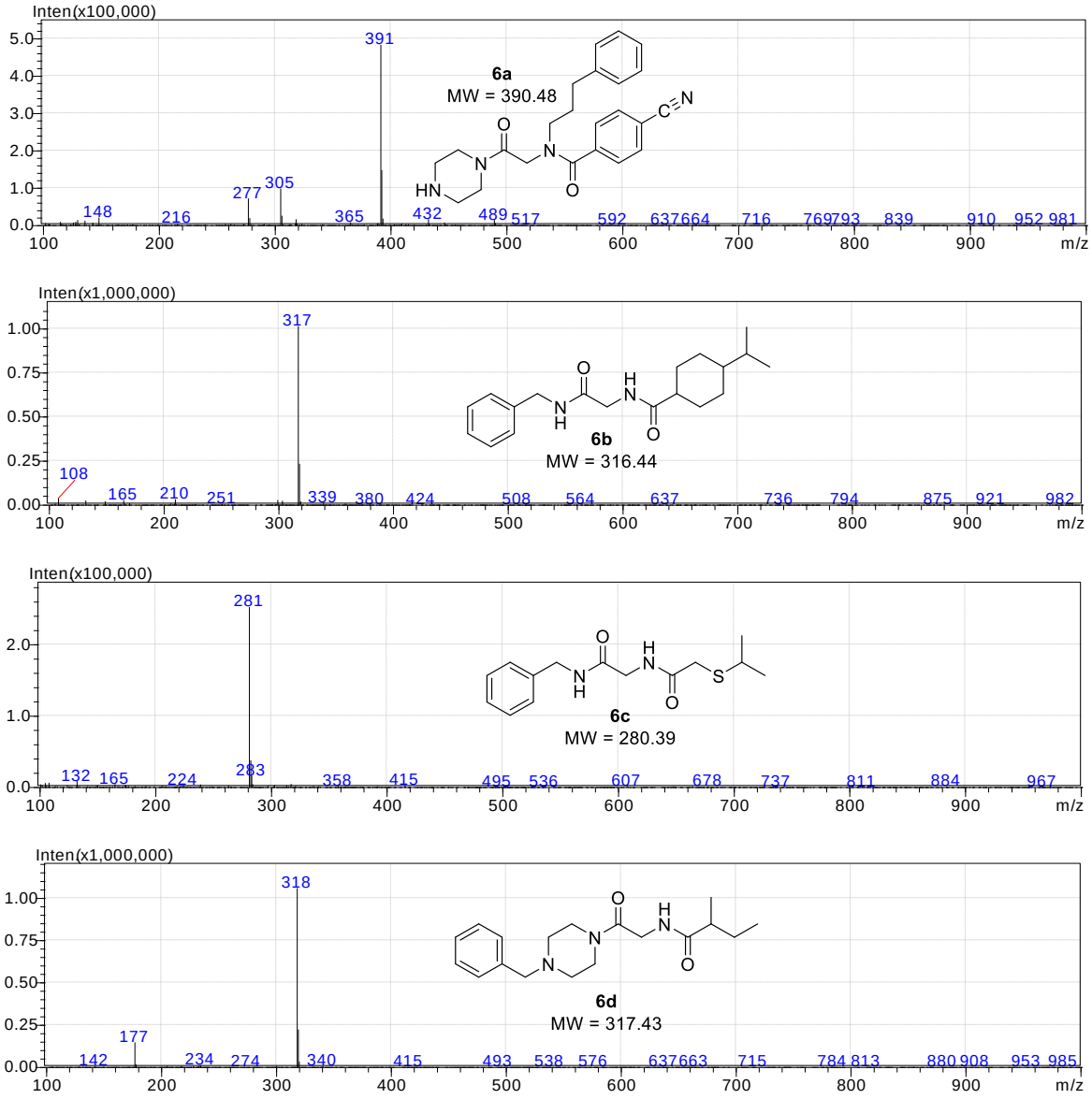

A.8 References

1. Nadler, S.G., et al., *Elucidating the Mechanism of Action of the Immunosuppressant 15-Deoxyspergualin.* Therapeutic Drug Monitoring, 1995. **17**(6): p. 700-703.
2. Umezawa, H., et al., *Structure of an Anti-Tumor Antibiotic, Spergualin.* Journal of Antibiotics, 1981. **34**(12): p. 1622-1624.
3. Ganesan, A., *The impact of natural products upon modern drug discovery.* Curr Opin Chem Biol, 2008. **12**(3): p. 306-17.
4. Neu, H.C., *The crisis in antibiotic resistance.* Science, 1992. **257**(5073): p. 1064-73.
5. Payne, D.J., et al., *Drugs for bad bugs: confronting the challenges of antibacterial discovery.* Nat Rev Drug Discov, 2007. **6**(1): p. 29-40.
6. Brodsky, J.L., *Selectivity of the molecular chaperone-specific immunosuppressive agent 15-deoxyspergualin - Modulation of HSC70 ATPase activity without compromising DnaJ chaperone interactions.* Biochemical Pharmacology, 1999. **57**(8): p. 877-880.
7. Lebreton, L., et al., *Structure-immunosuppressive activity relationships of new analogues of 15-deoxyspergualin. 1. Structural modifications of the hydroxyglycine moiety.* Journal of Medicinal Chemistry, 1999. **42**(2): p. 277-290.
8. Umeda, Y., et al., *Synthesis and Antitumor-Activity of Spergualin Analogs .3. Novel Method for Synthesis of Optically-Active 15-Deoxyspergualin and 15-Deoxy-11-O-Methylspergualin.* Journal of Antibiotics, 1987. **40**(9): p. 1316-1324.
9. Ohlman, S., et al., *Pharmacokinetics of 15-Deoxyspergualin Studied in Renal-Transplant Patients Receiving the Drug during Graft-Rejection.* Transplant International, 1994. **7**(1): p. 5-10.
10. Evans, C.G., et al., *Improved synthesis of 15-deoxyspergualin analogs using the Ugi multi-component reaction.* Bioorganic & Medicinal Chemistry Letters, 2011. **21**(9): p. 2587-2590.
11. Osipova, A., D.S. Yufit, and A. de Meijere, *Synthesis of new cyclopropylisonitriles and their applications in Ugi four-component reactions.* Synthesis-Stuttgart, 2007(1): p. 131-139.
12. Umeda, Y., et al., *Synthesis and Antitumor-Activity of Spergualin Analogs .1. Chemical Modification of 7-Guanidino-3-Hydroxyacyl Moiety.* Journal of Antibiotics, 1985. **38**(7): p. 886-898.
13. Feichtinger, K., et al., *Diprotected triflylguanidines: A new class of guanidinylation reagents.* Journal of Organic Chemistry, 1998. **63**(12): p. 3804-3805.
14. Johnston, J.W., *Laboratory growth and maintenance of Haemophilus influenzae.* Current protocols in microbiology, 2010. **Chapter 6**: p. Unit 6D.1-Unit 6D.1.